Blood vessel epicardial substance (BVES) and BVES binding partners in intestinal homeostasis and tumorigenesis

By

Joshua James Thompson

Dissertation

Submitted to the Faculty of the

Graduate School of Vanderbilt University

in partial fulfillment of the requirements

for the degree of

DOCTOR OF PHILOSOPHY

in

Cancer Biology

September 30, 2019

Nashville, Tennessee

Approved:

Barbara Fingleton, Ph.D. (committee chair)

R. Daniel Beauchamp, M.D.

Ethan Lee, M.D., Ph.D.

Christopher S. Williams, M.D., Ph.D. (advisor)

To Charlotte and Theodore – May all your dreams come true

ACKNOWLEDGEMENTS

My time in graduate school has been immensely rewarding and confirmed my passion for research that will ultimately affect the course of patient's lives. Graduate school, however, was not without challenges. From the vast number of failed Western blots to the difficult to interpret subtleties, I have grown as an individual and as a scientist, learning to think critically and integrate new literature to generate and refine hypotheses. None of that would have been possible without the help of a tremendous number of individuals with whom I am eternally grateful.

I would be remiss if I did not first thank my advisor, Dr. Christopher Williams. Chris, you have pushed me to be a better scientist, and you have always been a fearless advocate for your trainees. Your career advice and insight into navigating the complexities, whether it be grant writing or leadership, have been instrumental. Furthermore, I hope to emulate your alignment of priorities as it will make me a more well-rounded scientist, a better father, and a better husband. I am forever grateful for your mentorship and will look forward to continuing to seek out your advice through the many career transitions that lie ahead.

I am incredibly grateful for the members of my thesis committee, Dr. Barbara Fingleton, Dr. Ethan Lee, Dr. Daniel Beauchamp, Dr. David Bader, and Dr. Christopher Williams. They provided thoughtful and critical feedback of my data and also helped focus many of my studies, protecting me from those ever exciting but often risky tangents. It has been an honor to be mentored by such a talented committee of scientists and individuals whose careers I hope to emulate.

I would also like to thank the rest of the members of the Williams Lab for their support and comradery over the last three and a half years. The Williams Lab members are an incredible, hard-working, and collaborative family. Sarah, you make the lab go 'round and each and every one of us have benefitted immensely from your experimental and technical guidance. To Chase, Jasmine,

Jen, Niyati, Rachel, and Yash, as well as our former members Cody and Mukul, thank you for your friendship, critical data analysis, and willingness to always lend a hand. To my undergraduate mentees, Navu and David, thank you for your hard work and dedication. David, the projects that you have been working on have been incredibly difficult and you have shown tremendous diligence; you should be very proud of the contributions you have made.

Since arriving on campus six years ago, the Vanderbilt MSTP has welcomed my family with open arms. I am so grateful for both the past and present leadership's dedication, as well as that of the Vanderbilt School of Medicine, to the students and this program. We as students have the opportunity to succeed, in no small part, because of the framework that has been built and the support of this program.

I would also like to thank the core facilities here at Vanderbilt, with a special thank you to Sherry Smith and the staff in the TPSR core. Your technical expertise and guidance allowed us to capture some beautiful biology and push forward many of our studies.

To my previous research mentors, both at UNC and at CU Denver, it takes a village. Thank you for being a part of that. And to mouse 9787, thank you for keeping me humble.

Lastly, I would like to thank my family for making this all possible. To my parents, Scott and Tracy, thank you for instilling in me a love of learning and for providing me every opportunity, unreservedly. To my wife, Amy, this journey would not have been possible nor complete without you. You have taken on incredible responsibility caring for Charlotte and for me. From the countless weekend trips to the lab, to chasing Charlotte down the halls of Light Hall while I was upstairs splitting cells, there is no one I would have rather embarked on this journey with.

TABLE OF CONTENTS

Page

LIST OF TABLES

LIST OF FIGURES

LIST OF ABBREVIATIONS

AOM	Azoxymethane
APC	Adenomatous Polyposis Coli
β-TrCP	Beta-Transducin repeats-Containing Protein
BCAR3	Breast cancer anti-estrogen resistance 3
bFGF	basic Fibroblast Growth Factor
BMP	Bone Morphogenic Protein
BVES	Blood Vessel Epicardial Substance
cDNA	complementary DNA
CK1alpha	Casein Kinase 1 alpha
CBC	Crypt Based Columnar
CRC	Colorectal Cancer
DMEM	Dulbecco's Modified Eagle's Medium
DSS	Dextran Sodium Sulfate
DVL	Dishevelled
ECD	Extracellular Domain
EGF	Epidermal Growth Factor
EGFR	Epidermal Growth Factor Receptor
EMT	Epithelial-Mesenchymal Transition
ENR	Epidermal Growth Factor/Noggin/R-spondin
FZ	Frizzled
GAPDH	Glyceraldehyde 3-Phosphate Dehydrogenase
GEF	Guanine Nucleotide Exchange Factor
GEFH1	Guanine Nucleotide Exchange Factor H1
GEFT	Guanine Nucleotide Exchange Factor T
GSK3	Glycogen Synthase Kinase 3
HCE	Human Corneal Epithelial
HEK	Human Embryonic Kidney
HEPES	N-2-hydroxyethylpiperazine-N′-2- ethanesulfonic acid
hESC	human Embryonic Stem Cell
ICD	Intracellular Domain
JAM	Junctional Adhesion Molecule
KLF4	Kruppel Like Factor 4
LGMD	limb-girdle muscular dystrophy
Lgr5	Leucine-rich repeat-containing G-protein coupled receptor 5
LRP	lipoprotein receptor-related protein
LWRN	L-cell Wnt3a/R-spondin/Noggin
MEF	Mouse Embryonic Fibroblasts
MET	Mesenchymal-Epithelial Transition

MLC	Myosin Light Chain
NSP	Novel SH2-containing Protein family
OA	Okadaic Acid
OR	Odds Ratio
PBS	Phosphate-Buffered Saline
PCP	Planar Cell Polarity
PEI	Polyethylenimine
PKA	Protein Kinase A
PLA	Proximity Ligation Assay
PP2A	Protein Phosphatase 2A
PTM	Post-Translational Modification
PTP	Protein Tyrosine Phosphatase
RB	Retinoblastoma
RT	Room Temperature
shRNA	short hairpin RNA
siRNA	small interfering RNA
SMAP	small molecule activators of PP2A
STF	SuperTopFlash
TA	Transit Amplifying
TCGA	The Cancer Genome Atlas
TEAD	TEA domain transcription factor
TER	Transepithelial Resistance
TM	Transmembrane
VAMP3	Vesicle-Associated Membrane Protein 3
WT	Wild-Type
ZO	Zonula Occluden

CHAPTER I

THE INTESTINAL EPITHELIUM AND BVES

Introduction to the intestinal epithelium

The intestine is broadly divided into two distinct components: the small intestine (which can be further subdivided proximally to distally into the duodenum, jejunum, and ileum, respectively), and the large intestine, or colon (which can also be further subdivided into ascending, transverse, descending, and sigmoid segments). Functionally, the small intestine is specialized to digest and absorb food while the large intestine aids in the absorption of water and electrolytes. These specialized functions are facilitated predominately by the intestinal epithelium which is comprised of a single layer of simple columnar epithelial cells. This epithelium renews rapidly every 4-5 days and helps form a protective barrier against luminal antigens and pathogens[1]. Histologically, the small intestine is covered by finger-like projections known as villi which extend into the lumen of the intestine and increase the absorptive surface area. At the apical most surface of each intestinal villus are microscopic membranous protrusions known as microvilli which further increase the absorptive area and also aid in mechanotransduction, secretion, and cellular adhesion[2]. Collectively, this actin-rich bundle of microvilli is referred to as the intestinal "brush-border." At the base of the intestinal villi are the intestinal crypts, or crypts of Lieberkühn. Villi are restricted to the small intestine while the crypts are present in both the small intestine and the colon.

Rapid turnover of cells along the crypt-villus axis of the intestinal epithelium is fueled by constantly dividing stem cells located at the base of the crypts. Also referred to as crypt base

columnar (CBC) cells, these slender stem cells are anatomically distinct and, as is fundamental to all stem cells, they are long lived and multipotent[3,4]. They can self-renew and divide asymmetrically to give rise to additional cell types which in the case of the intestine is a proliferative progenitor cell known as a transit amplifying (TA) cell. TA cells migrate and differentiate into absorptive cells (enterocytes) or secretory cells (Paneth, goblet, and enteroendocrine cells) as they ascend towards the crypt-villus axis before being sloughed off into the intestinal lumen (Figure 1)[5,6]. Zonation, lineage specification, and proliferation along this axis are thought to be mediated by gradients of Wnt activity (higher at the crypt base) and BMP signaling (expressed in an opposite gradient to that of Wnt and increasing as cells move up the crypt) which is known to inhibit proliferation along with Notch signaling which is critical in the commitment towards secretory vs. absorptive lineages[7,8].

In 2007, Hans Clevers and his group identified the transmembrane receptor Leucine-rich repeat-containing G-protein coupled receptor 5 (Lgr5), a receptor for R-spondins which are Wnt pathway agonists, as a marker of CBCs and for the first time showed the capability of this population to repopulate all cell types in the intestinal epithelium[3,9,10]. The CBCs are nestled between crypt-resident Paneth cells which escape the upward thrust toward the villus and migrate downward to occupy the crypt base. Paneth cells secrete antimicrobial agents such as lysozyme and promote maintenance of stem cell function by secreting Wnt3a (a Wnt ligand), EGF, and Notch ligands[11]. While contributory, Paneth cells themselves are likely not essential as Lgr5+ intestinal stem cells can function even in the setting of Paneth cell ablation via deletion of the transcription factor Math1 (Atoh1)[12,13]. Additional niche cells such as the pericryptal mesenchymal cells have been shown to express potential niche-supporting factors[14]. Not surprisingly, CBC cells are not the only, and not the earliest, proposed resident stem cell populations. Potten's +4 cell was originally identified in 1977 due to its label-retaining

capacity[15]. It wasn't until 2008 that direct evidence of stemness in a +4 position cell was put forward by Sangio and Capecchi utilizing the Bmi1-CreER mouse[16]. Additional studies have identified Hopx, mTERT, and Lrig1 as +4 markers[17-20]. In general, lineage tracing from this +4 population appears to require damage to the intestinal crypt (and subsequently the Lgr5+ CBC) suggesting a stem cell hierarchy or plasticity within these reserve stem cell populations (reviewed in [21]). In summary, the intestinal epithelium is a complex, multi-faceted tissue that functions to absorb nutrients and partition luminal pathogens while undergoing continuous turnover in the setting of mechanical and chemical stress.

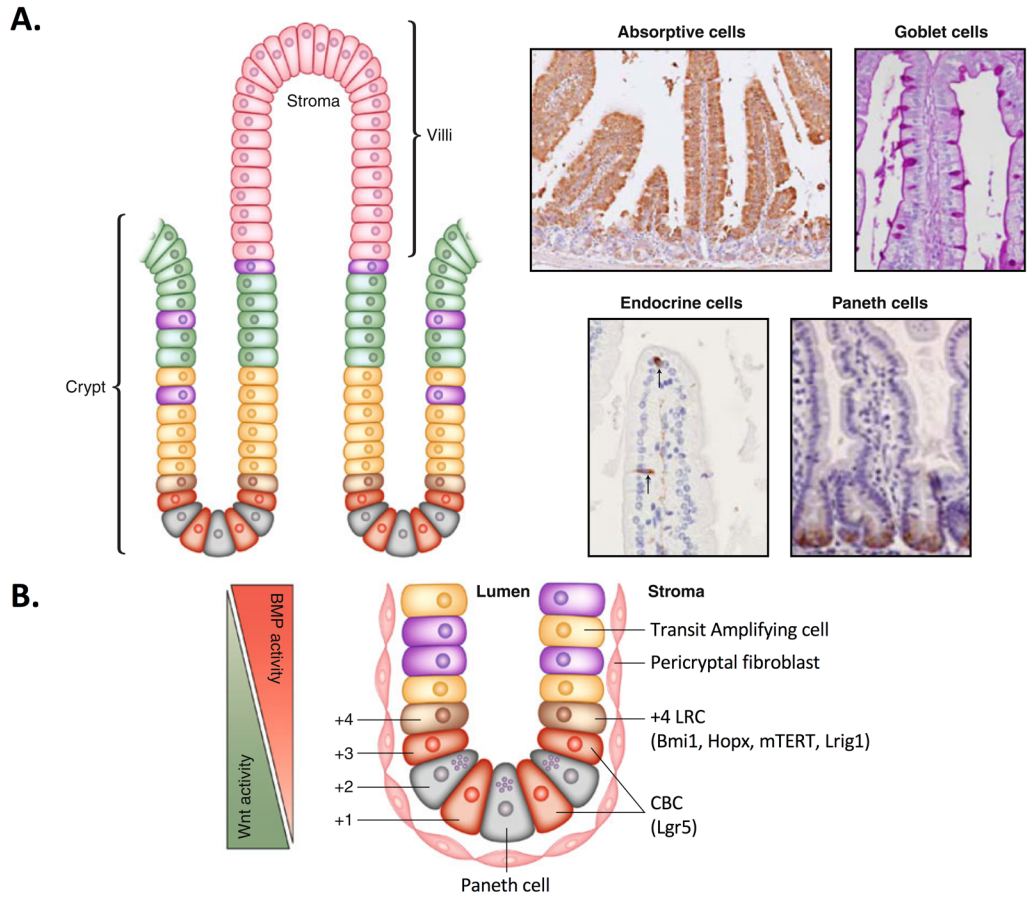

Figure 1. Cell populations of the intestinal epithelium. (A) The small intestine is composed of repeating crypt-villus units with intestinal stem cells residing at the base of the crypt and differentiated cells towards the villus. The following cell populations are stained: Absorptive cells (Fatty acid binding protein), Goblet cells (periodic acid/Schiff, PAS), enteroendocrine cells (synaptophysin, arrows), and Paneth cells (lysozyme). (B) An enlarged view of the constituent cells of the small intestinal crypt along with markers that have been demonstrated to label each cell population. Pericryptal fibroblasts are thought to supply niche factors to support crypt homeostasis. LRC, Label Retaining Cell; CBC, Crypt Based Columnar. This figure was adapted with permission [6].

Intestinal barrier function and junctional constituents

Cell-cell adhesions are critical for the epithelium to fulfill its role as a selectively permeable barrier allowing for the absorption of nutrients, water, and electrolytes while simultaneously preventing penetration of intestinal pathogens and other antigenic materials. Junctional complexes—such as tight junctions, adherens junctions, hemidesmosomes, and gap junctions — within these epithelial cells are critical for linkage of the cytoskeleton, cell-cell signaling, sub-cellular partitioning of membrane proteins, and for regulating para-cellular permeability that ultimately allows the intestinal epithelium to perform this function. Hemidesmosomes couple the basal membrane of the epithelium to the underlying basal lamina and coordinate with the more laterally localized desmosomes to help nucleate intermediate filament networks of the cytoskeleton[22]. Gap junctions connect neighboring cells and allow for direct cell-cell passage of ions, metabolites, and second messengers through hexamers consisting mainly of connexin proteins[23]. Adherens junctions initiate and maintain cell-cell contacts by coupling the transmembrane glycoprotein E-cadherin with the actin cytoskeleton through cytoplasmic constituents p120-catenin, β-catenin, and α-catenin[24]. Maintaining the integrity of these junctions is critical both in regulating barrier function and tumorigenesis. For example, expression of a dominant-negative N-cadherin in mice disrupts the adherens junction leading to the development of spontaneous colitis[25], and E-cadherin reductions in colorectal cancer are associated with increased invasive potential[26]. Interestingly, disruption of E-cadherin in the epidermis leads to alterations in the tight junction, highlighting the interconnectivity of the junctional barrier network[27].

Tight junctions are often closely associated with adherens junctions near the apical-lateral membrane and help form a selective, semipermeable barrier restricting the paracellular transport

of solutes, ions, and water. Additionally, tight junctions promote the sub-cellular partitioning of apical and basolateral proteins and help define cellular polarity[28]. Principal constituents of tight junctions include the transmembrane proteins of dial substance (BVES). Multiple adaptor proteins such as the zonula occludens (ZO-1-3) and cingulin as well as the RHOGEF, RHOA, and ZONAB signaling molecules are also located cytoplasmically in association with the tight junction[29].

BVES structure, expression, and localization

Blood vessel epicardial substance (BVES), otherwise known as POPDC1, is the founding member of the POPDC family. BVES shares about 25% sequence homology to the other two POPDC family members, POPDC2 and POPDC3 which themselves share about 50% homology (Figure 2)[30,31]. Human BVES is a 360-residue transmembrane protein with three alpha-helical membrane spanning, hydrophobic domains, two extracellular N-linked glycosylation sites[32], and a large intracellular domain, which is thought to serve as the scaffold for numerous protein-protein interactions to occur (Figure 3). The extracellular amino terminus of BVES extends from amino acid 1-42, and the two N-glycosylation sites potentially protect BVES from proteolysis or help traffic it to the cellular membrane[33,34]. Within the intracellular carboxy-terminus (a.a. 114-360) is the POPEYE domain (a.a.172-266), which displays nearly 80% sequence conservation across different vertebrates[31,35]. Functionally, Kawaguchi *et al.* showed that BVES exists as a dimer via interactions near the carboxy end of the POPEYE domain and that this homotypic interaction requires two lysine residues (K272 and K273)[36](Figure 3). Given its location at the membrane and that it possesses a three-pass transmembrane domain, it was postulated that BVES contributes to cell adherence, but interestingly, BVES lacks any motifs or domains commonly observed in other classes of adhesion molecules. To date, little is known about its protein folding,

translocation to the membrane, or how (and if) it is regulated post-translationally. Furthermore, sequence alignment analyses do not predict enzymatic activity. Accordingly, the novelty of the POPDC family structure implicates a unique cellular function.

While the structure of BVES does not provide immediate clues to its function, its expression pattern suggests some tissue specific capabilities. BVES is expressed in a variety of tissues and organs which may lend insight into its function and tissue-specific contributions. Specifically, BVES is expressed at high levels in the heart[37,38] as well as in smooth and skeletal muscle[39], and epithelial tissues in a variety of organs including the retina[40], intestine[41,42], lung[43], and breast[41]. A unifying feature of all of these tissues is a need for cell adherence. Not surprisingly, work by Osler *et al.* identified BVES dependent contributions to cell-cell adhesion. When cells are in a subconfluent state, BVES is primarily localized to the cytoplasm but BVES rapidly traffics to the cellular membrane at points of cell-cell contact[30,44] (Figure 4). Of note, the mechanisms and signals responsible for this trafficking are poorly understood and will require further investigation. At these points of cell-cell contact, BVES co-localizes with tight junction constituents ZO-1 and occludn, but not with adherens junction-associated proteins such as β-catenin and E-cadherin or desmosomal associated proteins[30]. Overall, based on BVES localization and its association with junctional complexes, it was hypothesized that BVES could be an important regulator of epithelial states.

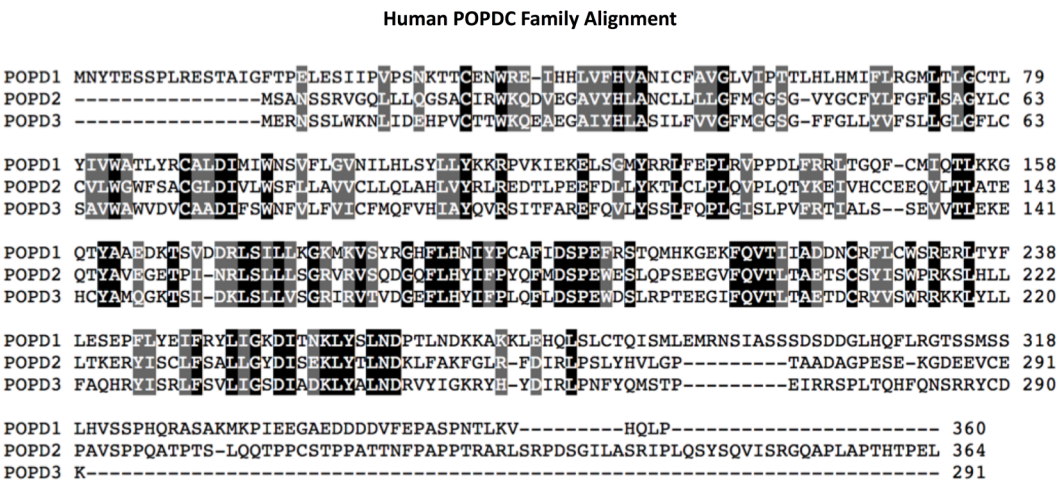

Figure 2. Human POPDC family sequence alignments. BVES or POPDC1 contains 360 amino acids. The extracellular domain extends from amino acids 1-42 and the intracellular domain is comprised of amino acids 114-360. A high degree of sequence homology exists among family members in the POPEYE domain which extends from amino acids 172-266 in POPDC1. Alignments generated using Clustal Omega from the European Bioinformatics Institute.

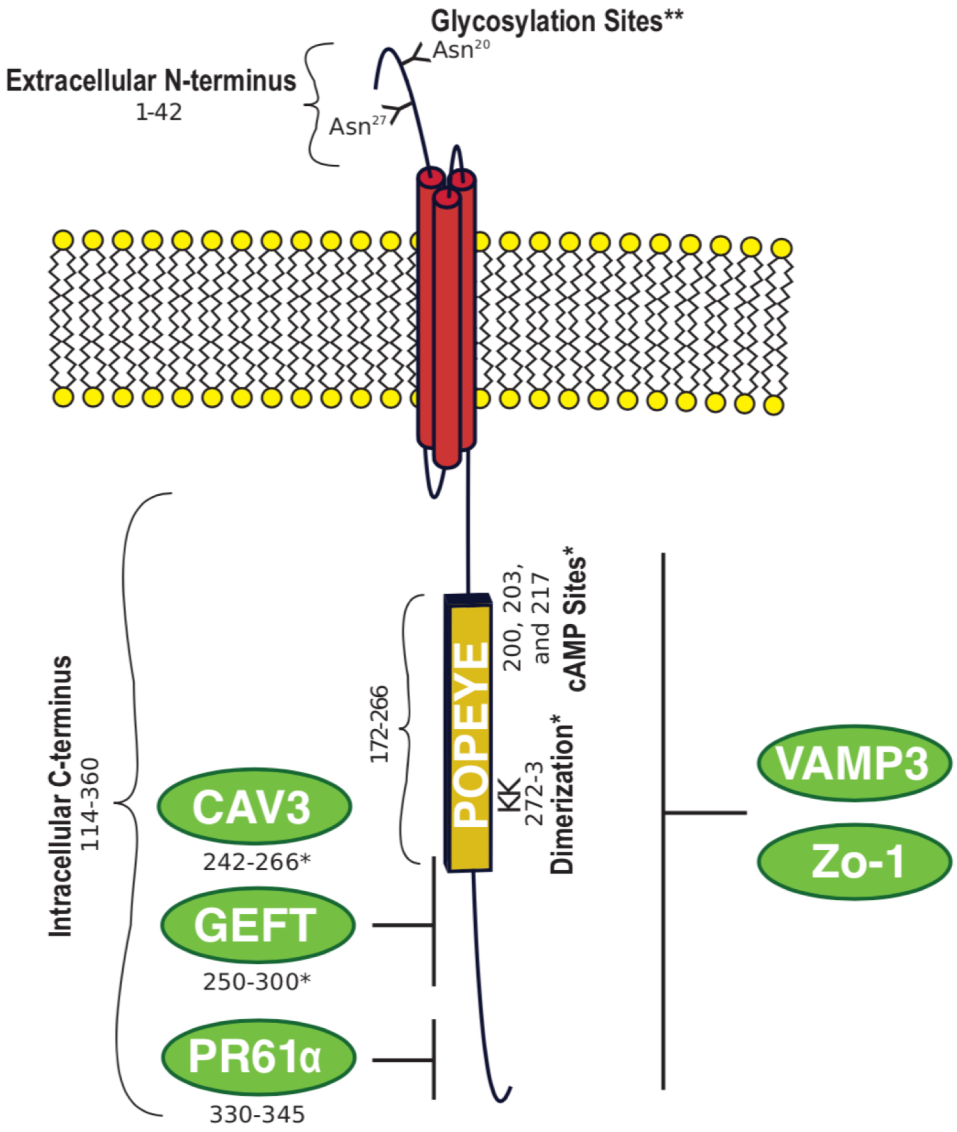

Figure 3. BVES structure. Human BVES protein is 360 amino acids with an extracellular N-terminus, a three-pass transmembrane domain, and a large intracellular C-terminus containing the highly conserved POPEYE domain.*mapped to murine BVES amino acids. ** mapped to chick BVES amino acids. Glycosylation[32]; POPEYE[35]; cAMP[58]; Dimerization[36]; GEFT[52]; PR61α[73]; VAMP3[55]; Zo-1[30].

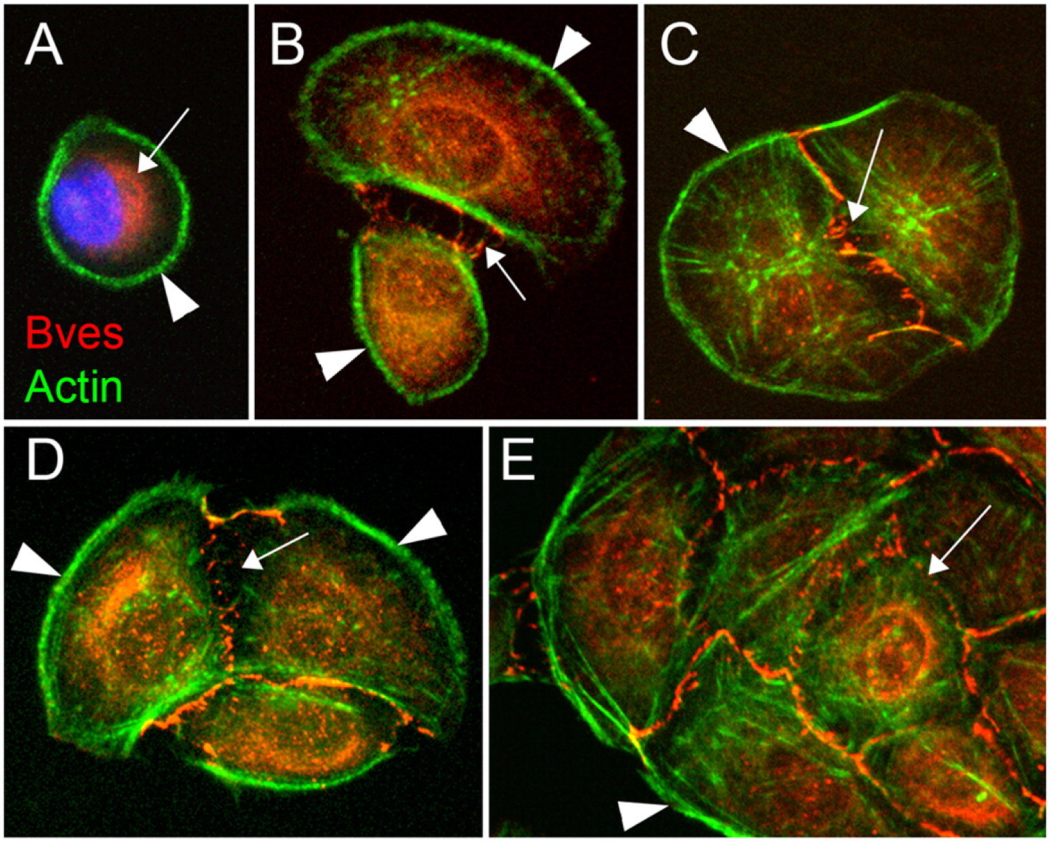

Figure 4. Dynamic subcellular localization of BVES at points of cell contact. Epicardial mesothelial cells (EMCs) are labelled with BVES (red) and phalloidin/Actin (green). (A) In the subconfluent state, BVES is predominately cytoplasmic. (B-D) As cells initiate contact, BVES traffics to these celllular adhesions. (E) In a mature cell monolayer, BVES localizes to the cell membrane. This figure was reproduced with permission[30].

Loss of BVES is associated with mesenchymal-like phenotype

A hallmark of epithelial cells is their ability to associate through cell-cell adhesion into an organized epithelium functioning, collectively, as a tissue[45]. Within the epithelium, there is coordinated differentiation, proliferation, and cell motility. This functional interplay is on display when there is loss of cell-cell contact, leading to individual epithelial cells assuming a fibroblast-like or mesenchymal-like morphology, a phenotypic change termed epithelial-mesenchymal transition (EMT)[46]. In many tissues, upon regaining cell-cell contacts, cells can undergo the reverse process which is termed mesenchymal to epithelial transition (MET). Cellular adhesion complexes, including tight and adherens junctions are key regulators of these transitions, providing a means for cellular signaling in addition to mechanical adhesion. For example, the role of E-cadherin and the adherens junction as a modulator of canonical WNT signaling through sequestration of β-catenin at the cell membrane is well established[47]. Dysregulation of β-catenin is strongly linked to the EMT phenotype as β-catenin has been shown to bind directly to the ZEB1 promoter, a key inducer of EMT, and activate its transcription[48]. Similarly, tight junctions play a fundamental role in outside-in signaling cascades (reviewed by Severson and Parkos[49]). RhoA downregulation following epithelial cell confluency leads to reductions in proliferation, which is due in part to an interaction with guanine nucleotide exchange factor H1 (GEFH1) and the tight junction protein Cingulin. In a similar fashion, ZO-1 can modify gene expression programs and cell growth by sequestering ZONAB (a Y-box transcription factor) at the tight junction, leading to coordinated regulation of cytoskeletal and transcriptional programs and providing a link between junctional integrity and cell signaling programs[50,51].

As BVES displays a dynamic subcellular localization and influences epithelial junctions, it was proposed that BVES may aid in maintaining epithelial states similar to junctional proteins

such as E-cadherin. Using the human corneal epithelial cell line (HCE), Osler *et al.* observed that BVES knockdown impaired tight junction and adherens junction formation (as evidenced by disrupted membrane localization of β-catenin, E-cadherin, ZO-1, and occludn)[30]. This alteration in junctional complexes following BVES knockdown led to functionally significant reductions in transepithelial resistance (TER), a readout for barrier competency and junctional integrity of an epithelium[30]. Conversely, BVES overexpression in HCE cells increased TER. Furthermore, overexpression of lysine 272 and 273 BVES mutants, which prevents homodimerization and endogenous BVES from localizing to the cell membrane, confers HCE cells with a more fibroblastic morphology. Concomitant increase in expression of the mesenchymal cell marker, vimentin, and enhanced mobility and invasion were also observed, together supporting a transition from an epithelial to a more mesenchymal phenotype[36]. This change in cellular phenotype was bolstered by *in vivo* observation that *Bves*$^{-/-}$ mice have markedly impaired recovery of skeletal muscle following cardiotoxin mediated muscle injury[39]. Together, these reports suggested that BVES promoted epithelial states and that loss of BVES promoted mesenchymal phenotypes.

Further studies would begin to provide mechanistic insight into the role BVES plays in promoting epithelial phenotypes. A yeast-two-hybrid screen performed by Smith *et al.* identified an interaction between Guanine nucleotide exchange factor T (GEFT) and murine BVES that was mapped to the cytoplasmic BVES domain between amino acids 250-300[52]. GEFs function principally to promote the exchange of GDP for GTP and can subsequently activate Rho GTPases[24]. GEFT has been shown to activate Rac1 and Cdc42 and promote lamellipodia and filopodia formation during cell migration. Importantly, Rho GTPases contribute to tight junction composition and conversely, tight junctions are implicated in the regulation of Rho GTPases. For example, the RhoA activator GEF-H1 can be sequestered through an interaction with ZO-1 and the adaptor protein cingulin to reduce RhoA activation[24]. Alternatively, expression of a

constitutively active RhoA leads to alterations in tight junction localization with redistribution of occludn and ZO-1[53]. Accordingly, it was shown via PAK-21 (which binds specifically to GTP-bound Rac and Cdc42 proteins) pulldown that overexpression of the C-terminal domain (amino acids 118-358) of murine BVES in NIH 3T3 cells reduced the activation of Rac1 and Cdc42 without a change in RhoA activation. This change in GTPase signaling also reduced the motility and increased the roundness of NIH 3T3 cells[52]. The exact mechanism by which BVES altered activation of CDC42 and Rac1 was still unclear. An additional study by Russ *et al.* utilized WT chick BVES and a C-terminal truncation mutant to further probe BVES function[54]. Overexpression of BVES reduced RhoA activation but RhoA activity was significantly higher in cells expressing the truncated BVES, likely because the truncated-BVES mutant disrupted the function and localization of endogenous BVES. The authors next demonstrate that BVES interacts with and colocalizes with ZO-1 and that this association is dependent on the carboxy-terminus of BVES. Overexpression of BVES confined both ZO-1 and BVES to the cell membrane but mutant BVES overexpression resulted in primarily intracellular ZO-1 and occludn. Overall, these data establish a complex, context-dependent regulation of junctional composition by BVES.

Further studies employing a yeast-two-hybrid approach identified Vesicle-associated membrane protein 3 (VAMP3) as a BVES interacting protein[55]. VAMP3 is a SNARE protein family member involved in vesicular transport and facilitates recycling of transferrin and β-1-integrin[56]. Previous studies have demonstrated that VAMP3 knockdown by siRNA inhibited cell migration without a change in cell proliferation. VAMP3 silencing reduced β-1-integrin levels at the cell membrane but did not alter total cellular levels, implicating VAMP3 in membrane trafficking[57]. Loss of BVES phenocopied VAMP3 loss and established a role for BVES in vesicular transport. Together, these studies highlight additional roles for BVES in modulating GEF activity, cell migration, and the balance between epithelial and mesenchymal phenotypes.

Non-epithelial roles of BVES

While many studies have demonstrated a role for BVES in modulating epithelial states, additional studies have identified novel non-epithelial roles for BVES. A LacZ-Neo cassette inserted during the generation of the POPDC1 knockout mouse by Thomas Brand allowed for identification of BVES expression patterns in murine tissue[39]. Andree *et al* demonstrated detectable LacZ activity in the cardiogenic mesoderm that would ultimately give rise to the ventricles and saw labelling in myocytes but not in endocardial or epicardial cells, confirming the results of previous cDNA screens which demonstrated enrichment of BVES/POPDC1 in cardiac tissue[37]. Subsequently, Froese *et al.* identified an important role for BVES in regulating cardiac myocytes[58]. *Bves*$^{-/-}$ mice demonstrated severe stress-induced bradycardia which worsened with increasing age and was linked to alterations in sinus node structure. They went on to show that the Popeye domain contains a high affinity cyclic-nucleotide-binding domain, that BVES can directly bind cAMP, and that the interaction between BVES and the stretch-activated potassium channel, TREK-1, is modulated by cAMP. Mutating single amino acids (D200A, E203A, and V217F) modulated the affinity of the BVES-cAMP interaction. The authors further suggested that BVES may be affecting TREK-1 channel trafficking and recruitment to the membrane to enhance conduction current in a cAMP dependent fashion[58]. This report expanded the known roles of BVES and showed its regulatory importance in cardiac pacemaking as well as supported a model whereby BVES can alter trafficking and recruitment of membrane proteins. A subsequent report in 2016 by Schindler *et al.* identified a BVES missense variant (S201F) by whole-exome sequencing in a family of four with cardiac arrhythmias and limb-girdle muscular dystrophy (LGMD)[59]. Skeletal muscle biopsies from the affected patients showed impaired BVES membrane localization. The variant, which was within the cAMP binding domain, showed 50%

reduction in cAMP affinity *in vitro* and impaired TREK-1 recruitment to the membrane. Furthermore, this BVES mutant, expressed in zebrafish, phenocopied the heart and skeletal muscle defects observed in the family carrying the homozygous allele. Thus, these studies revealed the powerful clinical implications of disrupting BVES function and continued to expand its widening regulatory role in cardiac myocytes and skeletal muscle tissue.

The role and functional impact of a BVES:cAMP interaction in normal epithelium is unknown; however, Amunjela *et al.* have recently demonstrated that BVES can immunoprecipitate with cAMP in breast cancer lines. Further, cAMP increases BVES protein levels and may influence cell migration[60]. Importantly, cAMP plays a key role in junctional integrity. Treatment of primary HUVEC cells with cAMP derivatives improves tight junction continuity and decreases paracellular permeability[61]. In ovarian cancer cells, the cAMP-dependent protein kinase (PKA) can phosphorylate claudin-3. A mutation in claudin-3 at the PKA phosphorylation site which mimics constitutive phosphorylation impairs junctional assembly as reflected by reductions in TER[62]. Additional studies defining the BVES:cAMP and its contribution to junctional integrity in the epithelium will be required.

BVES as a tumor suppressor

Epithelial state changes, such as EMT, occur during differing stages of tumor development and growth. It is thought that tumor cells at the leading/invasive front tend to possess mesenchymal traits (hypermigratory, reduced differentiation, and hyperproliferation[63]). They also tend to be incapable of cell-cell contact mediated growth arrest[63]. Accordingly, loss of adhesion junction molecules has been associated with increased tumor invasiveness[64,65], and colorectal cancers that retain E-cadherin expression are associated with decreased invasiveness[66]. Similarly, tight

junction proteins are implicated in tumor biology with claudin family members being overexpressed in CRC, gastric cancer, and ovarian cancers[67,68]. However, claudin-1 has also demonstrated tumor suppressive effects in gastric tumors[69], suggesting context and tissue dependence or tumor type-specific function. Similarly, high expression of ZO-1 is a good prognostic indicator in non-small cell lung cancer[70] and decreased expression of ZO-1 in breast and colon cancer are correlated with progression[71,72]. Thus, although our understanding is still incomplete, dysregulation of tight junction and adherens junction components is a feature of malignancies.

Studies focusing on BVES have provided further evidence of junctional dysregulation in cancer. Williams *et al.* showed that BVES was underexpressed and mislocalized in CRC compared to normal tissue and also downregulated in breast cancer samples[41]. Restoring BVES expression utilizing a chick Bll lines promoted an epithelial morphology and decreased migration (LIM2405 cells) and invasion (LIM2405 and

PyVmT cells), cellular proliferation (LIM2405 cells), subcutaneous xenograft growth (LIM2405), and metastasis in a splenic injection model (SW620)[41]. Alternatively, disrupting BVES using a dominant negative C-terminal truncation mutant in the non-malignant HCE cells induced a mesenchymal morphology and increased cellular proliferation and migration. Together, these results support a role for BVES in regulating cell migration/EMT and CRC. Building on previous studies, the authors showed that BVES interacts with GEFH1 (a cytoplasmic RhoA activator) and reduced RhoA activation as well as downstream phosphorylation of the RhoA target myosin light chain (MLC). To this point, however, no studies had directly looked at how BVES loss modified tumorigenesis.

Parang *et al.* performed the first *in vivo* study identifying BVES as a tumor modifier[73]. Using injections of azoxymethane followed by repeated cycles of dextran sodium sulfate

(AOM/DSS), a well characterized model of inflammatory carcinogenesis[74-76], they showed that BVES loss increased inflammatory injury and tumor multiplicity and led to a higher degree of intratumoral dysplasia. These phenotypes were associated with increased intratumoral Wnt signaling. RNA sequencing analysis of *Bves*$^{-/-}$ tumors identified c-Myc signaling network activation and subsequent immunohistochemistry demonstrated increased c-Myc protein. The authors hypothesized that BVES may regulate cellular c-Myc levels. Indeed, overexpressing a variant of human BVES that lacked the first 72 amino acids (and was subsequently more readily expressed) increased the presence of ubiquitinated c-Myc and lead to an overall decrease in c-Myc protein levels. Conversely, knocking down BVES by siRNA increased c-Myc protein. Co-immunoprecipitation and proximity ligation assays (PLA) revealed that BVES associated with c-Myc. As c-Myc stability is regulated post-translationally, they hypothesized that BVES may interact with PPP2R5A (PR61α), a regulatory subunit of the serine-threonine protein phosphatase 2A (PP2A) heterotrimeric complex that dephosphorylates c-Myc and promotes c-Myc ubiquitylation. By yeast-two-hybrid, co-immunoprecipitation, and proximity ligation assay, they showed that BVES interacted with PR61α and mapped the BVES: PR61α interaction to between amino acids 330-345 in human BVES. Deletion of these 15 residues uncoupled the interaction, and expression of this C-terminal truncation BVES mutant failed to alter c-Myc levels. These data suggest that BVES likely requires PR61α to promote c-Myc degradation. This was a key study illustrating that BVES can regulate oncogenic signaling pathways. Interestingly, in inflammatory bowel disease, c-Myc has been postulated to contribute to colitis-associated cancer progression[77-79]. Together, this study continued to broaden the known regulatory roles of BVES, from cardiac and skeletal muscle maintenance to tumor progression. As PP2A dephosphorylates a number of other targets, many of which are implicated in tumorigenesis[80,81], determining whether BVES directs additional PP2A activity may elucidate

novel regulatory roles. For instance, PP2A has been shown to dephosphorylate tight junction proteins such as ZO-1, occludin, and claudin-1 leading to increased paracellular permeability[82].

While several studies have demonstrated that BVES has an important role in intestinal malignancy, additional work implicates BVES in hepatocellular and breast cancer[60,83-85]. The tissue-specific functions of BVES in regulating tumorigenesis remain unclear, especially *in vivo*, but the recent literature strongly suggests BVES acts as a tumor suppressor in a variety of epithelial tissues, likely, at least in part, due to its role in promoting c-Myc degradation. The majority of phenotypes associated with BVES loss require cellular or physiologic stress, suggesting that under homeostasis, BVES loss has minimal deleterious effects. This may be due, in part, to physiologic redundancy via compensation by other POPEYE domain containing proteins such as POPDC2 and POPDC3.

BVES and its stem cell role

Numerous studies support the concept that BVES coordinately regulates multiple intracellular signaling pathways and that its expression helps in maintaining an epithelial phenotype. Furthermore, studies have supported the concept that BVES may regulate Wnt signaling which is inextricably tied to intestinal homeostasis, stem cell maintenance, and tumorigenesis[86,87]. Initial evidence of a link between BVES and Wnt signaling was provided in 2011 when Williams *et al.* showed that chick BVES overexpression attenuated TopFlash activity in HEK293 cells following inhibition of GSK3β with lithium chloride. Similarly, reductions in Wnt reporter activity were observed in LIM2405 cells stably overexpressing chick BVES. Notably, overexpression of a dominant negative chick BVES in HCE cells also lead to a redistribution of β–catenin away from the plasma membrane with concomitant increases in

cytoplasmic and nuclear β–catenin, indicative of higher levels of Wnt tone[41]. Further evidence for Wnt modulation by BVES was provided upon analysis of the AOM/DSS induced tumors in *Bves*$^{-/-}$ mice. *Bves*$^{-/-}$ tumors had an increased β–catenin staining index and upregulation of Wnt target genes by RNA-sequencing[73]. In further support of this paradigm, *Bves*$^{-/-}$ mice have increased intestinal proliferation at baseline in both the small intestine[88] and colon[89]. When *Bves*$^{-/-}$ mice were crossed with the *Lgr5-eGFP-IRES-creERT2* intestinal stem cell reporter mouse, there was an expansion of the stem cell compartment and an increase in the number of Lgr5+ stem cells in comparison to WT mice. Consistent with loss of BVES promoting "stemness," enteroid cultures derived from *Bves*$^{-/-}$ mice had a higher plating efficiency and increased stem-cell markers such as Axin2, CD44, and Cyclin-D1 by qRT-PCR[88]. The precise molecular mechanism underlying why *Bves*$^{-/-}$ mice have an expanded stem cell compartment and how, mechanistically, BVES is regulating Wnt signaling remains unknown which provided the rationale and laid the foundation for the studies presented in Chapter 3 of this dissertation.

CHAPTER II

PROTEIN PHOSPHATASE 2A IN THE REGULATION OF WNT SIGNALING, STEM CELLS, AND CANCER

Rationale

Given that prior yeast-two-hybrid screens identified interactions between BVES and multiple members of the PP2A family, and that previous studies have implicated BVES in the regulation of Wnt signaling, further understanding the complex interplay between protein phosphatases and the Wnt pathway as they pertain to human disease may elucidate novel mechanism by which BVES regulates Wnt signaling.

Introduction

Protein phosphorylation is an essential regulator of many cellular processes including metabolism, transcription, proliferation, cell motility, and apoptosis. Nearly 30% of all human proteins are covalently bound to a phosphate, a feat made possible by the 500+ different protein kinases encoded by the human genome[90]. Protein phosphatases make these modifications reversible, and the serine-threonine protein phosphatase 2A (PP2A) accounts for 30-50% of these protein dephosphorylation events[80,91]. PP2A is a heterotrimeric protein complex consisting of a structural (A), regulatory (B), and catalytic subunit (C)[92]. There exist two unique scaffolding isoforms, Aα and Aβ, two unique catalytic subunit isoforms, Cα and Cβ, and four structurally diverse families of regulatory (B) subunits that are referred to by a variety of naming conventions:

B (or PR55), B’ (PR56/61), B” (PR72/130), and B’” (PR93/110). As shown in Figure 5, Greek letters further identify individual regulatory subunit isoforms of the B and B’ family. These subunits determine the substrate specificity and subcellular localization of PP2A heterotrimers[91,93]. The precision with which PP2A regulatory subunits target individual phospho-residues was established by early studies on the phosphorylation of SV40 large T antigen. A holoenzyme with a B/PR55 family regulatory subunit dephosphorylates Thr124 of the SV40 large T antigen while a PP2A complex with the B”/PR72 regulatory subunit dephosphorylates Ser120 and Ser123[94]. The targeting specificity of the regulatory subunits allows a small pool of protein phosphatases to regulate numerous phosphoproteins with enhanced precision[92]. While individual regulatory subunits provide precision, the diversity of subunits also allows for the regulation of a variety of substrates.

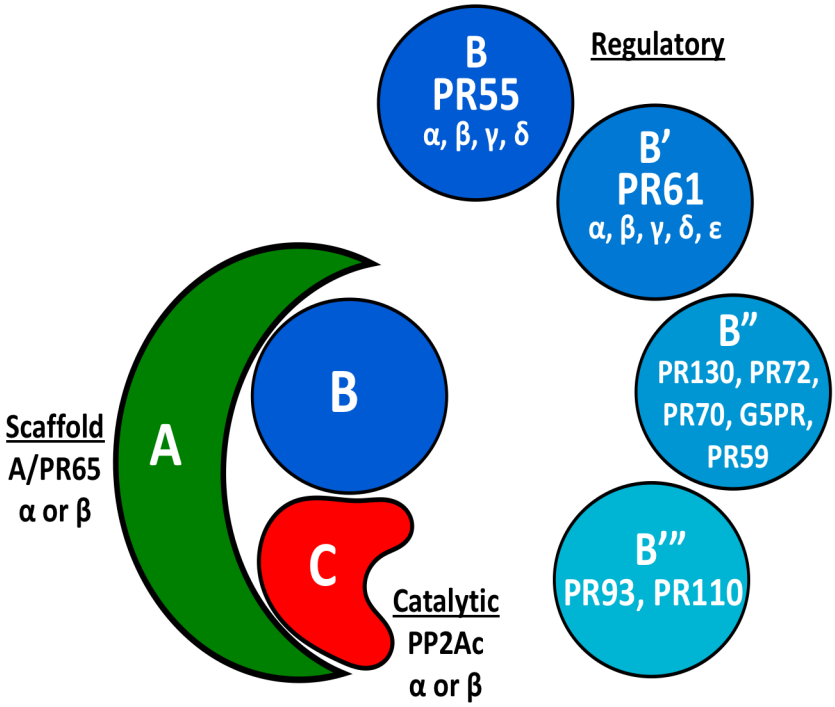

Figure 5. PP2A Holoenzyme. The PP2A holoenzyme consists of a scaffolding (A), regulatory (B), and catalytic subunit (C). There are two unique scaffolding subunits, PP2A Aα and PP2A Aβ, and two unique catalytic subunits, PP2Acα and PP2Acβ. The regulatory (B) subunits consist of four diverse families: B or PR55, B' or PR56/PR61, B", and B'". Within the B and B' regulatory subunit families are multiple isoforms, denoted using Greek letters. A number scheme using approximate molecular weights (i.e. PR55 or PR56) is also commonly utilized for referencing PP2A subunits.

Wnt signaling is known to regulate patterning and cell fate decisions during embryonic development and has been implicated in the pathogenesis of cancer[95]. Over 90% of colorectal carcinomas have alterations in Wnt signaling; mutations in the APC tumor suppressor or activating mutations in β-catenin account for ~80% of cases[96]. The key effector of canonical Wnt signaling, β-catenin, is tightly regulated within the cell predominantly through two distinct complexes: the adherens junction complex and the β-catenin destruction complex (Figure 6). The adherens junction helps initiate and stabilize cell-cell adhesion by coupling the transmembrane glycoprotein E-cadherin and associated cytoplasmic catenins with the actin cytoskeleton[97]. E-cadherin can recruit β-catenin to the cell membrane, thereby preventing its nuclear localization[47] in a cell-cell contact dependent fashion[98]. Cytoplasmic pools of β-catenin are also regulated through the β-catenin destruction complex. In the absence of Wnt ligand stimulation, the cytoplasmic β-catenin destruction complex (composed of the scaffolding proteins Axin and APC and the protein kinases GSK3 and CK1α) binds and phosphorylates β-catenin. This leads to its ubiquitinylation by the β-TrCP ubiquitin ligase and subsequent proteasomal degradation. CK1α phosphorylation of Ser45 on β-catenin primes the protein for subsequent phosphorylation by GSK3 at Ser33, Ser37, and Thr41 which are required for β-TrCP recognition and β-catenin ubiquitination[99]. In the presence of Wnt ligand, such as Wnt3a, Axin is sequestered at the membrane which prevents assembly of the destruction complex, stabilizes β-catenin[100,101], and allows its translocation to the nucleus for transcription of TCF/β-catenin target genes. Many components of the Wnt pathway can be modified via phosphorylation: the G protein-coupled Wnt receptor Frizzled[102], the Frizzled binding protein Dishevelled[103], the Frizzled co-receptor low density lipoprotein receptor-related protein-6 (LRP6), components of the β-catenin destruction complex (APC[104,105], Axin[106,107], CK1[108,109], and GSK3[110,111]) and β-catenin[99] (Figure 6). Determining

the Wnt components targeted by PP2A may identify novel regulatory mechanisms and opportunities for therapeutic intervention.

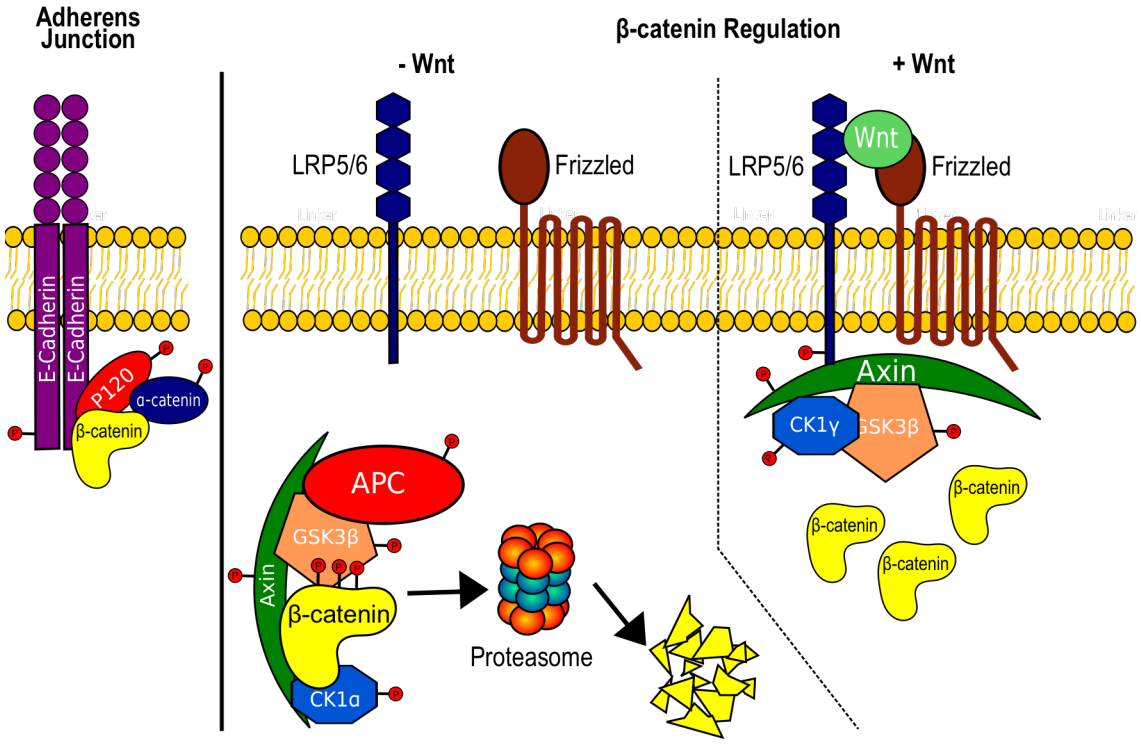

Figure 6. Phosphorylatable Proteins Involved in the Regulation of β-catenin. Left: The adherens junction, consisting of E-cadherin, P120, and the catenins sequesters β-catenin at the plasma membrane. Phosphorylation of E-cadherin at Ser834, Ser836, and Ser842 enhances β-catenin binding affinity while phosphorylation at Ser846 reduces β-catenin binding. Middle: In the absence of Wnt stimulation, β-catenin is bound to the β-catenin destruction complex. CK1α phosphorylation of β-catenin at Ser45 primes β-catenin for subsequent phosphorylation by GSK3β at Ser33, Ser37, and Thr41 which targets β-catenin for proteasomal degradation. Phosphorylation of Axin improves its stability and subsequent ability to negatively regulate Wnt signaling. Axin and APC also contain phosphorylation sites that improve binding to β-catenin. Right: In the presence of Wnt ligand, CK1γ phosphorylates LRP5/6, which sequesters Axin at the plasma membrane and prevents the destruction complex from phosphorylating β-catenin.

A tumor suppressive role for PP2A

Early studies using okadaic acid, a serine-threonine phosphatase inhibitor that targets the catalytic PP2Ac subunit, increased tumor formation in a cutaneous carcinogenesis challenge and provided early biochemical support for a tumor suppressive role of PP2A[112,113]. However, this model may suffer from off-target effects as PP2A is inhibited at low doses of okadaic acid[114,115], but increasing concentrations can inhibit multiple protein phosphatases[116]. Subsequent work has more specifically identified a role for PP2A in tumor suppression. The SV40 small T antigen, the gene product of two transforming DNA viruses, SV40 and polyoma virus, was found to interact with PP2A A and C subunits through co-immunoprecipitation experiments, likely inhibiting PP2A function through displacement of the regulatory subunits[117,118]. Human embryonic kidney cells expressing the catalytic subunit of telomerase, a G12V mutant H-ras, and the SV40 large T antigen (which inactivates the retinoblastoma (RB) and p53 tumor suppressors[119]), otherwise known as HEK TER cells, are immortalized but not tumorigenic (i.e. they lack anchorage independent growth in soft agar and cannot form tumors in immunocompromised mice[120,121]). However, addition of small T antigen, which interferes with PP2A function, imparts cells with anchorage independent growth and the ability to grow as subcutaneous xenografts[121]. Chen *et al.* determined that this phenotype partially depended upon the B' regulatory subunit PR61γ-isoform 3 (PR61γ3) as siRNA knockdown of PR61γ3 increased cell proliferation and conferred cells with the ability to grow in soft agar and form tumors in nude mice. Furthermore, overexpression of the regulatory subunit rescued the phenotype, partially reversing tumorigenicity in HEK TER cells as well as human lung cancer cell lines[122]. However, the HEK TER cells with PR61γ3 knockdown formed fewer tumors than HEK TER cells expressing small T antigen, suggesting additional tumor promoting effects of small T antigen aside from just

preventing PR61γ3 from incorporating into the PP2A complex. Finally, knockdown of the PP2A Aα scaffolding subunit activates AKT signaling and imparts tumorigenicity to HEK TER cells in immunocompromised mice[123].

Clinical evidence further supports a role for PP2A in tumor suppression. Cancer-associated mutations in the PP2A Aα scaffolding subunit impair binding to specific B subunits as well as the catalytic Cα subunit[124]. Mutations in PP2A Aα appear to act in a dominant negative fashion on wild-type Aα and also decrease B and C subunit stability, suggesting that an intact PP2A complex stabilizes individual holoenzyme subunits[123]. Additionally, mutations in the PP2A Aβ subunit have been found in human colon cancer, lung cancer, and breast cancer specimens. A list of reported mutations is reviewed in[81]. While the majority of these mutations appear to affect binding of subunits and holoenzyme formation[124], the functional consequences on Wnt signaling have yet to be determined. Clinically, the PP2A inhibitor SET is increased in human non-small cell lung cancer and leads to poorer overall survival rates, further supporting a tumor suppressive role for PP2A[125]. Additional endogenous inhibitors of PP2A, such as I_1^{PP2A} (PHAP), may also be clinically relevant; however, additional studies in cancer are needed[126,127]. Reciprocally, small molecule activators of PP2A (SMAPs) provide a promising avenue for tumor suppression via augmenting PP2A function. KRAS-mutant lung cancer cell lines and xenografts treated with SMAPs lead to inhibition of tumor growth and apoptosis with reductions in phosphorylated ERK[128]. The PP2A-activating drug FTY720 has also shown promising results in multiple hematologic malignancies[129-131]. It is unclear how effective these activators will be in the context of cancers harboring mutations in PP2A and given PP2A's dual role in regulating Wnt signaling, these activators may too have dichotomous effects.

PP2A regulation of E-Cadherin and β-catenin at the membrane

Two PP2A catalytic subunits, cα and cβ, share 97% sequence homology[132] yet mice lacking cα die at embryonic day 6.5, demonstrating that cβ cannot compensate for loss of cα[133]. cβ localizes to the cytoplasm and nucleus while cα is predominantly present at the plasma membrane[134,135]. Thus, subcellular localization may prevent cβ from compensating for loss of cα. Furthermore, β-catenin colocalizes with cα at the plasma membrane in the inner cell mass of early mouse embryos, and loss of cα results in E-cadherin and β-catenin redistribution to the cytoplasm[135]. Destabilization of membrane bound β-catenin reduces β-catenin levels, likely due to the action of a functional β-catenin destruction complex. While this leads to reductions in total cellular β-catenin levels, the remaining β-catenin is no longer sequestered at the membrane and thus free to translocate to the nucleus and induce transcription of β-catenin target genes[47]. Presumably, this makes the cells more responsive to Wnt stimulation. A similar phenomenon is observed in RKO cells which have a mutation in E-cadherin and low levels of cytoplasmic β-catenin[136] but are exquisitely sensitive to Wnt ligand. In a more recent study, Su *et al.* demonstrate that PP2Acα knockdown similarly leads to dramatic reductions in membrane associated and total levels of both β-catenin and E-cadherin in HT29, SW480, DLD1, and HEK293 cell lines[137].

The question of how PP2Acα loss alters E-cadherin localization remains unsolved but E-cadherin is highly phosphorylated within a serine enriched domain that comprises the β-catenin binding domain[138]. Phosphorylation of serine residues Ser834, Ser836, and Ser842 enhance β-catenin binding affinity over 300-fold [139,140]. Conversely, CK1 mediated phosphorylation of E-cadherin at Ser846 reduces β-catenin binding and leads to increased E-cadherin internalization[141]. It is plausible that a PP2A complex with a yet to be defined regulatory subunit

may specifically dephosphorylate Ser846 on E-cadherin and that loss of PP2Acα abrogates this interaction leading to reduced β-catenin binding and E-cadherin internalization.

PP2A's dual regulation of cytoplasmic Wnt signaling

Negative regulation of Wnt signaling

PP2A is unlikely to exert its Wnt-inhibitory effects through direct dephosphorylation of β-catenin as β-catenin dephosphorylation at Ser33, Ser37, and Thr41 removes β-TrCP recognition sites and subsequently stabilizes the protein[99]. Consequently, studies have focused on how PP2A affects other proteins involved in β-catenin regulation. Yokoyama *et al.* demonstrate PP2A inhibition via treatment with okadaic acid, knockdown of the PP2Ac catalytic subunit, or treatment with SV40 ST antigen potentiates Wnt signaling following Wnt3a stimulation. Furthermore, all three modifications lead to increases in phosphorylated-GSK3β[142]. Phosphorylation of GSK3β at Ser9 suppresses GSK3β kinase activity[110,111], and PP2A treatment can reverse this kinase activity in vitro[143]. Mitra *et al.* confirm this finding and show that PP2A mediated dephosphorylation of GSK3β occurs through recruitment of two heatshock proteins, DNAJB6 and HSPA8 (heat-shock cognate protein, HSC70) [144]. An intriguing report focusing specifically on PP2Acα knockout in cardiomyocytes may further elucidate tissue specific roles of individual PP2Ac isoforms[145]. These data support a potential role for PP2A in dephosphorylating, and thereby activating, GSK3β with resultant phosphorylation of β-catenin leading to its destruction.

Treatment with ST antigen potentiates Wnt signaling and also disrupts regulatory (B) subunit binding to the holoenzyme[116], suggesting that these regulatory subunits aid in inhibiting Wnt signaling. Seeling *et al.* show that overexpression of the B' regulatory subunits PR61α, PR61β, PR61δ, PR61ε, and PR61γ3 all decrease exogenous β-catenin in HEK293 cells[146],

although an effect on endogenous β-catenin was not evaluated. This decrease in β-catenin was inhibited with okadaic acid treatment, a non-degradable β-catenin mutant that lacks the GSK3β phosphorylation sites, and with proteasomal inhibition, which taken together suggests that PR61-dependent decreases in β-catenin are due to alterations in phosphorylation-induced proteasomal degradation or impaired targeting of β-catenin through the proteasomal degradation pathway. A yeast two-hybrid screen also identified that the PR61α and PR61δ subunits interact with the N-terminal third of APC (unpublished data referenced in [146]) which brings the subunits in close proximity to phospho-residues on Axin, APC, and GSK3β. Overexpression of PR61α in the colorectal cancer HCA7 cell line (wild-type APC) but not the SW480 cell line (APC truncation at 1338) recapitulates the decreases in β-catenin observed in HEK293 cells. These data suggest that PR61α promotes β-catenin degradation through an APC dependent signaling complex.

Axis duplication experiments in Xenopus embryos reveal that the PP2A A, PP2Ac, and B' PR61α regulatory subunit all have ventralizing activity, indicating Wnt inhibition. In Xenopus, β-catenin levels are higher dorsally than ventrally and higher Wnt tone leads to dorsalization/secondary axis formation[147]. Ventral injection of Wnt agonists leads to secondary body axis formation. To determine where in the Wnt pathway the PP2A regulatory subunits are inhibiting Wnt signaling, epistasis studies using lithium chloride (a GSK3β inhibitor that leads to dorsalization), dominant-negative Axin, and degradation resistant β-catenin, provide evidence that PR61α acts downstream of GSK3β and Axin but upstream of β-catenin to negatively regulate Wnt signaling. Furthermore, PP2A A, PP2Ac, and PR61α co-immunoprecipitate with Axin in Xenopus egg extracts, supporting a role for PP2A as a component of the β-catenin degradation complex[148]. Adding to the complexity, another group shortly thereafter demonstrated that two additional B' family regulatory subunits (PR61β and PR61γ) directly interact with Axin in COS cells. PR61β expression reduces Wnt reporter activity but did not decrease endogenous β-catenin

levels in wild-type L cells, suggesting that PR61β inhibits Wnt signaling through a mechanism independent of β-catenin stability[149]. Taken together, these data highlight the ability of various PP2A components and specifically the regulatory subunits to negatively regulate Wnt signaling at multiple levels.

Positive regulation of Wnt signaling

For every piece of evidence that PP2A negatively regulates Wnt signaling, there is evidence to the contrary. Teleological thinking would support a positive role for PP2A in regulating Wnt signaling as dephosphorylation of the main effector, β-catenin, increases its abundance[99]. Accordingly, Zhang *et al.* were the first to show that a B family regulatory subunit, PR55α, can interact with β-catenin[150]. Knockdown of PR55α increases β-catenin phosphorylation at Ser33, Ser37, and Thr41 (required for β-TrCP recognition and ubiquitination) in SW480 cells and also decreases β-catenin levels in HEK293 cells. PR55α overexpression increases Wnt reporter activity in HEK293T cells. Interestingly, phosphorylation of Ser675 (promotes β-catenin stability[151]) and Ser552 (causes β-catenin dissociation from cell-cell contacts and cytosolic/nuclear accumulation[152]) were also increased in SW480 cells with PR55α knockdown. While increased β-catenin stability due to reduced phosphorylation at Ser33, Ser37, and Thr41 appear to trump any effects of Ser675 and Ser552 phosphorylation, the dichotomy highlights the complexity of Wnt phosphorylation and the need for precise phosphatase activity. Hein *et al.* demonstrated similar results in CD-18/HPAF pancreatic cancer cells where knockdown of PR55α increased phosphorylation of β-catenin at Ser33, Ser37, and Thr41, destabilized the protein and reduced total levels of β-catenin. PR55α was increased in human pancreatic ductal adenocarcinoma tissue when compared to normal pancreatic tissue, suggesting that its elevated expression may maintain Wnt signaling and other oncogenic signaling cascades[153].

The scaffolding protein APC is also a putative target of PP2A dephosphorylation and subsequent Wnt activation as GSK3 phosphorylation of APC improves its ability to bind β-catenin[104,105]. A number of theories exist as to how APC regulates β-catenin levels. APC may promote export of nuclear β-catenin[154,155] or it may simply sequester β-catenin in the cytoplasm and prevent association with TCF4 in the nucleus[156]. The observation that APC truncations in human colorectal cancers increase total β-catenin levels suggests that APC has a direct role in β-catenin degradation. Su *et al.* support this hypothesis with evidence that WT APC "protects" phosphorylated β-catenin from dephosphorylation by a PP2AAα/PP2Acα dimer, which ensures that the β-TrCP ubiquitin ligase binding site remains intact[137]. This PP2AAα/PP2Acα dimer stabilizes β-catenin by dephosphorylating Ser33 and Ser37, thereby removing the β-TrCP ubiquitin ligase binding site. Mutations in APC abrogate this protective mechanism and allow the PP2AAα/PP2Acα dimer to dephosphorylate β-catenin, shunting it away from the ubiquitination pathway. It should be noted that the PP2Aα/PP2Acα complex identified in this study was isolated from bovine cardiac muscle and utilized in a cell-free system which may limit in vivo correlation. This study does, however, highlight the potentially promiscuous nature of PP2A in the absence of a regulatory subunit.

The scaffolding protein Axin has binding sites for both GSK3β and β-catenin and acts as a negative regulator of Wnt signaling by promoting β-catenin phosphorylation. Axin phosphorylation within the β-catenin binding domain increases binding to β-catenin, stabilizing Axin and increasing β-catenin degradation[107]. Using a combination of yeast-two hybrid screening and co-immunoprecipitation, Hsu *et al.* showed that Axin can bind directly to the PP2Ac catalytic subunit and mapped this interaction between amino acids 632 and 836 of Axin. Interestingly, this PP2AC-Axin binding domain is in close proximity to both the GSK3β binding domain (amino acids 477-561) and β-catenin binding domain (amino acids 561 – 630)[157], again

placing phosphatase activity within proximity of putative phosphorylation targets. Using a Wnt reporter assay, Strovel *et al.* showed that PP2Ac overexpression activates Wnt signaling and that PP2A likely mediates these effects through dephosphorylation of Axin, but the exact target of PP2Ac dephosphorylation has not been determined[158]. Taken together, these data suggest that PP2Ac mediated dephosphorylation of Axin activates the Wnt pathway.

PP2A regulation of stem cells and self-renewal

A role for Wnt signaling in the control of stem cells and cancer stem cells has been well established and previously reviewed ([100,159-162]), and the literature reviewed above supports an indirect role for PP2A in regulating stem cells through its modulation of Wnt signaling, yet few studies have looked at Wnt independent regulation of stemness and self-renewal by PP2A. Wang *et al.* show that PP2A mediates the equilibrium between self-renewal and differentiation of neural stem cells predominately through regulation of asymmetric division of neural stem cells [163]. Additionally, human embryonic stem cell (hESC) self-renewal has been linked to PP2A activity as forced expression of PP2A reduced levels of SSEA-4, a marker of undifferentiated hESCs [164]. Accordingly, inactivating PP2A via treatment with okadaic acid maintained hESC even in the absence of basic fibroblast growth factor (bFGF), a key factor known to maintain hESCs [165]. Mechanistically, PP2A inhibition leads to increased phosphorylation of AKT, GSK3β, and Ser62-c-Myc with reduced levels of Thr58-phosphorylated c-Myc [164]. Phosphorylation of c-Myc at these two key residues, Thr58 and Ser62, differentially affect c-Myc stability. Phosphorylation at Ser62 stabilizes c-Myc while phosphorylation on Thr58 signals c-Myc for degradation [166]. PR61α directs PP2A to c-Myc doubly phosphorylated at Thr58/Ser62 and dephosphorylates Ser62 thereby increases levels of phospho-Thr58 c-Myc. This shift in phosphorylation status signals c-

Myc to be degraded by the proteasome [166]. A recent study by Janghorban *et al.* utilizing a PP2A-PR61α hypomorph mouse with very low levels of PR61α demonstrated hyperproliferation of the epidermis, hair follicles, and sebaceous glands with increases levels of c-Myc phosphorylation at Ser62. Furthermore, PR61α deficiency increased the number of BrdU long-term label retaining skin stem cells in these mice and enhanced keratinocyte colony formation [167]. Additional studies have indicated c-Myc, a known Wnt target gene[168], as a regulator of stem cell self-renewal [169,170], highlighting the interplay and complexity of Wnt, c-Myc, and phosphatase signaling. Together, these data support a role for PP2A-PR61α mediated regulation of stem cell self-renewal and proliferation which may in large part be driven via PP2A mediated c-Myc de-phosphorylation and subsequent stabilization.

Conclusion

Protein dephosphorylation is a complex and nuanced process and the PP2A family of serine-threonine phosphatases play an important role in regulating multiple signaling pathways implicated in tumorigenesis, stem cell maintenance, and self-renewal. Early studies of PP2A inhibitors and genomic studies identifying mutations in PP2A subunits support its tumor suppressive role. While perturbations in Wnt signaling can help initiate a number of human malignancies, Wnt signaling is also critical for maintenance of normal tissue and stem cell homeostasis in the non-transformed state. Ample data supports a role for PP2A as a negative regulator of Wnt signaling; however, there is similarly strong data supporting PP2A's role in potentiating Wnt signaling. PP2A mediated regulation of Wnt signaling is likely cellular context specific and care must be taken to control for these variables. Given the specificity with which each regulatory subunit targets PP2A mediated dephosphorylation, future studies must continue to

identify how individual trimeric complexes function in regulating a target of interest – referring simply to PP2A provides scant biological relevance. Knockdown and overexpression studies must consider compensatory mechanisms given the high similarity, yet extreme specificity, of individual regulatory subunits and the numerous levels at which they appear to modulate Wnt signaling. Taken together, the PP2A family of serine/threonine phosphatases regulate Wnt signaling and stemness at multiple levels, both positively and negatively, and further understanding of this complex dynamic will aid in identifying key regulators of tumorigenesis and normal tissue homeostasis.

CHAPTER III

BVES REDUCES LRP6 RECEPTOR LEVELS TO MODULATE WNT SIGNALING AND INTESTINAL TUMORIGENESIS

Rationale

Previous reports have implicated BVES in the regulation of Wnt signaling and intestinal stem cells, however the mechanism underlying these BVES-dependent phenotypes is largely unknown. Therefore, the following studies seek to mechanistically address how BVES regulates Wnt signaling and its implications for intestinal tumorigenesis.

Introduction

Colorectal cancer (CRC) is the third most common cancer in men and the second most common cancer in women worldwide. In the United States, CRC is the second leading cause of cancer-related deaths[171,172]. Over 90% of CRC tumors exhibit disruptions in the Wnt signaling pathway with inactivating mutations in the tumor suppressor adenomatous polyposis coli (*APC*) or activating mutations in β-catenin present in ~80% of cases[96]. β-catenin is the key effector of canonical Wnt signaling, and cytoplasmic β-catenin is maintained at low levels via a destruction complex composed of the scaffolding proteins AXIN and APC and the protein kinases glycogen synthase kinase 3 (GSK3) and casein kinase 1 alpha (CK1α)[100]. CK1α phosphorylates β-catenin, priming it for subsequent phosphorylation by GSK3, which allows for recognition by the

β-transducin repeats-containing protein (β-TrCP) ubiquitin ligase and subsequent proteasomal degradation[99,173].

LRP6 is a Wnt co-receptor that, in the presence of ligand, complexes with the seven-transmembrane-domain receptor Frizzled (FZ) and the scaffold protein Dishevelled (DVL) [174,175]. LRP6 is ultimately phosphorylated by GSK3β and CK1α at multiple sites including Thr1479, Ser1490, and Thr1493 upon stimulation, which effectively recruits AXIN to the membrane, preventing the activity of the β-catenin destruction complex and allowing β-catenin to translocate to the nucleus to mediate TCF/β-catenin target gene transcription[176]. *AXIN2* is one such Wnt target gene and functions in a negative feedback loop to degrade β-catenin and attenuate Wnt signaling[177]. Given the dependence of CRC on hyperactive Wnt signaling, identifying novel regulators of this pathway will be essential to the development of targeted therapeutic strategies.

Blood vessel epicardial substance (BVES or POPDC1) is a tight junction-associated adhesion molecule that was isolated in a cDNA screen of the developing heart[37]. It is proposed that BVES promotes epithelial junctional competence and can set epithelial-mesenchymal states via sensing of cell-cell contacts. The *BVES* promoter is frequently hypermethylated in malignancy leading to its reduced expression[41]. Accordingly, *BVES* loss is observed in all stages of CRC, including in premalignant adenomas with APC loss, suggesting that its suppression may contribute to tumor initiation[41]. Restoring BVES in CRC cell lines results in attenuated growth, migration, and invasion[41] and BVES interacts with a protein phosphatase 2A (PP2A) regulatory subunit to reduce c-Myc protein levels[73]. Furthermore, in the inflammation-driven azoxymethane/dextran sodium sulfate (AOM/DSS) carcinogenesis model, tumors from *Bves*$^{-/-}$ mice displayed increased cytoplasmic and nuclear β-catenin staining[73]. RNA-sequencing analysis of these tumors also indicated hyperactive Wnt signaling networks[73]. Small intestinal crypts isolated from *Bves*$^{-/-}$

mice and grown in 3D-Matrigel™ cultures as enteroids displayed increases in plating efficiency and in the ratio of stem spheroids, a morphology associated with hyperactive Wnt signaling[88]. Importantly, *Bves*$^{-/-}$ enteroids are also hyper-responsive to Wnt activation upon Wnt3a stimulation[88]. Taken together, these data suggest that BVES may tune cellular responses to Wnt and growth factor signaling, however the mechanisms by which BVES influences Wnt signaling are unknown.

Given the baseline and Wnt-dependent phenotypes associated with BVES loss, we hypothesized that BVES may regulate Wnt signaling in a ligand-independent fashion that is enhanced upon ligand stimulation. We observed that *BVES* knockdown utilizing multiple approaches indeed increases Wnt pathway activation and β-catenin levels at baseline and coordinated with Wnt3a stimulation to further enhance Wnt signaling. Furthermore, BVES interacts with the Wnt co-receptor LRP6, and BVES loss increases LRP6 receptor levels and activation. Adenoma tumoroids isolated from a Wnt-driven genetic mouse model and human samples derived from normal colon also demonstrated increased LRP6 receptor levels and receptor activation, suggesting that BVES loss may aid in the transition from premalignant to malignant lesions by augmenting Wnt signaling. Finally, loss of BVES increased tumor multiplicity and dysplasia in two separate mouse models of colon tumorigenesis. Together, these results implicate BVES in the regulation of Wnt signaling through modulating LRP6 receptor levels and confirm its role as a tumor suppressor by inhibiting Wnt ligand-independent signaling cascades.

Results

BVES knockdown increases Wnt pathway activation

Previous reports have associated BVES loss with Wnt pathway activation, but the mechanisms by which this occurred were unclear[41,73,88]. In order to elucidate these mechanisms, we first turned to *in vitro* systems using HEK293 cells stably expressing the SuperTopFlash Wnt reporter (293STF)[178]. 293STF cells respond to canonical Wnt signaling and are a sensitive tool to determine the impact of BVES on Wnt pathway activation. *BVES* knockdown in these cells using a lentivirally delivered shRNA yielded a 90% reduction in BVES transcript and increased Wnt reporter activity at both baseline and following stimulation with Wnt3a conditioned media (Figure 7A, 15.6 ± 0.1 vs. 108.1 ± 1.1-fold activation over unstimulated control, $P < 0.0001$ and Figure 8A). A concomitant increase in the expression of the Wnt target gene *AXIN2* was also observed (Figure 7B). As β-catenin is the key effector of Wnt pathway activity, we next tested whether *BVES* knockdown increased β-catenin protein levels. Indeed, cytoplasmic fractionation followed by immunoblotting demonstrated increased β-catenin protein levels (Figure 7C). Pooled siRNAs targeting *BVES* also increased Wnt reporter activity and Wnt target gene expression both at baseline and following Wnt stimulation (Figure 7D and Figure 7E). Increases in β-catenin protein levels following *BVES* knockdown and cytoplasmic fractionation were also observed (Figure 7F). Similar results were obtained using individual siRNAs (Figure 8B and Figure 8C) and utilizing the HCT116 CRC cell line (Figure 9A-C). Together, these results support a role for BVES in modulating Wnt pathway activation through regulating cytoplasmic β-catenin protein levels.

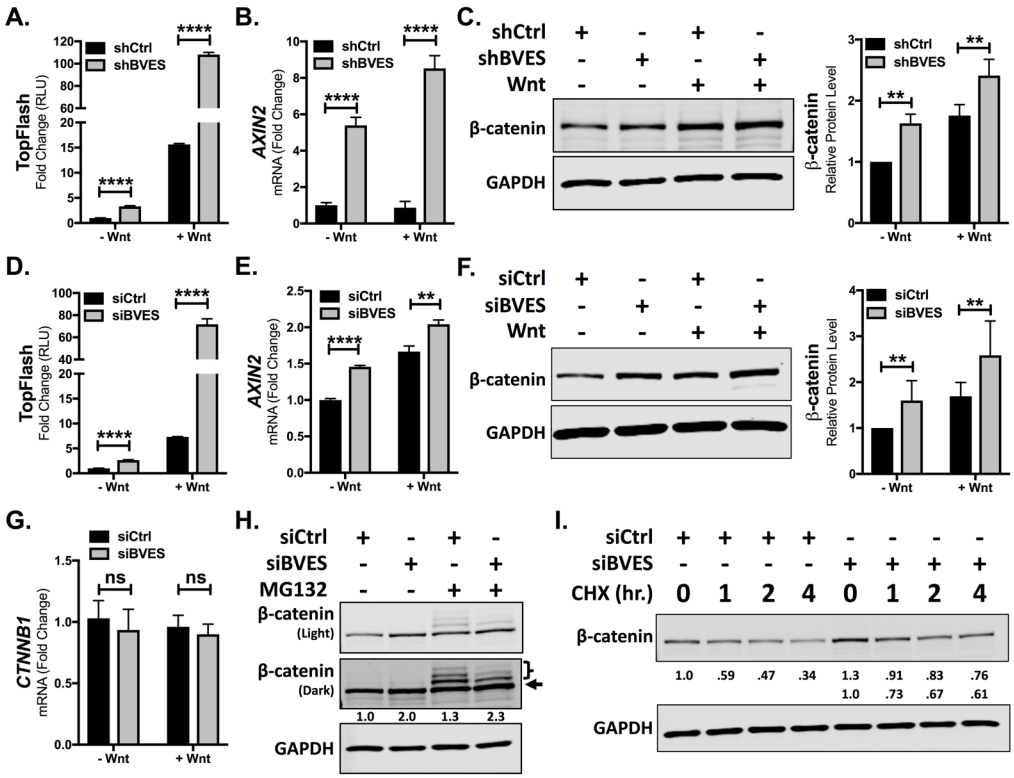

Figure 7. BVES loss increases Wnt signaling and β-catenin protein levels. (A) TopFlash activity in 293STF cells following *BVES* shRNA knockdown. (B) *AXIN2* fold change by qRT-PCR in 293STF cells with *BVES* shRNA knockdown. Cells were treated with 50% L-cell-conditioned media or 50% Wnt3a-conditioned media for 16 hours before isolation. (C) Cytoplasmic fractions of 293STF cells following shRNA knockdown of *BVES*. Cells were treated with 50% Wnt3a-conditioned media for 2 hours before harvest. (D) TopFlash activity in 293STF cells following siRNA knockdown. (E) *AXIN2* fold change by qRT-PCR in 293STF cells with siRNA knockdown. Cells were treated with 50% L-cell- or 50% Wnt3a-conditioned media for 16 hours before isolation. (F) Cytoplasmic fractions of 293STF cells following siRNA knockdown of *BVES*. Cells were treated with 50% Wnt3a-conditioned media for 2 hours before harvest. (G) β-catenin (*CTNNB1*) transcript levels in 293STF cells 56-72 hours following *BVES* siRNA knockdown. (H) 293STF cells were treated with 20 μM MG132 for 4 hours followed by cytoplasmic fractionation. Black arrow indicates β-catenin, and the relative intensity of only this lower band is quantified below. Bracket indicates ubiquitinated species. Western blot is representative of 2 independent experiments. (I) 293STF cells were treated with 100 μg/mL cycloheximide (CHX) dissolved in DMSO or DMSO vehicle control for the indicated time points followed by cytoplasmic fractionation. Western blot is representative of 2 independent experiments. For (A), (B), (D), and (E), data are representative of at least 4 independent experiments. $^{**}P < 0.01$, $^{****}P < 0.0001$ by Student's *t* test in the minus Wnt and plus Wnt conditions. For (C) and (F), data are pooled from n=5 independent experiments, each normalized to the control minus Wnt3a condition. $^{**}P < 0.01$ by Mann-Whitney test in the minus Wnt and plus Wnt conditions. For (G), Data are pooled from n=4 independent experiments. ns = non-significant by Mann-Whitney test in the minus Wnt and plus Wnt conditions.

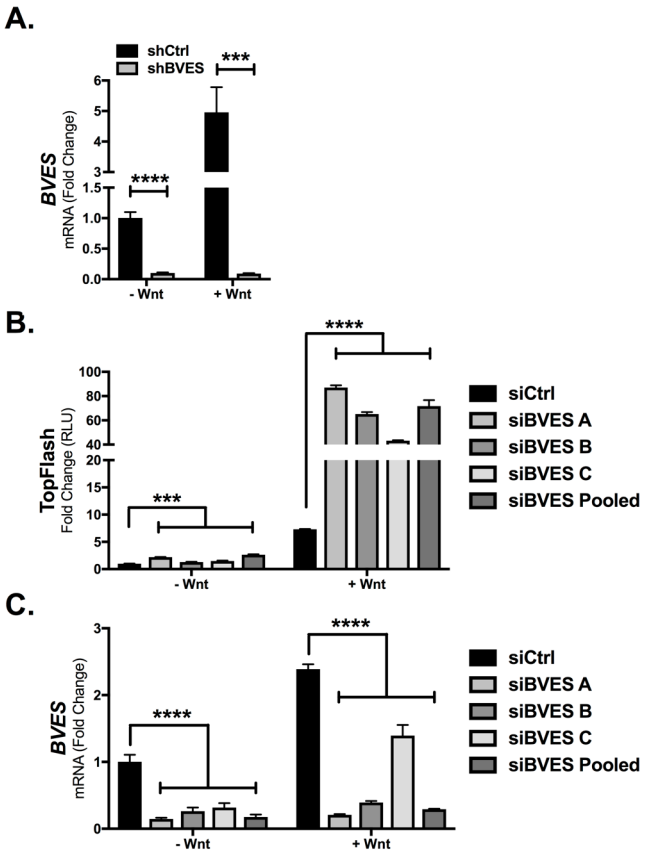

Figure 8. *BVES* knockdown increases TopFlash activity. (A) Confirmation of *BVES* knockdown by qRT-PCR in 293STF cells following shRNA knockdown. (B) TopFlash activity in 293STF cells utilizing both individual and pooled siRNAs. Cells were treated with 50% L-cell-conditioned media or 50% Wnt3a-conditioned media for 16 hours before reporter activity analysis. (C) Confirmation of B*VES* knockdown by qRT-PCR in 293STF cells from (B). All data are representative of at least n=3 independent experiments. For (A), ***$P < 0.001$, ****$P < 0.0001$ by Student's *t* test in the minus Wnt and plus Wnt conditions. For (B) and (C), ***$P < 0.001$, ****$P < 0.0001$ by one-way ANOVA with Tukey multiple comparison testing in the minus Wnt and plus Wnt conditions.

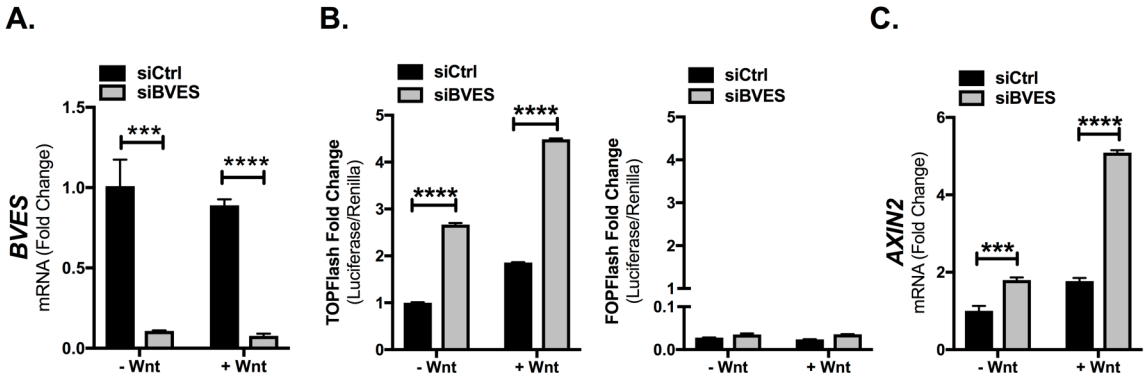

Figure 9. *BVES* knockdown increases Wnt signaling in HCT116 colorectal cancer cells. (A) Confirmation of *BVES* knockdown by qRT-PCR in HCT116 cells following siRNA knockdown. (B) TopFlash and FOPFlash activity in HCT116 cells following *BVES* knockdown. TopFlash activity was normalized to Renilla to control for transfection efficiency. Cells were treated with 50% L-cell-conditioned media or 50% Wnt3a-conditioned media overnight. (C) *AXIN2* fold change by qRT-PCR in HCT116 cells. Cells were treated with 50% L-cell-conditioned media or 50% Wnt3a-conditioned for 4 hours before RNA isolation. All data are representative of n=3 independent experiments. ***$P <$ 0.001, ****$P < 0.0001$ by Student's t test in the minus Wnt and plus Wnt conditions.

BVES loss leads to stabilization of β-catenin protein

β-catenin levels can be regulated transcriptionally or post-translationally, where it is sequentially phosphorylated by two kinases, GSK3β and CK1α[99,179,180]. This targets the protein for ubiquitination by β-TrCP and leads to its subsequent proteasomal degradation[173]. We tested whether the observed increases in β-catenin protein levels following BVES loss were due to alterations in β-catenin transcript levels or an effect on β-catenin ubiquitination and proteasomal degradation. *BVES* knockdown did not alter β-catenin transcript levels in 293STF or HCT116 cells (Figure 7G and Figure 10). Treatment of 293STF cells with the proteasome inhibitor MG132 led to an accumulation of higher molecular weight, ubiquitinated β-catenin species, as has been previously described (Figure 7H, Lane 3)[181]. In the setting of *BVES* knockdown, there was an increase in non-ubiquitinated β-catenin (Figure 7H, arrow) and a reduction in ubiquitinated species (Figure 7H, bracketed bands). To further these findings, we performed cycloheximide chase experiments to assess β-catenin stability. *BVES* knockdown cells maintained increased β-catenin protein levels after cycloheximide treatment (Figure 7I). Even when accounting for the overall increase in β-catenin protein levels in the setting of *BVES* knockdown, higher relative proportions of β-catenin were observed at each time point. Overall, this is consistent with BVES loss enhancing Wnt pathway activation through the accumulation of β-catenin due to reduced ubiquitination and proteasomal degradation leading to enhanced protein stability.

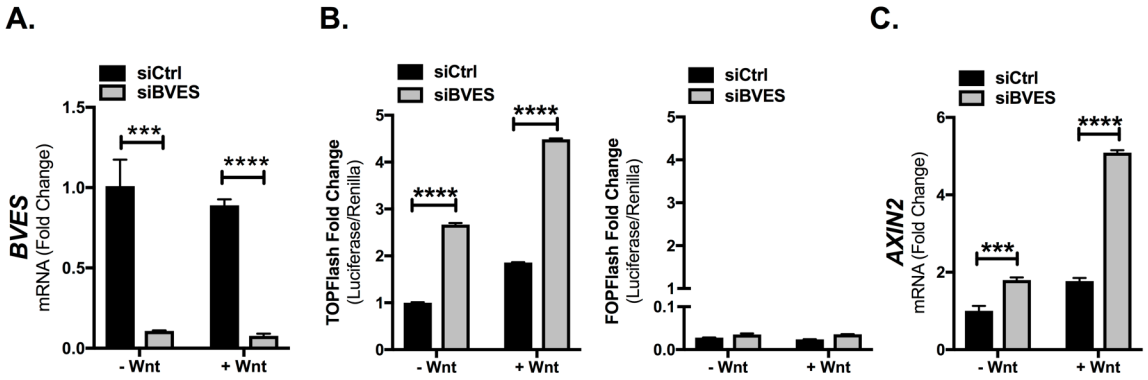

Figure 10. No increase in β-catenin transcript following *BVES* knockdown. (A) β-catenin (*CTNNB1*) mRNA levels by qRT-PCR in 293STF cells 72 hours after *BVES* shRNA knockdown. Representative data of n=4 independent experiments. (B) qRT-PCR analysis of HCT116 cells demonstrating no change in β-catenin transcript. $*P < 0.05$, ns = non-significant by Student's *t* test.

BVES inhibits Wnt receptor activation

Reductions in β-catenin ubiquitination lead to its stabilization and this can occur through multiple mechanisms, such as Wnt ligand binding and receptor activation, or through alterations in β-catenin destruction complex components (i.e. APC truncations)[182]. Because BVES rapidly traffics to the membrane upon cells reaching confluency, we hypothesized that BVES stabilization of β-catenin may be orchestrated via modulating Wnt receptor levels[30,183]. LRP6, and its homologue LRP5, are Wnt ligand co-receptors that, in the presence of Wnt ligand, bind the seven-transmembrane-domain receptor FZ and stabilize cytoplasmic β-catenin[184]. siRNA knockdown of *BVES* led to a reproducible 1.5-fold increase in LPR6 receptor levels in 293STF cells with concomitant increases in cytoplasmic β-catenin levels (Figure 11A). This increase in LRP6 protein levels was not due to an increase in *LRP6* mRNA transcript (Figure 11B), suggesting that BVES is affecting LRP6 protein stability.

We next determined if increases in total LRP6 levels also correlated with increased receptor activation. Cells were treated with or without Wnt3a conditioned media and immunoblotted for phospho-LRP6 (pLRP6, Ser1490), which is indicative of LRP6 receptor activation. *BVES* knockdown increased LRP6 phosphorylation both at baseline (without Wnt ligand) and with Wnt stimulation (Figure 11A and Figure 11C). Rapid phosphorylation of LRP6, within 1 hour, was observed with cytoplasmic levels of β-catenin peaking around 2 hours post-stimulation (Figure 11C). Consistently, pLRP6 levels were higher at baseline following *BVES* knockdown and remained elevated throughout the 3 hours of Wnt stimulation. Minimal change in LRP5 receptor levels were observed. Comparable results were observed in HCT116 cells (Figure 12A) and mouse embryonic fibroblasts (MEFs) isolated from littermate-controlled WT and *Bves*$^{-/-}$ embryos (Figure 12B and Figure 12C).

Interestingly, a mobility shift in DVL2 and DVL3 was also observed (Figure 11C). DVL proteins are key signal transducers that have roles in both canonical and noncanonical Wnt pathways[185]. DVL is phosphorylated in response to Wnt stimulation, which leads to a mobility shift[186], and it is these higher molecular weight, phosphorylated DVL species which are increased with *BVES* knockdown. To further analyze the level at which BVES alters Wnt signaling, we employed the HEK 293 DVL knockout cell line (293DVL TKO) which is null for all three *DVL* genes[187]. In agreement with a prior study that employed a combination of genetic knockout and *DVL* shRNA knockdown[188], the 293DVL TKO cells failed to phosphorylate LRP6 in response to Wnt3a (Figure 11D). Furthermore, *BVES* knockdown in this cell line led to small but reproducible increases in levels of the LRP6 receptor but did not result in changes in β-catenin levels, suggesting that the effects of BVES on Wnt signaling are upstream of DVL. These results indicate that DVL is not required for BVES-dependent changes in total LRP6, but is required for the downstream effects on β-catenin.

As we have previously shown that BVES directs PP2A phosphatase activity to dephosphorylate, and subsequently destabilize c-Myc[73], we next asked the question of whether BVES directed PP2A phosphatase activity reduces LRP6 receptor activation. 293STF cells with *BVES* knockdown were treated with Wnt3a conditioned media and an inhibitor of PP2A (Okadaic Acid, OA) or an activator of PP2A (Ceramide). Phospho-GSK3β (S9) and phospho-CREB (S133) are known PP2A targets and were included as reagent controls[189,190]. Reproducibly, *BVES* knockdown increased LRP6 phosphorylation both at baseline and with Wnt3a conditioned media (Figure 11E and Figure 12D). This effect was further augmented in the context of PP2A inhibition with OA, possibly owing to incomplete BVES knockdown or an indirect effect of BVES/PP2A on the activity of an intermediary protein such as GSK3β. In the setting of Wnt3a stimulation, activation of PP2A phosphatase activity with ceramide reduced LRP6 phosphorylation in the

presence of BVES. The ceramide mediated reduction in pLRP6 levels was abrogated following *BVES* knockdown, suggesting that BVES directs PP2A mediated dephosphorylation and subsequent inactivation of LRP6.

Overall, these data support a model in which the presence of BVES destabilizes the LRP6 co-receptor and reduces receptor activation, conceivably through directing the phosphatase activity of PP2A.

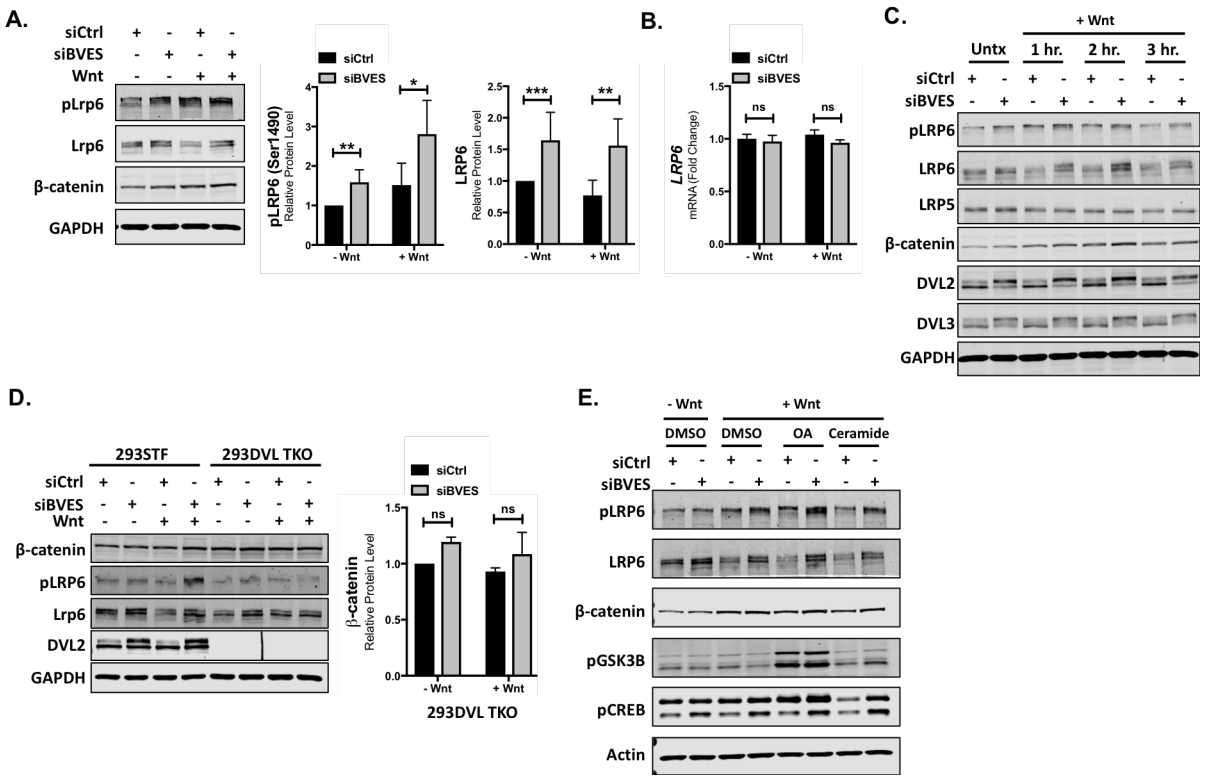

Figure 11. LRP6 levels and phosphorylation are increased with BVES loss. (A) Cytoplasmic fractionation of 293STF cells following siRNA knockdown of *BVES*. Cells were treated with 50% Wnt3a conditioned media for 2 hours before harvest. pLRP6 quantification is pooled from n=5 independent experiments, and total LRP6 quantification is pooled from n=7 independent experiments, each normalized to the control minus Wnt stimulation. (B) *LRP6* fold change by qRT-PCR in 2923STF cells with *BVES* siRNA knockdown. Cells were treated with 50% L-cell-conditioned media or 50% Wnt3a-conditioned media for 8 hours before isolation. (C) Cytoplasmic fractionations of 293STF cells with Wnt stimulation time course following *BVES* knockdown. Cells were treated with 50% Wnt3a-conditioned media for indicated time points. (D) Cytoplasmic fractionations of 293STF or 293 Dishevelled Triple-Knockout (293DVL TKO) cells following BVES knockdown. Cells were stimulated with 50% Wnt3a-conditioned media for 2 hours and immunoblotted. b-catenin quantification in the 293DVL TKO is pooled from n=3 independent experiments. Black line between lanes 6 and 7 is debris on the membrane. (E) Cytoplasmic fractionations of 293STF cells stimulated with 50% control or 50% Wnt3a-conditioned media for 2 hours. At the time of Wnt3a stimulation, cells were concurrently treated with DMSO, okadaic acid (OA) at 100 nM, or ceramide at 50mM and probed for pLRP6 (S1490), pGSK3b (S9), and pCREB (S133). Data is representative of two independent experiments. For (A), (B), and (D), *P < 0.05, **P < 0.01, ***P < 0.001 by Mann-Whitney test in the minus Wnt and plus Wnt conditions. ns = non-significant by Mann-Whitney test.

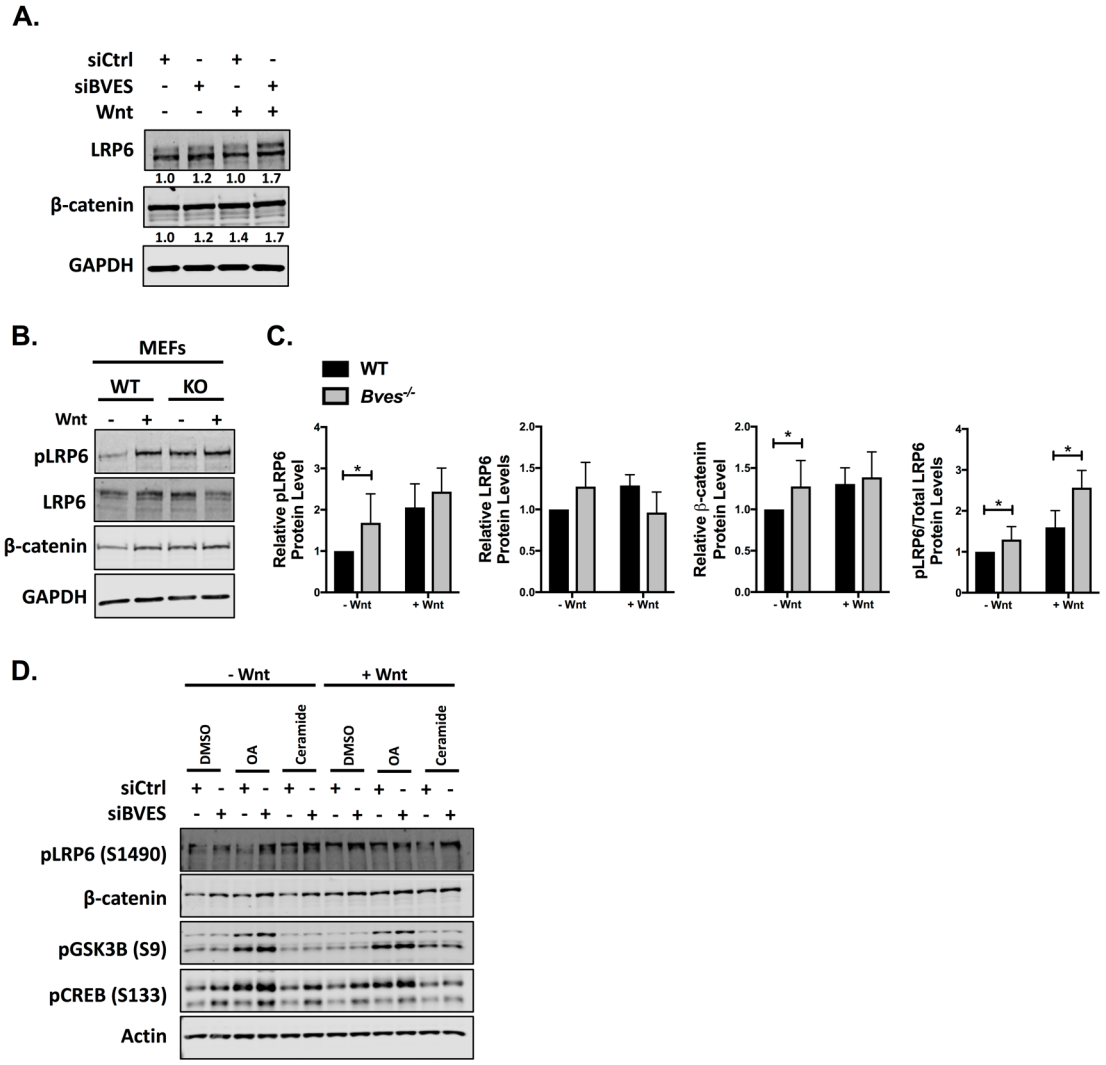

Figure 12. BVES loss increases LRP6 levels and activation in multiple cell types. (A) Western Blot demonstrating small but observable increases in LRP6 and β-catenin levels following *BVES* knockdown in HCT116 cells. Cells were treated with 50% L-cell-conditioned media or 50% Wnt3a-conditioned media for 2 hours. For (B) and (C), WT and BVES KO mouse embryonic fibroblasts (MEFs) were derived from littermates of $Bves^{+/-}$ by $Bves^{+/-}$ crosses and analyzed 1-2 passages after isolation. (B) Representative Western blot from one WT and one $Bves^{-/-}$ MEF line. Cells were stimulated for 2 hours with 50% L-cell-conditioned media or 50% Wnt3a-conditioned media before cytoplasmic fractionation. (C) Quantification of relative protein abundance from n=4 $Bves^{WT}$ and n=4 $Bves^{-/-}$ lines. (D) Cytoplasmic fractionations of 293STF cells stimulated with 50% control or 50% Wnt3a-conditioned media for 2 hours. At the time of Wnt3a stimulation, cells were concurrently treated with DMSO, okadaic acid (OA) at 100 nM, or ceramide at 50μM and probed for pLRP6 (S1490), pGSK3β (S9), and pCREB (S133). Data is representative of two independent experiments. $*P < 0.05$ by Mann-Whitney test in the minus Wnt and plus Wnt conditions.

BVES interacts with LRP6

As BVES is recognized to orchestrate changes in cellular state via protein interactions in the carboxy-terminus, we next hypothesized that BVES regulates LRP6 levels through a protein-protein interaction and performed co-immunoprecipitation experiments. Reciprocal co-immunoprecipitations of overexpressed Flag-tagged chick BVES (Flag-BVES) and GFP-tagged LRP6 (GFP-LRP6) demonstrated a BVES-LRP6 interaction (Figure 13A). Overexpression of BVES also reduced exogenous levels of LRP6 in the input samples, complementing our previous observations utilizing *BVES* knockdown. Overexpression of BVES followed by immunoprecipitation with anti-Flag resin also demonstrated an interaction with endogenous LRP6 as well as LRP5 (Figure 13B) and again confirmed that BVES levels are inversely correlated with LRP6 levels. To narrow the putative BVES-LRP6 interaction domain, we utilized an LRP6 construct spanning amino acids 1364 to 1539 which comprises the transmembrane (TM) and proximal intracellular domain (ICD) along with an amino-terminal Myc tag (Myc-LRP6ICD). These mapping studies demonstrate that the extracellular domain is dispensable for the BVES-LRP6 interaction and narrow the interaction domain to around 175 amino acids (Figure 13C). To test whether Wnt3a augments the BVES-LRP6 interaction, cells were stimulated for 2 hours with Wnt3a conditioned media before immunoprecipitation (Figure 13D). A subtle increase in the BVES-LRP6 interaction upon ligand stimulation was observed but overall, BVES and LRP6 appear to associate quite readily even in the absence of ligand. Together, these data demonstrate that BVES interacts with LRP6 and that BVES overexpression leads to reductions in LRP6 protein levels.

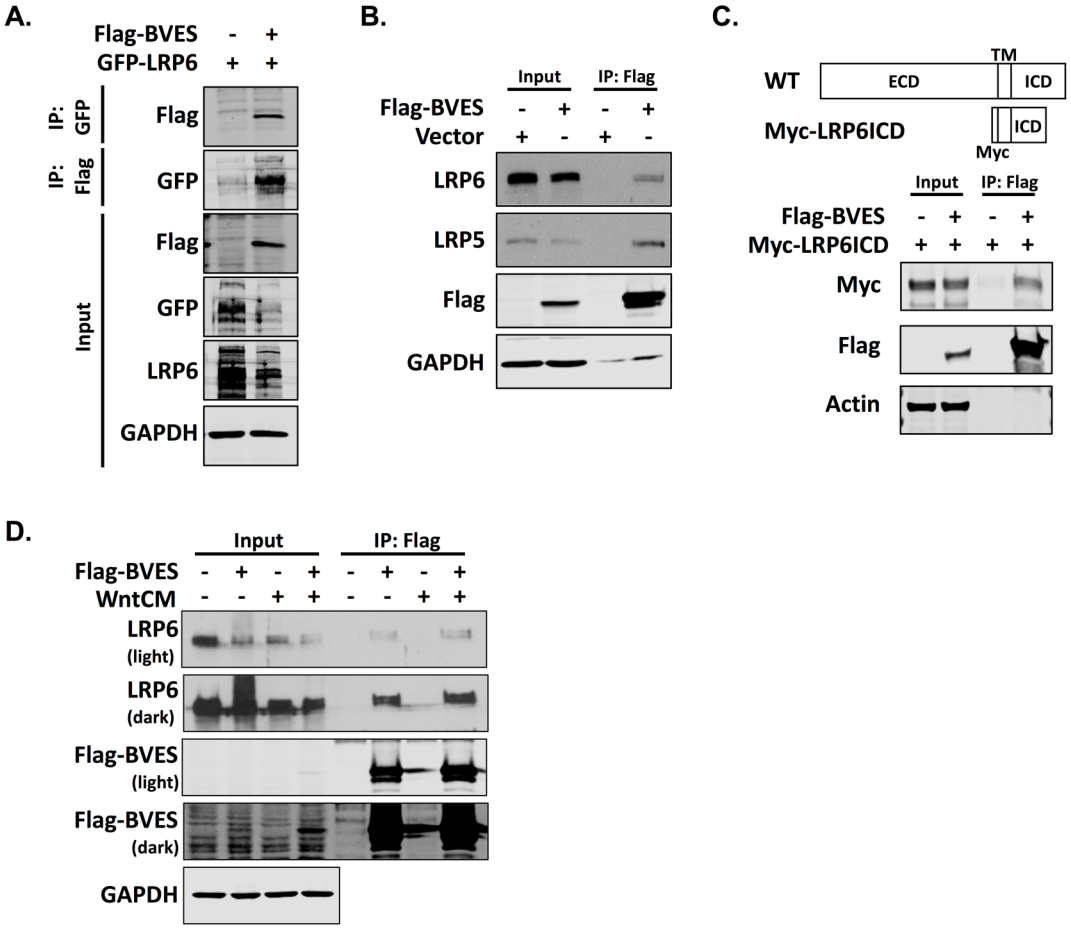

Figure 13. BVES interacts with LRP6 and LRP5. (A) Reciprocal co-immunoprecipitation of Flag-tagged BVES (Flag-BVES) and GFP-tagged LRP6 (GFP-LRP6). HEK293T cells were transiently transfected with 4 μg of each plasmid using PEI. Filler plasmid was used to maintain equal DNA quantities. GFP-LRP6 was immunoprecipitated with GFP binding protein magnetic beads following by immunoblotting with anti-Flag antibodies. Flag agarose resin was utilized to immunoprecipitate BVES followed by immunoblotting with anti-GFP antibodies. (B) Immunoprecipitation of Flag-BVES followed by immunoblotting for endogenous LRP5 and LRP6. 4 μg of vector or Flag-BVES was transfected into HEK293T cells using PEI. The LRP5 and LRP6 blots were developed using ECL and film, while the rest of the blots were immunoblotted using Odyssey infrared reagents as discussed in Methods. (C) Schematic of the amino-terminal myc-tag LRP6 (Myc-LRP6ICD) construct which spans amino acids 1364-1539 and contains the LRP6 transmembrane domain (TM) and proximal intracellular domain (ICD). Myc-LRP6ICD was transfected into HEK293T cells along with Flag-BVES as in (A) and immunoprecipitation experiments performed 48 hours later. (D) Cells were transfected with 4 μg of Flag-BVES and then 48 hours later treated with 50% L-cell-conditioned media or 50% Wnt3a-conditioned media for 2 hours before flag immunoprecipitation.

BVES regulates LRP6 and Wnt activation in human colonoids

To expand our studies into the intestinal epithelium, we performed *BVES* knockdown using lentivirally delivered shRNAs in a primary human colonoid line. Human colonoids more faithfully recapitulate intestinal physiology and are an excellent tool for studying junctional biology[191]. Following *BVES* knockdown, levels of both pLRP6 and total LRP6 increased (Figure 14A). This occurred despite only about a 50% reduction in *BVES* message (Figure 14B). Concomitant increases in *AXIN2* transcript levels were also observed with *BVES* knockdown (Figure 14C). Utilizing robust human intestinal models, these data further demonstrate that BVES loss enhances Wnt signaling and increases LRP6 receptor levels and phosphorylation.

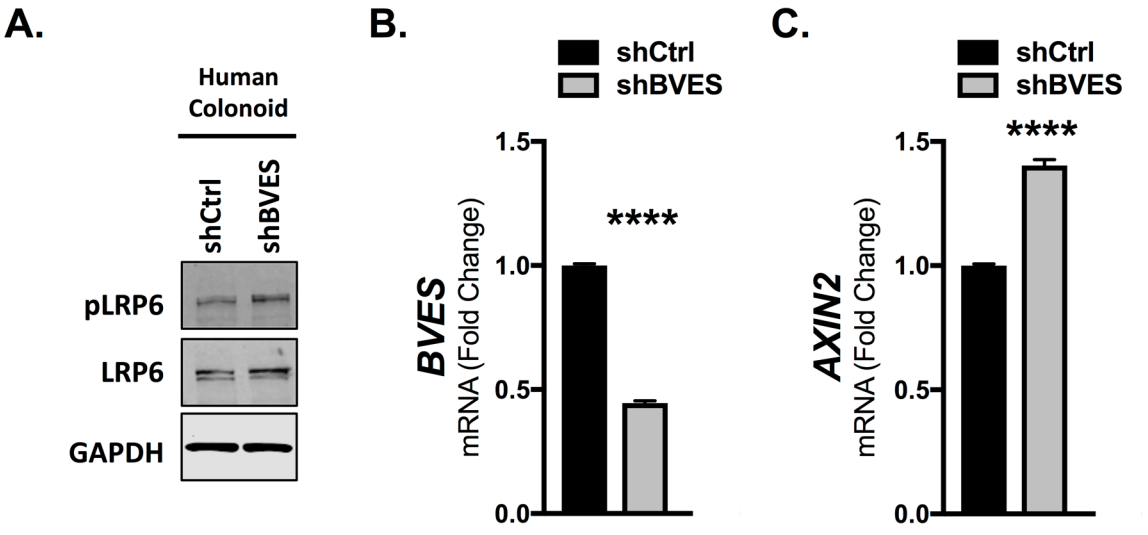

Figure 14. *BVES* knockdown increases LRP6 levels and Wnt activity in human colonoids. (A) Whole cell lysates from human colonoids maintained in human culture media (see Methods). Analysis was performed 96 hours following lentiviral shRNA knockdown. (B) *BVES* fold change by qRT-PCR in human colonoids from (A). (C) *AXIN2* fold change by qRT-PCR in human colonoids from (A). Data are representative of n=2 independent experiments. ****$P < 0.0001$ by Student's t test.

BVES loss increases Wnt receptor activation in *Apc*-deficient organoids

As our data supports a role for BVES in modulating Wnt receptor activation in non-transformed cells, we next sought to determine whether BVES loss can alter Wnt receptor activation in pathologic conditions such as in the setting of *APC* loss. We utilized the *Lrig1-CreER* driver to induce loss of one allele of *Apc* in intestinal stem cells. Lrig1 is a pan-ErbB family inhibitor that marks stem/progenitor cells in the intestinal crypt base[19]. Heterozygous loss of *Apc* driven by *Lrig1-CreER* leads to the development of intestinal adenomas upon stochastic loss of the second *Apc* allele[19]. Intestinal adenomas were isolated from tumor-bearing *Lrig1-CreER;Apc$^{fl/+}$;Bves^{WT}* mice and grown in 3D-Matrigel™ cultures. Importantly, *Bves^{WT}* adenoma tumoroids grown in basal media supplemented with purified Wnt3a and R-spondin grew larger than adenoma tumoroids grown without growth supplementation (Figure 15A) indicating that adenoma tumoroids, despite homozygous loss of *Apc*, were still responsive to Wnt stimulation. These data support prior observations by Saito-Diaz *et al.* and demonstrate that even in the absence of functional APC, modulating upstream Wnt receptors further activates the Wnt pathway and increases organoid growth[192].

We then isolated adenoma tumoroids from additional *Lrig1-CreER;Apc$^{fl/+}$;Bves^{WT}* and *Lrig1-CreER;Apc$^{fl/+}$;Bves$^{-/-}$* mice. As expected, the *Bves$^{-/-}$* tumoroids exhibited increases in both total LRP6 and activated pLRP6 levels (Figure 15B). Immunofluorescence analysis of formalin-fixed paraffin embedded adenoma tumoroids demonstrated an increased percentage of phospho-Histone H3 (pH3) positive proliferative cells with no change in cleaved caspase 3 (CC3) positive apoptotic cells (Figure 15C). These data demonstrate that BVES loss increases LRP6 receptor levels and activation in the setting of APC loss with concurrent increases in adenoma tumoroid proliferation.

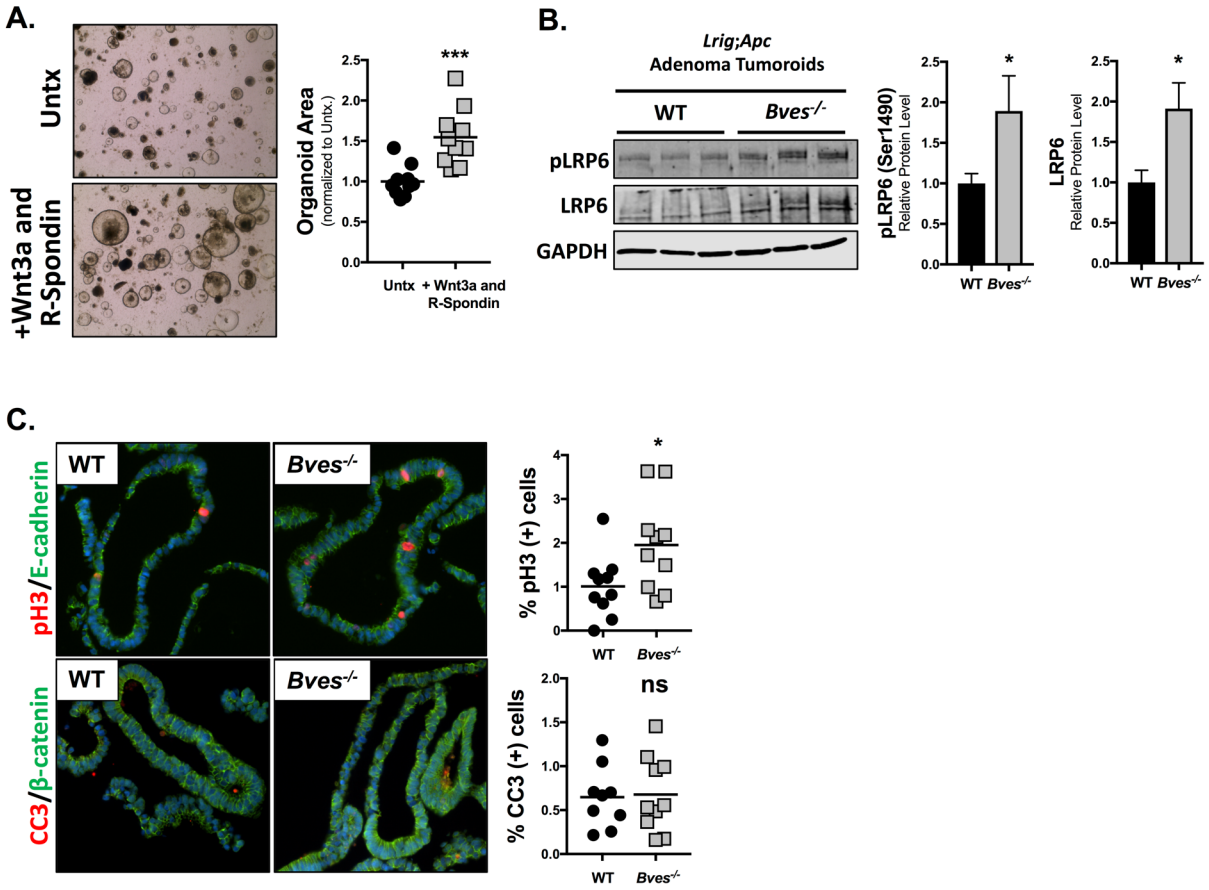

Figure 15. BVES loss increases LRP6 receptor activation and proliferation in *Lrig1-CreER;Apcfl/+* adenoma tumoroids. *Bves*^{WT} and *Bves*$^{-/-}$ mice were crossed with *Lrig1-CreER;Apc*$^{fl/+}$ mice and injected with 2 mg Tamoxifen for 3 consecutive days. Tumors were harvested at 100 days. (A) Established WT adenoma tumoroid lines were passaged and plated in basal media (Untx) or basal media supplemented with purified Wnt3a and R-spondin for 4 days. Representative 4x brightfield images are shown, and organoid area is quantified to the right. Data are from n=2 WT mouse tumoroid lines and representative of n=3 independent experiments. Quantification was performed on 5 images per condition. (B) Adenoma tumoroids from 3 *Bves*^{WT} and *Bves*$^{-/-}$ mice were maintained in WENR media and harvested for Western Blot. (C) Adenoma tumoroids were fixed, embedded, and stained for phospho-Histone H3 (pH3) to measure proliferation and cleaved caspase 3 (CC3) to measure apoptosis. Data are from n=2 WT mouse tumoroid lines and n=2 *Bves*$^{-/-}$ tumoroid lines. Quantification was performed on 5 images per line. *$P < 0.05$, ***$P < 0.001$ by Student's *t* test.

BVES loss augments intestinal tumorigenesis

Given that mutations in Wnt signaling components are among the most common initiating events in CRC, we next determined whether BVES could modify Wnt-dependent tumorigenesis[96]. Utilizing a purely Wnt-driven genetic model, we analyzed tumor burden in *Lrig1-CreER;Apc*$^{fl/+}$*;Bves*^{WT} and *Lrig1-CreER;Apc*$^{fl/+}$*;Bves*$^{-/-}$ mice. *Apc* loss was induced with three consecutive daily doses of Tamoxifen administered intraperitoneally. Mice were sacrificed after 100 days and analyzed for tumor burden. There was no difference in survival between cohorts, and all mice developed tumors independent of *Bves* genotype. There was no difference in tumor size; however, *Bves*$^{-/-}$ mice displayed an almost 2-fold increase in tumor multiplicity over littermate-matched controls (Figure 16A, 35.1 ± 5.1 vs. 68 ± 13.1, $P < 0.05$) and an increased incidence of high-grade dysplasia upon histologic review by a pathologist (MKW) who was blinded to the genotypes of the samples (Figure 16B and Figure 16C).

We also utilized a chemically-induced model of tumorigenesis to confirm these findings. Cohorts of 8-week-old WT and *Bves*$^{-/-}$ mice were treated with 5 weekly injections of AOM, which can induce β-catenin mutations but can also promotes *Apc* loss[193,194]. Mice were harvested at 30 weeks of age and assessed for tumor burden. Increased tumor incidence (Figure 16D and Figure 16E) and tumor multiplicity (Figure 16F) were observed in *Bves*$^{-/-}$ mice. The tumors in AOM-treated *Bves*$^{-/-}$ mice also demonstrated higher degrees of dysplasia upon histologic review. Together, these tumor models are in agreement in supporting a role for BVES as a tumor suppressor and highlight that BVES loss can increase both tumor multiplicity as well as histologic progression.

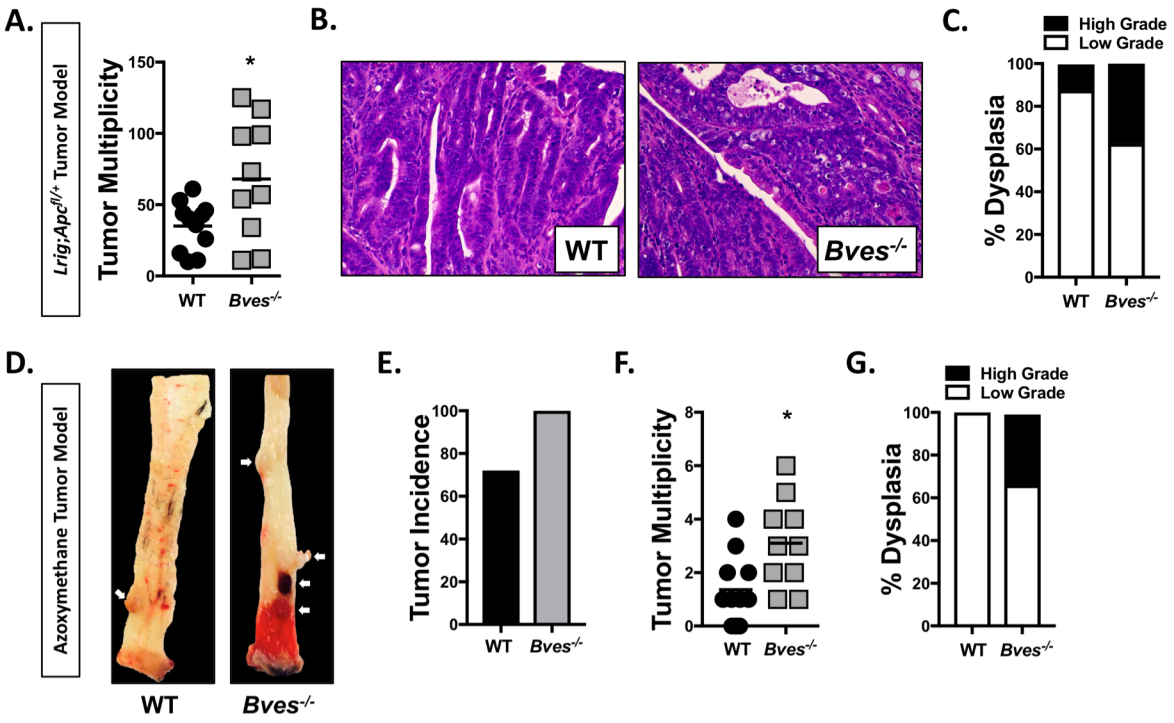

Figure 16. BVES loss increases tumorigenesis. (A) Tumor multiplicity in small and large intestine of *Lrig1-CreER*;*Apc*$^{fl/+}$ mice crossed with *Bves*$^{-/-}$ mice. (B) Representative histology from *Lrig1-CreER*;*Apc*$^{fl/+}$ and *Lrig1-CreER*;*Apc*$^{fl/+}$;*Bves*$^{-/-}$ tumor bearing mice. (C) Dysplasia scoring in *Lrig1-CreER*;*Apc*$^{fl/+}$ and *Lrig1-CreER*;*Apc*$^{fl/+}$;*Bves*$^{-/-}$ mice. (D) Representative images from AOM-treated *Bves*^{WT} and *Bves*$^{-/-}$ colons at sacrifice. Tumors indicated by white arrows. (E) Tumor incidence, (F) tumor multiplicity, and (G) dysplasia scoring in AOM-treated mice. For (A-C), n=11 WT and n=10 *Bves*$^{-/-}$ mice. For (D-G), n=11 WT and n=10 *Bves*$^{-/-}$ mice. $*P < 0.05$ by Student's *t* test.

Discussion

Multiple mechanisms regulate β-catenin levels and activity within the cell. Classically, the transmembrane glycoprotein E-cadherin sequesters β-catenin at the cell membrane, thereby preventing its nuclear translocation and repressing Wnt signaling[47]. However, there is little evidence that tight junctions can regulate Wnt signaling and β-catenin levels. Here, we demonstrate a novel role for BVES, a tight junction-associated molecule, in modulating Wnt signaling by controlling LRP6 receptor levels and activation state, thereby determining cellular β-catenin levels.

As a tight junction protein, BVES is implicated in regulating a variety of diverse cellular phenotypes such as cell migration and epithelial-mesenchymal transition. *BVES* is downregulated in multiple epithelial malignancies and, notably, is reduced in the earliest stages of CRC[41]. Furthermore, BVES interacts with a protein phosphatase 2A (PP2A) regulatory subunit to reduce c-Myc protein levels, and loss of BVES increases tumor formation in a mouse model of colitis-associated cancer[73]. BVES also demonstrates high affinity for cAMP, and aberrant cyclic nucleotide signaling has been implicated in tumorigenesis[58,195]. This suggests that BVES suppression may cooperate with multiple oncogenic factors in promoting tumorigenesis. Our previous studies have also associated BVES loss with Wnt pathway activation, a foundational step in the initiation of CRC[96]. We now demonstrate that BVES directly regulates Wnt signaling by altering cellular β-catenin levels via an effect on LRP6 activity and that such regulation increases *APC*-dependent tumorigenesis.

We show that BVES loss increases TopFlash reporter activity, Wnt target gene transcription, and β-catenin protein levels at baseline, in the absence of Wnt ligand. Additionally,

BVES loss coordinates with Wnt ligand to robustly increase pathway activation. This suggests cells lacking BVES are "primed" and more responsive to Wnt ligand binding. Thus, it follows that BVES may influence receptor level dynamics, and indeed, we observed that BVES loss increased LRP6 receptor levels in the absence and in the presence of Wnt ligand. No changes in Frizzled 8 or the E3 ubiquitin-ligase RNF43 were observed (data not shown), suggesting that this is a direct effect on LRP6. Across multiple experiments and models, BVES loss increased Ser1490 phosphorylation of the LRP6 receptor even in the absence of Wnt ligand, suggesting that BVES inhibits ligand-independent receptor activation and Wnt signalosome formation. Phosphorylated LRP6 can subsequently recruit AXIN2 to the plasma membrane which ultimately leads to stabilization of β-catenin. This effect appears to be upstream of the scaffolding DVL proteins because no changes in β-catenin levels were observed in the DVL TKO cells following BVES loss. Because DVL is required for LRP6 receptor phosphorylation and signalosome formation[196], one working model is that BVES prevents LRP6 receptor activation by disrupting the DVL-LRP6 interaction. Interestingly, BVES interacts with ZO-1, a tight junction protein that, like DVL, contains a PDZ domain[54,197]. While this protein motif could link BVES and DVL, an interaction between BVES and DVL2 was not observed (data not shown). Instead, immunoprecipitation studies demonstrate that BVES interacts with both LRP5 and LRP6. Chick BVES was utilized for these experiments because it is much more readily expressed than full length human BVES, is nearly 80% homologous with even higher homology in key functional domains[35], and has been extensively utilized for many key studies describing BVES function[32,41,54]. LRP5 and LRP6 share a high degree of sequence homology[198], therefore it is not surprising that BVES could interact with both proteins. However, why *BVES* knockdown differentially increase LRP6 levels with minimal changes to LRP5 levels will require further exploration. Mapping studies place the BVES-LRP6 interaction within the

transmembrane/intracellular domain of LRP6 and confirm that the extracellular domain (ECD) of LRP6 is not required for the interaction. As the effects of BVES loss on LRP6 occur even in the absence of Wnt ligand, it is unlikely that BVES is altering ligand-receptor dynamics which is consistent with a BVES-LRP6 interaction that is independent of the LRP6 ECD. While a direct interaction between BVES and LRP5/6 cannot be ruled out, we believe that this interaction exists within a larger complex and is indirect as BVES-LRP6 direct interactions have not been observed in prior yeast two hybrid screens[41,55]. Interestingly, we also observed increases in BVES transcript following stimulation with Wnt3a conditioned media, suggesting that BVES itself is a Wnt target gene. Overall, this supports a potential model whereby BVES is upregulated in response to Wnt stimulation in a negative feedback loop that subsequently attenuates Wnt signaling, a well described phenomenon in Wnt signaling exemplified by studies of AXIN2[177].

Our studies utilizing OA and ceramide highlight a novel and unexplored mechanism of Wnt receptor regulation. A model by which BVES-directed, PP2A-mediated, dephosphorylation of the LRP6 co-receptor occurs at the membrane would not be without precedent as PP2A dephosphorylates a number of Wnt signaling components and appears to have dual (both activating and inhibiting) roles in this regulation similar to other pathway components such as GSK3β[81]. The role of BVES in directing PP2A activity appears to be more critical in the setting of Wnt3a stimulation, when phosphorylated LRP6 levels are highest. This is consistent with the dramatically enhanced TopFlash activity in the setting of BVES loss and Wnt3a stimulation and suggests that while the BVES-LRP6 interaction itself appears to be ligand independent, some components of this regulatory mechanism may be ligand dependent.

In the setting of tumorigenesis, the question remains as to whether or not modulating Wnt receptor activity upstream of mutations in *APC* is functionally relevant. Inactivating mutations in *APC* are potent drivers of CRC development and lead to stabilization of β-catenin. Teleological

thinking would suggest that downstream *APC* mutations subsequently render cells insensitive to upstream ligand stimulation; however, a recent study by Saito-Diaz *et al.* highlights a novel role for APC in preventing ligand-independent LRP6 activation and proposes a model by which the APC homologue APC2 functions within the destruction complex to degrade β-catenin [192]. We also know that despite *APC* mutations, cellular β-catenin levels do not rise indefinitely, which may be in part due to APC2's function in the destruction complex[192,199]. Therefore, in the setting of APC loss, ligand stimulation may enhance Wnt signaling by preventing APC2-dependent destruction complex formation. In support of this, we show that WT adenoma tumoroids derived from *Lrig1-CreER;Apc*$^{fl/+}$*;Bves*^{WT} tumors are still responsive to Wnt ligand stimulation, growing significantly larger in the setting of Wnt3a and R-spondin.

Tumoroids derived from *Apc*^{Min} adenomas are sensitive to LRP6 knockdown[192], highlighting a critical dependency of Wnt receptor signaling in the context of APC loss. Our studies reveal that adenoma tumoroids derived from *Lrig1-CreER;Apc*$^{fl/+}$*;Bves*$^{-/-}$ adenomas display increased LRP6 and pLRP6 levels. These changes in receptor activation were associated with an increase in the number of pH3-positive proliferating cells. Expanding these observations, we show that *BVES* knockdown increases LRP6 phosphorylation in non-transformed human colonoids with associated increases in *AXIN2* mRNA. Utilizing the HCT116 CRC cell line, we also observed increases in Wnt pathway activation and LRP6 and β-catenin protein levels following *BVES* knockdown despite a stabilizing mutation in one allele of β-catenin[200]. The more nuanced effect on β-catenin protein levels in this cell line is likely due to the reduced pool of modifiable β-catenin. Together, these data demonstrate that BVES loss increases LRP6 receptor levels and activation in the setting of an intact destruction complex, in adenoma tumoroid models with homozygous APC truncations, and in CRC cell lines.

Given the preponderance of *APC* mutations in CRC, it was important to show that BVES loss can alter tumorigenic phenotypes in the context of these strong pro-tumorigenic mutations. Utilizing the *Lrig1-CreER;Apc*$^{fl/+}$ tumor model, we confirm that BVES loss leads to increased tumor multiplicity and higher degrees of dysplasia. Importantly, this model mimics human CRC progression where BVES loss and APC truncations occur early in the tumorigenic cascade. Surprisingly, we did not observe an overall change in tumor size but the increased tumor multiplicity suggests that BVES loss increases tumor initiation, a process associated with higher levels of Wnt tone[41,201,202]. We suspect that the strong pro-proliferative signal generated by loss of both alleles of *Apc* in these tumors masks the increase WNT signaling observed in the *Bves*$^{-/-}$ setting. AOM is a known chemical mutagen and tumor initiator and we again observed increased tumor multiplicity and dysplasia in the setting of BVES loss. Together, these tumor models support a role for BVES as a tumor suppressor and highlight that BVES loss can increase both tumor multiplicity and tumor progression. While the effects of BVES loss on tumorigenesis are multifactorial, it is likely that the disinhibition of Wnt signaling plays a prominent role.

This report has focused on BVES in regulating canonical Wnt signaling; however, a role for BVES in regulating non-canonical Wnt signaling cannot be excluded. In fact, previous reports have demonstrated that BVES reduces RhoA activity by sequestering GEF-H1 and Wnt ligands can activate Rho signaling through the non-canonical Planar Cell Polarity pathway (PCP)[182]. Future studies will be required to determine whether BVES coordinately inhibits RhoA through multiple mechanisms.

In summary, our current working model is that BVES tunes Wnt signaling at the receptor level by interacting with LRP6 and subsequently inhibiting signalosome formation (Figure 17). This prevents ligand-independent LRP6 receptor and Wnt pathway activation. In the absence of BVES, the LRP6 receptor is phosphorylated, the β-catenin destruction complex is inhibited, and

β-catenin protein levels increase. Given this primed receptor state, Wnt stimulation then further increases pathway activation. Because of the increased Wnt tone and sensitivity to ligand stimulation, the loss of BVES early in tumorigenesis facilitates growth of transformed cells, thereby augmenting tumorigenesis and progression.

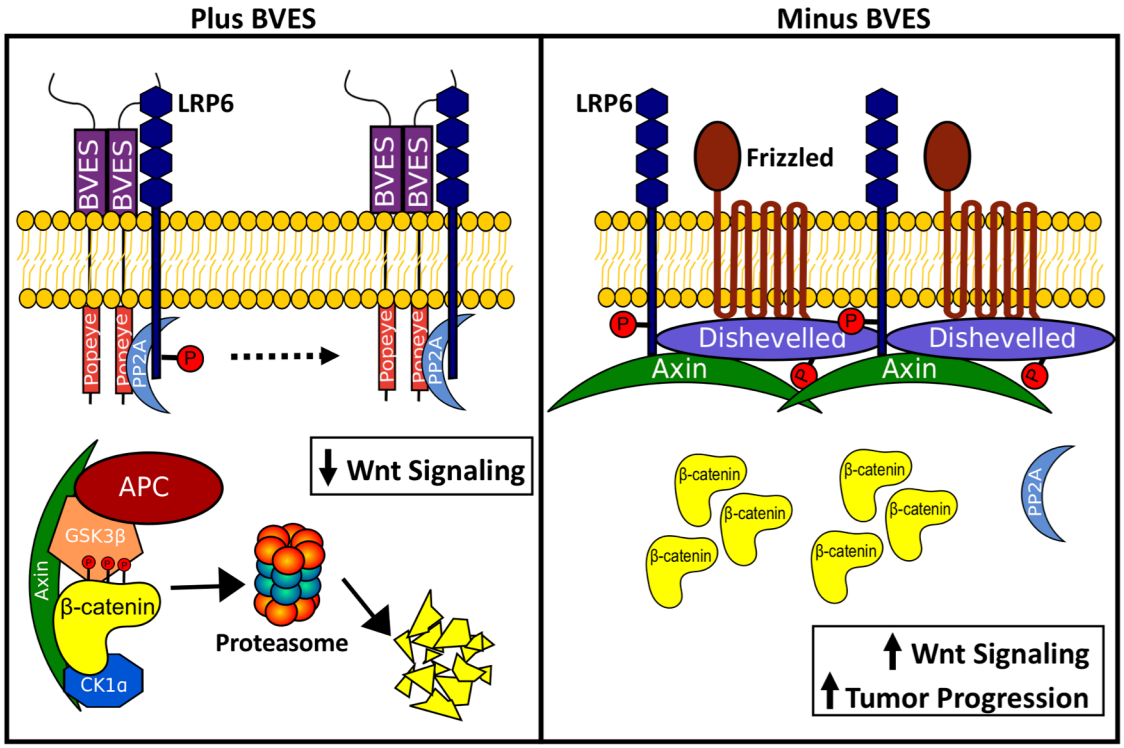

Figure 17. Proposed model by which BVES regulates Wnt signaling. (A) Schematic and proposed model for the role of BVES in the regulation of Wnt signaling. In the presence of BVES, BVES directs PP2A activity to dephosphorylate and inactivate LRP6. The β-catenin destruction complex remains intact and degrades β-catenin. In the absence of BVES, LRP6 remains phosphorylated which recruits Axin and DVL to the plasma membrane and prevents assembly of the β-catenin destruction complex which leads to stabilization of β-catenin, enhanced Wnt signaling, and increased tumor progression.

Acknowledgements

This chapter would not have been possible without support from a number of key individuals. Sarah Short, Ph.D. performed the *Lrig1-CreER;Apc*$^{fl/+}$ tumor studies, isolated the adenoma tumoroid lines, performed the shRNA knockdown in the human colonoid lines, and performed the pH3 and CC3 staining and quantification. Bobak Parang, M.D., Ph.D. performed the AOM only tumor modeling. An additional thank you to the members of the Williams, Lee, and Coffey labs for their many helpful discussions and a special thank you to Kenyi and Victoria from the Lee lab for providing technical expertise and reagents. Victoria's expertise was critical for teaching me how to develop the HRP/film blots demonstrating an endogenous BVES-LRP6 interaction. The thrill and excitement of developing that blot in the dark room and seeing that crisp glowing doublet on the membrane as our eyes adjusted will remain one of my fondest graduate school memories.

Chapter IV

BREAST CANCER ANTI-ESTROGEN RESISTANCE 3 IN COLORECTAL CANCER MIGRATION AND INTESTINAL TUMORIGENESIS

Rationale

Protein-protein interactions are the foundation of cellular signaling cascades and alterations in many of these interactions predispose to the development of cancer. This chapter builds on a prior yeast-two-hybrid screen performed in the Williams lab which identified an interaction between BVES and BCAR3. Before determining how the BVES-BCAR3 interaction impacts tumorigenesis, it was deemed important to individually characterize the role of BCAR3 in colon homeostasis and disease.

Introduction

Breast cancer anti-estrogen resistance 3 (BCAR3) is a member of the novel SH2-containing protein family (NSP) which, in humans, is comprised of three related proteins, NSP1/SH2D3A, NSP2/BCAR3, and NSP3/SH2D3C/CHAT/SHEP1. Two of these family members exist in mice; the murine homolog of NSP2/BCAR3 is AND-34 and the homolog of NSP3 is known as CHAT/SHEP. In humans, the *BCAR3* gene codes for 5 different splice variants[203]. The first three splice variants (NM_001261408, NM_001261409, and NM_003567) differ in their 5' untranslated regions and encode for the same 825 amino acid, 93 kDa, protein (human BCAR3 Isoform 1, NP_003558.1). The product from the fourth transcript variant (NM_001261410)

encodes a 734-amino acid (83 kDa) protein (human BCAR3 Isoform 2, NP_001248339). BCAR3 protein Isoform 2 differs in its amino terminus from Isoform 1, however Exons 9 through 17 (corresponding to amino acids 118-825) are identical. The fifth splice variant (NM_001308251) differs in the 5' UTR, lacks portions of the 5' coding region, and initiates translation at a downstream start codon to generate a significantly shorter 501 amino acid (~56 kDa) protein product (NP_001295180). While most of the isoforms are detectable in multiple tissues[203], little is known about how these different isoforms function within the cell. Structurally, human BCAR3 isoform 1 contains an amino-terminal SH2 domain, which allows for docking to phosphorylated tyrosine residues, a central proline/serine-rich domain, and a C-terminal domain that is homologous to the guanine nucleotide exchange factor (GEF) domain of the Cdc25 family[204]. There is controversy over whether the GEF domains of NSP family members, including BCAR3, have any catalytic activity[204-208]. There may be additional NSP binding partners that help modulate GEF domain activity or these domains may bind GTPases without actually promoting the exchange of GDP for GTP and further investigation will be required.

Discovery and characterization of BCAR3 function

BCAR3 was originally identified as a gene that confers resistance to the antiestrogen, tamoxifen, through a retrovirus-mediated insertional mutagenesis screen in the estrogen dependent human ZR-75-1 breast cancer cell line[209]. Of the 80 tamoxifen-resistant clones, 6 of them were shown to contain retroviral insertion in the BCAR3 promoter which resulted in up-regulation of BCAR3 expression and growth in the presence of 4-hydroxy-tamoxifen. A similar approach also identified a gene product that was termed BCAR1[210]. While unknown at the time, BCAR1 had been previously identified as the crk-associated substrate, p130Cas, a protein which is highly phosphorylated on tyrosine residues following v-Src and v-Crk mediated transformation[211,212].

The study confirming that "BCAR1" was homologous to the p130Cas adaptor protein came a few years later[213].

The predominant body of literature suggests that BCAR3 functions as an adapter protein downstream of p130Cas to mediate cell migration. p130Cas itself, likely via its extensive tyrosine and serine phosphorylation, also functions as an adaptor protein and is important in nucleating protein-protein complexes downstream of focal adhesion. Furthermore, p130Cas has been implicated in cells survival and apoptosis by integrating extracellular matrix signaling with signaling downstream of soluble growth factors (and their receptors). Specifically, p130Cas helps activate the GTPases Rac and Ras, as well as JNK and the ERK1/2-Map kinase pathway (reviewed in [214]). The first association between BCAR3 and p130Cas was described in NIH3T3 fibroblasts, both of which demonstrated enhanced tyrosine phosphorylation following serum stimulation[215]. Murine BCAR3 overexpression in NIH3T3 cells results in membrane ruffling (actin rich membrane protrusions which are essential for cell motility[216]) and alterations in F-actin stress fibers, similar to the morphology changes observed when overexpressing a constitutively activate RacV12 construct. Accordingly, the BCAR3 mediated changes were linked with activation of Rac and Cdc42 and p21-activated serine threonine kinase (PAK1), a protein that is autophosphorylated and activated in response to GTP-bound Rac and Cdc42 binding. Confirming BCAR3's namesake, Cai *et al.* went on to shown that overexpression of BCAR3 in ZR-75-1 promotes cell proliferation even in the presence of the antiestrogen ICI 182,780. As Rac activation can induce cyclin D1, the authors suggest that BCAR3-mediated antiestrogen resistance could be mediated, at least to some extent, by Rac and PAK1-mediated activation of the cyclin D1 promoter[217]. Cross *et al.* determined that the "entire cellular pool of BCAR3 is in complex with p130Cas, that the BCAR3-p130Cas interaction increases active GTP-bound Rac1, and that BCAR3 overexpression increases cell migration and invasion in MDA-MB-231 cells[218].

Furthermore, studies have shown that the BCAR3-p130Cas interaction is required for promoting antiestrogen resistance[219], highlighting the importance of the BCAR3-p130Cas interaction. Importantly, nearly all of the studies examining BCAR3 function have been carried out in breast cancer cell lines and very little is known about BCAR3's role in other tissues and other cancers.

A role for BCAR3 in immunology

The second earliest report in the literature mentioning BCAR3 (AND-34) came via identification of transcripts that were up-regulated in the thymus following induction of apoptosis in immature CD4+CD8+ thymocytes. Interestingly, while upregulated in total thymic RNA, *Bcar3* expression was considerably lower in purified thymocytes suggesting that *Bcar3* may be expressed within the thymic stromal cells. Indeed, *Bcar3* expression was elevated in thymic cortical reticular cells, thymic nurse cells, and fibroblast cell lines. This study also demonstrated that *Bcar3* transcript and protein levels increased in response to IL-1β and TNFα stimulation, suggesting that BCAR3 may play a role in mediating cellular signaling downstream of inflammatory cytokines[215]. In 2003, another report by *Cai* et al. demonstrated that BCAR3 is expressed at high levels in murine splenic B cells, that BCAR3 associated with p130Cas and another Cas family member, HEF1, that BCAR3 overexpression activates Cdc42 and PAK1, and that BCAR3 overexpression inhibits stromal cell-derived factor-1α-induced B cell polarization ([205]. The high levels of expression in B-cells and lymphoid-derived stromal cells is in agreement with expression data from the Immunological Genome Project (www.immgen.org) that demonstrates robust expression in B-cell populations, alveolar macrophages, and stromal cells with a relative paucity of expression in T-cell, natural killer cell, and ILC3 cell populations (Figure 18). Accordingly, analysis by The Imunological Genome Project Consortium identified *Bcar3* as one of the "Top 100" B cell signature genes and a transcript that most distinguished T and B cells[220]. While

lowly expressed in most macrophage populations, multiple studies have implicated BCAR3 in macrophage polarization. Specifically, *Bcar3* enrichment was identified in M2 (classically thought to be pro-tumorigenic) macrophages in two independent experiments [221,222]. Similarly, while *Bcar3* expression is also relatively low in most T-cell populations, it may play a role in certain cell populations in specific contexts. One study identified differential *Bcar3* expression in an asbestos-induced, apoptosis-resistant polyclonal T-cell line (MT-2)[223] and *BCAR3* expression was enhanced in a signature of Th2 cells compared to naïve and non-polarized "Th0" cells[224]. Overall, these relatively disparate pieces of data at the very least provide some preliminary data and evidence to support further investigation of BCAR3 in immune cell and immune-stromal cell compartments. As B-cells appear to have the highest levels of BCAR3, characterizing B-cell homing, lineage allocation, and activity in the BCAR3 knockout mice may provide useful insight into how an adapter protein that predominately regulates cell migration and adhesion can influence immune cell populations.

While the above is evidence for the role of BCAR3 in immune cell populations and previous studies have highlighted the role of BCAR3 in breast cancer cell lines, the function of BCAR3 in other tissues, such as the intestine, is unknown. The following studies were initiated because of a newly identified interaction between BVES and BCAR3. Before determining the significance of this interaction, we sought to determine the role of BCAR3 alone in colorectal cancer cell migration and intestinal tumorigenesis. Here we show that BCAR3 is overall downregulated in colorectal cancer but displays heterogeneous protein and RNA expression. BCAR3 interacts with p130Cas and augments colorectal cancer cell migration and invasion and loss of BCAR3 increases intestinal tumorigenesis. Overall, these data provide novel insights into the role BCAR3 in intestinal tumorigenesis.

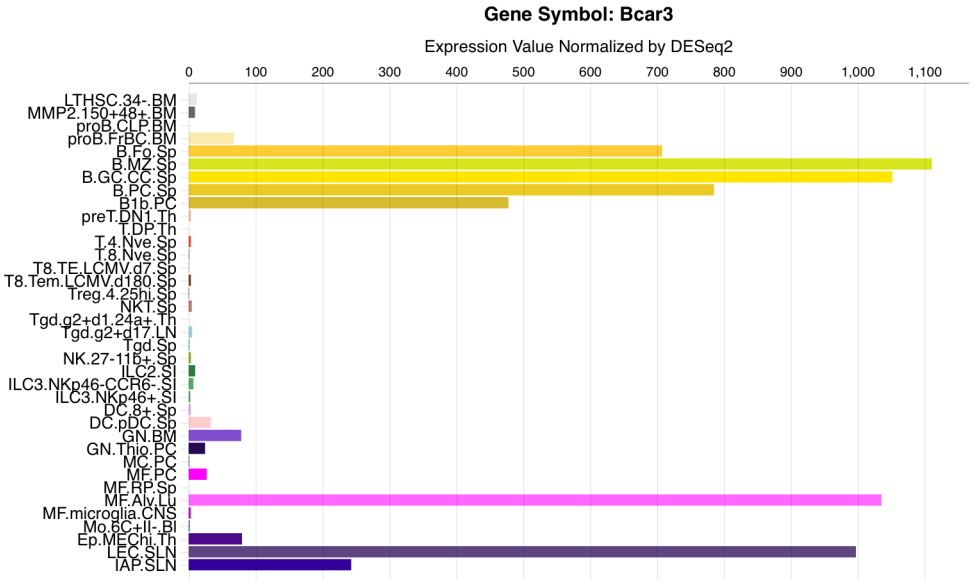

Figure 18. BCAR3 expression in Immune Cell Populations. Ultra-low-input RNA-seq analysis of sorted mouse cell populations generated from the Immunological Genome Project (www.immgen.org). The indicated cell populations with enrichment of BCAR3 expression based on flow sorting label are: proB_FrBC_BM: Pro-B cells, B_Fo_Sp: Splenic Follicular B cells, B_MZ_Sp: Splenic Marginal Zone B cells, B_GC_CC_Sp: Splenic Germinal Center Centrocytes, B_PC_Sp: Splenic Plasma Cells, B1b_PC: Peritoneal B1b cells, GN.BM: Bone Marrow Neutrophils, MF_Alv_Lu: Alveolar Macrophages, Ep_MEChi_Th: Thymic Medullary Epithelial Cells, LEC_SLN: Subcutaneous Lymph Node Lymphatic Endothelial cell, IAP_SLN: Subcutaneous Lymph Node.

Results

BVES interacts with BCAR3 and may influence DSS-induced colitis

As has been previously discussed, BVES is a tight junction-associated protein that regulates EMT and functions as a tumor suppressor in CRC. To identify novel BVES interactors that may influence BVES dependent phenotypes, the Williams lab had previously commissioned a yeast-two-hybrid screen which identified BCAR3 as a BVES interacting protein (Figure 19A). A direct yeast-two-hybrid was also performed using full length BCAR3 and BVES protein fragments in an effort to map the interaction domain within BVES. The directed yeast-two-hybrid domain mapping results confirmed the BVES-BCAR3 interaction but did not conclusively narrow the putative interaction domain (Figure 19B). To confirm this interaction in eukaryotic cells, HEK293 cells were transfected with a V5-tagged BVES construct (containing amino acids 72-360) and a His-tagged BCAR3 vector followed by V5-immunoprecipitation (Figure 19C).

In order to test whether the BVES-BCAR3 interaction can impact cellular phenotypes, compound *Bves*$^{-/-}$*;Bcar3*$^{-/-}$ global knockout mice were generated and subjected to DSS-colitis modeling. In this pilot experiment, the *Bcar3*$^{-/-}$ mice appear to be more sensitive to DSS-induced colitis, though this observation is not statistically significant by two-way ANOVA. The *Bves*$^{-/-}$*;Bcar3*$^{-/-}$ double knockout appeared less sensitive than the *Bcar3*$^{-/-}$ mice, suggesting that BVES may be functioning downstream of BCAR3 to mediate colitis sensitivity. These results must be interpreted carefully as the complex genotypes precluded the use of littermate controls and mice were instead derived from single or double knockout colonies. We have observed significant cage and sub-colony effects with these types of DSS experiments which can be mitigated, at least to some degree, by using age-matched littermate controls and carefully controlling for the microbiome by admixing bedding before these experiments begin. Nonetheless, this preliminary

data confirms a BVES-BCAR3 interaction, suggests that the *Bcar3*$^{-/-}$ mice are more sensitive to DSS-induced colitis, and highlights a potential interplay between BVES and BCAR3 in mediating this phenotype. As both proteins have been shown to modulate migratory phenotypes, further investigating the role of BCAR3 loss alone, as well is in addition to BVES, will be required.

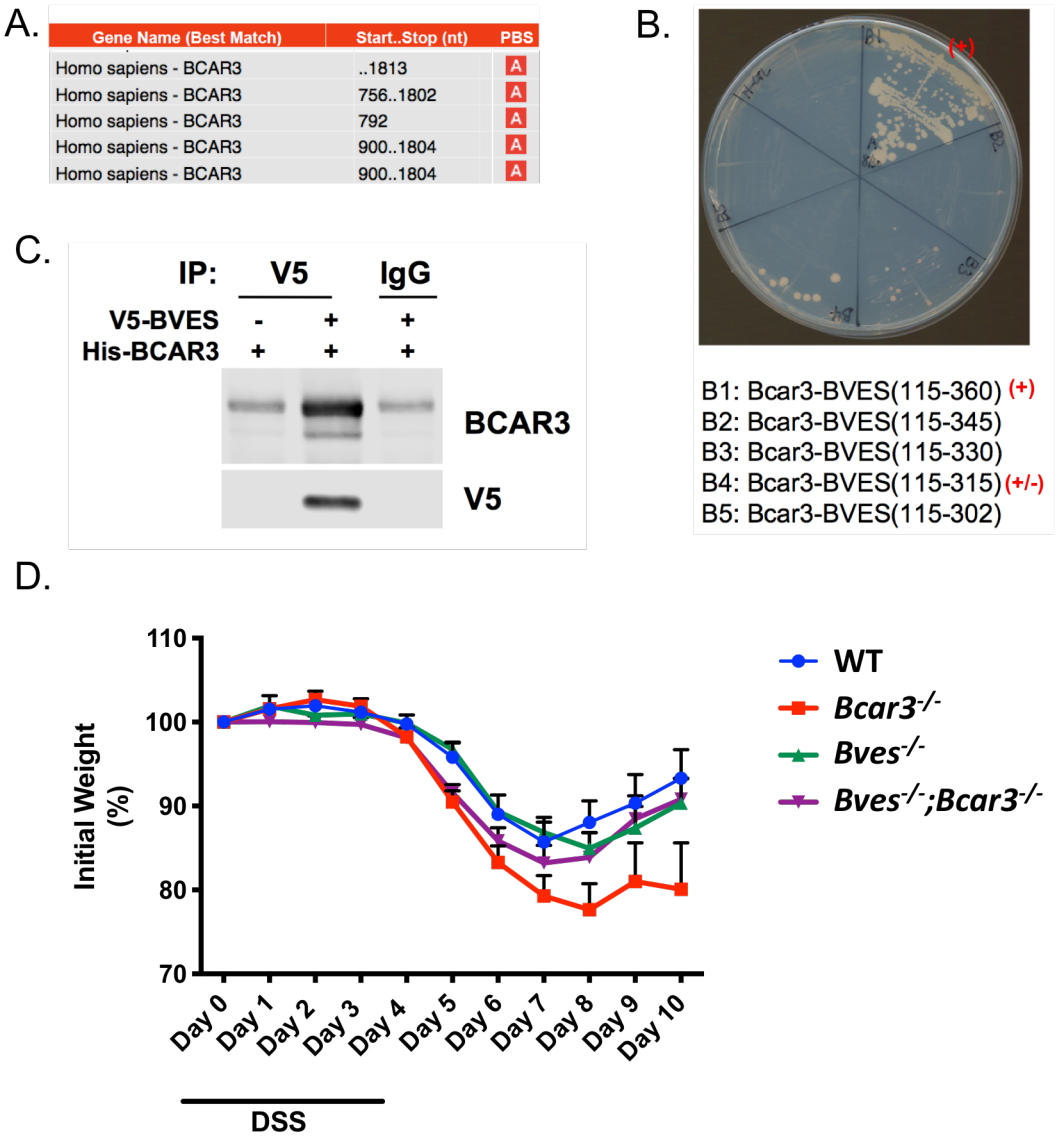

Figure 19. BCAR3 is a BVES binding partner and may coordinate to alter response to DSS colitis. (A) Yeast 2-hybrid commissioned by Hybrigenics identified BCAR3 as a BVES binding partner (B) Direct yeast 2-hybrid using full-length BCAR3 and BVES protein fragments as indicated. Confirmed interaction (+) and likely interaction domain (+/-) (C) V5-tagged BVES (72-350) and a His-tagged BCAR3 were transfected into HEK293 cells. Cells were immunoprecipitated for V5 and IP samples probed for V5 and BCAR3. (D) Mice (WT: n = 8, *Bcar3*$^{-/-}$: n = 7, *Bves*$^{-/-}$: n = 9; , *Bves*$^{-/-}$; *Bcar3*$^{-/-}$: n = 9) were subjected to 4 days of 2% DSS followed by 6 days of recovery with weights measured daily and plotted as a percent of initial starting weight.

BCAR3 is differentially expressed in CRC

Before further characterizing the functional significance of the BVES-BCAR3 interaction, we surveyed BCAR3 expression in human tissue and CRC cell lines. We began by assessing *BCAR3* expression in the Moffitt/Vanderbilt-Ingram Cancer Center colorectal cancer expression array data set (Figure 20A, [41,225]). *BCAR3* was downregulated in early stages of tumorigenesis (Adenoma) as well as throughout all stages of CRC progression. Of note, there was a subset of tumors that appeared to express higher levels of *BCAR3* than the normal mucosa control. Similar results were obtained when analyzing RNA-sequencing data from the TCGA COAD data set (Figure 20B, [96]). To specifically look at matched sets of normal-tumor data, we analyzed *BCAR3* mRNA expression in samples provided through the Cooperative Human Tissue Network (CHTN). Reduced *BCAR3* expression was observed in 64% (7/11) of tumor samples in comparison to patient matched normal colon Figure 20C. Notably, there was considerable heterogeneity in *BCAR3* expression in this subset of samples. We next assessed for BCAR protein levels in 8 of the matched normal and tumor samples from (Figure 20C) and observed similar heterogeneity in protein expression levels. Despite abundant transcript, levels of BCAR3 protein were difficult to detect in the whole tumor tissue lysates so we next assessed BCAR3 protein levels in a panel of CRC cell lines. Overall, we observed heterogeneous BCAR3 protein expression. There was a trend towards lower levels in more epithelial cell lines such as Caco2s and HCA7s. In comparison, the majority of cell lines expressed higher levels of BCAR3 than the matched normal and tumor samples (for example, Figure 21A). The predominant lower band indicated with the black arrow in Figure 20F is BCAR3 (confirmed by shRNA knockdown and overexpression of BCAR3 Isoform 1, Figure 21B) while the upper band (indicated with an *) is only detectable in some cells and may represent a post-translationally modified species or non-specific binding. Finally, to determine how levels of *BCAR3* transcript compare to protein levels, we performed qRT-PCR on

the cell lines from Figure 20F. Overall, there was correlation between transcript levels and protein levels with the highest levels of both protein and mRNA observed in LIM2405 cells. We did note that even within a single cell line, baseline BCAR3 levels varied and therefore performed a density experiment to assess BCAR3 mRNA and protein levels with varying levels of cellular confluency. In HCT116 cells, BCAR3 protein and mRNA levels were dynamic in response to cellular confluency with higher levels of BCAR3 observed with lower confluency. The changes in BCAR3 protein levels cannot be accounted for entirely with changes in mRNA transcript levels, suggesting confluency mediated regulation of BCAR3 protein stability (Figure 21C). Normal colonic epithelial tissue contains robust cell-cell adhesions, mimicking a confluent state, which may partially explain the low levels of BCAR3 observed in the matched normal colonic mucosal tissue (Figure 20E).

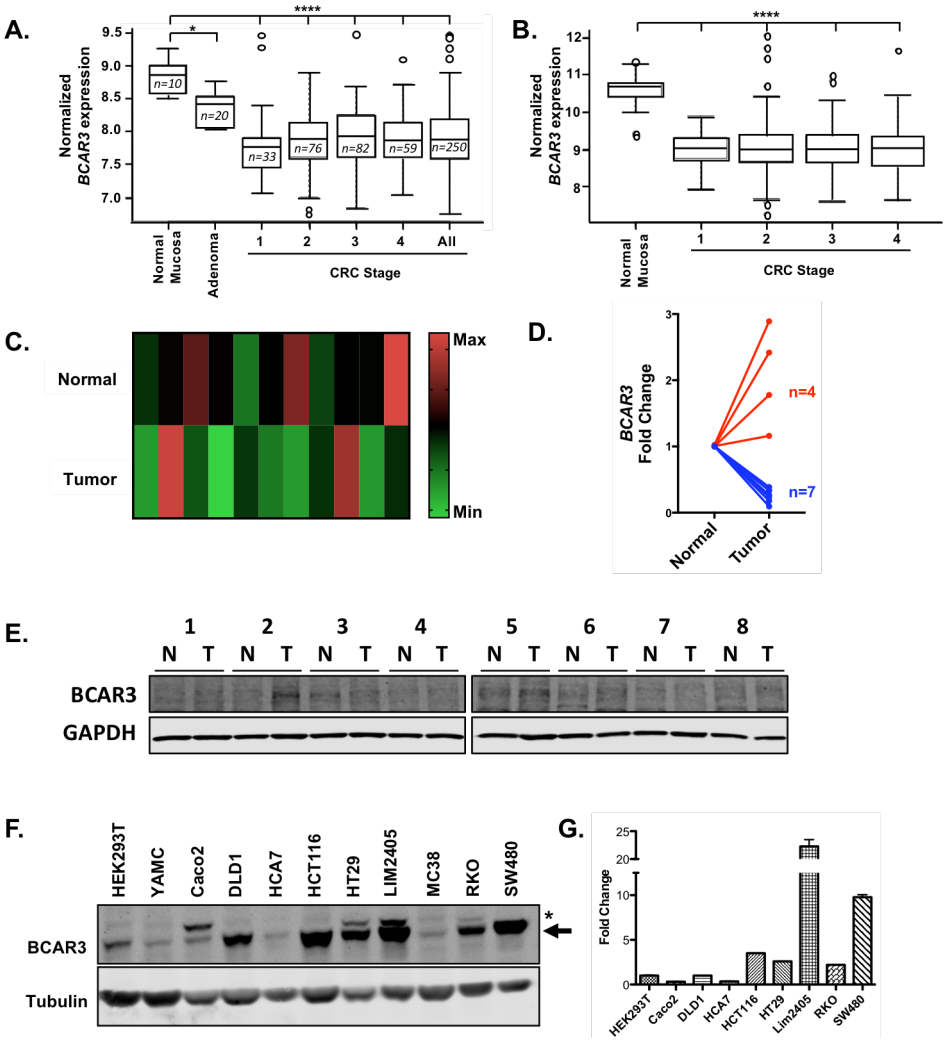

Figure 20. BCAR3 is downregulated in a subset of CRC. (A) Analysis of tumor samples from the combined Moffitt Cancer Center and Vanderbilt Medical Center colon tumor expression array data set. For whisker plots, the bottom and top of the boxes are the 25th and 75th percentile, respectively (the lower and upper quartiles, respectively), and the band near the middle of the box is the 50th percentile (median). The whiskers extend to the most extreme data points, which are no more than 1.5 times the interquartile range from the box. * P = 0.01, **** P < 0.0001. (B) Analysis of TCGA normalized RSEM expression data. Log2 transformed for visualization **** P < 0.0001. (C) Taqman qRT-PCR heatmap of samples from the Cooperative Human Tissue Network (CHTN) demonstrates reduced BCAR3 expression in 64% (n=11) of tumor samples (vs. patient matched normal colon). Values displayed are 1/dCT for each matched sample. (D) Fold change in BCAR3 expression between matched normal and tumor samples from (C). (E) Western blot analysis of n=8 paired normal and tumor samples from (C).(F) BCAR3 protein levels in a panel of CRC cell lines. Band indicated with black arrowis BCAR3. Upper band indicated with * may be non-specific band or a post-translationally modified BCAR3 species. (G) SYBR Green qRT-PCR for human BCAR3 Isoform 1 in human cell lines from (F).

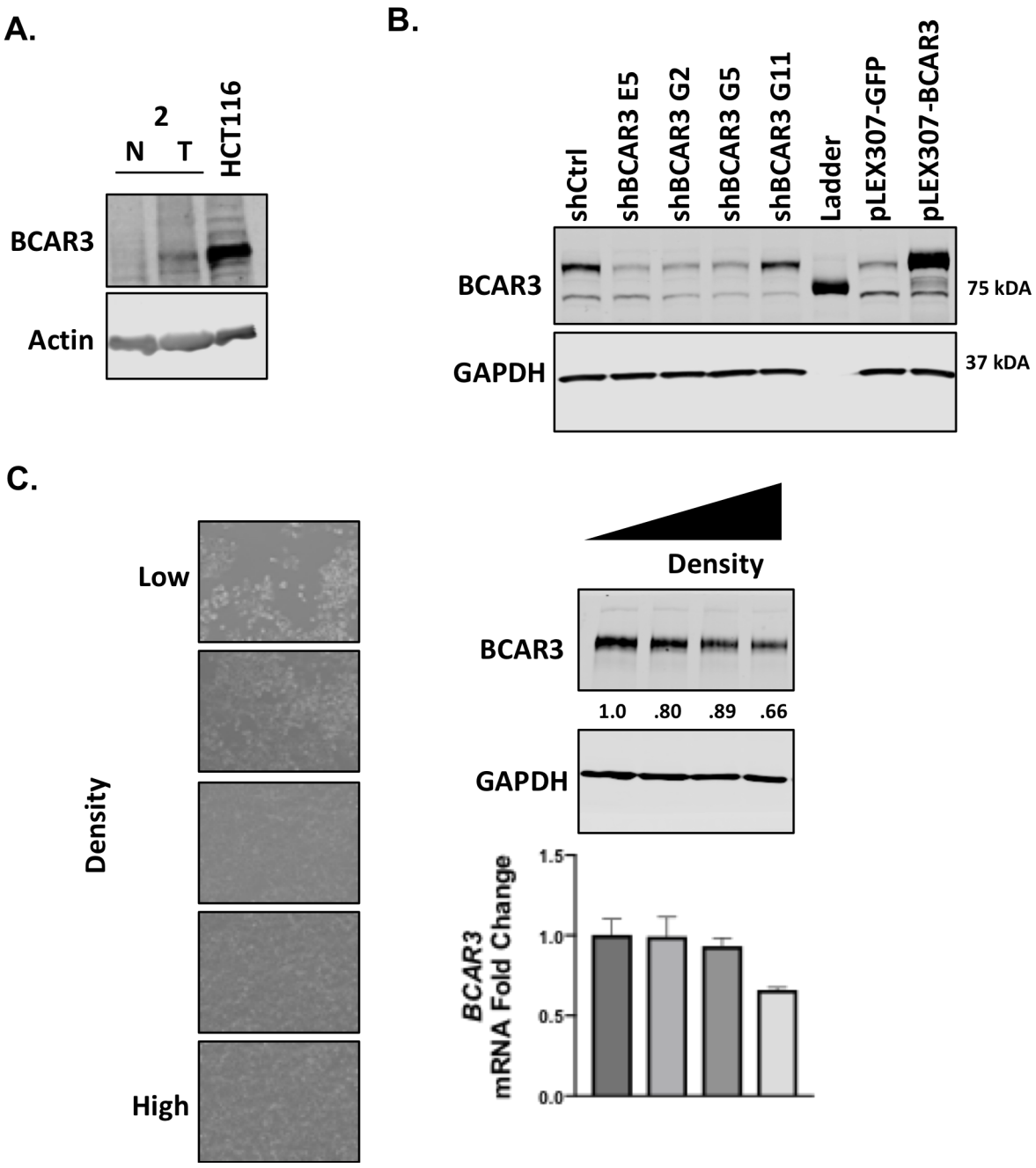

Figure 21. BCAR3 antibody validation and density dependency. (A) Comparison of BCAR3 expression levels between HCT116 cells and matched normal and tumor tissue, set 2 from Figure 20E. (B) Validation of BCAR3 antibody specificity demonstrating reductions in BCAR3 protein levels using a panel of BCAR3 shRNAs. Cells were stably transduced with pGIPZ shCtrl or indicated shBCAR3 constructs. For stable overexpression, cells were transduced with pLEX307-GFP or pLEX307-BCAR3.

BCAR3 augments cellular migration in CRC cells

Previous reports of BCAR3's impact on cellular morphology and migration have focused predominately on its effects in fibroblasts([226]) and breast cancer cell lines ([217], [227], [228], [229], [230], [218]). To our knowledge, there is only one report that identifies a role for BCAR3 in colorectal cancer cell migration [231]. Ibrahim *et al.* show that BCAR3 interacts with HEF1, a Cas family member, and that BCAR3 is required for HEF1-induced cell migration. We therefore sought to further define the role of BCAR3 in CRC cell migration and invasion by generating both shRNA (shBCAR3) and CRISPR/Cas9 (crBCAR3) mediated knockout stable cell lines. For the shRNA lines, a single shRNA construct was used. For the CRISPR/Cas9 knockout lines, 3 different sgRNAs targeting Exon 4 of BCAR3 Isoform 1 were cloned into the lentiCRISPR v2 construct to generate knockout clones with each guide RNA. Individual clones were confirmed to be knockout for BCAR3 by western blot and then 2-3 confirmed knockout clones were pooled together. A similar approach was employed to generate the crCtrl line, which consisted of 6 pooled vector-only control clones. shRNA knockdown and CRISPR/Cas9 knockout were confirmed by western blot (Figure 22A). Transwell migration assays were subsequently performed and demonstrated that BCAR3 knockout reduced migration by over 50% (Figure 22B). In parallel, we utilized an MC38 mouse colorectal cancer cell line that stably overexpressed luciferase (MC38 pLenti-Luc) and overexpressed murine BCAR3/AND34 (mBCAR3) which was confirmed by western blot (Figure 22C). mBCAR3 overexpression increased transwell migration (Figure 22D) and invasion through Matrigel coated chambers (Figure 22E). Together, these data indicate that BCAR3 loss attenuates cell migration and BCAR3 overexpression can augment CRC cell migration.

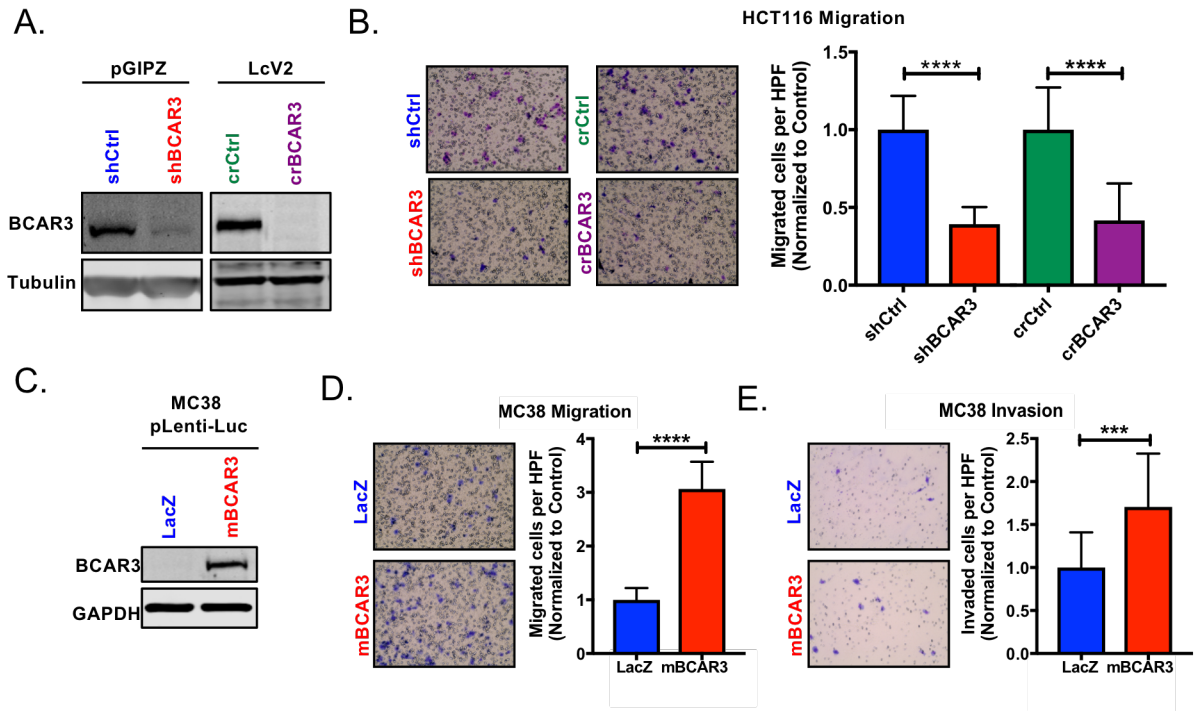

Figure 22. BCAR3 influences CRC cell migration. (A) Western blot confirming BCAR3 shRNA knockdown (shBCAR3) and CRISPR/Cas9 mediated knockout in HCT116 cells (crBCAR3). For the HCT116 LentiCRISPR V2 knockout line, single cell clones from three different guide RNAs were screened for BCAR3 knockout and 8 BCAR3 knockout clones were then pooled. Similarly, the control line (crCtrl) consists of 6 pooled single cell clones. (B) 75,000 cells of the indicated cell lines were plated in the upper chamber of a Boyden chamber and allowed to migrate for 24 hours. Migrated cells were stained using Diff-Quick. Five images were obtained for each insert in triplicate. Representative results from n=3 independent experiments. (C) MC38 murine colon adenocarcinoma cells expressing luciferase were transduced with LacZ or mouse BCAR3 (mBCAR3). Expression was confirmed by western blot. (D) MC38 cells assayed for migration as above at 12 hours and invasion (E) through matrigel coated transwells at 24 hours using Diff-Quick, n=3. All images are original magnification, ×20. Student's t-test was used *P < 0.05, ***P = 0.003, ****P < 0.0001, Student's t-test.

BCAR3 induced cell migration is dependent on p130Cas

The adaptor protein p130Cas has been implicated in a multitude of signaling pathways linked to colorectal cancer progression such as cellular adhesion, migration, invasion, and apoptosis. Additionally, p130Cas is one of two confirmed BCAR3 interacting proteins. Given the link between p130Cas, BCAR3, and cell migration, we sought to determine whether the pro-migratory effects of BCAR3 were dependent on the interaction with p130Cas. p130Cas tyrosine phosphorylation predominately by SRC family kinases at distinct residues such as Tyr249, Tyr410, Tyr668, and Tyr670 have been implicated as direct mediators of signaling downstream of p130Cas but it is well reported that p130Cas can also be extensively serine phosphorylated. Phosphorylation of either tyrosine or serine residues causes an electrophoretic mobility shift of p130Cas on SDS-PAGE gels[228,232-234] and Makkinje *et al.* show that mouse BCAR3 induces this phosphomobility shift predominately via increasing p130Cas serine phosphorylation. Notably, this study utilized murine BCAR3 overexpressed in MCF-7 which may be confounding as murine and human BCAR3 only share ~85% sequence homology. Previous investigations have raised questions as to whether direct binding of BCAR3 with p130Cas is required for the p130Cas phosphomobility shift and BCAR3-mediated augmentation of cell migration. Accordingly, multiple approaches to uncouple the BCAR3-p130Cas interaction have been utilized with somewhat discrepant results. Vanden Borre *et al.* reported that murine BCAR3 can signal independently of p130Cas and that the p130Cas/BCAR3 interaction is not required for BCAR3-mediated anti-estrogen resistance, Rac activation, lamellipodia formation or morphologic changes in BALB/c-3T3 cells[229]. These studies utilized a 743A point mutant in murine BCAR3 and overexpressed BCAR3 in either MCF-7 cells or BALB/c-3T3 cells. Many of the interaction studies addressed interactions between different species of proteins and there are questions as to whether the 743A point mutation completely uncouples the p130Cas/BCAR3 interaction (which may be

dependent on how strong of an ionic detergent is utilized in the lysis buffer). Wallez *et al.* demonstrated that even the more drastic 748E mutation in human BCAR3 (equivalent to residue 743 in mouse BCAR3) can still interact with overexpressed p130Cas to induce p130Cas hyperphosphorylation. To address these discrepancies, we developed a CRISPR/Cas9 knockout/knock-in system to determine the effects of BCAR3 alterations on p130Cas phosphorylation and cell migration in HCT116 cells. Three BCAR3 CRISPR knockout clones generated from a single guide RNA were pooled together and we then took advantage of wobble base pairing to generate a guide RNA-resistant BCAR3 cDNA by introducing point mutations in and around the PAM sequence of our BCAR3 cDNA. This allow for BCAR3 expression in cells constitutively expressing Cas9 and the BCAR3 sgRNA. To generate the p130Cas uncoupling mutant, we introduced two point mutations at L744E and R748E (744/748E) in our sgRNA-resistant BCAR3 construct[219,235]. We had previously confirmed that the 744/748E double mutant more successfully uncoupled the BCAR3-p130Cas interaction compared to either the R748A or R748E mutation alone. While BCAR3 knockout did not appear to reduce p130Cas mobility, BCAR3 overexpression (but not the 744/748E p130Cas uncoupling mutant) lead to an enrichment of the upper p130Cas band (Figure 23A). Admittedly, it does not appear that these bands resolve as well in HCT116 cells as compared to previously reported studies using MCF7 cells. We then confirmed that BCAR3 interacts with p130Cas via reciprocal co-immunoprecipitations (Figure 23B). BCAR3 loss impairs transwell migration which can be rescued with WT BCAR3 expression but not with the 744/748E uncoupling mutant, suggesting that BCAR3-mediated tumor cell migration is dependent on an interaction with p130Cas (Figure 23C). To expand these findings, we utilized the low BCAR3 expressing MC38 cells and overexpressed WT mouse BCAR3, or two different point mutants (R743A and the more drastic R743E, Figure 23D) to determined their interactions with endogenous murine p130Cas and effects

on cell migration. As expected, WT mouse BCAR3 strongly interacts with p130cas while both the 743A and 743E mutants abrogate the BCAR3-p130Cas interaction (Figure 23E). Surprisingly, while both the 743A and 743E mutations significantly reduce the interaction with p130Cas, they still appear to promote p130Cas stabilization and hyperphosphorylation. With regards to migration, overexpression of WT mouse BCAR3 augmented cell migration which returned to near baseline in the 743A or 743E lines. Consistently, the 743E mutant line tended to migrate less robustly than the LacZ control line, suggesting that this mutant may be having a dominant negative effect on endogenous BCAR3 or some neomorphic-anti-migratory effect. Together, these results identify a robust role for the BCAR3-p130Cas interaction in mediating colorectal cancer cell migration.

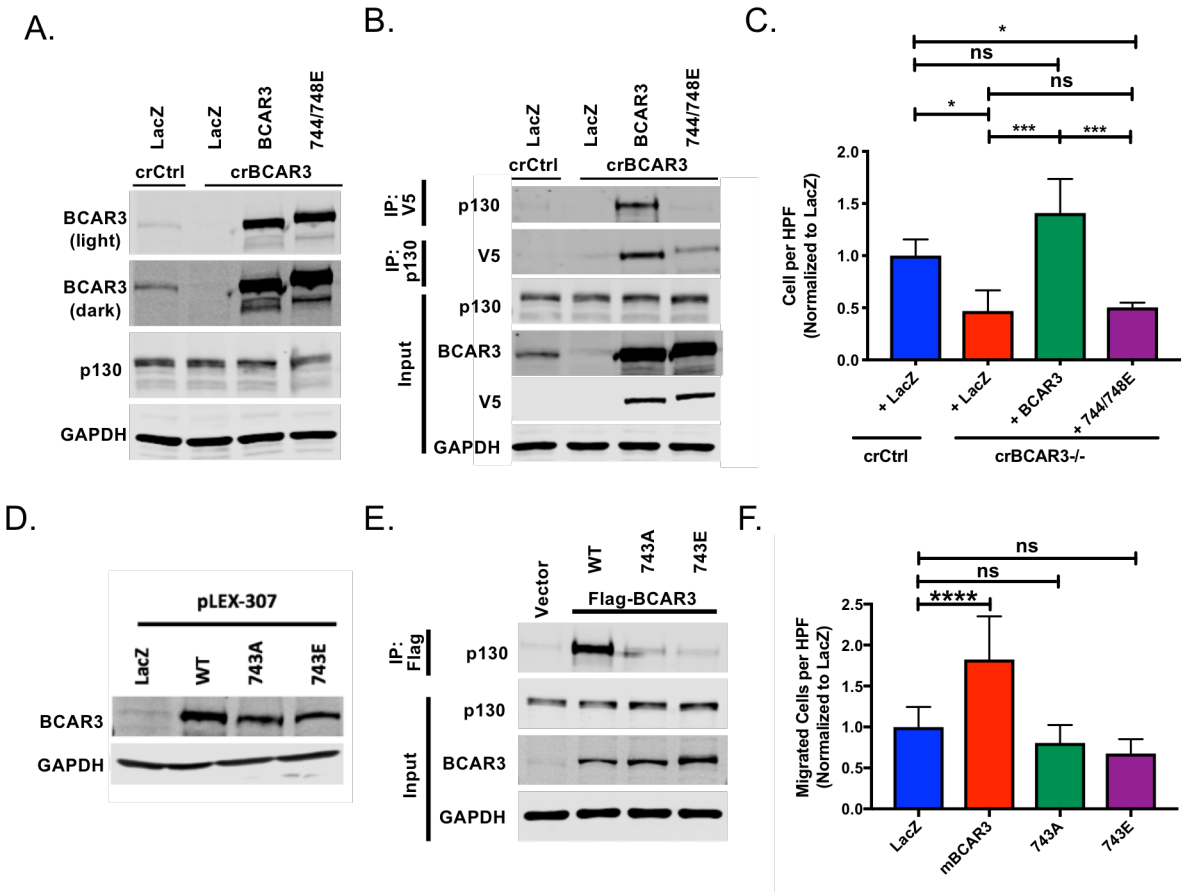

Figure 23. BCAR3's promigratory effects are dependent on an interaction with p130Cas. (A) Western blot confirming cDNA rescue in HCT116 cells with Cas9 guide RNA resistant V5-tagged WT BCAR3 or V5-tagged mutant BCAR3 (744/748E containes two point mutations: L744E and R748E). (B) Reciprocal co-immunoprecipitation with V5 and p130 in HCT116 cells demonstrates marked uncoupling of the BCAR3-p130cas interaction in the 744/748E double mutant. (C) Transwell migration in HCT116 derivatives. 75,000 cells of the indicated cell line were plated in a Boyden chamber and allowed to migrate for 24 hours. Migrated cells were stained using Diff-Quick and five images were obtained per insert in triplicate wells. Data representative of n=3 independent experiments. (D) Western blot confirming stable expression of untagged mBCAR3 and two p130 uncoupling mutants (743A and 743E) in MC38 cells. (E) MC38 cells transiently transfected with flag-tagged WT BCAR3 or point mutants (R743A or R743E equivalent to R748A/E in human BCAR3). Lysates were co-immunoprecipitation with Flag and proved for p130. (F) Transwell migration at 16 hours with stable MC38 cell lines from (D). ns = non-significant, **P = 0.0012, ***P = 0.0009, ****P < 0.0001 by One-Way ANOVA with Tukey multiple comparison testing.

BCAR3 mediated phenotypes are also dependent on the BCAR3 SH2 domain

BCAR3 is a member of the novel SH2-containing protein family and contains an SH2 domain which may mediate interactions with phosphorylated tyrosine residues on proteins that bind BCAR3. Sun *et al.* reported that protein tyrosine phosphatase α (PTPα), a receptor-like protein tyrosine phosphatase, when tyrosine phosphorylated at residue 789, binds BCAR3 and helps recruit p130Cas to PTPα at focal adhesions[236]. An additional report demonstrated that GST-tagged full-length BCAR3 and the SH2 domain of BCAR3 interacted with EGFR only after stimulation with EGF. As expected, full-length BCAR3 also interacted with p130Cas but the SH2 domain alone did not[237]. Analysis of the publicly available BioGRID database identified ERB family members ERBB2 (HER-2) and ERBB3 (HER3) by yeast-two-hybrid as BCAR3 interactors. Functionally, BCAR3 upregulation has also been identified in Trastuzumab resistant clones of the SkBr3 breast cancer cell line, which overexpresses HER2, suggesting that BCAR3 may regulate signaling downstream of HER2 and that BCAR3 may be involved in resistance to multiple therapeutic agents[238]. To test whether the BCAR3 SH2 domain may play a role in modulating cell migration or alter the BCAR3-p130Cas interaction, an interstitial mutant lacking the conserved BCAR3 SH2 domain (amino acids 154-234) was created. Both WT BCAR3 and the Delta SH2 mutant interact with p130Cas (Figure 24A, top panel). Treatment with the EGFR ligand EGF did not significantly alter the BCAR3-p130Cas interaction. Notably, overexpression of full-length V5-tagged BCAR3 but not the Delta SH2 mutant increased p130Cas hyperphosphorylation. As the Delta SH2 mutant still interacts with p130Cas but BCAR3 has no known kinase or phosphatase activity, the SH2 domain may be required to recruit an intermediary protein that augments p130Cas phosphorylation. Notably, WT BCAR3 increased SRC electrophoretic mobility in a similar fashion to that of p130Cas but in this instance, the SH2 mutant did as well. Therefore, BCAR3 and the BCAR3 SH2 mutant differentially affect p130Cas electrophoretic

mobility but similarly augment SRC electrophoretic mobility. SRC electrophoretic mobility has been reported to change with cell density[239] and with tyrosine phosphorylation [240] but the exact post-translational modification induced by BCAR3 expression is unknown and will require further investigation. Src phosphorylation at Tyr416 increases Src kinase activity while phosphorylation at Tyr 527 reduces enzyme activity[241] and both likely augment electrophoretic mobility so while the SRC migration pattern is similar between WT-BCAR3 and SH2-mutant BCAR3, SRC activation may be different. Despite prior reports, we were unable to detect an interaction with EGFR (without or with EGF stimulation). To assess the effect of the SH2 domain on transwell migration, we plated serum starved cells in the upper transwell chamber in low serum media and added complete media or complete media + EGF to the lower chamber. Consistent with our prior observations, BCAR3 overexpression increased cell migration which was dependent on the BCAR3 SH2 domain (Figure 24B). Treatment with EGF minimally affected cell migration, perhaps owing to the use of complete media as the chemoattractant which alone promotes significant migration. These data implicate the SH2 domain in altering p130Cas phosphorylation and BCAR3-induced cell migration.

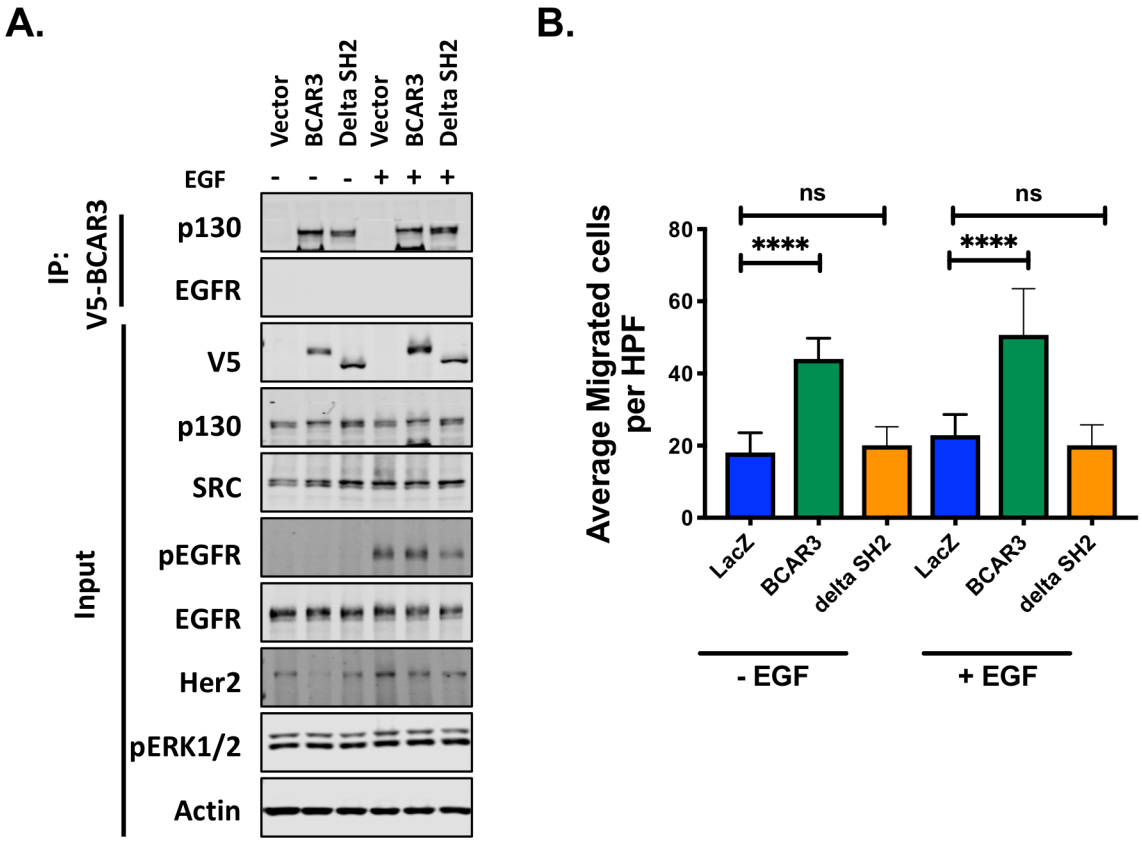

Figure 24. The SH2 domain of BCAR3 is required for p130Cas hyperphosphorylation and enhanced cell migration. (A) Western blot demonstrating overexpression of WT-BCAR3 or the BCAR3 Delta SH2 interstitial mutant (which lacks the conserved SH2 domain, amino acids 154-234). Cells were serum starved overnight (0.1% FBS) then treated with EGF 100 ng/mL for 15 minutes before harvest. V5-tagged BCAR3 was immunoprecipitated with anti-V5-magnetic beads and subjected to Western Blotting. (B) Cells were serum starved overnight (0.1% FBS) then 100,000 cells were plated in the upper chamber of the transwell and complete media or complete media + 100 ng/mL EGF was added to the bottom. Cells were allowed to migrate for 24 hours. Migrated cells were stained using Diff-Quick and five images were obtained per insert in triplicate wells. Data representative of n=3 independent experiments. ns = non-significant, ****P < 0.0001 by One-Way ANOVA with Tukey multiple comparison testing.

Time and cell line dependency of BCAR3 mediated cell migration

To further assess the contribution of BCAR3 to CRC cell migration, we performed additional experiments looking at longer time points and also utilized additional cell lines. Utilizing the HCT116 CRISPR knockout/rescue cell lines from Figure 23C, we assessed transwell migration at 24, 33, and 48 hours, plating all cells at the same density at the same time. At 24 hours, BCAR3's effects on cell migration were identical to that observed previously. BCAR3 knockout reduced transwell migration which could be rescued with WT, but not the p130Cas uncoupling mutant (Figure 25A). However, as the time point was extended, there was a trend towards increased cell migration with BCAR3 knockout (Figure 25B and Figure 25C). Consistently, rescued BCAR3 expression increased cell migration (Figure 25A, Figure 25B, and Figure 25C, Green bars) while the p130Cas uncoupling mutant demonstrated lower transwell migration than WT-BCAR3 (Figure 25A, Figure 25B, and Figure 25C, Purple Bar). As time progressed, cells with BCAR3 knockout actually began to migrate better. We do not believe that these changes are due to proliferative changes as we have not seen significant changes in *in vitro* proliferation and if anything, we would expect BCAR3 knockout cells to proliferative less readily. To determine if this observation was limited to one cell line, we used CRISPR to knockout BCAR3 in the SW480 CRC cell line. Because of the concern for clonal effects with CRISPR knockout screening, we generated high-titer lentivirus and used pooled populations of control or crBCAR3 knockout cells. Surprisingly, BCAR3 knockout in SW480s consistently increased transwell migration (Figure 25D) at 24 hours. Notably, BCAR3 expression is nearly 8-fold lower in the SW620 cell line, an isogenic cell line derived from a lymph node metastasis in the same patient (GEO Dataset GDS1780), supporting the notion that BCAR3 loss can promote cell migration and metastasis. One hypothesis for these results stems from findings that BCAR3 interacts with PTPα. This interaction could direct PTPα to dephosphorylate any number of RTKs, with EGFR being a

prime candidate, thereby reducing downstream signaling which would otherwise promote cell migration. Thus, BCAR3 knockout cells may be more sensitive to chemoattractant gradients because of a higher level of RTK activation. We tested this hypothesis by looking at baseline ERB family receptor levels and phosphorylation (Figure 26A). Initially results were encouraging as we observed increased total EGFR receptor levels as well as increased phosphorylation of EGFR after EGF stimulation (Figure 26A). ERBB2/HER-2 levels were relatively unchanged but there was a subtle increase in ERBB3/HER-3 and phospho-AKT (S473) with BCAR3 knockout. However, upon repeating this experiment, total EGFR levels and pEGFR levels were lower with BCAR3 knockout. The subtle increases in ERBB3/HER-3 and phospho-AKT (S473) were reproducible (Figure 26B). In this experiment, p130Cas levels were reduced with BCAR3 loss (which is consistent with the literature) and low dose EGF stimulation appeared to increase p130Cas levels, which again were reduced with BCAR3 knockout. The higher (100 ng/μL) dose of EGF did not dramatically alter p130Cas levels, suggesting complex dose and time-dependent interplay within the EGFR/BCAR3/p130Cas axis. Tight temporal and dose-dependent regulation of EGFR signaling have been previously reported[242-244]. We then rescued BCAR3 loss with WT-BCAR3, the p130Cas uncoupling mutant (744/748E), or the SH2 domain mutant (Delta SH2). BCAR3 knockout and rescue were confirmed by western blot (Figure 26C). In this experiment, BCAR3 knockout increased transwell migration which was reduced with WT-BCAR3 expression. Both the p130Cas uncoupling mutant and the Delta SH2 mutant migrated better than control lines. Perhaps, as was hypothesized with the HCT116 cells, BCAR3 sets the tone by which cells respond to environmental stimuli. Under the right conditions, BCAR3 loss could enhance growth factor responsiveness to overcome any actin/cytoskeletal remodeling deficiencies also conferred by BCAR3 loss. These data further add to the complexity of BCAR3 mediated transwell migration

and suggest distinct, cell-line, temporal, and context specific contributions to migration and cell signaling.

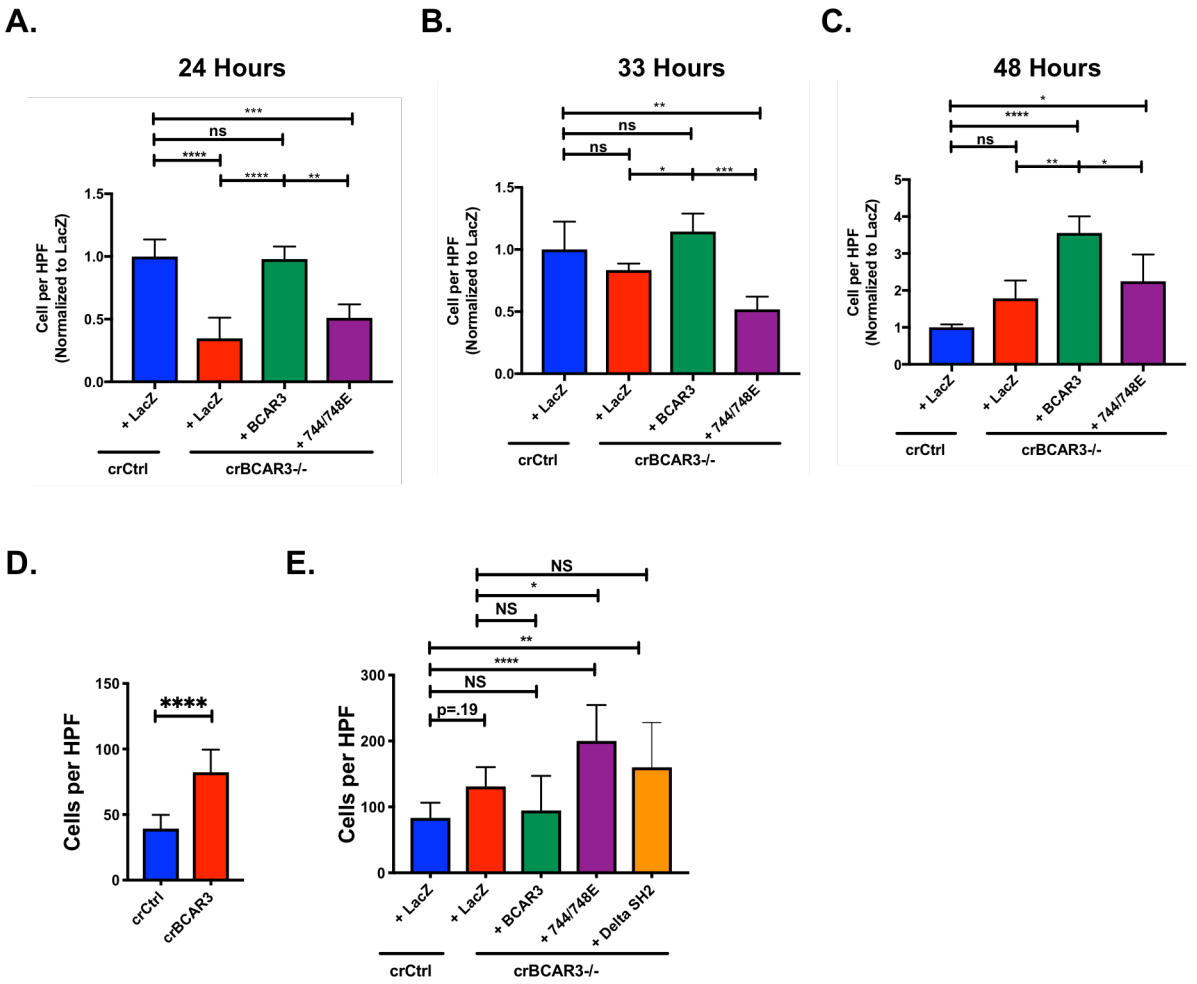

Figure 25. Temporal and cell-line dependent modulation of cell migration by BCAR3. Transwell migration in HCT116 derivatives. 100,000 cells of the indicated cell line were serum starved overnight and then plated in a transwell migration chamber and allowed to migrate for (A) 24 hours, (B) 33 hours, or (C) 48 hours. Migrated cells were stained using Diff-Quick and five images were obtained per insert in triplicate wells. Data representative of n=1 independent experiments. (D) Transwell migration assay in SW480 crCtrl and crBCAR3 lines. Cells were serum starved overnight and then 100,000 cells were plated in the upper chamber of a transwell. Cells were allowed to migrate for 24 hours before staining and imaging as in (C). (E) SW480 crCtrl and crBCAR3 with or without BCAR3 rescue for transwell migration as in (D). For (A), (B), (C), and (E), ns = non-significant, *P < 0.05, **P < 0.01, ***P < 0.001, ****P < 0.0001 by One-Way ANOVA with Tukey multiple comparison testing. For (D), ****P < 0.0001 by Student's *t* test.

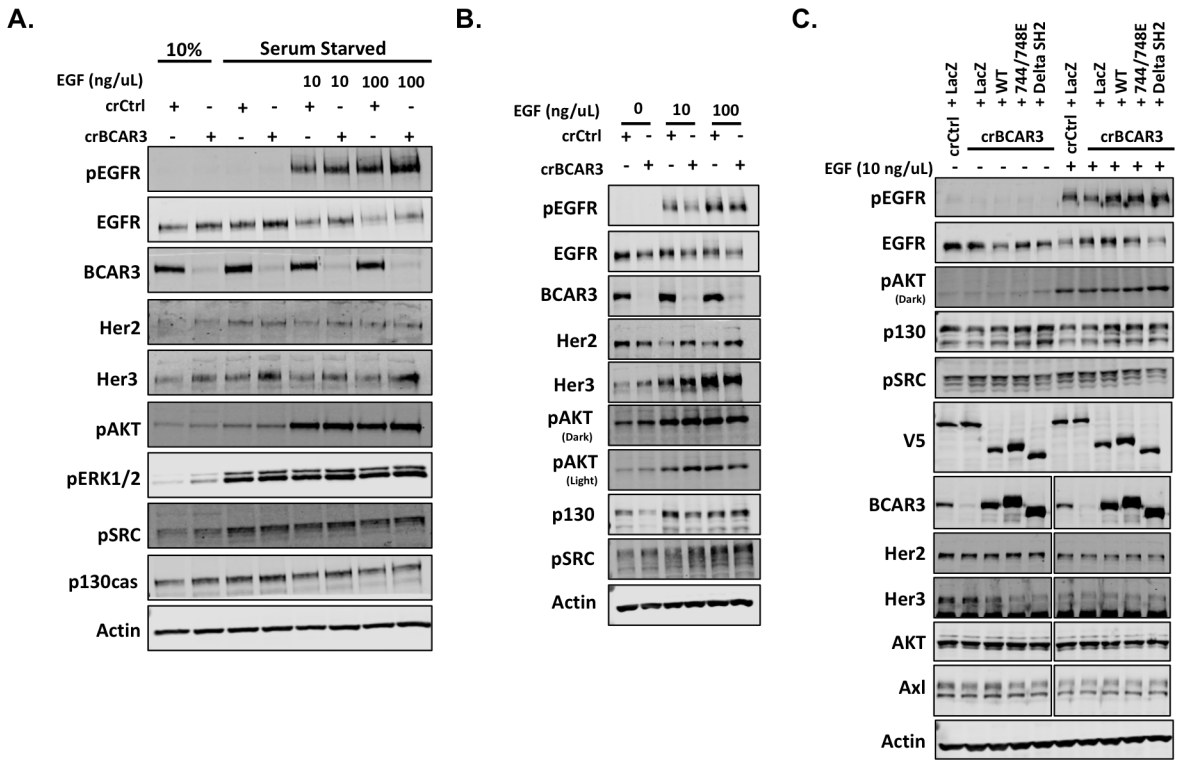

Figure 26. Effects of BCAR3 loss on ErbB members and downstream signaling. (A) and (B) SW480 crCtrl and crBCAR3 lines were grown in complete media or serum-starved (0.1% FBS) overnight as indicated. The following morning, low-serum media (0.1% FBS) or low-serum media plus 10 ng/mL or 100 ng/mL EGF were added to the serum starved cells. Cells were lysed in RIPA buffer and western blotting performed. (C) SW480 crCtrl and crBCAR3 with or without LacZ addback (control transduction) or rescue with WT BCAR3, p130Cas uncoupling mutant (744/748E), or Delta SH2 mutant were serum starved overnight then stimulated with 10 ng/mL EGF. For the BCAR3, Her2, Her3, AKT, and AXL blots, a lane was skipped between the minus EGF and plus EGF conditions. This lane has been cropped to allow proper alignment with the rest of the panel but the images shown are from the same western blot with identical exposures.

BCAR3 increases tumor growth *in vivo*

We next examined whether BCAR3 alters *in vivo* tumor growth using subcutaneous tumor injections. We observed no differences in cell viability (as measured using Cell-titer Glo, a luminescent ATP-based assay) *in vitro* which led us to hypothesize that BCAR3 may be mediating signaling downstream of growth factors or tumor cell-extracellular matrix interactions that cannot be appropriately modeled in tissue culture plates. We injected the HCT116 CRISPR knockout/rescue cell lines subcutaneously into NOD/SCID mice and monitored tumor growth every three days once palpable tumors were observed. Tumor volumes were calculated using the modified ellipsoidal formula (volume = ½(Length x ($Width^2$))[245]. BCAR3 overexpression in the "crBCAR3 + BCAR3" significantly augmented tumor volumes when compared to both the "crCtrl + LacZ" cell line and the "crBCAR3 + LacZ" cell lines (Figure 27A and Figure 27B). This mitigates any concern that the observed differences were due to clonal effects during the derivation of individual cell clones as the same three pooled BCAR3 knockout clones expressed either the LacZ-control or BCAR3. The p130Cas uncoupling mutant (744/748E) did not augment tumor volume, suggesting that BCAR3 may be acting in concert with p130Cas to promote tumor growth. We next isolated the xenografts and fixed the tissue to allow immunohistochemical analysis. Consistent with the tumor size data, BCAR3 overexpression significantly increased intratumoral proliferation as measured by phosphor-Histone H3 (Figure 27C). The LacZ control vector and BCAR3 expression vectors contained a V5-epitope tag, which allowed for co-staining and quantification specifically of V5/pH3 double positive proliferating tumor cells. Similar experiments were performed using the MC38-BCAR3 expressing cell lines in syngeneic C57Bl/6 mice. BCAR3 overexpression augmented subcutaneous allograft tumor volume and tumor weight (Figure 27D, Figure 27E, and Figure 27F). These data support a pro-proliferative role for BCAR3 in HCT116 and MC38 subcutaneous tumor models.

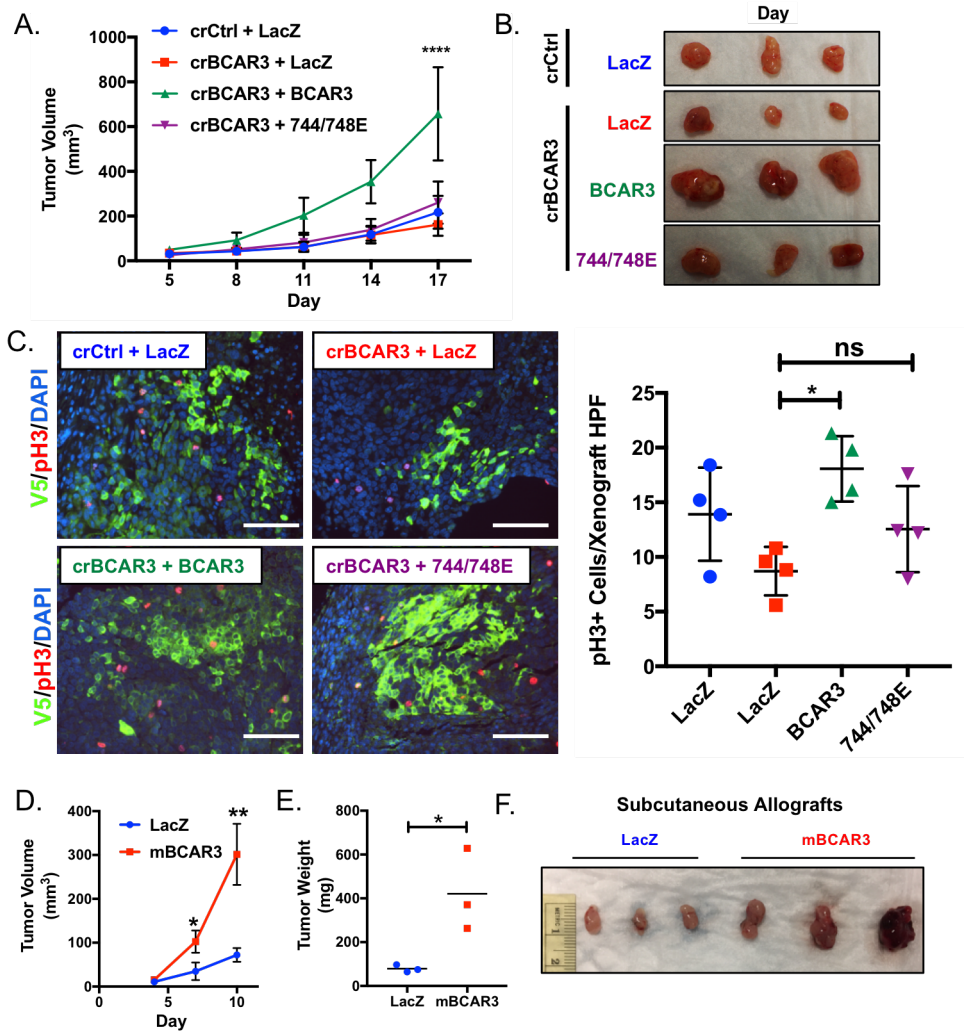

Figure 27. BCAR3 augments tumor growth *in vivo*. (A) $5x10^6$ HCT116 cells with CRISPR knockout or rescue were injected subcutaneously into NOD/SCID mice and allowed to grow. Once palpable tumors were observed, tumors were measured and volumes calculated using the modified ellipsoidal formula. n=6 mice per group. (B) Representative xenografts at harvest. (C) HCT116 xenografts immunohistochemistry. V5 labels tumor cells and phospho-Histone H3 (pH3) indicates proliferating cells of which only the double positive cells were quantified. Data are from n = 4 tumors per line with quantification from at least five images per tumor. (D) (E) (F) Luciferase expressing MC38 cells were transduced with LacZ or mouse BCAR3 (mBCAR3) and injected subcutaneously into syngeneic C57BL/6 mice. (D) Tumor volume and (E) tumor weights at harvest. (F) Gross images of resected tumors. For (A), **** $P < 0.0001$ compared to crCtrl + LacZ or crBCAR3 + LacZ group by Two-Way ANOVA with Dunnett multiple comparison testing. For (C), * $P < 0.05$ by Kruskal-Wallis test with Dunn's multiple comparisons testing. ns = non-significant. For (D) and (E), * $P < 0.05$ and ** $P < 0.01$ by Student's t-test.

BCAR3 loss augments *in vivo* tumorigenesis

BCAR3 is downregulated in human colorectal cancer, therefore we next asked the question of whether BCAR3 loss could modify Wnt-dependent tumorigenesis. Mutations in the Wnt signaling pathway are common initiating events, occurring in nearly 90% of all CRCs[96]. We utilized the *Lrig1-CreER* driver[19], which facilitates Cre expression in stem and progenitor cells within the intestinal epithelium to drive loss of one allele of *Apc.* Through stochastic loss of the second *Apc* allele, these mice develop Wnt-driven tumors in the small intestine and distal colon. This model has been previously utilized in our laboratory [246]. The *Bcar3*$^{-/-}$ mice have been previously reported. Phenotypically, the *Bcar3*$^{-/-}$ mice develop eye lesions and posterior lens rupture along with reductions in AKT S473 phosphorylation but no other over phenotypes[247]. Tamoxifen was administered to drive *Lrig1-CreER* activation and mice were harvested after 100 days to assess for tumor burden (Figure 28A). Prior to sacrifice, colonoscopies were performed to assess tumor burden (Figure 28B). *Lrig1-CreER*;*Apc*$^{fl/+}$;*Bcar3*$^{-/-}$ mice exhibited increased colonic tumor multiplicity compared to age-matched littermate controls (Figure 28C), suggesting that *Bcar3* loss augments tumorigenesis which is consistent with the human expression data. Interestingly, the *Bcar3*$^{-/-}$ tumors were also smaller (Figure 28D and Figure 28E). Upon histologic examination of tumors of similar size, the *Bcar3*$^{-/-}$ tumors also demonstrated a reduction in complex crypt architecture suggestive of reduced dysplasia. Together, these data reinforce the prior findings demonstrating that reductions in BCAR3 promote intestinal tumorigenesis but higher levels of BCAR3 within a tumor can promote tumor growth.

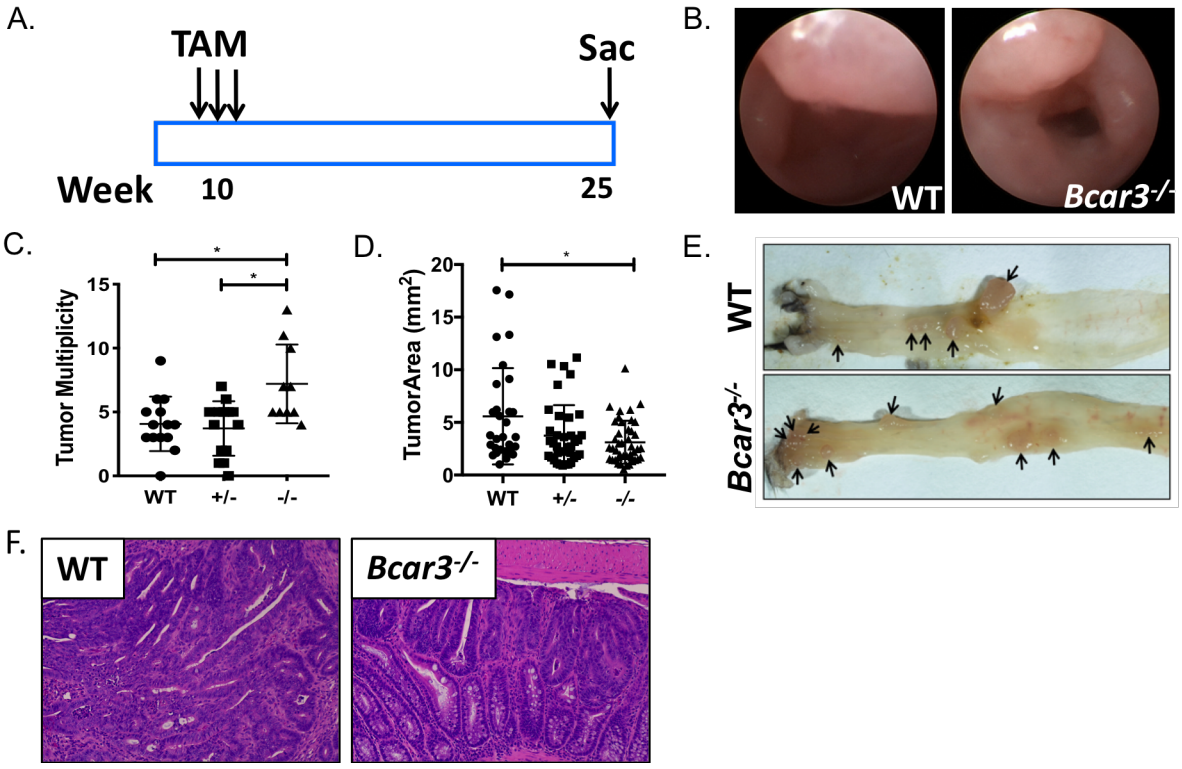

Figure 28. BCAR3 loss augments tumor number but reduces tumor size *in vivo*. (A) Schematic demonstrating *Lrig1-CreER*;*Apc*$^{fl/+}$;*Bcar3* tumor induction scheme. 10-week old mice are injected intraperitoneally with 2mg of Tamoxifen on 3 sequential days. Mice are then aged 15 weeks (~105 days) before harvest. (B) Representative endoscopic tumors in *Lrig1-CreER*;*Apc*$^{fl/+}$;*Bcar3*^{WT} and *Lrig1-CreER*;*Apc*$^{fl/+}$;*Bcar3*$^{-/-}$ mice. (C) Colonic Tumor multiplicity. n = 14 WT, n =14 *Bcar3*$^{+/-}$, and n = 10 *Bcar3*$^{-/-}$ mice per group. (D) Average tumor Area calculations (Area = Length x Width) from *Lrig1-CreER*;*Apc*$^{fl/+}$;*Bcar3* mice. (E) Gross image of *Lrig1-CreER*;*Apc*$^{fl/+}$;*Bcar3*^{WT} and *Lrig1-CreER*;*Apc*$^{fl/+}$;*Bcar3*$^{-/-}$ distal colons. Black arrows indicate quantified tumors. (F) Representative histology from *Lrig1-CreER*;*Apc*$^{fl/+}$;*Bcar3*^{WT} and *Lrig1-CreER*;*Apc*$^{fl/+}$;*Bcar3*$^{-/-}$ tumor bearing mice. For (C) and (D), * $P < 0.05$ by Kruskal-Wallis test with Dunn's multiple comparisons testing.

Enteroid morphology and Wnt pathway alterations in *Bcar3*$^{-/-}$ mice

Increased Wnt signaling helps initiate colorectal cancer and promote tumor progression[248]. Given the increased tumor multiplicity with *Bcar3* knockout, we hypothesized that BCAR3 loss may be enhancing Wnt signaling to promote tumor initiation. To test this, we isolated small intestinal enteroids from non-tumor bearing WT and *Bcar3*$^{-/-}$ mice to assess for morphological and transcriptional changes suggestive of enhanced Wnt signaling. *Bcar3*$^{-/-}$ enteroids displayed increased branching patterns compared to WT mice (Figure 29A). Additionally, a majority of the branches displayed a more cystic structure (Figure 29B) which has been linked with hyperactive Wnt signaling (tumoroids derived from *Apc*^{Min} adenomas grow as large cystic spheroids). While the branching phenotype is less well described, we posited that it may be due to expansion of the stem cell compartment, which is closely linked with hyperactive Wnt signaling[249]. In support of this, *Bcar3*$^{-/-}$ enteroids displayed increased expression of the Wnt targets *Lgr5, Axin2, and c-Myc* (Figure 29C). To further assess this, we crossed the *Lgr5-eGFP-IRES-creERT2* reporter mouse with the *Bcar3*$^{-/-}$ mice and assessed the number of LGR5+ stem cells in each crypt. There were no significant differences in LGR5+ stem cell number in the small intestine (Figure 29D) or the colon (Figure 29E), suggesting that the increased branching of *Bcar3*$^{-/-}$ enteroids is not due to an increase in the number of stem cells. Additionally, there were no changes in *Lgr5* or *Axin2* transcript levels in the small intestine (Figure 29F and Figure 29G) or colon (Figure 29H and Figure 29I). These data suggest that the enhanced tumorigenesis in the *Bcar3*$^{-/-}$ mice is not a direct result of differences in basal Wnt tone between the WT and *Bcar3*$^{-/-}$ mice.

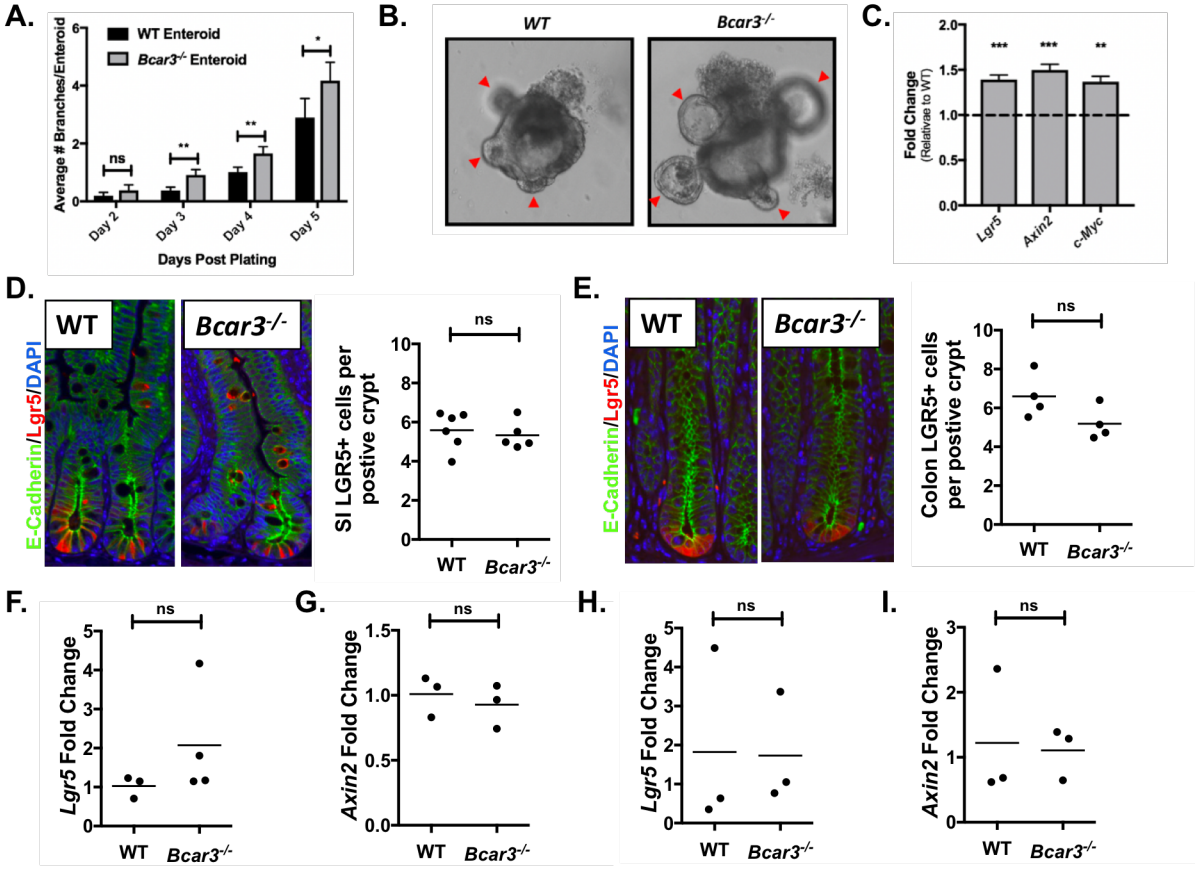

Figure 29. Loss of BCAR3 increases enteroid branching and expression of Wnt targets *in vitro* but not *in vivo.* WT and *Bcar3*$^{-/-}$ small intestine crypts were isolated from 8-week old mice and plated in 3D matrigel cultures. (A) *Bcar3*$^{-/-}$ enteroids have increased branches at Day 3, Day 4, and Day 5 post plating. (B) Day 5 *Bcar3*$^{-/-}$ enteroids branches are larger and exhibit more spheroidal morphologically than WT enteroids. Arrows indicate quantified branches in each image. (C) Expression of Wnt targets Lgr5, Axin2, and Myc is increased in *Bcar3*$^{-/-}$ enteroids. Fold change values are relative to WT. (D) and E) *Lgr5*-eGFP reporter mice were crossed with *Bcar3*$^{-/-}$ mice. Lgr5+ stem cells were stained via GFP immunofluorescence and quantified in the small intestine (D) and colon (E). n = 4-5 mice per group with a minimum of 20 crypts quantified and averaged per mouse. (F) Small intestine expression of *Lgr5* and (G) *Axin2*. n = 3-4 mice per group. (H) Colonic expression of *Lgr5* and (I) *Axin2*. ns = nonsignificant, * $p<0.05$, ** $p<0.01$, *** $p<0.001$ by Mann-Whitney test.

BCAR3 regulation of TGFβ dependent phenotypes and signaling

The duality of phenotypes associated with BCAR3 loss (some pro-tumorigenic and some anti-tumorigenic) are reminiscent of another well described pathway in colorectal cancer progression: the TGFβ pathway. Nearly 30 percent of non-hypermutated CRCs and 87% of hypermutated tumors harbor genomic alterations in TGFβ signaling[96]. Paradoxically, TGFβ can inhibit the proliferation of normal colonic epithelial cells, thereby supporting its role as a tumor suppressor, but TGFβ also promotes the survival, invasion, and metastasis of cells by regulating cell intrinsic qualities such as adhesion and motility as well as cell extrinsic factors such as the composition of the extracellular matrix [250,251]. Guo *et al.* reported that BCAR3 can inhibit TGFβ induced phosphorylation of Smad3 in MCF-7 cells and that BCAR3 knockdown promotes TGFβ induced cell migration. Furthermore, in this study of human breast cancer patients, low BCAR3 expression was associated with poor prognosis (reduced disease-free survival, reduced distant metastasis-free survival, and reduced relapse-free survival with low BCAR3 expression), indicating that higher BCAR3 expression promotes disease-free survival[252]. Therefore, BCAR3 may be acting as a putative tumor suppressor in breast cancer by inhibiting prometastatic signaling downstream of TGFβ. Similarly, van Agthoven *et al.* reported that high levels of BCAR3 were associated with favorable progression free survival in a cohort of 242 estrogen receptor-positive patients treated with Tamoxifen (OR: 1.55; 95% Confidence Interval 1.06 – 2.66, P = 0.022). Further adding to the allure of this enigmatic protein is the fact that BCAR3, named as such because its upregulation promoted tamoxifen resistance, is actually associated with a favorable response to tamoxifen therapy (OR: 1.52; 95% Confidence Interval 1.00 – 2.30, P = 0.045). The authors highlight this finding elegantly, stating that BCAR3 "exhibits discordant associations" and that "findings in breast cancer cell models may differ from observations in clinical tumor samples"

[253]. To test whether or not BCAR3 modulates TGFβ signaling in CRC, we first performed siRNA knockdown of BCAR3 in SW480 cells as we had previously observed pro-migratory phenotypes in this cell line following BCAR3 knockout. Of note, SW480 and HT29 cells are Smad4 deficient and therefore lack canonical TGFβ signaling[254], though there are reports that they may still exhibit some EMT associated phenotypes following TGFβ treatment[255]. To that end, TGFβ treatment following BCAR3 knockdown in SW480 cells did not significantly alter cell morphology or expression of genes associated with TGFβ-induced mesenchymal phenotypes (Figure 30A and Figure 30B). There was, however, a trend towards increased expression of Fibronectin following BCAR3 knockdown. Aberrant expression of Fibronectin, a matrix glycoprotein, is common in cancer and may promote tumor progression[256]. While downstream signaling is likely inhibited in SW480 cells, both SW480 and HT29 cells express wildtype TGFBR2 and may remain responsive to upstream signaling, therefore allowing for assessment of phospho-Smad2 and phospho-Smad3 levels. In contrast to prior reports demonstrating regulation of phospho-Smad3 levels by BCAR3, we observed no significant changes in Smad phosphorylation following BCAR3 knockout (Figure 30C). Additionally, Smad phosphorylation was nearly undetectable in HT29 cells. Further studies, particularly in cells with an intact TGFβ signaling axis, will be required to determine whether BCAR3 loss may promote tumorigenesis by altering signaling cascades downstream of TGFβ.

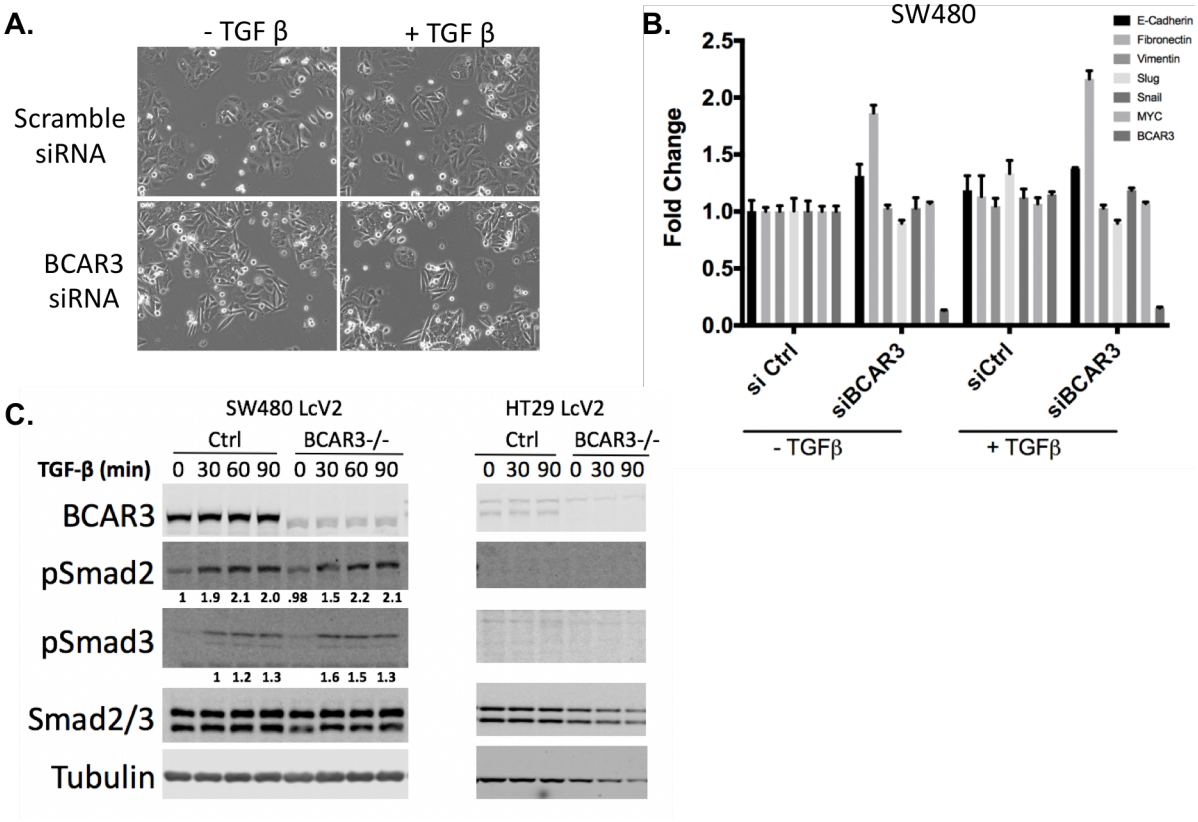

Figure 30. BCAR3 loss does not alter TGFβ signaling in CRC cell lines. (A) SW480 cells were transfected with siRNAs targeting BCAR3 or with scramble control siRNAs using Lipofectamine RNAiMAX. 24 hours later, the media was changed to 0.5% FBS + 10 ng/mL TGFβ or vehicle control. Cells were maintained for 48 hours (72 hours post siRNA knockdown) before imaging. (B) SW480 cells treated in parallel to cells from (A) harvested for RNA and qRT-PCR. (C) Western blot analysis of pooled SW480 and HT29 CRISPR Ctrl and CRISPR BCAR3 knockout cell lines. Cells were serum starved overnight then treated with 5 ng/mL TGFβ diluted in 0.5% FBS for the indicated time points.

Discussion

Originally identified as a gene that confers resistance to the anti-estrogen tamoxifen, BCAR3 has subsequently been implicated in the regulation of a number of cellular processes related to cell adhesion and migration. *In vitro* studies have demonstrated that BCAR3 expression promotes breast cancer cell proliferation, motility, and invasion. Thus, one may expect that BCAR3 functions as an oncogene and that tumors would select for cells with high BCAR3 expression. However, we observed significant downregulation of *BCAR3* expression across a large sample of human colorectal cancers suggesting that BCAR3 may function as a tumor suppressor and that loss of BCAR3 promotes tumorigenesis. Whether the observed BCAR3 levels within a tumor cell (high or low) are actually drivers of disease progression or set secondarily by extracellular and environmental stimuli is unknown. Clinically, low BCAR3 expression has been associated with poor prognosis in breast cancer patients while patients with high BCAR3 expression demonstrated an increase in progression free survival[252,253]. More recently, Zhang *et al.* found that high BCAR3 expression predicted a better prognosis in patients with multiple myeloma and that low BCAR3 expression may predict early relapse. Notably, within our data there were subsets of tumors that expressed high levels of BCAR3 when compared to normal mucosa. Perhaps there is a subset of CRC tumors, likely with distinct mutational profiles, that coordinate with differential BCAR3 expression to augment tumorigenesis. Efforts to define distinct molecular subtypes of colorectal cancer, such as those proposed by Guinney *et al.*, will be invaluable moving forward in determining these functional interactions[257]. While BCAR3 levels overall were nearly undetectable in bulk tumor and adjacent normal tissue samples, abundant levels of BCAR3 protein were detected in most colorectal cancer cell lines. Of the human colorectal cancer lines tested, BCAR3 protein levels were lowest in two lines, Caco2 and HCA7, and relatively low in

HT29 cells, all of which are cells capable of forming prominent adherens junctions with robust membrane localization of E-cadherin and α-catenin. Determining whether BCAR3 regulates junctional composition and formation of cell-cell adhesions may yield insight into how it regulates cell migration.

With regards to cell migration, we demonstrate that BCAR3 loss can both reduce and augment transwell migration. One possible explanation is that the initial loss of BCAR3 reduces the cells ability to initiate and maintain focal adhesions required for cell migration but that this loss can be compensated, and possibly overcompensated, for by the two other NSP family members, NSP1 and NSP3. NSP3, like BCAR3/NSP2, interacts with p130Cas and can similarly promote its hyperphosphorylation[219,235]. In HCT116 cells, we consistently observed that BCAR3 expression enhanced cell migration – both when overexpressing BCAR3 in cells that still express endogenous levels of BCAR3 (Figure 24) and when rescuing BCAR3 in cells where BCAR3 has been knocked out (Figure 23 and Figure 25). It is plausible in the cells that have lost endogenous BCAR3 that NSP family member compensation could be playing a role. Another possible explanation for the dichotomous migration results is that BCAR3 knockout cells may be more sensitive to chemoattractant gradients because of a higher level of RTK activation. We have observed that BCAR3 loss can increase levels of multiple different receptor tyrosine kinases (EGFR, HER3, AXL, and c-MET), however, paradoxically, BCAR3 overexpression also appears to increase levels of many of these proteins as well. Likely there are temporal and cell-context specific factors contributing to this dynamic phenotype and further investigation will be required to determine whether these changes are occurring predominately at the transcriptional or post-translational level.

The BCAR3-p130Cas interaction has been widely studied in breast cancer cell lines but we are among the first to demonstrate this functional interaction in colorectal cancer cell lines.

Utilizing the BCAR3 744/748E mutant, we demonstrate that BCAR3 mediated transwell migration is dependent on the BCAR3-p130Cas interaction. Furthermore, we show that BCAR3-mediated hyperphosphorylation of p130Cas is dependent on both the physical association of BCAR3 with p130Cas and on BCAR3's SH2 domain. While the SH2 domain is dispensable for the BCAR3-p130Cas interaction, it appears critical for promoting the observed upregulation of p130Cas serine phosphorylation. One model for this dynamic interaction is that BCAR3, via its SH2 domain, binds another tyrosine-phosphorylated protein that either directly, or indirectly, phosphorylates p130Cas. Identifying the phosphorylated residues on p130Cas that are altered by the association with BCAR3, along with the kinases recruited to this complex, will be critical. Furthermore, given that we observed significantly reduced growth in HCT116 xenografts expressing the BCAR3-p130Cas uncoupling mutant, identifying these interactors may allow for the development of small molecules or peptides that prevent these interactions and reduce mitogenic signaling in cancer cells. Approaches to prevent protein-protein interactions, such as with the use of the MDM2 inhibitor AMG-232 (which prevents MDM2-p53 binding and restores p53-transcriptional activity), are currently being evaluated in clinical trials. Utilizing the HCT116 xenografts expressing either WT BCAR3 or the p130Cas uncoupling mutant would provide an excellent model to test these types of therapies as we would expect the cells expressing WT BCAR3 (but not the uncoupling mutant) to be far more sensitive to disruption of the BCAR3-p130 interaction.

While we observed no significant differences *in vitro* with regards to proliferation, the robust differences observed with subcutaneous xenograft/allograft tumor modeling in HCT116 and MC38 cells suggests an important role for BCAR3 in mediating and integrating extracellular matrix and growth factor signaling. *In vitro* experiments may simply lack the complex milieu of mitogenic factors needed to augment signaling cascades regulated by BCAR3. There is strong preliminary evidence that BCAR3 can interact with multiple ErbB family members. We observed

changes in EGFR receptor levels and activation and in HER3 levels with BCAR3 loss but these changes were difficult to reproduce and may be context dependent. Additional variables such as cell density, which we report here can regulate BCAR3 levels, and number of passages since BCAR3 knockout will need to be carefully controlled in future studies. Nonetheless, the interaction between BCAR3 and ErbB family members, as well as other tyrosine phosphorylated receptors, will be important areas of future study given their strong association with colorectal cancer. Specifically, analysis of BCAR3's role in the 5% of HER2 amplified colorectal cancers may be noteworthy[258].

While many of the phenotypes associated with BCAR3 overexpression could be characterized as pro-tumorigenic (increased cell migration and invasion, increased *in vivo* proliferation), we also observed increased tumor multiplicity in a Wnt-driven model of colorectal cancer. These mouse studies mirror the human expression data, both of which suggest that low levels of BCAR3 can promote tumorigenicity. Paradoxically, however, the tumors in *Bcar3*$^{-/-}$ mice were smaller and further studies will be needed to understand this complex dynamic. We do not believe that the loss of BCAR3 is promoting increased tumor multiplicity via enhanced Wnt signaling or alterations in TGFβ signaling.

Here we report previously uncharacterized roles for BCAR3 in colorectal cancer. BCAR3 is under expressed at all stages of colorectal cancer yet exhibits significant heterogeneity within CRC cell lines. BCAR3 loss promotes intestinal tumorigenesis in a Wnt driven model yet high levels of BCAR3 led to increases in tumor size. Furthermore, loss of BCAR3 can both reduce and augment cell migration, which may be secondary to BCAR3's influence on receptor tyrosine kinase activation. Overall, these data highlight the complex and dynamic contributions of BCAR3 to intestinal tumorigenesis and lay the foundation for future studies examining the role of this promiscuous protein.

Acknowledgements

I would like to thank David Fei-Zhang, a talented Vanderbilt undergraduate student for his help over the past three years. David was instrumental in preparing plasmid DNA, isolating and extracting RNA, performing transwell migration assays, and maintaining many of the cell lines utilized in these studies. Furthermore, David helped generate and characterize the BCAR3 SH2 mutant and has spearheaded the optimization of crosslinking co-immunoprecipitation studies seeking to confirm the BCAR3-EGFR interaction. I would also like to acknowledge Rachel Brown for her help staining and quantifying the *Lgr5-eGFP;Bcar3* tissue.

CHAPTER V

MATERIALS AND METHODS

Animal Care

Animals were provided water and standard chow diet from Harlan Laboratories *ad libitum* and kept on a 12-hour light/12-hour dark cycle. All mice were bred and housed in the same facility throughout the duration of the experiments. *Bves*^{WT}, *Bves*$^{+/-}$, and *Bves*$^{-/-}$ as well as *Bcar3*^{WT}, *Bcar3*$^{+/-}$, and *Bcar3*$^{-/}$ mice were maintained in the same room for a year prior to beginning the experiment to ensure a controlled microenvironment. *Bves*$^{-/-}$ mice were previously characterized[73,89]. *Bcar3*$^{-/-}$ mice were previously characterized[247] as are the *Lgr5-eGFP-IRES-creERT2* mice*[3]*. All *in vivo* procedures were carried out in accordance with protocols approved by the Vanderbilt Institutional Animal Care and Use Committee.

AOM and *Lrig1-CreER;Apc* Tumorigenesis Protocols

For the AOM tumorigenesis study, eight week old C57BL/6 wild type (WT; n = 11) or *Bves*$^{-/-}$ (n = 10) mice were injected with 5 weekly injections of AOM at 12.5 mg/kg (Sigma-Aldrich) intraperitoneally as previously described[193] and harvested at 30 weeks.

For the *Lrig1-CreER;Apc*$^{fl/+}$;*Bves* experiments, *Lrig1-CreER*;*Apc*$^{fl/fl}$;*Bves*$^{+/-}$ mice were crossed with *Bves*$^{+/-}$ mice to generate both WT and *Bves*$^{-/-}$ mice with appropriate age-matched littermate controls. Similarly, for the *Lrig1-CreER;Apc*$^{fl/+}$;*Bcar3* experiments, *Lrig1-CreER*;*Apc*$^{fl/fl}$;*Bcar3*$^{+/-}$ mice were crossed with *Bcar3*$^{+/-}$ mice to generate *Bcar3*^{WT}, *Bcar3*$^{+/-}$, and

Bcar3$^{-/-}$ mice with appropriate age-matched littermate controls. Between 8-12 weeks of age, mice were injected intraperitoneally on 3 sequential days with 2 mg of Tamoxifen (Sigma-Aldrich). Briefly, a 10 mg/mL Tamoxifen solution was prepared by dissolving 10 mg of Tamoxifen in 100 μL of 100% ethanol. This solution was vortexed for 15 minutes at room temperature and pre-warmed corn oil was then added to bring the total volume up to 1 mL. 200 μL was injected intraperitoneally per mouse. Mice were harvested 100 days after tamoxifen injection.

All mice were sacrificed using isoflurane followed by cervical dislocation and intestines resected. Intestines were irrigated with phosphate-buffered saline (PBS) then opened longitudinally and tumor numbers/size were quantified visually. The sections were then rolled from distal to proximal and the tissues were fixed in 10% formalin overnight prior to paraffin-embedding. Five micron sections were cut and stained with hematoxylin and eosin (H&E) by the Vanderbilt Translational Pathology Shared Resource Core (TPSR Core).

Human RNA expression

BCAR3 levels were queried from the combined Moffitt Cancer Center/Vanderbilt Medical Center colon cancer expression array data set (GEO accession number GSE17538) as previously described [41,225,259]. Similarly, *BCAR3* levels were also analyzed from Illumina HiSeq and Illumina RNASeqV2 data in The Cancer Genome Atlas (TCGA) colon adenocarcinoma (COAD) data sets[96]. Normalized RSEM expression data were log2 transformed for visualization.

Cell Lines and Culture

HEK293 SuperTopFlash (293STF) cells were a kind gift from Dr. Ethan Lee, Vanderbilt University and J. Nathans, Johns Hopkins University[192,260] and 293DVL TKO were a kind gift from Dr. Ethan Lee, Vanderbilt University and S. Angers, University of Toronto[187]. 293STF cells were not authenticated in our laboratory but demonstrate expected TopFlash activity in response to Wnt pathway activation and expected G418-resistance conferred during generation of the cell line[260]. 293DVL TKO cells were confirmed to be DVL knockout by western blot. L-cells, L-Wnt3a, HEK293T, and HCT116 cells were purchased from ATCC which characterizes cell lines using short tandem repeat (STR) DNA profiles. HCT116, SW480, and HT29 cells were maintained in McCoy's 5A while MC38 cells and all other cell lines were maintained in DMEM, all supplemented with 10% FBS and 1% penicillin/streptomycin at 37°C in 5% CO_2. All cells used were passaged in our laboratory for less than 3 months after resurrection. Cells were tested using the PCR Mycoplasma Detection Kit (ABM).

Transfections

For siRNA knockdown experiments, Control siRNA-A (SantaCruz, sc-37007) and individual as well as pooled BVES siRNAs (sc-60295) were transfected into 293STF and HCT116 cells using Lipofectamine RNAimax (Life Technologies) as per manufacturer's instructions. BCAR3 siRNAs (sc-60265) were similarly transfected into SW480 cells. The overexpression plasmid for chick-BVES and V5-BVES have been previously described[30,73]. LRP6-GFP was a gift from Dr. Ethan Lee and Randall Moon[261], and Myc-LRP6ICD was a gift from Dr. Ethan Lee. The murine Flag-BCAR3 construct was purchased from OriGene (Catalog number

MR210814). In all experiments, pcDNA3.2/V5/GW-CAT (Thermo Scientific) was utilized as filler to maintain equivalent DNA concentrations.

TopFlash Assays

293STF cells were seeded into 12-well plates and knockdown was performed when cells were at ~50% confluency. 48 hours after knockdown cells were stimulated with 50% L-cell-conditioned media or 50% Wnt3a-conditioned media overnight. Cells were then lysed in 250 μL of 1X Glo lysis buffer (Promega). 30 μL of lysate was mixed 1:1 with the Steady-Glo Luciferase Assay solution (Promega) in 96-well polystyrene white opaque plates (Thermo Scientific) and luminescence measured using a GloMax Discover plate reader (Promega). Assays were performed in triplicate and repeated at least 4X. TopFlash experiments in HCT116 were performed by co-transfection of 1 μg of M50 Super8x TopFlash (gift from Randal Moon, Addgene plasmid #12456) or M51 Super 8x FOPFlash (gift from Randal Moon, Addgene plasmid #12457) with 0.1 μg of pRL-TK (Promega) to normalize transfection efficiency and assayed using the Dual-Glo Luciferase Assay System (Promega).

Lentivirus Generation

Lentivirus was packaged using pMD2.G (a gift from Didier Trono, Addgene plasmid # 12259) and psPAX2 (a gift from Didier Trono, Addgene plasmid # 12260) vectors and the pLKO.1 non-target shRNA (Sigma-Aldrich) or pLKO.1 shBVES (Mission shRNA – Sigma, TRCN0000153094). The pGIPZ shCtrl (RHS4346) and shBCAR3 constructs were purchased from Dharmacon (G11: V2LHS_33013, G2: V3LHS_370110, G5: V3LHS_370111, E5:

V3LHS_370113). HEK293T at 50% confluency in 10-cm plates were transfected with 1 μg each of pMD2.G and psPAX2 and 2 μg of shRNA, lentiCRISPR v2, or indicated pLEX304/307 using polyethylenimine (PEI). Media was changed the following morning then viral supernatant was harvested 48 hours later, centrifuged, and filtered through a 0.45 μM filter. For transient shRNA knockdown, polybrene was added to 5 μg/mL and target cells were transduced overnight then assayed 48-60 hours later. Lentiviral transduction of human colonoids and human tumoroids was performed as previously described[192].

BCAR3 CRISPR Knockout

For the CRISPR/Cas9 knockout lines, guide RNAs were designed against Exon 4 of human BCAR3 (after the ATG start codon of transcript variants 1/2/3) through the portal at crispr.mit.edu. 3 different sgRNAs targeting were cloned into the lentiCRISPR v2 construct, a gift from Feng Zhang (addgene plasmid #52961, [262]). The guide sequences were as follows: sgRNA1: 5'-AGGTGAAGGTTTCGCCGTGC-3' (antisense), sgRNA2: 5'-TCACAGGCGAGTTCTGCCGT–3' (antisense), sgRNA3: 5'-AGCCCATGGCAGGACCGGCA– 3' (sense). Lentiviral particles were packaged with each individual sgRNA and HCT116 cells were transduced. 48 hours after transduction, 100 cells were plated per 10-cm plate in 1.0 μg/mL Puromycin to allow for selection and clonal expansion. Individual clones were expanded and confirmed to be knockout for BCAR3 by immunoblot. Then 2-3 confirmed knockout clones per guide RNA were pooled together. A similar approach was employed to generate the crCtrl line, which consisted of 6 pooled vector-only control clones. For rescue experiments, only clones harboring sgRNA1 were pooled together.

To generate the pooled crBCAR3 SW480 lines, the lentiCRISPR v2_sgRNA1 construct was packaged, concentrated, and utilized to transduce a pooled population of SW480 cells.

Expression Constructs

To generate the c-terminal V5-tagged human BCAR3 expression vectors, a Gateway™ compatible human BCAR3 cDNA vector was obtained from the Harvard Plasmid Bank (HsCD00376429). BCAR3 was cloned into the lentiviral pLEX304 vector (a gift from David Root, Addgene plasmid #25890) to generate pLEX304-hBCAR3 using Gateway™ LR Clonase ™ (Invitrogen) according to manufacturer recommendations. pLEX304 was utilized as it confers Blasticidin resistance and allowed for rescue experiments in cells expressing puromycin resistance from the lentiCRISPRv2 lines. Recombined plasmids were transformed into STBL3 (ThermoFisher) and transformants were sequence verified. In parallel, LR recombinase reactions were also performed with the pDONR223_LacZ plasmid (a gift from David Root, Addgene plasmid #25893) to generate the LacZ control vector. For the mouse BCAR3 lentiviral expression vector, pCMV-Sport6-mouse BCAR3 (Plasmid ID MmCD00318547) was obtained from the Harvard Plasmid Bank. A BP Clonase™ reaction was performed with pDONR221 (Invitrogen) to generate the intermediary pDONR221-mBCAR3 vector which was sequence verified. The pDONR221-mBCAR3 construct or the pDONR223_LacZ constructs were then utilized for the LR reaction with pLEX307 (a gift from David Root, Addgene plasmid #41392) to generate pLEX307-mBCAR3 and pLEX307-LacZ. Because the mouse BCAR3 cDNA vector contained a stop codon, translation was halted and the pLEX307-mBCAR3 vector does not contain a c-terminal V5 tag (despite being in the pLEX307 vector which can generate c-terminal V5 tagged proteins). The BVES expression constructs were purchase from Genecopoeia: EX-EGFP-LV102 (Control), EX-

T3443-Lv102 (N-terminal Flag Tag), EX-T3443-Lv103 (N-terminal GFP Tag), EX-T3443-Lv121 (C-terminal Flag Tag), EX-T3443-Lv122 (C-terminal GFP Tag), and EX-T3443-Lv205 (Untagged, IRES GFP).

Site Directed Mutagenesis

Site directed mutagenesis was performed using the QuikChange XL Site-Directed Mutagenesis Kit (Agilent) according to manufacturer recommendations. For lentiviral constructs, STBL3 cells (ThermoFisher) were utilized to culture positive transformants. The guide RNA resistant silent wobble mutations were introduced into pLEX304-hBCAR3 to generate pLEX304-sgRNA resistant hBCAR3. Generation of the BCAR3 744/748E double mutant was performed on pLEX304-sgRNA resistant hBCAR3 in one mutagenesis step. To generate the BCAR3 Delta SH2 interstitial mutant (which lacks amino acids 154-234), "Round the Horn PCR" was utilized on the pLEX304-sgRNA resistant hBCAR3. Briefly, primers abutting the SH2 domain were designed with melting temperatures within 5°C of each other and going away from the region to be deleted. This allowed for amplification of the entire plasmid, excluding the interstitial SH2 region. Primers were phosphorylated in T4 DNA ligase buffer with T6 polynucleotide kinase for 30 minutes at 37°C. PCR amplification was performed with 2x Q5 Hot-start, high fidelity PCR master mix (NEB). The PCR product was purified via gel extraction and circularized with T4 DNA ligase (NEB). Generation of the mBCAR3 743A and 743E point mutations were performed on the pDONR221-mBCAR3 intermediary before flipping these inserts into the pLEX307 vector. The BVES degron mutants and truncation mutants were performed on the EX-T3443-LV102 N-terminal Flag-BVES. A list of primers is included in Table 1.

SDM Primer	Sequence
BCAR3_sgRNA1degres_F	CCTGAAGGTGAAGGTTTCCCCATGTCTATCCTGCCATGGGCTCTCC
BCAR3_sgRNA1degres_R	GGAGAGCCCATGGCAGGATAGACATGGGGAAACCTTCACCTTCAGG
BCAR3_R748A_R	GCCTCGGCCATGAATGCCGCTGTTGCCAAATG
BCAR3_R748A_F	CATTTGGCAACAGCGGCATTCATGGCCGAGGC
BCAR3_R748E_R	GCAGCCTCGGCCATGAACTCCGCTGTTGCCAAATGGT
BCAR3_R748E_F	ACCATTTGGCAACAGCGGAGTTCATGGCCGAGGCTGC
BCAR3_L744E/R748E_F2	CTGTGAAATCATGCTGAACCATGAGGCAACAGCGGAGTTCATGGCCGAGGC
BCAR3_L744E/R748E_R2	GCCTCGGCCATGAACTCCGCTGTTGCCTCATGGTTCAGCATGATTTCACAG
hBCAR3_deltaSH2_F:	GTGGGCAACCGCCGGCCC
hBCAR3_deltaSH2_R:	GGCATGGCTGCGCAGGTCC
mBCAR3_R743A_F	GCCTCAGCCATGAACGCGGCTGTTGCCAAGTG
mBCAR3_R743A_R	CACTTGGCAACAGCCGCGTTCATGGCTGAGGC
mBCAR3_R743E_F	GAAGCCTCAGCCATGAACTCGGCTGTTGCCAAGTGATT
mBCAR3_R743E_R	AATCACTTGGCAACAGCCGAGTTCATGGCTGAGGCTTC
BVES_D-Box_Mut_F	CGTCTGGGCCACTCTCTACGCATGTGCCGCGGATATAATGATCTGGAAC
BVES_D-Box_Mut_R	GTTCCAGATCATTATATCCGCGGCACATGCGTAGAGAGTGGCCCAGACG
BVES_FBW7_Mut_F	GAATCAACTGCCATAGGTTTTGCAGCTGAGTTAGCAAGTATCATACCTGTGC
BVES_FBW7_Mut_R	GCACAGGTATGATACTTGCTAACTCAGCTGCAAAACCTATGGCAGTTGATTC
BVES330_F	CCCACACCAGCGAGCCTCTTAGAAGATGAAACCGATAGAAG
BVES330_R	CTTCTATCGGTTTCATCTTCTAAGAGGCTCGCTGGTGTGGG

SDM Primer	Sequence
BVES300_F	GAACAGTATAGCCAGCTCCTAGGACAGTGACGACGGCTTGC
BVES300_R	GCAAGCCGTCGTCACTGTCCTAGGAGCTGGCTATACTGTTC
BVES270_F	TACTCATTGAATGATCCCACCTTATAGGATAAAAAAGCCAAAAAGCTGGAA
BVES270_R	TTCCAGCTTTTTGGCTTTTTTATCCTATAAGGTGGGATCATTCAATGAGTA
BVES240_F	CAAGAGAAAGATTAACATACTTTCTGTAATCAGAACCTTTCTTGTATGAAATC
BVES240_R	GATTTCATACAAGAAAGGTTCTGATTACAGAAAGTATGTTAATCTTTCTCTTG
BVES210_F	CTGAATTTAGATCAACTCAGATGTAGAAAGGTGAAAAATTCCAGGTCAC
BVES210_R	GTGACCTGGAATTTTTCACCTTTCTACATCTGAGTTGATCTAAATTCAG
BVES180_F	GAGTATTCTCTTGAAGGGATAAATGAAGGTCTCCTATCG
BVES180_R	CGATAGGAGACCTTCATTTATCCCTTCAAGAGAATACTC
BVES150_F	TTTGTTCAGAAGACTAACTGGACAGTTTTAGATGATCCAAACCTTGAAAAA
BVES150_R	TTTTTCAAGGTTTGGATCATCTAAAACTGTCCAGTTAGTCTTCTGAACAAA
BVES120_F	TTATACAAGAAGAGACCGGTAAAGTAGGAAAAGGAACTCAGTGGCATGTAC
BVES120_R	GTACATGCCACTGAGTTCCTTTTCCTACTTTACCGGTCTCTTCTTGTATAA
BVES_K122A_F	GTACATGCCACTGAGTTCCGCTTCAATCTTTACCGGTCTCTTC
BVES_K122A_R	GAAGAGACCGGTAAAGATTGAAGCGGAACTCAGTGGCATGTAC
BVES_K166A_F	ACGGTCATCAACTGAGGTTGCATCCTCTGCAGCATAAGTTTG
BVES_K166A_R	CAAACTTATGCTGCAGAGGATGCAACCTCAGTTGATGACCGT
BVES_K272A_F	TGATGTTCCAGCTTTTTGGCTTTTGCATCATTTAAGGTGGGATCATTCAATG
BVES_K272A_R	CATTGAATGATCCCACCTTAAATGATGCAAAAGCCAAAAAGCTGGAACATCA

Table 1. Site directed mutagenesis primers.

RNA Isolation and qRT-PCR

Cells in 6-well plates at 50% confluency were treated with *BVES* siRNA or transiently transduced with *BVES* shRNA lentivirus overnight. 36-48 hours after knockdown cells were stimulated with 50% L-cell-conditioned media or 50% Wnt3a-conditioned media overnight. Cells were harvested in TRIzol Reagent (Invitrogen) and RNA purified using the Direct-zol RNA Miniprep kit (Zymo Research). RNA (2 μg) was reverse transcribed to cDNA using qSCRIPT XLT cDNA SuperMix (QuantaBio) according to manufacturer's protocol. The 20 μL cDNA reaction was diluted in 380 μL H_20 and 2 μL was used as a template in each subsequent PCR reaction. Taqman reactions were performed using Taqman Universal PCR Master Mix (Applied Biosystems, #4304437) with probes listed in Table 2. SYBR Green reactions were performed using PerfeCTa SYBR Green FastMix (QuantaBio) using the primers listed in Table 2. All qRT-PCR reactions were normalized to *GAPDH* and fold changes calculated using the delta-delta Ct method.

SYBR Green	
Primer Name	Sequences/IDs
*hAXIN2_* F	CAACACCAGGCGGAACGAA
*hAXIN2_* R	GCCCAATAAGGAGTGTAAGGACT
hβ-catenin/*CTNNB1_* F	AAAGCGGCTGTTAGTCACTGG
hβ-catenin/*CTNNB1_* R	CGAGTCATTGCATACTGTCCAT
hGAPDH _F	GGCCTCCAAGGAGTAAGACC
*hGAPDH_* R	AGGGGTCTACATGGCAACTG
*hBCAR3_ISO_1_* F	CAGAAACATGCCGGTGAATCA
*hBCAR3_Iso_1_* R	GTGGGGATTTGGAGTGGGG
hE-cadherin_RT_F	CGAGAGCTACACGTTCACGG
hE-cadherin_RT_R	GGGTGTCGAGGGAAAAATAGG
hFibronectin1_RT_F	CGGTGGCTGTCAGTCAAAG
hFibronectin1_RT_R	AAACCTCGGCTTCCTCCATAA
hVimentin_RT_F	AGTCCACTGAGTACCGGAGAC
hVimentin_RT_R	CATTTCACGCATCTGGCGTTC
hSNAI2_RT_F	TGTGACAAGGAATATGTGAGCC
hSNAI2_RT_R	TGAGCCCTCAGATTTGACCTG
hSNAI1_RT_F	TCGGAAGCCTAACTACAGCGA
hSNAI1_RT_R	AGATGAGCATTGGCAGCGAG
hMYC_RT_F	GTCAAGAGGCGAACACACAAC
hMYC_RT_R	TTGGACGGACAGGATGTATGC
mLgr5 _F	CCAATGGAATAAAGACGACGGCAACA
mLgr5 _R	GGGCCTTCAGGTCTTCCTCAAAGTCA
mAxin2 _R	TGACTCTCCTTCCAGATCCCA
mAxin2 _F	TGCCCACACTAGGCTGACA
mMyc _F	ATGCCCCTCAACGTGAACTTC
mMyc _R	GTCGCAGATGAAATAGGGCTG
*mBVES_Exon4_* F	CTGGGTGGTGTCTACCATCG
*mBVES_Exon4_* R	CTGGCCCCTTTTCAAGGTCT
*mBVES_Exon3/4_* F	TATGTGGTCTGGGCCACTCT
*mBVES_Exon3/4_* R	CGATGGTAGACACCACCCAG
mGapdh _F	CCGCATCTTCTTGTGCA
mGapdh _R	CGGCCAAATCCGTTCA

Taqman	
hBVES	Hs00362584_m1
hBCAR3	Hs00182488_m1
hFBXW7	Hs00217794_m1
hGAPDH	Hs02786624_g1
mBves (Exon 5-6)	Mm00517902_m1
mBves (Exon 3-4)	Mm01192020_m1
mBves (Exon 4-5)	Mm01192021_m1
mGAPDH	Mm99999915_g1

Table 2. SYBR Green Primers and Taqman probes.

Genomic Analysis of *Bves*$^{fl/fl}$ Mice

Lrig1-CreER;Bves$^{fl/fl}$*;mTmG*$^{+/-}$ enteroids were treated with vehicle or with 500 μM 4-Hydroxytamoxifen (4OHT) dissolved in DMSO for 96 hours before harvesting genomic DNA or RNA. Genomic DNA was isolated using the DNeasy Blood & Tissue Kit (Qiagen) according to the manufacturer. Genomic DNA amplification was using GoTaq Green Master Mix (Promega) with the following primers: mBVES_GenomicF: TGTGAAGTGGTGAGTGTTGG and mBVES_GenomicR1: GGGGGTCTTAGAGGGTTAG, mBVES_GenomicR2 (same as mBVES_Exon4_R): CTGGCCCCTTTTCAAGGTCT, and mBVES_GenomicR3: AGGCAGGCCTGGTAACGGGC.

Human Normal Colon and Tumor Samples

Deidentified human normal colon tissue was acquired from the Vanderbilt Cooperative Human Tissue Network in accordance with the Vanderbilt Institutional Review Board. Samples were homogenized in Trizol followed by RNA extraction using the Direct-zol RNA MiniPrep Kit (Zymo Research) or lysed in RIPA buffer, homogenized, then sonicated and quantified as above.

Murine Enteroid Isolation and Maintenance

Enteroids were cultured as previously described[88,263]. Briefly, proximal small intestines of age-matched littermate control *Bcar3*^{WT} or *Bcar3*$^{-/-}$ mice were flushed with ice cold PBS and then minced. Tissue was rocked in PBS at 4°C for 15 minutes then vortexed for 10 second to remove the villi. After two additional PBS washes, the tissue was resuspended in 2mM EDTA in

PBS and chelated at 4°C for 30 minutes. Tissue was again washed two times in PBS and resuspended in cold shaking buffer (PBS with 43.3 mM sucrose and 54.9 mM sorbitol). Tissue fragments were then filtered through a 70 micron cell strainer and intact crypts were counted. 300 *Bcar3*^{WT} or *Bcar3*$^{-/-}$ enteroids per well were pelleted at 200 g for 5 minutes, the supernatant discarded, and the enteroids resuspended in growth-factor-reduced Matrigel™ (Corning). 50 µL Matrigel™ plugs were spotted in the middle of a 12 well plate and allowed to polymerize at 37°C for 30 minutes before overlaying with 500 µL of epidermal growth factor/Noggin/R-spondin (ENR) media which consists of basal media [(Advanced DMEM/F12 (Gibco), 1X Glutamax (Gibco), 100 U/mL Pen-Strep (Invitrogen #15140-148), 10 mM HEPES (Cellgro MT25060CI), 1X N2 Supplement (GIBCO), 1X B27 Supplement (GIBCO)] supplemented with 20% R-spondin conditioned media (produced from R-spondin-expressing cells kindly provided by Dr. Jeff Whitsett, Cincinnati Children's Hospital Medical Centre and The University of Cincinnati College of Medicine, Cincinnati, USA), 10% Noggin conditioned media (made from Noggin-producing cells kindly provided by G.R. van den Brink, Amsterdam, The Netherlands [described in[264]], and 50ng/ml mouse recombinant EGF (R&D 2028EG200)]. Media was replenished every 3-4 days. For splitting, Matrigel™ plugs were scraped into 1 mL of ice cold PBS and sheared by pulling through a 25G needle 1-2x. Sheared enteroids were pelleted at 200g for 5 minutes and remaining PBS and Matrigel™ aspirated off before re-suspending in fresh Matrigel™ and spotting new 50 µL plugs in 12 well plates.

Murine Adenoma Tumoroid Isolation, Maintenance, and Treatments

Tumoroids were cultured as previously described[263]. Briefly, colons and small intestines of *Lrig1-CreER*;*Apc*$^{fl/+}$;*Bves*^{WT} *or Bves*$^{-/-}$ mice were flushed with ice cold PBS and multiple macroscopic tumors from each mouse were resected and pooled. Tissue was digested with constant agitation at 37°C in 10ml pre-warmed digestion buffer (9.7 mL DMEM + 250 µL FBS + 100 µL Pen Strep + 1 mg Collagenase XI + 1.25 mg Dispase II) for 30 minutes. Digested tumor fragments were then shaken 2-3x to loosen cell clusters. Larger fragments were allowed to settle to the bottom of the tube and the supernatant was collected, spun at 200g for 5 minutes, and then washed with 5mL cold PBS to remove remaining digestion buffer. Samples were pelleted at 200g for 5 minutes, the supernatant discarded, and the tumor fragments resuspended in 300-500 µL of growth-factor-reduced Matrigel™ (Corning) depending on the size of the pellet.

50 µL Matrigel™ plugs were spotted in the middle of a 12 well plate and allowed to polymerize at 37°C for 30 minutes before overlaying with 500 µL of epidermal growth factor/Noggin/R-spondin (ENR) media which consists of basal media [(Advanced DMEM/F12 (Gibco), 1X Glutamax (Gibco), 100 U/mL Pen-Strep (Invitrogen #15140-148), 10 mM HEPES (Cellgro MT25060CI), 1X N2 Supplement (GIBCO), 1X B27 Supplement (GIBCO)] supplemented with 20% R-spondin conditioned media (produced from R-spondin-expressing cells kindly provided by Dr. Jeff Whitsett, Cincinnati Children's Hospital Medical Centre and The University of Cincinnati College of Medicine, Cincinnati, USA), 10% Noggin conditioned media (made from Noggin-producing cells kindly provided by G.R. van den Brink, Amsterdam, The Netherlands [described in[264]], and 50ng/ml mouse recombinant EGF (R&D 2028EG200)]. Media was replenished every 3-4 days. For splitting, Matrigel™ plugs were scraped into 1 mL of ice cold PBS and sheared by pulling through a 25G needle 1-2x. Sheared tumoroids were pelleted

at 200g for 5 minutes and remaining PBS and Matrigel™ aspirated off before re-suspending in fresh Matrigel™ and spotting new 50 µL plugs in 12 well plates.

For Wnt3a and R-spondin treatment of WT adenoma tumoroids, tumoroids were split and maintained in basal or basal media supplemented with 100 ng/mL mouse recombinant Wnt3a (Vanderbilt Antibody and Protein Resource, VAPR Core) and 250 ng/mL mouse recombinant R-spondin (VAPR Core) for 4 days before imaging and size quantification using ImageJ.

Human Colonoid and Tumoroid Isolation and Maintenance

Deidentified human normal colon tissue was acquired from the Vanderbilt Cooperative Human Tissue Network in accordance with the Vanderbilt Institutional Review Board. Human tumor organoids were established according to previously published protocols[263]. Briefly, minced colon tissue was incubated in PBS with 2mM EDTA for 30 minutes at 4^{o}C. Tissue fragments were then washed and resuspended in 5ml PBS containing with 43.4mM sucrose and 54.9mM D-sorbitol. Tissue was then gently shaken for 1-2 minutes to release intestinal crypts which were then collected, resuspended in Matrigel™, and spotted in 10µl plugs in the bottom of a 12 well plate. After polymerization, Matrigel™ plugs were overlaid with human culture media containing Advanced DMEM F12 (Gibco), 50% LWRN conditioned media (produced from L-cells expressing Wnt, R-spondin, and Noggin, ATCC), 1x B27 (Gibco), 1x N2 (Gibco), 1x Glutamax (Gibco), 1mM HEPES, 100 U/ml penicillin, 100 µg/ml streptomycin, 50 ng/ml EGF (R&D), 10nM [Leu15]-Gastrin 1 (Sigma-Aldrich), 1mM n-Acetylcysteine (Sigma-Aldrich), 10µM SB202190 (Sigma-Aldrich), 10mM Nicotinamide (Sigma-Aldrich), 500nM A83-01 (Tocris), and 10nM Prostaglandin E2.

Adenoma Tumoroid Embedding and Staining

Tumoroids were collected in ice-cold PBS and fixed in 10% neutral buffered formalin on ice for 20 minutes. Fixed enteroids were then pelleted at 200g for 3 minutes and washed 3X with ice-cold PBS. After the final centrifugation, the supernatant was aspirated and the enteroid pellet was resuspended in 2% agarose dissolved in PBS. The agarose was allowed to solidify for 10 minutes then placed in 70% ethanol and paraffin embedded by the Vanderbilt Translational Pathology Shared Resource Core.

Subcutaneous Xenografts and Allografts

1 x 10^7 HCT116 cells were injected subcutaneously into NOD/SCID mice (Jackson Laboratory 001303) or 1 x 10^6 MC38 cells were injected subcutaneously into C57BL/6J mice and allowed to grow. Once palpable tumors were observed, tumors were measured every three days and volumes calculated using the modified ellipsoidal formula (volume = ½(Length x ($Width^2$))[245]. At harvest, tumors were isolated and flash frozen for protein, placed in RNAlater (ThermoFisher) or fixed in 10% neutral buffered formalin overnight prior to paraffin-embedding.

Immunoblots and Immunoprecipitation

For cytoplasmic fractionation, cells were incubated on ice for 15 minutes in cytoplasmic fractionation lysis buffer (10 mM HEPES (pH 7.8), 10 mM KCl, 2 mM $MgCl_2$, 0.1 mM EDTA with phosphatase inhibitor cocktail 2 (Sigma-Aldrich), phosphatase inhibitor cocktail 3 (Sigma-Aldrich), and protease inhibitor (Sigma-Aldrich), then scraped and transferred to microfuge tubes.

NP-40 was added to 0.5% and lysates were vortexed then sheared through a 23-gauge needle 6 times, and spun at 16,000Xg for 2 minutes. This protocol enriches for cytoplasmic and membrane proteins but significantly reduces nuclear protein contamination. Supernatants (cytoplasmic fractions) were recovered and protein concentrations determined using the Pierce BCA Protein Assay Kit (Thermo Scientific). Samples were combined with 5x Laemmli buffer and then boiled for 5 minutes. 20-30 μg of protein was loaded per lane followed by SDS-PAGE electrophoresis. Lysates were transferred to a 0.2 micron Nitrocellulose membrane (PerkinElmer) and then blocked using Odyssey TBS blocking buffer (LI-COR) for 30 minutes. Membranes were probed overnight at 4°C with antibodies diluted in Odyssey blocking buffer with 0.1% Tween-20 as listed in Table 3. IRDye Goat-anti rabbit 800 (LI-COR #827-08365) or IRDye Goat anti-Mouse 680LT (LI-COR #925-68020) secondary antibodies were diluted 1:10,000 in TBS + 0.1% Tween-20 and incubated for 30 minutes at RT. Blots were imaged on a LI-COR Clx Near-infrared system and quantification of western blot band intensity was conducted using the LI-COR Image Studio with samples normalized to GAPDH. All western blots are representative of at least 3 independent experiments unless otherwise noted.

For co-immunoprecipitations, cell lysates were prepared using CellLytic M (Sigma-Aldrich) with protease and phosphatase inhibitors. 1 mg of lysate was incubated with anti-GFP binding protein magnetic beads (VAPR Core) or Anti-flag M2 affinity gel (Sigma-Aldrich) for 2 hours at 4°C with constant agitation. Beads/resin were washed 3X with lysis buffer and proteins were eluted from beads with 2X Laemmli buffer. The Flag-BVES IPs probed for endogenous LRP5 and LRP6 was developed using Supersignal West Femto (Sigma-Aldrich) chemiluminescence and HyBlot CL film (Denville Scientific).

Tumoroids were harvested based on standard passage protocols described above with the addition of a 30-minute incubation step in Cell Recovery Solution (Corning #354253) to digest

away the Matrigel™. Tumoroids were then washed 1x in PBS, pelleted, and resuspended in RIPA buffer (50 mM Tris pH 7.4, 150 mM NaCl, 1% NP-40, 0.5% Deoxycholic Acid, 0.1% Sodium Dodecyl Sulfate).

For the immunoblots in Chapter 4, cells were washed twice with ice cold PBS, incubated on ice with gentle agitation in RIPA Buffer (50 mM Tris pH 7.4, 150 mM NaCl, 1% NP-40, 0.5% Deoxycholic Acid, 0.1% Sodium Dodecyl Sulfate) with phosphatase inhibitor cocktail 2 (Sigma-Aldrich), phosphatase inhibitor cocktail 3 (Sigma-Aldrich), and protease inhibitor (Sigma-Aldrich), then scraped and transferred to microfuge tubes. Lysates were sonicated 6-8 times with 1 second pulses at power 3 and then cleared by centrifugation at 16,000Xg for 10 minutes. Protein concentrations were determined using the Pierce BCA Protein Assay Kit (Thermo Scientific). Samples were combined with 5x Laemmli buffer and then boiled for 5 minutes. 20-30 μg of protein was loaded per lane followed by SDS-PAGE electrophoresis. Lysates were transferred to a 0.2 micron Nitrocellulose membrane (PerkinElmer) and then blocked using Odyssey TBS blocking buffer (LI-COR) for 30 minutes. Membranes were probed overnight at 4°C with antibodies diluted in Odyssey blocking buffer with 0.1% Tween-20 as listed in Table 3.

IRDye Goat-anti rabbit 800 (LI-COR #827-08365) or IRDye Goat anti-Mouse 680LT (LI-COR #925-68020) secondary antibodies were diluted 1:10,000 in TBS + 0.1% Tween-20 and incubated for 30 minutes at RT. Blots were imaged on a LI-COR Clx Near-infrared system and quantification of western blot band intensity was conducted using the LI-COR Image Studio with samples normalized to the indicated loading control (GAPDH, β-actin, or Tubulin).

For co-immunoprecipitations, cell lysates were prepared using CellLytic M (Sigma-Aldrich) with protease and phosphatase inhibitors. For V5 immunoprecipitation, 1 mg of lysate was incubated with anti-V5 magnetic beads (MBL International Corporation) for 2 hours at 4°C with constant agitation. For p130Cas immunoprecipitation, 1 μg of p130 Cas antibody was incubated with

lysates for 1 hour at 4°C then washed Protein G Magnetic Beads (Millipore) were added and samples incubated an additional 1 hour at 4°C. Beads/resin were washed 3X with lysis buffer and proteins were eluted from beads with 2X Laemmli buffer.

	Antibody	Company	Catalog Number	Dilution
Chapter 3	β-Actin	Sigma-Aldrich	A5441	1:5000
	β-catenin	BD Biosciences	610153	1:2000
	DVL-2	Cell Signaling	3224	1:1000
	DVL-3	Cell Signaling	5731	1:1000
	Flag	Sigma-Aldrich	F1804	1:1000
	GAPDH	Cell Signaling	5174	1:5000
	GFP	Cell Signaling	2956	1:1000
	LRP5	Cell Signaling	5731	1:1000
	LRP6	Cell Signaling	3395	1:1000
	pLRP6 (Ser1490)	Cell Signaling	2568	1:750
Chapter 4 and Appendix	β-Actin	Sigma-Aldrich	A5441	1:5000
	AKT	Cell Signaling	9272	1:1000
	pAKT	Cell Signaling	9271	1:1000
	Axl	Cell Signaling	8661	1:1000
	BCAR3	Sigma-Aldrich	HPA014858, Lot A86849	1:1000
	EGFR	Cell Signaling	4267	1:1000
	pEGFR (Y1068)	Cell Signaling	2234	1:1000
	GAPDH	Cell Signaling	5174	1:5000
	HER2	Cell Signaling	2165	1:1000
	HER3	Cell Signaling	12708	1:1000
	p130	BD Transduction Laboratories	610271	1:1000
	pERK1/2 (T202/Y2040	Cell Signaling	9101	1:1000
	pSmad2 (Ser465/467)	Cell Signaling	3108	1:1000
	pSmad3 (Ser423/425)	Cell Signaling	9520	1:1000
	Smad2/3	Cell Signaling	8685	1:1000
	SRC	Cell Signaling	2108	1:1000
	pSRC Family (Y416)	Cell Signaling	2101	1:1000
	Tubulin	Cell Signaling	15115	1:4000
	V5	Abcam	ab27671	1:2000
	BVES	Abcam	ab196551, Lot GR237218-1	1:1000

Table 3. Antibodies used for immunoblotting.

Immunohistochemistry

Protocols for fluorescent staining of paraffin-embedded sections were previously described[89]. Primary antibodies include anti-phospho Histone H3 (1:400, Millipore #06-570), Cleaved Caspase 3 (1:400, Cell Signaling Technologies #9661), β-catenin (1:400, BD Biosciences #610153), and E-cadherin (1:500, BD Biosciences #610181). For the xenograft staining, primary antibodies include anti-phospho Histone H3 (1:400, Millipore #06-570) and V5 (1:400, Abcam # ab2761). Staining in the *Lgr5-eGFP*;*Bcar3* tissue was performed similarly with the exception of the antigen retrieval which was performed using Citrate Buffer, pH 6 (DAKO) for 15 minutes in a pressure cooker. Primary antibodies used were Rabbit α-GFP (1:500, Novus NB600-308 and E-cadherin (1:500, BD Biosciences #610181).

Statistical Analysis

Statistical analysis comparing was performed in Graphpad Prism Software as indicated in the figure legends. For all studies, error is represented by standard deviation and $P < 0.05$ is considered significant.

CHAPTER 6

FUTURE DIRECTIONS

BVES detection and subcellular localization

A significant barrier to studying the functional relevance of BVES in colorectal cancer has been the relative inability to express full-length human BVES at detectable levels *ex vivo*, especially in CRC cell lines. Furthermore, the lack of sensitive immunoreagents to detect endogenous, untagged BVES has necessitated a reliance on protein tags that could affect BVES function and localization. As seen in Figure 33B, the location (N-terminal vs. C-terminal) of the epitope tag alters BVES banding patterns and electrophoretic mobility and may influence subcellular localization. Therefore, developing new immunoreagents to more thoroughly characterize endogenous BVES levels will be critical. One limiting factor in this is simply that overall, BVES levels are relatively low in a majority of colorectal cancer cell lines[41], whole intestinal tissue, intestinal crypts, and pure intestinal epithelium (See *Bves* CT values from *Bves*$^{fl/fl}$ troubleshooting, Table 7). Therefore, utilizing a CRISPR activation system like dCas9-VPR[265] to enhance BVES expression from the endogenous locus would be beneficial in screening new immunoreagents. Adding an epitope tag to the endogenous locus via CRISPR/Cas9 and a homology directed repair (HDR) template would also be very beneficial. Combing these two approaches into one cell line (endogenously tagging BVES and being able to inducibly increase endogenous gene transcription) would provide a powerful tool for further functional studies. While powerful, an approach of this nature would require a significant amount of investment in a single cell line which may not accurately depict BVES function in all cell contexts. Therefore,

determining the subcellular location and stability of each of the human BVES expression constructs (Figure 33) through a combination of membrane/cytoplasmic fractionation and immunofluorescence with and without cycloheximide treatment would provide a tremendous amount of information and help identify the constructs that may be functioning most similarly to endogenous BVES. It is hypothesized that membrane bound BVES is likely much more stable than the cytoplasmic pools of BVES but this hypothesis has not been formally tested. By performing true membrane and cytoplasmic fractionations following a cycloheximide time-course and using ultracentrifugation to isolate the cell fractions (as opposed to commercial kits which can be more prone to cross-contamination), the most stable pools of BVES can be identified. Furthermore, adding an N-terminal myristoylation tag (along with a fluorescent reporter such as Addgene plasmid #32602) could help tease apart differential roles for cytoplasmic vs. membrane BVES. For example, with the BVES/LRP6/β-catenin story, attempts at overexpressing BVES did not attenuate Wnt signaling as would be expected based on the knockdown data. This could certainly be due to the difficulties in expressing full length human BVES, but overexpression of a more readily expressed V5-tagged BVES truncation construct (containing amino acids 72-360) and full length chick BVES also failed to attenuate Wnt signaling. It is possible that the cells simply have enough BVES and therefore adding more to the system has little effect. Another hypothesis is that overexpressed BVES is mislocalized and that cytoplasmic BVES is sequestering other proteins, preventing their translocation to the nucleus. Perhaps BVES is indirectly affecting the localization/activity of GSK3β through an association with PP2A (which is known to bind both BVES and GSK3β) and therefore overexpressing BVES is having a dominant negative effect on some components of the Wnt signaling pathway. Overall, a more detailed understanding of BVES protein levels and localization will allow for more carefully controlled and informative experiments when studying a protein that can exhibit such dynamic subcellular localization.

Further characterizing BVES degrons and post translational modifications

While the identification of putative D-Box and FBXW7 degrons was initially encouraging, overall it is felt that these motifs are not contributing to BVES stability by influencing degradation and proteasomal degradation directly. Nonetheless, the BVES D/F double mutant demonstrated significantly enhanced protein expression which provides a valuable tool to further probe BVES function. Furthermore, WT BVES and the D/F double overall shared very similar protein-protein interactions by mass spectroscopy (Table 5), suggesting that the higher expressing D/F double mutant can be utilized in functional studies. Additional studies to elucidate the mechanism by which the D-Box and FBXW7 mutations confer enhanced stability are necessary. As the D-Box motif is a target of the anaphase-promoting complex (APC/C) which ubiquitinates predominately cell cycle proteins for subsequent degradation by the 26S proteasome [266], it will be important to determine how BVES protein levels change throughout the cell cycle. Perhaps the subcellular localization of BVES as cells reach confluency is not just due to cell-cell proximity but is also a byproduct of cells progressing towards an arrest/contact inhibited state which indirectly stabilizes BVES. By performing cell synchronization experiments using a double thymidine block, cells will arrest at the G1/S boundary and can then be assessed at 0, 2, 6, 8, 10, 12, 14, and 24 hours after release/serum addition. Levels of CyclinA and CyclinB along with BVES can be monitored by western blot. Alternatively, if these experiments are performed using a GFP-tagged BVES construct, cells can be analyzed by flow cytometry for GFP-BVES levels concurrently with cell cycle analysis using PI. It would not be surprising if BVES protein levels change throughout the cell cycle as significant junctional remodeling occurs during cell division, at least in the *Xenopus laevis* embryo[267]. Another key experiment to determine the functional contribution of the putative D-Box and FBXW7 degrons would be to transfer these motifs to a different protein, such

as GFP which is frequently used in these types of functional studies because of its relative stability and ease of detection[268]. As the FBXW7 degron is a phospho-dependent degron, an in depth analysis of phosphorylated residues within BVES will be essential. PhosphoSitePlus compiled a list of phosphorylated residues within human, mouse, and rat BVES (Y3, S7, Y194, T218, S295, S315, S318, S322, and S323). The functional significance of these residues has not been determined but a broader understanding of the BVES-phospho proteome may be gained by introducing individual alanine point mutations at these residues and assessing BVES stability and subcellular localization. Of note, none of these phosphorylated residues fall within the putatively predicted GSK3β sites, suggesting that the FBXW7's phospho-degron may not be dependent on priming phosphorylation by GSK3β. One way to test this would be to treat cells with the GSK3β inhibitor CHIR99021 and assess for BVES stability. Overall, it is also important to determine the location of these motifs when factoring in membrane topology. Based on the known BVES membrane topology, both the D-Box and FBXW7 degrons would be extracellular when BVES is inserted in the plasma membrane. However, when BVES is cytoplasmic or when BVES is being processed in the endoplasmic reticulum, these motifs would be cytoplasmic. Finally, while generating C-terminal truncation mutants and individual lysine point mutations at putatively ubiquitinated residues was unsuccessful, a more thorough analysis may be beneficial. Namely, it has been reported that mutating individual lysine residues can lead to ubiquitination at different lysine residues within the protein and therefore it may be necessary to generate pan-lysine mutants[269,270]. Mutating all three putative BVES lysine residues, and even a more drastic pan-BVES lysine mutant, is therefore a reasonable approach. As an aside, one of the putatively ubiquitinated BVES residues, K272, has been previously implicated in homotypic BVES interactions. Perhaps homodimerization of BVES at that K272 lysine residue protects those residues and subsequently BVES from ubiquitination and proteasomal degradation. For the

truncation mutations, N-terminal Flag tagged BVES was utilized due to the ease of inserting stop codons to generate truncated proteins. However, a more elegant approach would be to introduce interstitial mutants utilizing 'round the horn PCR (such an approach was utilized to generate the BCAR3 SH2 domain interstitial mutant). Additionally, making these interstitial mutants in both the N-terminal and C-terminal tagged constructs would provide for robust confirmation of any important functional domains that affect BVES stability. There is a tremendous opportunity to study some of these basic questions pertaining to BVES structure, function, and stability and doing so will likely generate important reagents and address fundamental questions about BVES's dynamic function.

Notable BVES interactors identified by mass spectroscopy

Overall, it is hypothesized that BVES orchestrates changes in cellular and epithelial states through complex and dynamic protein-protein interactions, many of which are thought to occur within the BVES POPEYE domain and therefore may be conserved across all POPDC family members. The two mass spectroscopy experiments performed over the course of these studies provide a trove of data and putative interactors that may further elucidate novel BVES directed regulatory mechanisms. In the first mass-spec experiment, over 10% of the identified interactors (15/140) were related to ubiquitination and proteasomal degradation such as ubiquitin itself (Polyubiquitin-B/UBB) and a multitude of 26S proteasome regulatory subunits. Many of these same subunits were identified in the second BVES mass spectroscopy experiment as well (Table 6). While it is possible that these are contaminants, an unrelated mass spectroscopy experiment assessing STK17A and BCAR3 interactors did not identify any of the 26S protease or proteasome regulatory subunits (data not shown). Conversely, multiple heterogeneous nuclear

ribonucleoproteins (HNRNPs) and 60S ribosomal proteins were identified in all three experiments (both BVES experiments and the unrelated STK17A/BCAR3 mass spectroscopy experiments) and therefore are likely indicative of contamination. Together, the enrichment of proteasome regulatory subunits binding to BVES is supportive of a proteasomal degradation pathway regulating BVES protein levels.

One of the more notable hits identified in both mass spectroscopy screens is Proteasomal ubiquitin receptor, ADRM1, otherwise known as Adhesion Regulating Molecule 1. ADRM1, as its name suggests, functions as a ubiquitin receptor that works in concert with shuttle factors to supply the 26S proteasome [271]. Therefore, it is hypothesized that ADRM1, an interferon-inducible, heavily glycosylated membrane protein, may be contributing to the proteasomal degradation of BVES. Interestingly, ADRM1 gene amplification may drive metastatic gastric cancer [272] and it is consistently overexpressed in ovarian high-grade serous carcinoma[273]. Confirming the BVES-ADRM1 interaction and also knocking down ADRM1 then assessing BVES stability would help determine whether ADRM1 is contributing to BVES degradation and worth investigating further.

Additional mass spectroscopy hits may also lead to further understanding of BVES function. In both mass spectroscopy experiments, a cAMP-dependent protein kinase regulatory subunit, PRKAR1A, was identified. Additionally, in the first mass spectroscopy experiment cAMP-dependent protein kinase catalytic subunit beta (PRKACB), and another cAMP-dependent protein kinase regulatory subunit, PRKAR2A, were identified. A previously commissioned yeast-two-hybrid screen performed in a placental library with BVES as the bait protein also identified a likely direct interaction between A-kinase anchor protein 220 (AKAP220) and BVES. AKAPs are large docking proteins which provide a scaffold and help localize the cAMP-dependent protein kinase (PKA) to various locations within the cell[274,275]. PKA itself is a tetrameric holoenzyme

which consists of two regulatory subunits and two catalytic subunits. The regulatory subunits bind cAMP which leads to a conformational shift, freeing the catalytic subunits from the complex and allowing them to phosphorylate serine and threonine residues. It is known that BVES binds cAMP with high affinity[58] and given the number of PKA-directing proteins that BVES interacts with, it seems quite reasonable to purpose that BVES has considerable influence over PKA activity. In support of this, *BVES* siRNA knockdown in HEK293T cells increased CREB phosphorylation at S133 (Figure 11E and Figure 12D), a residue that is phosphorylated in response to cAMP by PKA[276]. CREB pS133 is also a known target of PP2A and in the aforementioned experiments, CREB phosphorylation was assayed as a positive control to confirm activity of the PP2A inhibiting and activating compounds, OA and Ceramide, respectively. As BVES can also direct PP2A activity, the role of BVES in modulating CREB activity may be multifaceted: both in modulating PKA activity to phosphorylate CREB and in directing PP2A to dephosphorylate PP2A. Specifically with regards to PKA, these data suggest that BVES may be inhibiting PKA activation which has tremendous implications with regards to multiple cellular signaling processes such (reviewed in [277]). To address this question, looking at levels of known target genes downstream of CREB such as *Pck1, Ppargc1a, and Crem* following BVES knockdown will be informative. Performing these studies in the setting of enhanced cAMP signaling, such as following forskolin stimulation[278], should lead to more dramatic differences. Furthermore, performing rescue experiments with BVES or the BVES:cAMP uncoupling mutant (D200A) would further validate that this modulation is dependent on BVES binding cAMP. Given the link between CREB signaling and metabolism, along with the fact that BVES regulates c-Myc[73], another key regulator of cellular metabolism[279], it might also be fruitful to do baseline characterization of glucose levels in the fed and fasted state in the *Bves*$^{-/-}$ animals[280].

Any proteins identified as putative interactors in two independent, well controlled, mass spectroscopy experiments are worth additional exploration. One such protein is TGF-Beta-Activated Kinase 1 and MAP3K7-binding protein 1, or TAB1 which was identified in the first mass spectroscopy experiment and was also shown to interact with all 3 BVES constructs in the second mass spectroscopy experiment (Table 6). Additionally, mitogen-activated protein kinase kinase kinase 7 (MAP3K7) otherwise known as TGF-Beta-Activated Kinase 1 or TAK1 was also identified in the second mass spectroscopy experiment as interacting with all three BVES constructs Table 5). TAB1 is a specific activator of TAK1, therefore these studies identify BVES as a putative interactor mediating TAK1 signaling. TAK1 is activated by TGF-β, bone morphogenic protein (BMP), interleukin-1, and TNFα and has been shown to strongly induce NF-κB activation[281] as well as AP-1 mediated transcription downstream of JNK/p38MAPKs[282]. Previous studies have demonstrated that in response to TNFα, the JNK/p38MAPK pathway is activated downstream TAK1 and that activation of this pathway enhanced cell migration on fibronectin *in vitro* and *in vivo* lung metastasis using a tail vein injection of colon 26 cells[283]. Furthermore, the TAK1-NF-κB pathway has been linked with establishing and maintaining EMT[284,285]. Additionally, there is also considerable evidence for the role of TAK1 in immunity, which is not surprising given the pivotal roles NF-κB and AP-1 play in the immune system[286-288]. Correspondingly, we have previously shown that BVES is underexpressed in moderate to severe ulcerative colitis and that BVES loss increases colonic injury after both *Citrobacter rodentium* infection and DSS induced colitis[89]. Overall, a review of the TAB1/TAK1 literature reveals a multitude of phenotypes that closely align with phenotypes regulated, at least in part, by BVES and it would seem that BVES may be inhibiting activation of TAK1 to attenuate NF-κB and AP-1 mediated programs. Therefore, a careful analysis of a putative

BVES-TAK1/TAB1 interaction and whether this interaction mediates inflammatory programs and TAK1 regulated signaling cascades is necessary.

Optimization and validation of BVES conditional knockout mice

Overall, the data generated while characterizing the BVES conditional knockout mice is encouraging. As expected, it appears that Exon 4 of *Bves* is flox-able but the recombination at this site is very inefficient. One possible explanation for this is the presence of the PGK promoter and neomycin cassette which adds nearly 2600 bp to the genomic region between the loxP sites. Ultimately, it will likely be necessary to cross the $Bves^{fl/fl}$ mice with the FLP delete mouse (Jackson Laboratory mouse strain 003946). This mouse constitutively expresses FLP recombinase from the ROSA26 allele and will allow for the deletion of the neomycin cassette (which is flanked by FRT sites). In the interim, treating the $Lrig1\text{-}CreER;Bves^{fl/fl};mTmG^{+/-}$ enteroids with a lentivirally delivered FLP recombinase and then repeating the experiments outlined in Figure 38 and Figure 39 would provide proof of principal and confirm the need to perform additional breeding to delete the neomycin cassette. Alternatively, these enteroid cultures could be transduced with a lentiviral or adenoviral cre recombinase which would likely provide much higher levels of cre recombinase than what is produced from the endogenous *Lrig1* locus and this may enhance recombination efficiency. It may also be worth isolating MEFs from $Bves^{fl/fl}$ mice and treating these sequentially with a lentiviral FLP recombinase followed by a lentiviral cre recombinase. MEFs are a highly functional system for this type of assay because they are easy to isolate, cheaper to maintain than enteroid cultures, and provide ample amounts of DNA and RNA (which can be somewhat difficult to obtain with enteroid cultures).

Assuming that deleting the neomycin cassette significantly increases the recombination efficiency, the conditional *Bves* knockout mice will be an invaluable tool to probe epithelial intrinsic vs. extrinsic roles. Overall, an analysis of the ImmGen database suggests that *Bves* transcript levels are low across the majority of immune cell populations, suggesting that *Bves* loss may be having minimal effect in immune cells in the global knockout mice, though this has not been formally tested. By crossing the *Bves* floxed mice with a LysMcre driver mouse and performing an AOM/DSS inflammatory carcinogenesis challenge, how non-epithelial *Bves* expression, specifically in myeloid cell lineages (monocytes, mature macrophages, and granulocytes), can be assessed. Alternatively, epithelial-cell intrinsic contributions of *Bves* can be assessing using the *Lrig1-CreERT2[19]* driver or the inducible *vil-Cre-ERT2*[289]. Studies looking at crypt/stem cell dynamics following conditional deletion of *Bves* utilizing the *Lrig1-CreERT2;mTmG*$^{+/-}$ mice (to lineage trace recombined cells) would also help confirm prior studies demonstrating enhanced Wnt tone and stemness following *Bves* loss with the added benefit of conditional deletion. The conditional deletion in this setting is important as it will delineate how transient loss of *Bves* alters cellular phenotypes without confounding effects from cellular compensation. Assessing the contribution of the other POPDC family members (POPDC1 and POPDC3) after conditional epithelial deletion vs. global epithelial loss from birth may highlight functional redundancy among the family members). In a panel of CRC cell lines, *POPDC2* expression was higher than *BVES* expression while *POPDC3* expression is lower and more approximate to *BVES* expression levels; this suggests that perhaps *BVES* and *POPDC3* are both downregulated in tumorigenesis and therefore may be acting more similarly to each other than *POPDC2* which has similar levels in "normal" cell lines (YAMCs) and CRC cell lines[41]. Similar to CRC, *BVES* is also downregulated in breast tumors compared to normal breast tissue, therefore the conditional knockout mice would also be useful to investigate the role of *Bves* in breast

epithelial tissues, breast cancers, and breast cancer metastasis. One approach would be to cross the *Bves*$^{fl/fl}$ mice with the MMTV-Cre mouse and the MMTV-PyVmT and assess tumor burden and metastasis[290]. A simpler approach would be to just cross the *Bves* global knockout mice with the MMTV-PyVmT mice but the caveat again would be the use of a global knockout as opposed to an epithelial specific knockout. Perhaps using the global knockout first to assess for any increase in tumor burden/metastasis would be worthwhile with follow up studies taking advantage of the epithelial specific knockout.

Further characterization of BCAR3 regulation and post-translational modifications

Our studies provide new insight into BCAR3 function within the cell, however little is known about how BCAR3 itself is regulated within the cell. A study by Guo *et al.* demonstrated that TGFβ led to reductions in BCAR3 protein levels[252] and determining whether this phenotype is also observed in TGFβ responsive CRC cell lines (such as the SW480 cells co-expressing exogenous Smad4 and TGF-β type II receptor[254]). Lerner and colleagues demonstrated that murine *Bcar3* transcript and BCAR3/AND-34 protein levels are increased in response to IL-1β and TNFα stimulation[215], suggesting that BCAR3 may be responsive to inflammatory signaling. This could explain why a subset of queried human CRC samples express higher levels of BCAR3 as there are reports that sporadic CRC can contain high degrees of inflammation[291,292]. Treatment of WT enteroids with TNFα and characterization of *Bcar3* transcript and protein levels would be informative. Furthermore, there is evidence to suggest that BCAR3 itself undergoes tyrosine phosphorylation in response to both serum stimulation and adhesion to fibronectin. Defining the phosphorylated BCAR3 residues with mass spectroscopic

approaches and determining how these phosphorylation events alter binding of BCAR3 interactors may help elucidate context specific roles for BCAR3 signaling and clarify some of the discrepant phenotypes observed. Additionally, the upper band observed in some cell lines with the BCAR3 antibody (Figure 20F) is uncharacterized. Interestingly, with transient BCAR3 knockdown via siRNA, the intensity of this upper band increases in some cell lines. However, stable CRISPR mediated knockout of BCAR3 in the HT29 cells (Figure 30C) did not lead to deletion of this upper band, suggesting that it may not be a BCAR3 product. It is unlikely that this upper BCAR3 band is another NSP family member as NSP1 is around 63 kDa and NSP3 is about 77 kDa, decreasing the likelihood of these being identified as proteins running higher than BCAR3/NSP2 (which runs at about 93 kDa) and the family members only share between 25 and 39% homology[293]. Analysis of NSP1 and NSP3 protein and transcriptional changes in response to both transient and chronic BCAR3 depletion will help address whether these family members aid in compensating for BCAR3 loss.

Identification of BCAR3 interactors

The key to further elucidating cellular signaling cascades regulated by BCAR3 will likely depend on identifying BCAR3 protein-protein interactions as only modest changes in gene expression have been observed with BCAR3 overexpression[294]. A previous report focusing on breast cancer associated apoptotic genes identified an interaction between BCAR3 and both proteasome 26S subunit ATPase 3 interacting protein (PSMC3IP) and epithelial-stromal interaction 1 (EPSTI1). Focusing on how these interactions, and how BCAR3 in general, regulate apoptosis will be essential. Quantification of apoptosis by cleaved caspase 3 and TUNEL in *Bcar3*$^{-/-}$ tumors may provide one explanation for why these tumors were smaller on average. Furthermore,

looking at how altering BCAR3 expression in CRC cell lines modifies response to commonly used chemotherapeutics in colon cancer such as 5-Fluorouracil (5-FU) and platinum based compounds such as oxaliplatin may allow for stratification and treatment prognostication by BCAR3 levels.

To identify novel BCAR3 interacting proteins, we have generated BCAR3 constructs fused to a promiscuous biotin ligase (BioID2) allowing for capture of biotinylated proteins in close proximity to BCAR3 and are currently optimizing conditions for immunoprecipitation and mass spectroscopic analysis[295]. These data will allow for further identification of BCAR3 interactors, specifically those that may be transient or context dependent. Additionally, we are very interested in further exploring a potential interaction between BCAR3 and the receptor tyrosine kinase c-Met. Using both protein microarrays and high throughput fluorescence polarization, Leung and colleagues identified an interaction between c-MET and BCAR3's SH2 domain, possibly localized to phosphorylated Y1365 residues. While we have been unable to confirm an interaction by co-immunoprecipitation, it is possible that this interaction is low affinity or mediated by additional proteins that are lowly expressed in HCT116 cells, in which the preliminary studies have been carried out. Utilizing additional approaches (overexpressing c-MET, proximity ligation assay, directed yeast-two-hybrid) would aid in confirming a biologically relevant interaction. Overall, the preliminary data suggest that BCAR3 loss can lead to increases in total c-MET and that, paradoxically, overexpression of BCAR3 (in cells with BCAR3 knockout) further increases total c-Met levels with varying effects on phosphorylation of c-Met tyrosine residues (Figure 31). This increase in c-MET levels was not observed with siRNA knockdown of BCAR3, suggesting that constitutive loss of BCAR3 promotes cellular reprogramming which either enhances c-MET protein stability or increased gene transcription. Further understanding these dichotomous effects will be critical to the understanding of the putative BCAR3-c-MET interaction in colorectal and other cancers. To address the varying phenotypes, performing unbiased proteomic (SILAC) and

transcriptional (RNA-sequencing) analysis following acute and chronic loss of BCAR3 will be beneficial. Careful attention to cellular confluency and substrate composition (performing these experiments with and without fibronectin coated tissue culture plates) will be essential.

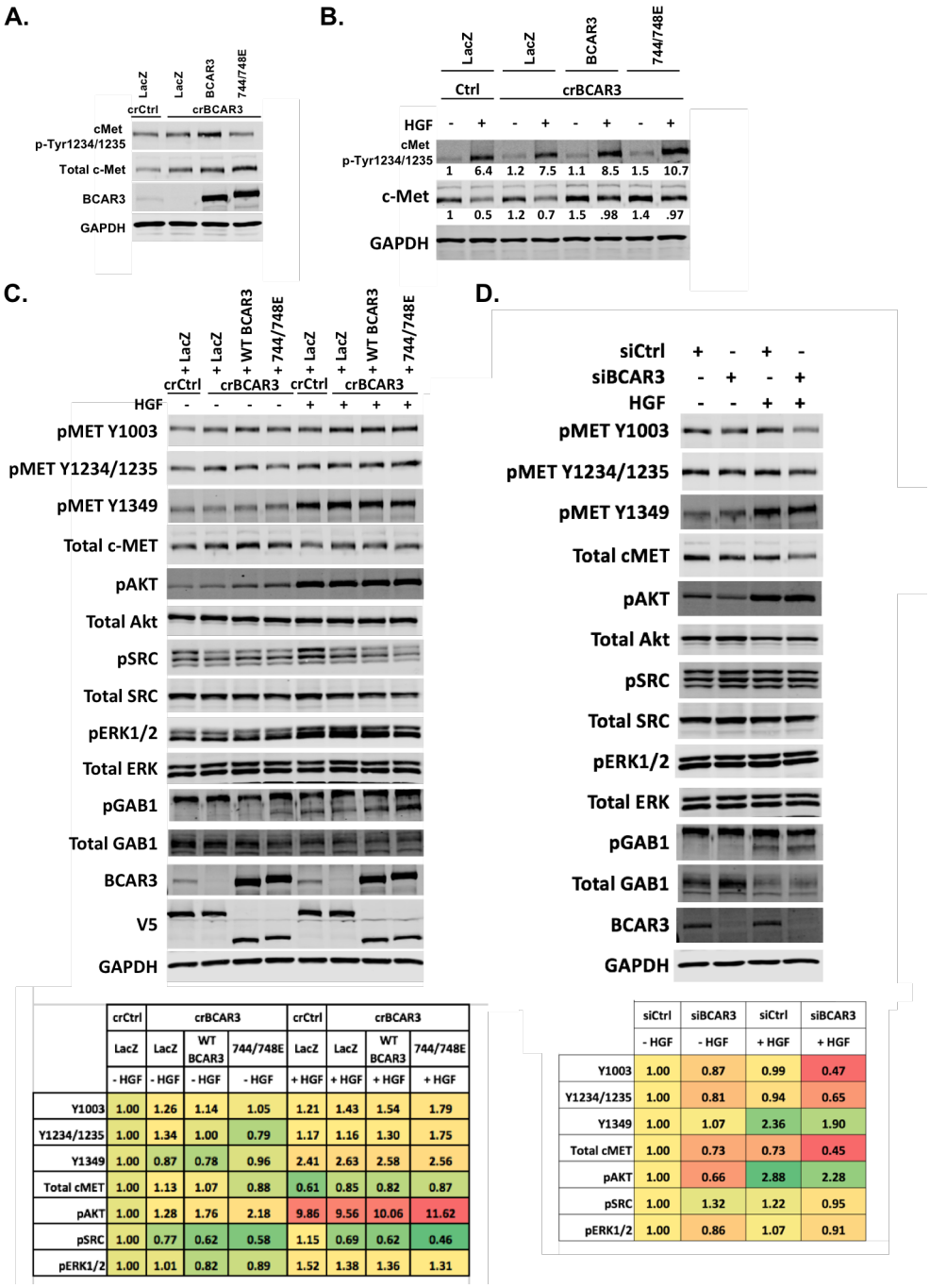

	crCtrl	crBCAR3			crCtrl	crBCAR3		
	LacZ	LacZ	WT BCAR3	744/748E	LacZ	LacZ	WT BCAR3	744/748E
	- HGF	- HGF	- HGF	- HGF	+ HGF	+ HGF	+ HGF	+ HGF
Y1003	1.00	1.26	1.14	1.05	1.21	1.43	1.54	1.79
Y1234/1235	1.00	1.34	1.00	0.79	1.17	1.16	1.30	1.75
Y1349	1.00	0.87	0.78	0.96	2.41	2.63	2.58	2.56
Total cMET	1.00	1.13	1.07	0.88	0.61	0.85	0.82	0.87
pAKT	1.00	1.28	1.76	2.18	9.86	9.56	10.06	11.62
pSRC	1.00	0.77	0.62	0.58	1.15	0.69	0.62	0.46
pERK1/2	1.00	1.01	0.82	0.89	1.52	1.38	1.36	1.31

	siCtrl	siBCAR3	siCtrl	siBCAR3
	- HGF	- HGF	+ HGF	+ HGF
Y1003	1.00	0.87	0.99	0.47
Y1234/1235	1.00	0.81	0.94	0.65
Y1349	1.00	1.07	2.36	1.90
Total cMET	1.00	0.73	0.73	0.45
pAKT	1.00	0.66	2.88	2.28
pSRC	1.00	1.32	1.22	0.95
pERK1/2	1.00	0.86	1.07	0.91

Figure 31. BCAR3 augments c-MET levels. (A) HCT116 BCAR3 CRISPR knockout/resuce lines were probed for basal c-MET and phospho c-MET (Tyr1234/1235) in complete serum. (B) and (C) HCT116 lines as in (A) were serum starved overnight then treated with 30 ng/mL HGF for 30 minutes. (D) HCT116 were treated with control or BCAR3 siRNAs. 48 hours later, cells were serum starved overnight then treated with 30 ng/mL HGF for 30 minutes.

BCAR3, BVES, and YAP

Hippo-YAP-TAZ signaling is a potent regulator of cell differentiation, tissue homeostasis, proliferation, and contact growth inhibition in cells and contributes to cell polarity downstream of both tight-junctions and adherens junctions[296]. The Hippo pathway is also regulated by soluble growth factors such as EGF, BMP/TGFβ, and Notch pathways. While classically thought to promote tumorigenesis[297], there are also report that YAP acts as a tumor suppressor[298]. Integration of upstream activators leads to a kinase cascade which activates the serine/threonine kinases LATS1/2 which go on to phosphorylate YAP, thereby promoting its cytoplasmic retention[299]. Specifically, YAP1 phosphorylation at S127 by LATS promotes cytoplasmic sequestration reduced YAP signaling. Given the abundance of pathways regulating YAP, it is not surprising that YAP and TAZ have been implicated in dual roles within the intestinal epithelium: both promoting the proliferation of intestinal stem/progenitor cells and increasing their differentiation into goblet cells via binding of TEA domain transcription factors (TEADs) and Kruppel Like Factor 4 (KLF4), respectively[300]. For nearly every YAP/TAZ associated phenotype, one can recall a study or an experiment that could foreseeably link BVES and/or BCAR3 to this pathway. For example, BVES is a tight-junction associated protein and both BVES and BCAR3 appear to be regulated by cellular confluency, as is YAP. Excitingly, in the previously discussed yeast-two-hybrid screen performed in the Williams lab, YAP1 was identified as a very high confidence interaction. Additionally, a recent study demonstrated that the orphan receptor tyrosine kinase ROR1 phosphorylates HER3 at Tyr1307 in response to neuregulin stimulation which can ultimately modify YAP phosphorylation. The SH2 domain of BCAR3 was found to bind HER3-phospho-Tyr1307 and recruit additional complex proteins to modify YAP signaling[301]. This study affirmed that studying BCAR3 and ErbB family members is worthwhile

and highlighted the nuances of BCAR3 interactions (BCAR3 only bound to the HER3-phospho-Tyr1307 following neuregulin stimulation, doing so without modifying its phosphorylation levels). Further, this study provided the rational to test whether or not modifying BCAR3 levels in other cell lines can modify YAP signaling. Exciting, BCAR3 knockout promoted increased YAP1 Ser127 phosphorylation in the H1299 lung adenocarcinoma cell line, the SW480 CRC cell line, and in primary human tumoroids. Conversely, overexpression of WT BCAR3 appeared to rescue the phenotype. This preliminary study provides strong rationale to further assess BCAR3's influence on YAP1 signaling. Assessing expression of YAP1 target genes such as connective tissue growth factor (CTGF) and cysteine rich angiogenic inducer 61(CYR61) in human cell lines and *Bcar3*$^{-/-}$ intestinal tissues/tumors will be of value. Furthermore, immunofluorescence analysis determining the ratio of YAP nuclear/cytoplasmic localization on a per cell basis, especially within the intestinal crypts, may identify specific zones of regulation.

Overall, this story began with the characterization of a novel role for BVES in regulating Wnt signaling and then focused on the BVES binding partner, BCAR3. Given the striking similarities between phenotypes linked with BVES and YAP1 signaling, it seems only fitting to conclude by proposing that the BVES-BCAR3 interaction may be controlling YAP mediated transcription, thereby providing a novel mechanism by which BVES, through its interaction with a complex of proteins recruited by BCAR3, can regulate YAP1, a key regulator of tumorigenesis.

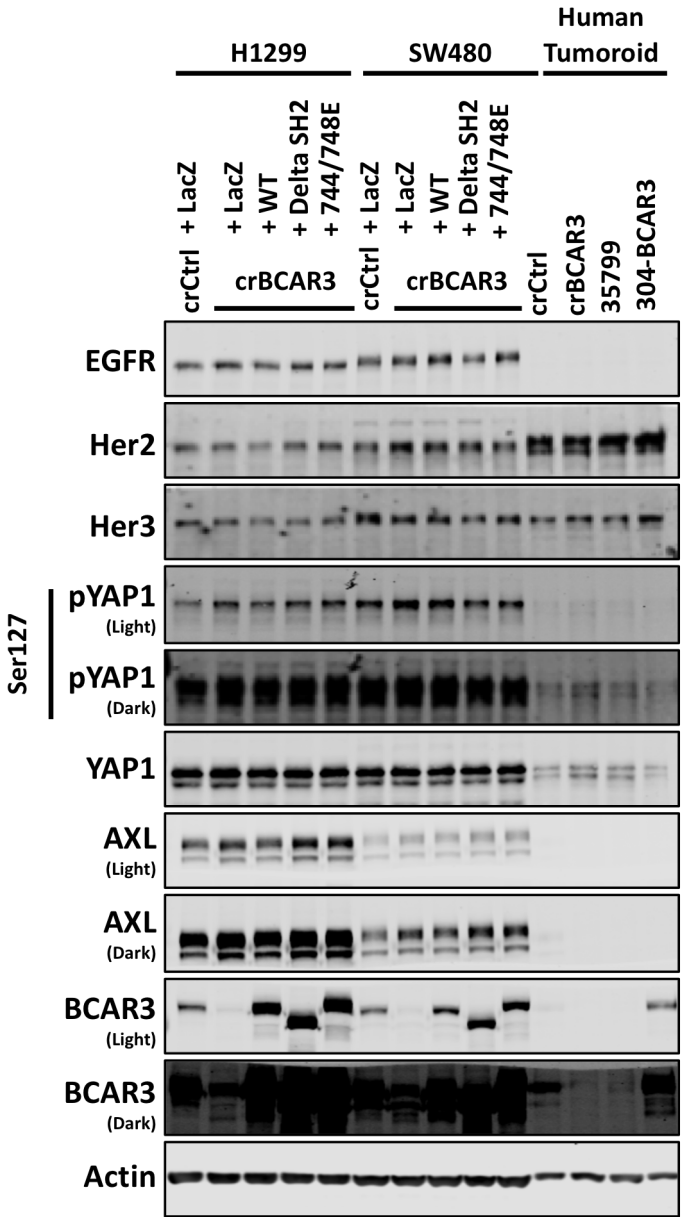

Figure 32. BCAR3 regulation of YAP1 phosphorylation. BCAR3 knockout and rescue in the lung adenocarcinoma H1299 line, the SW480 colorectal cancer cell line, and a primary human tumoroid line.

APPENDIX

A. Generation of full-length human BVES expressing cell lines

Previous studies of BVES have identified key residues within the BVES protein that are important for BVES function including the previously mentioned lysine residues (K272 and K273)[36] which are required for BVES homodimerization, the cAMP binding residues (D200A, E203A, and V217F), and two consensus asparagine residues (Asn20 and Asn27) which are heavily glycosylated[32]. Beyond the studies identifying glycosylation sites in BVES, there is little if any other data that identified how (or if) post-translational modifications (PTMs) affect BVES structure or function. Furthermore, most of the studies on BVES have utilized Chick, murine, or truncated BVES expression constructs to study BVES function. One possible reason for these approaches is that, at least in our experience, full-length Human BVES has been relatively difficult to express. Based on personal experience and that of others in the lab, expressing BVES in colorectal cancer cell lines has been especially difficult while detectable protein expression is more readily observed in non-cancerous cell lines such as HEK293Ts. Others have also observed that treating BVES expressing cells with the proteasome inhibitor MG132 can increase BVES protein levels, suggesting that BVES degradation may be occurring through ubiquitination followed by subsequent proteasomal degradation.

To evaluate these observation, stable cell lines were generated in the RKO colorectal cancer cell line and the noncancerous HEK293T human embryonic kidney cell line utilizing 5 different lentiviral BVES expression constructs with various epitope tags (Figure 33). BVES expression was nearly undetectable in the RKO stable cell lines even after antibiotic selection allowed for stable cell line generation, however robust levels of expression were observed in the

293T cells. Interestingly, differential banding patterns were observed depending on whether BVES was expressed with N-terminal vs. C-terminal protein tags. Specifically, the N-terminal Flag-BVES (N-Flag-BVES) demonstrated a triplet banding pattern while only a single prominent band was observed with the C-terminal Flag-BVES (C-Flag-BVES). Similarly, the C-terminal GFP tagged BVES demonstrated a mobility shift upward relative to the N-terminal GFP tagged BVES. These mobility shifts, along with the differential banding pattern are suggestive of PTMs. Specifically, the triplet banding pattern in the N-Flag-BVES construct is reminiscent of observations made by Knight *et al.* utilizing Chick BVES and may be due to differential glycosylation[32].

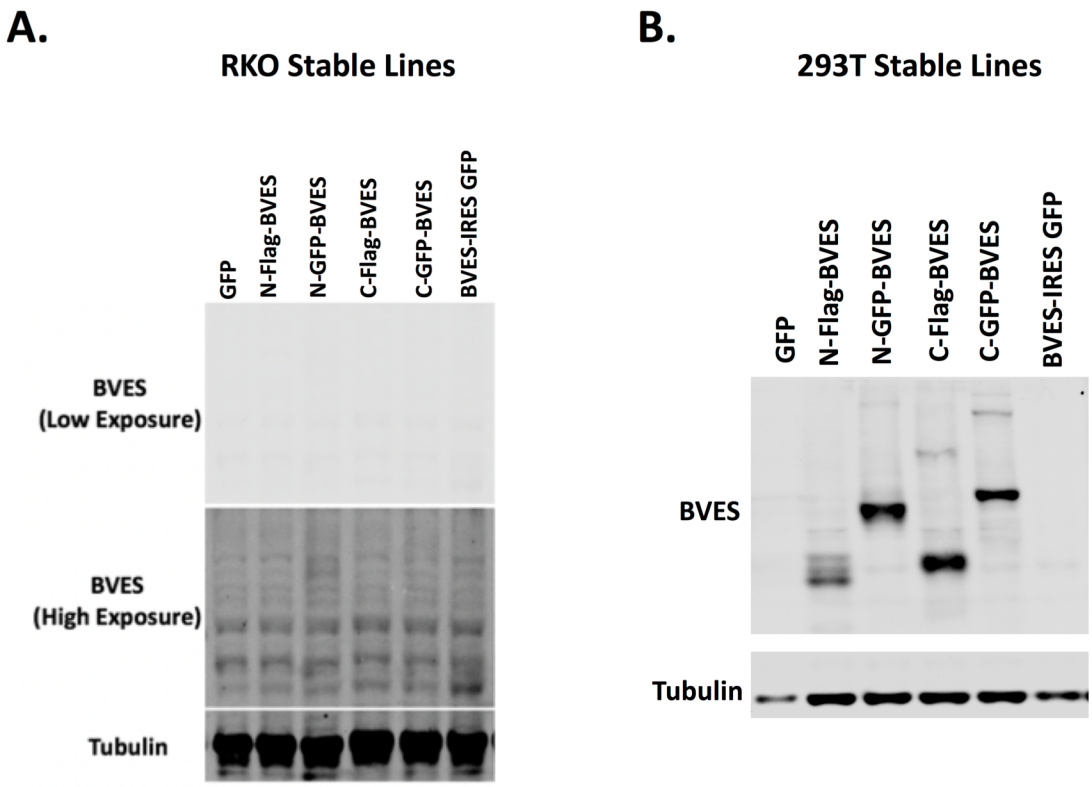

Figure 33. Generation of stable BVES expressing cell lines. (A) Western blot demonstrating minimal detectable levels of full length human BVES protein in the RKO CRC cell line. Cell lines were transduced with lentiviral particles expressing control GFP, N-terminal and C-terminal flag tagged BVES, N-terminal and C-terminal GFP tagged BVES, or an untagged BVES construct. Successful transduction was confirmed via GFP expression and puromycin selection. (B) Western blot as in (A) of HEK293T cells stably expressing BVES expression constructs.

B. Identification of BVES motifs impacting protein stability

To identify additional protein motifs present within the primary BVES amino acid sequence that may be amenable to PTMs, an insilico approach was employed. Analysis utilizing the Eukaryotic Linear Motif (ELM) [302] and Protein Domain Prediction E Pipeline reveled multiple conserved sequences with putative functional significance. As proof of principle, this pipeline identified N-terminal glycosylation motifs within BVES which had been experimentally demonstrated previously[32]. Of particular interest were two different protein degron motifs, hereby referred to as the D-Box and FBW7/FBXW7 (or simply F-Box) motifs (Figure 34). The D-Box consist of an RxxL consensus motif (Arginine followed by any two amino acids and then a Leucine) and was first identified as a degron promoting the degradation of Cyclin B[303]. Additional studies have identified the D-Box motif as a target of the anaphase-promoting complex (APC/C), a large complex of proteins directing E3 ubiquitin ligase activity to ubiquitinate predominately cell cycle proteins for subsequent degradation by the 26S proteasome[266]. The F-Box is a phospho-dependent degron that consists of a slightly more complex TPxxE motif (Threonine-Proline-X-X-Glutamate) which targets the F-box protein FBW7 (F-box and WD repeat domain-containing 7) and the accompanying SCF (SKP, Cullin, F-box containing) E3 ubiquitin ligase complex to degrade target proteins. FBW7 is considered to be a tumor suppressor and has been shown to target key proteins involved in proliferation, differentiation, apoptosis, and metabolism such as Myc, Notch, Cyclin E, and c-Jun[304]. Data from the TCGA supports this notion as FBXW7 is mutated in 10% of non-hypermutated CRC samples and 43% of hypermutated CRC samples[96]. Notably, FBW7 phospho-dependent degradation is, at least in some situations, dependent on the activity of GSK3β[305]. This is of particular interest as two GSK3β phosphorylation motifs within BVES were identified via ELM. Teleologically, the high rates of

FBXW7 mutations are not entirely consistent with our experiences expressing BVES as one would hypothesize that if FBXW7 is mediating BVES degradation in CRC cell lines, then cell lines with mutant FBXW7 may be more amenable to BVES overexpression. Nonetheless, RKO cells are FBXW7 wildtype[306]and a good model for assessing the contributions of the FBXW7 motif on BVES stability. Should the FBXW7 story prove a promising lead, a comparative analysis of BVES stability in WT vs. FBXW7 mutant cell lines (or WT vs. FBXW7 CRISPRKO cell lines) may prove enlightening. As both the D-Box and F-Box degrons are dependent on the activity of E3 ubiquitin ligases, additional insilico analysis using the curated PhosphoSitePlus website was performed to ask whether or not global proteomic screens had identified ubiquitinated residues on BVES by mass spectroscopy. Encouragingly, three highly conserved lysine residues (K122, K166, and K272) were identified by Wagner *et al.* in a global proteomic analysis of ubiquitylation sites in murine tissue[307]. To test the functional contribution of these various protein motifs on BVES stability, degron mutations were generated in full length human BVES by introducing R88A and L91A point mutations in the D-Box degron (hereby referred to as the D-Box mutant) and T18A, P19A, and E22A point mutations in the F-Box degron (hereby referred to as the FBXW7 mutant). An additional mutant containing all 5 amino acid substitutions in both degrons (D/F double mutant) was also generated. These constructs were then introduced via lentiviral transduction into HEK293T cells and the RKO CRC cell line. Expression of the D-Box mutant had a modest effect on BVES protein stability Figure 34) while the F-Box mutant increased BVES protein levels nearly 9-fold over WT. The D-Box/F-Box double mutant also demonstrated considerably higher levels of BVES protein expression Figure 34C and Figure 34D). To confirm that the observed differences in BVES protein levels were due to changes in protein stability and not transduction efficiency/mRNA transcript levels, qRT-PCR was performed on all cell line derivatives to measure BVES transcript levels. No observable difference in the levels of BVES transcript were detected,

suggesting that the changes in BVES protein levels were due to alterations in BVES protein stability or translational efficiency. Notably, differential banding patterns were again observed, especially upon introduction of the FBXW7 mutant.

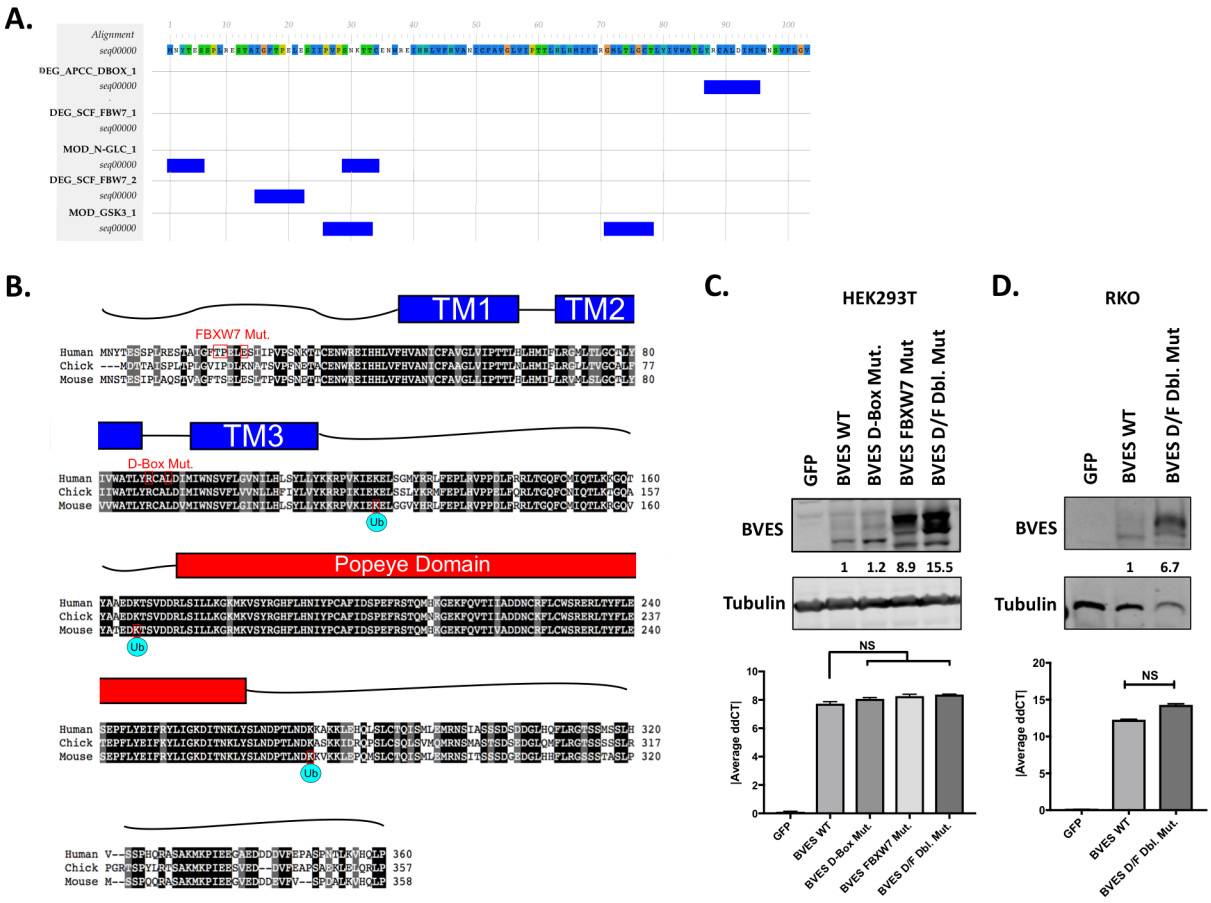

Figure 34. BVES degron mapping and generation of degron mutants. (A) Putative degrons within the primary sequence of BVES were identified using the Eukaryotic Linear Motif (ELM) resource (http://elm.eu.org). (B) BVES sequence alignment of Human, Chick, and Mouse BVES along with mapping of the BVES degrons to the BVES protein domains. TM1,2, and 3 in blue are membrane spanning regions while the Popeye Domain is aligned in Red. Ubiquitinated residues within murine BVES were identified using PhosphoSitePlus. (C) Stable HEK293T cells expressing WT BVES, D-Box mutant BVES, FBXW7 mutant BVES, or a D-Box/FBXW7 double mutant were generated via lentiviral transduction and probed for BVES expression. Below, BVES qRT-PCR was performed in all cell lines to assess BVES transcript level. (D) RKO stable cell lines were generated as in (C) and BVES expression confirmed by western blot. NS = by one-way ANOVA with Tukey multiple comparison testing.

C. Functional validation of BVES degrons

To determine whether the observed increase in protein levels in the BVES D/F double mutant was due to changes in protein stability, cycloheximide chase experiments were performed. Cells were treated with cycloheximide for up to 6 hours before protein harvest and western blot detection (Figure 35A). As seen previously, the D/F double mutant demonstrated significantly higher levels of BVES protein at baseline and had higher detectable levels out to 6 hours. However, given the higher starting levels of BVES, an end point analysis (comparing levels of WT BVES to the D/F double mutant only at 6 hours post cycloheximide) is insufficient. Instead, a half-life calculation utilizing the equation in Figure 35B was performed based on the signal intensity from all observed BVES bands at each time point, respectively. Upon initial evaluation, it appears that the BVES D/F double mutant demonstrates increased protein stability Figure 35C with a greater than 2-fold increase in the protein half-life. However, upon more critical review of this data, it appears that the lower band (presumably the unglycosylated band) actually demonstrates a very similar decay rate to that of WT BVES. The upper band in the D/F double mutant persists longer and demonstrate higher stability than the lower bands. It was subsequently hypothesized that, perhaps, the introduced mutations, are not directly affecting BVES ubiquitination and proteasomal degradation to alter stability but instead are altering PTMs, such as glycosylation, which are indirectly affecting BVES stability. To test this, mutant lines were treated with tunicamycin to inhibit N-linked glycosylation or the proteasome inhibitor MG132. If those upper BVES bands were indeed glycosylated, we would anticipate seeing a collapsing of those bands to a lower molecular weight species (as has been observed previously [32]) and if glycosylation was stabilizing BVES, we would expect that tunicamycin treatment (and subsequent inhibition of glycosylation) would reduce BVES protein levels. Indeed, this is what was observed suggesting

that the introduced D-Box and FBXW7 mutations may simply be altering glycosylation or ER processing of BVES to subsequently alter its stability (Figure 35D). Similar results were observed with the D/F double mutant (data not shown). In support of this, if the D-Box and FBXW7 mutations were preventing BVES ubiquitination and proteasomal degradation, then treating the mutant BVES derivatives with a proteasome inhibitor should have minimal stabilizing effect (as BVES is "maximally stabilized" already). However, it was observed that treatment of the D-Box and FBXW7 mutants with MG132 lead to further stabilization of the protein. This was particularly striking in the RKO cell line where baseline BVES express is very low (Figure 35D). This again supports the notion that these D-Box and FBXW7 mutations are not acting entirely by preventing BVES ubiquitination and proteasomal degradation. One possible explanation for this is that the introduced mutations (alanine point mutants) are insufficient to uncouple the BVES-E3 ubiqutin ligase interaction and further studies utilizing larger interstitial mutations or more hydrophobic point mutations (such as point mutations to glutamate) may be required. To more specifically test whether the introduced FBXW7 mutations were altering FBXW7-mediated proteasomal degradation, knockdown experiments in both BVES WT and the D/F double mutant were performed (Figure 35E). With similar rationale to the MG132 experiments, if the FBXW7 mutation is preventing FBXW7-mediated ubiquitination and proteasomal degradation, then knocking down FBXW7 specifically should increase WT BVES protein levels with little effect on the mutant BVES constructs. However, despite admittedly low levels of all around BVES expression in this experiment, and only a slight increase in WT BVES protein levels following FBXW7 knockdown, we observed that FBXW7 knockdown could further stabilize the D/F double mutant BVES protein. Partial knockdown of FBXW7 was confirmed by qRT-PCR (Figure 35E). Together, these data begin to address possible ways in which the D-Box and FBXW7 mutations

are affecting human BVES stability, likely in certain contexts and in some but not all cell types, and further investigation will be required.

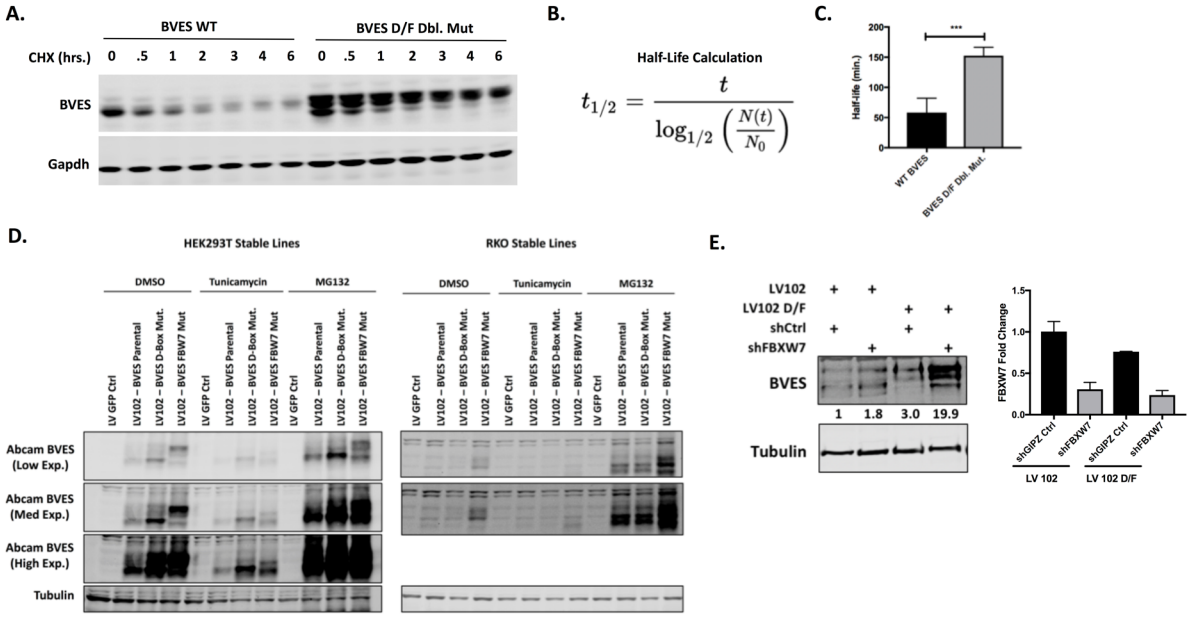

Figure 35. BVES degron functional validation. (A) HEK293T cells expressing either WT BVES or the BVES D/F double mutant were treated with 100 µg/mL cycloheximide (CHX) for the indicated time points. (B) Half-Life equation utilized to calculate BVES protein half-life from (A). All detectable signal (all bands) were quantified utilizing the Licor Imaging software for the BVES western blots to generate signal intensity. (C) Average BVES half-life quantification generated by comparing calculated BVES half-life from 0-0.5, 0-1, and 0-2 hrs. (D) Indicated HEK293T and RKO stable cell lines were treated with DMSO, 0.25 µg/mL Tunicamycin, or 0.5 µM MG132 for 18 hours before protein harvest and western blot detection. (E) LV102 (GFP Control) or BVES D/F double mutant stable HEK293T cells were transduced with a control shRNA or shRNA targeting FBXW7. 48 hours later, cells were harvested for protein and RNA. *FBXW7* transcript levels were assessed by qRT-PCR to validate partial knockdown.

D. Mass spectroscopic analysis for BVES PTMs and interacting proteins

Concurrently with the targeted approach focusing on specific degrons, a more unbiased approach was also pursued in hopes of identifying BVES PTMs and BVES interactors that may mediate BVES stability. A series of C-terminal truncation mutants were generated in the N-terminal Flag-tag full length human BVES expression construct by introducing stop codons by site-directed mutagenesis every 30 amino acids in the hopes of identifying regions contributing to BVES instability. Full-length human BVES is a 360 amino acid protein, therefore 8 truncation mutants were generated (BVES 330, BVES 300, BVES 270, BVES 240, BVES210, BVES180, BVES150, and BVES120). Unfortunately, none of these constructs, when transiently transfected into HEK293T cells, demonstrated detectable levels of expression. Similarly, 3 lysine point mutants (K122A, K166A, and K272A) were generated in full length human BVES (ubiquitination of these residues was identified in murine BVES and human and mouse BVES are highly homologous at these residues, Figure 34B). However, individual point mutations at these residues also did not lead to observable augmentation of BVES expression. Instead, a completely unbiased approach utilizing immunoprecipitation followed by mass spectrometry was pursued to identify PTMs within full length human BVES and to evaluate for potential interacting proteins that may be contributing to BVES protein degradation. In the first mass spec experiment, full length human BVES was treated with MG132 to increase BVES protein levels and enrich for potential post translational modifications followed by Flag-immunoprecipitation and flag peptide elution (Figure 36A). 10% of the sample was analyzed by western blot and the remaining 90% was run on a separate gel and coomassie stained. The band on the coomassie stained gel that was also detected by anti-flag western blot was excised and further processed for mass spec analysis. This approach

was taken to enrich specifically for high levels of BVES in sample with the hope of enriching for and subsequently identifying post translational modifications. BVES was the second highest abundant protein in the analysis behind Actin, confirming that the experiment worked from a technical aspect. Interestingly, a number of ubiquitin-related and proteasome related regulatory subunits also co-immunoprecipitated with BVES and serendipitously were similar in size (so as to co-migrate with the excised BVES band, Figure 36B). This supports a model of proteasomal degradation that may be contributing to BVES instability. Despite approaches taken to specifically increase the relative abundance of BVES within the sample, BVES spectral coverage was only 22%, meaning that a significant majority of digested BVES peptides were not identified in the analysis (Figure 36C). This may be due to a lack of tryptic digestion sites within these larger protein sequences. Importantly, of the putatively ubiquitinated residues (K122, K166, and K272), K166 and K272 had spectral coverage but were not identified as post-translationally modified or ubiquitinated. More sensitive, targeted approaches utilizing antibodies that specifically recognize ubiquitinated lysine residues such as those proposed by Udeshi *et al.* may be required [308]. A complete list of proteins identified by mass spectroscopic analysis is provided in Table 4. To confirm the identified mass spectroscopy hits and to expand the analysis to all interacting proteins (as opposed to just the proteins/protein fragments that co-migrated around the same molecular weight as BVES, a second mass spectroscopy experiment was performed. For this experiment, the following samples were immunoprecipitated and the entire sample was sent for analysis: Flag-tagged GFP control, N-terminal Flag-tagged BVES, N-terminal Flag-tagged BVES D/F double mutant, and C-terminal Flag-tagged BVES. The identified proteins, along with protein probability metrics, are provided in Table 5. Overall, there were many functionally relevant proteins and quite a few overlapping proteins identified in the two mass spectroscopy experiments that could prove

to be important mediators of BVES function in colorectal cancer. A more thorough analysis and discussion of the BVES mass spectroscopy hits is included in the Future Directions chapter.

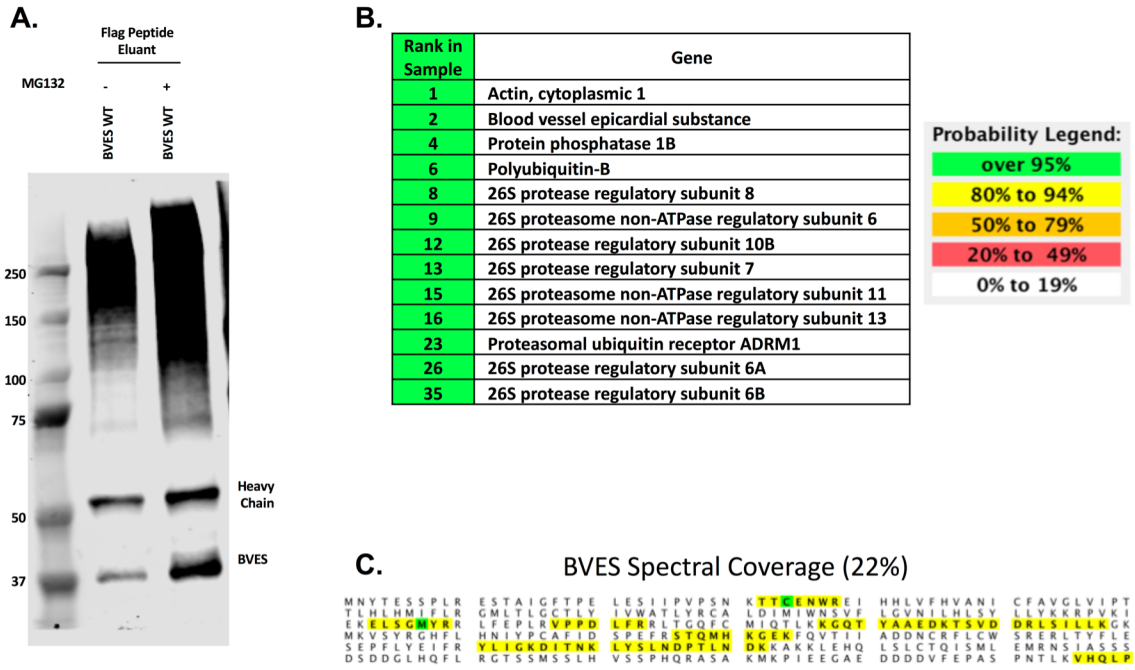

Figure 36. Mass spectroscopic analysis of full-length human BVES. (A) N-terminal flag tagged BVES was stably overexpressed in HEK293T cells. A total of 5 10-cm plates were treated with 1 μM MG132 for 14 hours followed by protein harvest and immunoprecipitation with anti-Flag M2 affinity resin. Proteins were eluted with 200 μL of 150 ng/μL 3X Flag Peptide. The eluent was concentrated using an Amicon Ultra centrifugal filter and then analyzed by western blot or coomassie blue staining. The 37 kDa band on the coomassie gel corresponding with immunoreactive BVES was excised and analyzed by mass spec. (B) A curated list of proteasome and ubiquitin related proteins identified in the BVES mass spec analysis. The left column indicates the overal abundance rank for each protein across the entire sample. The Probability Legend (right) indicates the protein threshold or confidence interval with which the peptide spectra are likely to belong to the indicated protein. For analysis, the protein and peptide thresholds were set to a 5% FDR with a minimum requirement of 2 peptides for each identified protein. (C) Spectral coverage and peptide sequences for BVES. Overall, 45 total spectra and 15 unique spectra comprising 12 unique peptide fragments were identified.

Rank in Sample	Gene Name	Gene ID
1	Actin, cytoplasmic 1	ACTB
2	Blood vessel epicardial substance	BVES
3	Heterogeneous nuclear ribonucleoproteins C1/C2	HNRNPC
4	Protein phosphatase 1B	PPM1B
5	Elongation factor 1-alpha 1	EEF1A1
6	Polyubiquitin-B	UBB
7	PIG TRYPSIN PRECURSOR	
8	26S protease regulatory subunit 8	PSMC5
9	26S proteasome non-ATPase regulatory subunit 6	PSMD6
10	Methylosome protein 50	WDR77
11	DnaJ homolog subfamily A member 2	DNAJA2
12	26S protease regulatory subunit 10B	PSMC6
13	26S protease regulatory subunit 7	PSMC2
14	RNA-binding motif protein, X chromosome	RBMX
15	26S proteasome non-ATPase regulatory subunit 11	PSMD11
16	26S proteasome non-ATPase regulatory subunit 13	PSMD13
17	Erlin-2	ERLIN2
18	Bovine Albumin	
19	Titin	TTN
20	Fructose-bisphosphate aldolase A	ALDOA
21	Elongation factor 1-gamma	EEF1G
22	Eukaryotic translation initiation factor 3 subunit E	EIF3E
23	Proteasomal ubiquitin receptor ADRM1	ADRM1
24	60S ribosomal protein L3	RPL3
25	cAMP-dependent protein kinase catalytic subunit beta	PRKACB
26	26S protease regulatory subunit 6A	PSMC3
27	DnaJ homolog subfamily B member 12	DNAJB12
28	Spliceosome RNA helicase DDX39B	DDX39B
29	Titin	TTN
30	Keratin 10	KRT10
31	DnaJ homolog subfamily A member 1	DNAJA1
32	60S ribosomal protein L4	RPL4
33	Eukaryotic initiation factor 4A-III	EIF4A3
34	RNA-binding protein 4B	RBM4B
35	26S protease regulatory subunit 6B	PSMC4
36	Protein arginine N-methyltransferase 5	PRMT5
37	Poly(rC)-binding protein 1	PCBP1
38	Guanine nucleotide-binding protein G(s) subunit alpha isoforms short	GNAS
39	Beta-actin-like protein 2	ACTBL2
40	Histone H1	HIST1H1D
41	Keratin, type II cytoskeletal 1	KRT1
42	Heterogeneous nuclear ribonucleoproteins A2/B1	HNRNPA2B1
43	Multifunctional protein ADE2	PAICS
44	Macrophage erythroblast attacher	MAEA
45	Erlin-1	ERLIN1
46	7-dehydrocholesterol reductase	DHCR7
47	Keratin, type II cytoskeletal 6A	KRT6A
48	Stomatin-like protein 2	STOML2
49	Acylglycerol kinase, mitochondrial	AGK
50	Basic leucine zipper and W2 domain-containing protein 1	BZW1
51	cAMP-dependent protein kinase type I-alpha regulatory subunit	PRKAR1A
52	Trifunctional enzyme subunit beta, mitochondrial	HADHB
53	Eukaryotic translation initiation factor 3 subunit G	EIF3G
54	Eukaryotic translation initiation factor 3 subunit F	EIF3F
55	Nuclear migration protein nudC	NUDC
56	Cytochrome b-c1 complex subunit 2, mitochondrial	UQCRC2
57	Eukaryotic translation initiation factor 3 subunit H	EIF3H
58	Ancient ubiquitous protein 1	AUP1
59	40S ribosomal protein SA	RPSA
60	Keratin 14	KRT14
61	Heat shock 70 kDa protein 1A/1B	HSPA1A
62	Heterogeneous nuclear ribonucleoprotein A/B	HNRNPAB
63	Ornithine aminotransferase, mitochondrial	OAT
64	Lupus La protein	SSB
65	Tubulin beta chain	TUBB
66	Alpha-centractin	ACTR1A
67	Nuclease-sensitive element-binding protein 1	YBX1
68	Heterogeneous nuclear ribonucleoprotein D0	HNRNPD
69	Glyceraldehyde-3-phosphate dehydrogenase	GAPDH
70	DnaJ homolog subfamily B member 2	DNAJB2

Rank in Sample	Gene Name	Gene ID
71	Basic leucine zipper and W2 domain-containing protein 2	BZW2
72	Eukaryotic translation initiation factor 4B	EIF4B
73	S-adenosylmethionine synthase isoform type-2	MAT2A
74	Eukaryotic initiation factor 4A-I	EIF4A1
75	Ubiquitin fusion degradation protein 1 homolog	UFD1L
76	Creatine kinase U-type, mitochondrial	CKMT1A
77	Citrate synthase, mitochondrial	CS
78	Keratin 9	KRT9
79	26S proteasome non-ATPase regulatory subunit 12	PSMD12
80	Heterogeneous nuclear ribonucleoprotein A3	HNRNPA3
81	Transcriptional activator protein Pur-alpha	PURA
82	Ataxin-10	ATXN10
83	Protein pelota homolog	PELO
84	Minor histocompatibility antigen H13	HM13
85	Interleukin enhancer-binding factor 2	ILF2
86	Phosphoribosyl pyrophosphate synthase-associated protein 2	PRPSAP2
87	Tubulin alpha-1B chain	TUBA1B
88	Lamina-associated polypeptide 2, isoforms beta/gamma	TMPO
89	ADP/ATP translocase 2	SLC25A5
90	E3 ubiquitin-protein ligase TRIM21	TRIM21
91	Transmembrane protein 43	TMEM43
92	WD repeat-containing protein 18	WDR18
93	39S ribosomal protein L37, mitochondrial	MRPL37
94	BRISC and BRCA1-A complex member 1	BABAM1
95	Transducin beta-like protein 2	TBL2
96	Squalene synthase	FDFT1
97	Protein arginine N-methyltransferase 1	PRMT1
98	Mitochondrial import receptor subunit TOM40 homolog	TOMM40
99	Actin-like protein 6A	ACTL6A
100	Mitotic checkpoint protein BUB3	BUB3
101	Uveal autoantigen with coiled-coil domains and ankyrin repeats	UACA
102	Cytokeratin 5	CK5
103	Nucleophosmin	NPM1
104	cAMP-dependent protein kinase type II-alpha regulatory subunit	PRKAR2A
105	Adenosylhomocysteinase	AHCY
106	Cytochrome b-c1 complex subunit 1, mitochondrial	UQCRC1
107	MARCKS-related protein	MARCKSL1
108	Emerin	EMD
109	Cyclin-dependent kinase 9	CDK9
110	26S proteasome non-ATPase regulatory subunit 4	PSMD4
111	Histone H2B type 1-D	HIST1H2BD
112	Eukaryotic translation initiation factor 3 subunit I	EIF3I
113	Hsp90 co-chaperone Cdc37	CDC37
114	Sushi, nidogen and EGF-like domain-containing protein 1	SNED1
115	Endophilin-B1	SH3GLB1
116	Nesprin-1	SYNE1
117	TGF-beta-activated kinase 1 and MAP3K7-binding protein 1	TAB1
118	26S proteasome non-ATPase regulatory subunit 7	PSMD7
119	Endoplasmic reticulum-Golgi intermediate compartment protein 3	ERGIC3
120	B-cell scaffold protein with ankyrin repeats	BANK1
121	Elongation factor 1-delta (Fragment)	EEF1D
122	Leucine-rich PPR motif-containing protein, mitochondrial	LRPPRC
123	39S ribosomal protein L38, mitochondrial	MRPL38
124	Isovaleryl-CoA dehydrogenase, mitochondrial (Fragment)	IVD
125	Tripeptidyl-peptidase 1	TPP1
126	Collagen alpha-1(XVI) chain	COL16A1
127	Olfactory receptor 1C1	OR1C1
128	DnaJ homolog subfamily B member 14	DNAJB14
129	COP9 signalosome complex subunit 4	COPS4
130	Dehydrogenase/reductase SDR family member 13	DHRS13
131	RING finger protein 126	RNF126
132	Collagen alpha-1(XXII) chain	COL22A1
133	Protein FAM8A1	FAM8A1
134	Pachytene checkpoint protein 2 homolog	TRIP13
135	Protein transport protein Sec61 subunit alpha isoform 1	SEC61A1
136	Sodium channel protein type 10 subunit alpha	SCN10A
137	Brefeldin A-inhibited guanine nucleotide-exchange protein 3	ARFGEF3
138	Protein PRRC2A	PRRC2A
139	Snurportin-1 (Fragment)	SNUPN
140	Dynein heavy chain 2, axonemal	DNAH2

Table 4. Complete list of proteins identified by mass spectroscopy from excised BVES band. (A) A complete list of proteins identified by mass spectroscopic analysis of the excised, MG132 treated full length human BVES band. Green is >95% probability, yellow is 80-94% probability that the identified peptide spectra are likely to belong to the indicated protein.

Gene Name	Gene ID	Molecular Weight	GFP	N-Flag WT BVES	N-Flag D/F Mut. BVES	C-Flag WT BVES
Blood vessel epicardial substance	BVES	41 kDa	0	45	75	35
Kinesin-like protein KIF11	KIF11	119 kDa	2	53	27	56
Heat shock 70 kDa protein 1A/1B	HSPA1A	70 kDa	3	48	49	30
Heat shock cognate 71 kDa protein	HSPA8	71 kDa	3	40	44	22
Tubulin beta chain	TUBB	50 kDa	1	23	26	16
Tubulin alpha-1B chain	TUBA1B	50 kDa	0	17	28	16
Protein arginine N-methyltransferase 5	PRMT5	73 kDa	0	19	11	27
Calnexin	CANX	68 kDa	0	10	25	14
Nucleolin	NCL	77 kDa	1	19	14	14
Eukaryotic translation initiation factor 4B	EIF4B	69 kDa	0	17	11	17
Serine/threonine-protein kinase 38	STK38	54 kDa	0	18	13	13
RNA-binding protein 10	RBM10	104 kDa	0	18	8	13
Heat shock protein HSP 90-beta	HSP90AB1	83 kDa	0	21	12	4
Complement component 1 Q subcomponent-binding protein, mitochondrial	C1QBP	31 kDa	0	19	18	0
ATP synthase subunit beta, mitochondrial	ATP5B	57 kDa	0	12	11	8
Histone H1.4	HIST1H1E	22 kDa	5	6	7	8
Actin, cytoplasmic 1	ACTB	42 kDa	3	6	6	10
Heterogeneous nuclear ribonucleoprotein A1	HNRNPA1	39 kDa	0	7	8	10
78 kDa glucose-regulated protein	HSPA5	72 kDa	0	8	16	8
Filamin-A	FLNA	281 kDa	0	5	5	13
ATP synthase subunit alpha, mitochondrial	ATP5A1	60 kDa	0	8	8	6
Methylosome protein 50	WDR77	37 kDa	0	7	7	7
DnaJ homolog subfamily A member 1	DNAJA1	45 kDa	0	7	9	5
Elongation factor 1-alpha 1	EEF1A1	50 kDa	2	5	5	8
Non-POU domain-containing octamer-binding protein	NONO	54 kDa	3	10	2	6
ADP/ATP translocase 2	SLC25A5	33 kDa	0	8	8	3
Thyroid hormone receptor-associated protein 3	THRAP3	109 kDa	0	12	3	5
Heterogeneous nuclear ribonucleoproteins A2/B1	HNRNPA2B1	37 kDa	2	5	5	6
Nucleophosmin	NPM1	33 kDa	2	5	7	4
Ubiquitin-60S ribosomal protein L40	UBA52	15 kDa	1	7	7	2
Bcl-2-associated transcription factor 1	BCLAF1	106 kDa	0	5	4	8
Heterogeneous nuclear ribonucleoprotein K	HNRNPK	51 kDa	0	4	4	9
26S proteasome non-ATPase regulatory subunit 2	PSMD2	100 kDa	0	12	3	2
TGF-beta-activated kinase 1 and MAP3K7-binding protein 1	TAB1	55 kDa	0	8	2	6
Splicing factor, proline- and glutamine-rich	SFPQ	76 kDa	1	6	4	4
Histone H2A type 2-C	HIST2H2AC	14 kDa	1	6	3	5
DNA-dependent protein kinase catalytic subunit	PRKDC	469 kDa	1	6	7	1
Sodium/potassium-transporting ATPase subunit alpha-1	ATP1A1	113 kDa	0	4	7	3
60S acidic ribosomal protein P0	RPLP0	34 kDa	0	3	5	6
Heat shock protein HSP 90-alpha	HSP90AA1	85 kDa	0	16	9	4
40S ribosomal protein SA	RPSA	33 kDa	0	3	5	5
Lamin-B1	LMNB1	66 kDa	0	5	6	2
60S acidic ribosomal protein P2	RPLP2	12 kDa	0	4	3	5
RING finger protein 219	RNF219	81 kDa	0	3	5	4
Voltage-dependent anion-selective channel protein 2	VDAC2	32 kDa	0	4	6	2
Heat shock protein 105 kDa	HSPH1	97 kDa	0	6	4	2
BAG family molecular chaperone regulator 2	BAG2	24 kDa	0	6	3	3
ATP synthase lipid-binding protein, mitochondrial	ATP5G1	14 kDa	0	6	3	3
OTU domain-containing protein 4	OTUD4	124 kDa	0	6	0	6
Emerin	EMD	29 kDa	0	4	3	4
60S ribosomal protein L15	RPL15	24 kDa	0	4	2	5
Enhancer of rudimentary homolog	ERH	12 kDa	0	4	1	6
FAS-associated factor 2	FAF2	53 kDa	0	4	7	0
60 kDa heat shock protein, mitochondrial	HSPD1	61 kDa	1	4	2	3
3-hydroxyacyl-CoA dehydratase 3	PTPLAD1	43 kDa	0	4	3	3
40S ribosomal protein S3a	RPS3A	30 kDa	0	3	2	5
Reticulocalbin-2	RCN2	37 kDa	0	4	5	1
Stress-70 protein, mitochondrial	HSPA9	74 kDa	0	5	6	1
Cytoskeleton-associated protein 4	CKAP4	66 kDa	0	2	7	1
60S ribosomal protein L13	RPL13	24 kDa	1	3	2	3
Plasminogen activator inhibitor 1 RNA-binding protein	SERBP1	45 kDa	2	4	1	2
Polyadenylate-binding protein 1	PABPC1	71 kDa	0	3	2	4
Lamina-associated polypeptide 2, isoforms beta/gamma	TMPO	51 kDa	0	4	3	2
Heterogeneous nuclear ribonucleoprotein U	HNRNPU	91 kDa	0	2	3	4
Histone H4	HIST1H4A	11 kDa	0	2	2	5
Transitional endoplasmic reticulum ATPase	VCP	89 kDa	0	5	4	1
40S ribosomal protein S13	RPS13	17 kDa	0	3	5	1
26S protease regulatory subunit 7	PSMC2	49 kDa	0	3	6	0
40S ribosomal protein S10	RPS10	19 kDa	0	2	4	2
Histone H2B type 1-K	HIST1H2BK	14 kDa	0	2	3	3
60S ribosomal protein L4	RPL4	48 kDa	0	2	3	3
40S ribosomal protein S19	RPS19	16 kDa	0	1	4	3
Heterogeneous nuclear ribonucleoproteins C1/C2	HNRNPC	34 kDa	0	3	4	1
Probable ATP-dependent RNA helicase DDX5	DDX5	69 kDa	0	4	3	1
Eukaryotic translation initiation factor 5A-1	EIF5A	17 kDa	0	5	1	2
Spindlin-1	SPIN1	30 kDa	0	4	0	4
60S ribosomal protein L7a	RPL7A	30 kDa	1	3	1	2
Heterogeneous nuclear ribonucleoprotein H	HNRNPH1	49 kDa	1	1	2	3
Nuclease-sensitive element-binding protein 1	YBX1	36 kDa	1	2	2	2
60S ribosomal protein L12	RPL12	18 kDa	0	2	2	3
Nucleosome assembly protein 1-like 1	NAP1L1	45 kDa	0	2	3	2
60S ribosomal protein L3	RPL3	46 kDa	0	2	2	3
Serine/threonine-protein kinase RIO1	RIOK1	66 kDa	0	2	2	3
Mitogen-activated protein kinase kinase kinase 7	MAP3K7	29 kDa	0	3	1	3
40S ribosomal protein S8	RPS8	24 kDa	0	2	1	4
Dolichyl-diphosphooligosaccharide--protein glycosyltransferase subunit 2	RPN2	69 kDa	0	1	4	2
Prohibitin	PHB	30 kDa	0	0	3	4
Dolichyl-diphosphooligosaccharide--protein glycosyltransferase subunit 1	RPN1	69 kDa	0	2	5	0
Proteasome subunit alpha type-3	PSMA3	28 kDa	0	5	2	0
26S proteasome non-ATPase regulatory subunit 13	PSMD13	43 kDa	0	4	3	0
Splicing factor 3B subunit 3	SF3B3	136 kDa	0	1	0	6

Gene Name	Gene ID	Molecular Weight	GFP	N-Flag WT BVES	N-Flag D/F Mut. BVES	C-Flag WT BVES
60S ribosomal protein L9	RPL9	22 kDa	0	2	2	2
Putative pre-mRNA-splicing factor ATP-dependent RNA helicase DHX15	DHX15	91 kDa	0	2	2	2
40S ribosomal protein S12	RPS12	15 kDa	0	3	1	2
40S ribosomal protein S4, X isoform	RPS4X	30 kDa	0	2	1	3
Spliceosome RNA helicase DDX39B	DDX39B	49 kDa	0	3	1	2
40S ribosomal protein S2	RPS2	31 kDa	0	2	3	1
26S protease regulatory subunit 8	PSMC5	46 kDa	0	4	2	1
60S ribosomal protein L29	RPL29	18 kDa	0	3	2	1
Calumenin	CALU	37 kDa	0	1	3	2
60S ribosomal protein L18	RPL18	22 kDa	0	2	3	1
Importin subunit beta-1	KPNB1	97 kDa	0	3	2	1
BTB/POZ domain-containing protein KCTD5	KCTD5	26 kDa	0	4	1	1
60S ribosomal protein L17	RPL17	21 kDa	0	3	3	0
Exportin-T	XPOT	110 kDa	0	2	4	0
40S ribosomal protein S9	RPS9	23 kDa	0	2	0	4
Proteasome subunit alpha type-2	PSMA2	26 kDa	0	4	2	0
26S protease regulatory subunit 6B	PSMC4	47 kDa	0	3	3	0
BolA-like protein 2	BOLA2	10 kDa	1	2	1	1
Titin	TTN	3816 kDa	1	1	2	1
Importin-8	IPO8	120 kDa	0	2	1	2
Far upstream element-binding protein 2	KHSRP	73 kDa	0	2	1	2
Small nuclear ribonucleoprotein Sm D1	SNRPD1	13 kDa	0	1	2	2
60S acidic ribosomal protein P1	RPLP1	12 kDa	0	2	2	1
40S ribosomal protein S11	RPS11	18 kDa	0	2	2	1
Voltage-dependent anion-selective channel protein 3	VDAC3	31 kDa	0	2	2	1
Calcium-binding mitochondrial carrier protein Aralar2	SLC25A13	74 kDa	0	2	2	1
60S ribosomal protein L8	RPL8	28 kDa	0	2	2	1
Src substrate cortactin	CTTN	62 kDa	0	2	1	2
Serine/threonine-protein phosphatase 2A 65 kDa regulatory subunit A alpha isoform	PPP2R1A	65 kDa	1	3	1	0
Lamin-B2	LMNB2	68 kDa	0	2	4	2
Spectrin alpha chain, non-erythrocytic 1	SPTAN1	285 kDa	0	2	1	2
Serine/threonine-protein kinase 38-like	STK38L	54 kDa	0	3	3	4
Proteasome subunit alpha type-4	PSMA4	29 kDa	0	3	1	1
40S ribosomal protein S28	RPS28	8 kDa	0	2	2	1
Histone-binding protein RBBP7	RBBP7	48 kDa	0	3	1	1
Phosphate carrier protein, mitochondrial	SLC25A3	40 kDa	0	1	3	1
Tubulin beta-4B chain	TUBB4B	50 kDa	0	24	25	15
Membrane-associated progesterone receptor component 1	PGRMC1	22 kDa	0	3	1	1
Proteasome subunit beta type-6	PSMB6	25 kDa	0	3	1	1
Proteasome subunit alpha type-1	PSMA1	30 kDa	0	3	1	1
Peptide deformylase, mitochondrial	PDF	27 kDa	0	1	3	1
Proteasome subunit alpha type-5	PSMA5	26 kDa	0	3	2	0
U4/U6 small nuclear ribonucleoprotein Prp31	PRPF31	55 kDa	0	3	0	2
Pre-mRNA-processing factor 19	PRPF19	55 kDa	0	2	0	3
Proteasome subunit beta type-5	PSMB5	28 kDa	0	3	2	0
Heterogeneous nuclear ribonucleoprotein A3	HNRNPA3	40 kDa	0	0	2	3
Cleavage and polyadenylation specificity factor subunit 5	NUDT21	26 kDa	0	2	0	3
DnaJ homolog subfamily A member 2	DNAJA2	46 kDa	0	2	3	0
26S proteasome non-ATPase regulatory subunit 1	PSMD1	106 kDa	0	4	1	0
Monocarboxylate transporter 1	SLC16A1	54 kDa	0	4	1	0
60S ribosomal protein L6	RPL6	33 kDa	0	1	0	4
High mobility group protein B1	HMGB1	25 kDa	0	1	1	2
Small nuclear ribonucleoprotein-associated proteins B and B'	SNRPB	25 kDa	0	1	1	2
60S ribosomal protein L7	RPL7	29 kDa	0	1	1	2
40S ribosomal protein S20	RPS20	13 kDa	0	1	1	2
40S ribosomal protein S15a	RPS15A	15 kDa	0	1	1	2
Cleavage and polyadenylation specificity factor subunit 6	CPSF6	59 kDa	0	1	1	2
40S ribosomal protein S3	RPS3	27 kDa	0	2	1	1
60S ribosomal protein L5	RPL5	34 kDa	0	2	1	1
40S ribosomal protein S30	FAU	7 kDa	0	2	1	1
Thioredoxin	TXN	12 kDa	0	1	2	1
ADP/ATP translocase 3	SLC25A6	33 kDa	0	5	6	4
Transmembrane protein 33	TMEM33	28 kDa	0	1	2	1
40S ribosomal protein S6	RPS6	29 kDa	0	1	2	1
40S ribosomal protein S26	RPS26	13 kDa	0	1	2	1
T-complex protein 1 subunit beta	CCT2	57 kDa	0	1	2	1
60S ribosomal protein L18a	RPL18A	21 kDa	0	1	2	1
40S ribosomal protein S23	RPS23	16 kDa	0	2	1	1
RNA-binding motif protein, X chromosome	RBMX	42 kDa	0	1	2	1
60S ribosomal protein L35	RPL35	15 kDa	0	1	2	1
Heterogeneous nuclear ribonucleoprotein L	HNRNPL	64 kDa	0	2	0	2
Methylosome subunit pICln	CLNS1A	26 kDa	0	2	0	2
Calmodulin	CALM1	17 kDa	0	2	0	2
Spectrin beta chain, non-erythrocytic 1	SPTBN1	275 kDa	0	2	0	2
Proteasomal ubiquitin receptor ADRM1	ADRM1	42 kDa	0	2	2	0
T-complex protein 1 subunit alpha	TCP1	60 kDa	0	2	2	0
26S proteasome non-ATPase regulatory subunit 4	PSMD4	41 kDa	0	2	2	0
26S protease regulatory subunit 10B	PSMC6	44 kDa	0	3	2	0
Proteasome subunit beta type-1	PSMB1	26 kDa	0	2	2	0
Proteasome subunit alpha type-7	PSMA7	28 kDa	0	3	1	0
ATP-dependent RNA helicase DDX3X	DDX3X	73 kDa	0	0	1	3
Reticulocalbin-1	RCN1	39 kDa	0	1	3	0
Heterogeneous nuclear ribonucleoprotein Q	SYNCRIP	70 kDa	0	0	3	1
Pre-mRNA-processing-splicing factor 8	PRPF8	274 kDa	0	3	0	1
D-3-phosphoglycerate dehydrogenase	PHGDH	57 kDa	0	1	3	0
60S ribosomal protein L19	RPL19	23 kDa	0	1	3	0
Heterogeneous nuclear ribonucleoprotein D0	HNRNPD	38 kDa	0	2	3	0
26S proteasome non-ATPase regulatory subunit 3	PSMD3	61 kDa	0	4	0	0
HCLS1-associated protein X-1	HAX1	32 kDa	0	2	1	0
TRAF-type zinc finger domain-containing protein 1	TRAFD1	65 kDa	0	2	1	0

Gene Name	Gene ID	Molecular Weight	GFP	N-Flag WT BVES	N-Flag D/F Mut. BVES	C-Flag WT BVES
26S proteasome non-ATPase regulatory subunit 7	PSMD7	37 kDa	0	2	1	0
40S ribosomal protein S24	RPS24	15 kDa	0	0	1	2
Collagen alpha-1(XIV) chain	COL14A1	194 kDa	0	2	1	0
C-Myc-binding protein	MYCBP	12 kDa	0	0	1	2
Voltage-dependent anion-selective channel protein 1	VDAC1	31 kDa	0	2	3	0
Elongation factor 1-gamma	EEF1G	50 kDa	0	1	0	2
40S ribosomal protein S14	RPS14	16 kDa	0	1	0	2
Lamin-B receptor	LBR	71 kDa	0	1	2	0
Insulin-like growth factor 2 mRNA-binding protein 1	IGF2BP1	63 kDa	0	1	0	2
Heterogeneous nuclear ribonucleoprotein A/B	HNRNPAB	30 kDa	0	1	2	0
cAMP-dependent protein kinase type I-alpha regulatory subunit	PRKAR1A	43 kDa	0	0	2	1
Proteasome subunit beta type-3	PSMB3	23 kDa	0	2	0	1
40S ribosomal protein S16	RPS16	16 kDa	0	2	0	1
Heterogeneous nuclear ribonucleoprotein A0	HNRNPA0	31 kDa	0	2	0	1
Serine/threonine-protein phosphatase PGAM5, mitochondrial	PGAM5	32 kDa	0	2	0	1
Sigma non-opioid intracellular receptor 1	SIGMAR1	25 kDa	0	2	0	1
Prothymosin alpha (Fragment)	PTMA	16 kDa	2	0	0	1
Uncharacterized protein C11orf84	C11orf84	41 kDa	0	1	0	2
26S proteasome non-ATPase regulatory subunit 11	PSMD11	47 kDa	0	2	1	0
Vesicle-trafficking protein SEC22b	SEC22B	25 kDa	0	1	2	0
Heat shock 70 kDa protein 4L	HSPA4L	95 kDa	0	2	3	0
Serine/arginine-rich splicing factor 3	SRSF3	19 kDa	0	1	0	2
Splicing factor 3A subunit 3	SF3A3	59 kDa	0	1	0	2
ATP synthase subunit gamma, mitochondrial	ATP5C1	33 kDa	0	0	2	1
ATP-dependent RNA helicase A	DHX9	141 kDa	0	1	0	2
Microtubule-associated protein 1B	MAP1B	271 kDa	0	2	0	1
Importin-4	IPO4	119 kDa	0	2	1	0
Transmembrane protein 43	TMEM43	45 kDa	0	1	2	0
REV Probable ATP-dependent RNA helicase DDX31	DDX31	94 kDa	2	0	0	1
Latent-transforming growth factor beta-binding protein 1	LTBP1	187 kDa	0	2	0	1
Poly(rC)-binding protein 1	PCBP1	37 kDa	0	0	2	1
REV Periaxin	PRX	155 kDa	0	2	1	0
39S ribosomal protein L12, mitochondrial	MRPL12	21 kDa	0	3	0	0
GTP-binding nuclear protein Ran	RAN	24 kDa	0	3	0	0
Protein arginine N-methyltransferase 1	PRMT1	42 kDa	0	0	0	3
Prohibitin-2	PHB2	33 kDa	0	3	0	0
Calmodulin-regulated spectrin-associated protein 3	CAMSAP3	135 kDa	0	0	0	3
ATP synthase subunit b, mitochondrial	ATP5F1	29 kDa	0	3	0	0
Ribosomal protein S6 kinase alpha-3	RPS6KA3	81 kDa	0	0	3	0
26S proteasome non-ATPase regulatory subunit 12	PSMD12	53 kDa	0	2	0	0
Exportin-1	XPO1	123 kDa	0	0	2	0
Cytochrome b-c1 complex subunit 6, mitochondrial	UQCRH	11 kDa	0	0	2	0
CTP synthase 1	CTPS1	67 kDa	0	0	0	2
Serine/arginine-rich splicing factor 1	SRSF1	28 kDa	0	2	0	0
DNA damage-binding protein 1	DDB1	127 kDa	0	2	0	0
Coiled-coil domain-containing protein 47	CCDC47	56 kDa	0	2	0	0
Pre-mRNA branch site protein p14	SF3B14	15 kDa	0	0	0	2
Protein transport protein Sec16A	SEC16A	252 kDa	0	2	0	0
Structure-specific endonuclease subunit SLX4	SLX4	200 kDa	2	0	0	0
Nitric oxide synthase, brain	NOS1	165 kDa	2	0	0	0
26S protease regulatory subunit 6A	PSMC3	49 kDa	0	3	0	0
Nebulin	NEB	987 kDa	0	0	0	2
Ankyrin repeat domain-containing protein 34B	ANKRD34B	56 kDa	0	2	0	0
Methyl-CpG-binding domain protein 5	MBD5	160 kDa	0	2	0	0
4F2 cell-surface antigen heavy chain	SLC3A2	68 kDa	0	2	0	0
Pre-mRNA 3'-end-processing factor FIP1	FIP1L1	67 kDa	0	0	0	2
Numb-like protein	NUMBL	65 kDa	0	2	0	0
Alanine--tRNA ligase, cytoplasmic	AARS	107 kDa	0	0	2	0
Golgin subfamily B member 1	GOLGB1	376 kDa	0	2	0	0
Protein FAM47B	FAM47B	74 kDa	0	2	0	0
RING finger and transmembrane domain-containing protein 2	RNFT2	46 kDa	0	0	2	0
Laminin subunit beta-1	LAMB1	198 kDa	2	0	0	0
C2 domain-containing protein 2	C2CD2	76 kDa	0	2	0	0
Dynein heavy chain 8, axonemal	DNAH8	515 kDa	0	0	2	0
Kinesin-like protein KIF21B	KIF21B	183 kDa	0	2	0	0
Lymphoid-specific helicase	HELLS	97 kDa	2	0	0	0

Table 5. BVES interacting proteins identified by mass spectroscopy. Four Flag-tagged constructs (GFP, N-Flag WT BVES, N-Flag D/F double mutant BVES, and C-Flag WT BVES) were immunoprecipitated with anti-Flag M2 affinity resin, Flag-peptide eluted, and subjected to mass spectroscopy. The gene name, gene ID, and molecular weight of proteins identified in the analysis are listed. The values to the right are the total spectral counts that map to each identified protein. The color coding indicates protein probability confidence intervals: Green is >95% probability, yellow is 80-94%, orange is 50-79%, and red is 20-49% probability that the identified peptide spectra belong to the indicated protein.

Gene Name	Gene ID	Likely contaminants
Actin, cytoplasmic 1	ACTB	*
Proteasomal ubiquitin receptor ADRM1	ADRM1	
Blood vessel epicardial substance	BVES	
Spliceosome RNA helicase DDX39B	DDX39B	
DnaJ homolog subfamily A member 1	DNAJA1	
DnaJ homolog subfamily A member 2	DNAJA2	
Elongation factor 1-alpha 1	EEF1A1	*
Elongation factor 1-gamma	EEF1G	*
Eukaryotic translation initiation factor 4B	EIF4B	
Emerin	EMD	
Heterogeneous nuclear ribonucleoproteins A2/B1	HNRNPA2B1	*
Heterogeneous nuclear ribonucleoprotein A3	HNRNPA3	*
Heterogeneous nuclear ribonucleoprotein A/B	HNRNPAB	
Heterogeneous nuclear ribonucleoproteins C1/C2	HNRNPC	
Heterogeneous nuclear ribonucleoprotein D0	HNRNPD	
Heat shock 70 kDa protein 1A/1B	HSPA1A	*
Nucleophosmin	NPM1	*
Poly(rC)-binding protein 1	PCBP1	
cAMP-dependent protein kinase type I-alpha regulatory subunit	PRKAR1A	
Protein arginine N-methyltransferase 1	PRMT1	
Protein arginine N-methyltransferase 5	PRMT5	
26S protease regulatory subunit 7	PSMC2	
26S protease regulatory subunit 6A	PSMC3	
26S protease regulatory subunit 6B	PSMC4	
26S protease regulatory subunit 8	PSMC5	
26S protease regulatory subunit 10B	PSMC6	
26S proteasome non-ATPase regulatory subunit 11	PSMD11	
26S proteasome non-ATPase regulatory subunit 12	PSMD12	
26S proteasome non-ATPase regulatory subunit 13	PSMD13	
26S proteasome non-ATPase regulatory subunit 4	PSMD4	
26S proteasome non-ATPase regulatory subunit 7	PSMD7	
RNA-binding motif protein, X chromosome	RBMX	*
60S ribosomal protein L3	RPL3	*
60S ribosomal protein L4	RPL4	*
40S ribosomal protein SA	RPSA	
ADP/ATP translocase 2	SLC25A5	
TGF-beta-activated kinase 1 and MAP3K7-binding protein 1	TAB1	
Transmembrane protein 43	TMEM43	
Lamina-associated polypeptide 2, isoforms beta/gamma	TMPO	
Titin	TTN	*
Tubulin alpha-1B chain	TUBA1B	*
Tubulin beta chain	TUBB	*
Methylosome protein 50	WDR77	
Nuclease-sensitive element-binding protein 1	YBX1	*

Table 6. Overlapping proteins identified in both BVES mass spectroscopy experiments. A list of proteins identified in both mass spectroscopy experiments (Table 4 and Table 5). * proteins were also identified in an unrelated experiment utilizing V5-magnetic beads and therefore likely represent consistent protein contaminants as opposed to true hits.

E. Characterization of BVES conditional knockout mice

While utilization of global knockout mice allows for robust analysis of genotypic:phenotypic correlations with relatively simple breeding schemes[309], conditional knockout mice allow for tissue specific gene deletion and can help overcome barriers associated with embryonic lethality when critical genes are deleted globally[310]. While the BVES global knockout mice are fertile and display no evidence of embryonic lethality[58,73], developing targeted intestinal epithelial cell specific mouse models of BVES deletion will undoubtedly further our understanding of the role BVES is playing in intestinal homeostasis and disease. Conditional gene targeting can be achieved by flanking a genomic locus of interest with loxP sites and then crossing these mice with mice that express Cre recombinase under a tissue-specific or cell-type specific promoter[311]. To that end, we sought to generate BVES intestinal epithelial cell conditional knockout mice utilizing the *Lrig1-CreER* driver and BVES conditional knockout mice generated by our collaborator, Dr. Thomas Brand at the Imperial College of London. Lrig1 marks stem/progenitor cells in the intestinal crypt base and previous studies have demonstrated the utility of the *Lrig1-CreER* driver to promote intestinal epithelial cell specific gene deletion [19,246,312]. As detecting BVES loss is difficult given the lack of immunoreagents, we also sought to cross these mice with a fluorescent reporter to lineage trace cells where Cre was activated. We first crossed the *Lrig1-CreER* driver with the *mTmG* reporter mice, a double-fluorescent Cre reporter mouse that expresses a membrane-targeted mTomato (*mT*) fluorescent protein prior to cre-mediated recombination and then a membrane-targeted green fluorescent protein (*mG*) after cre-mediated recombination. The *Lrig1-CreER* driver is tamoxifen inducible, allowing for temporal control of recombination based on when Tamoxifen is delivered *in vivo* or when the metabolite 4-hydroxytamoxifen (4OHT) is delivered *ex vivo*. These *Lrig1-CreER* reporter mice were then

backcrossed with the *Bves*$^{fl/fl}$ mice. In separate experiments, the *Lrig1-CreER*;mTmG mice were also crossed with *Apc*$^{fl/fl}$ mice to assess the contribution of hyperactive Wnt signaling on crypt dynamics. Overall, this model performed as expected with robust lineage tracing throughout the intestinal epithelium (Figure 37) that increased in a dose dependent fashion with increasing dose/frequency of Tamoxifen administration. At low doses of Tamoxifen, this reporter mouse also labelled small subsets of cells in the submucosa, corroborating previous reports utilizing the *Lrig1-Apple/+* mouse that Lrig1 marks interstitial cells of cajal within the deep muscle layers[313]. With higher doses of Tamoxifen, the majority of the submucosal muscle layer was labelled, again supporting findings by Kondo *et al.* that Lrig1 marks smooth muscle progenitor cells.

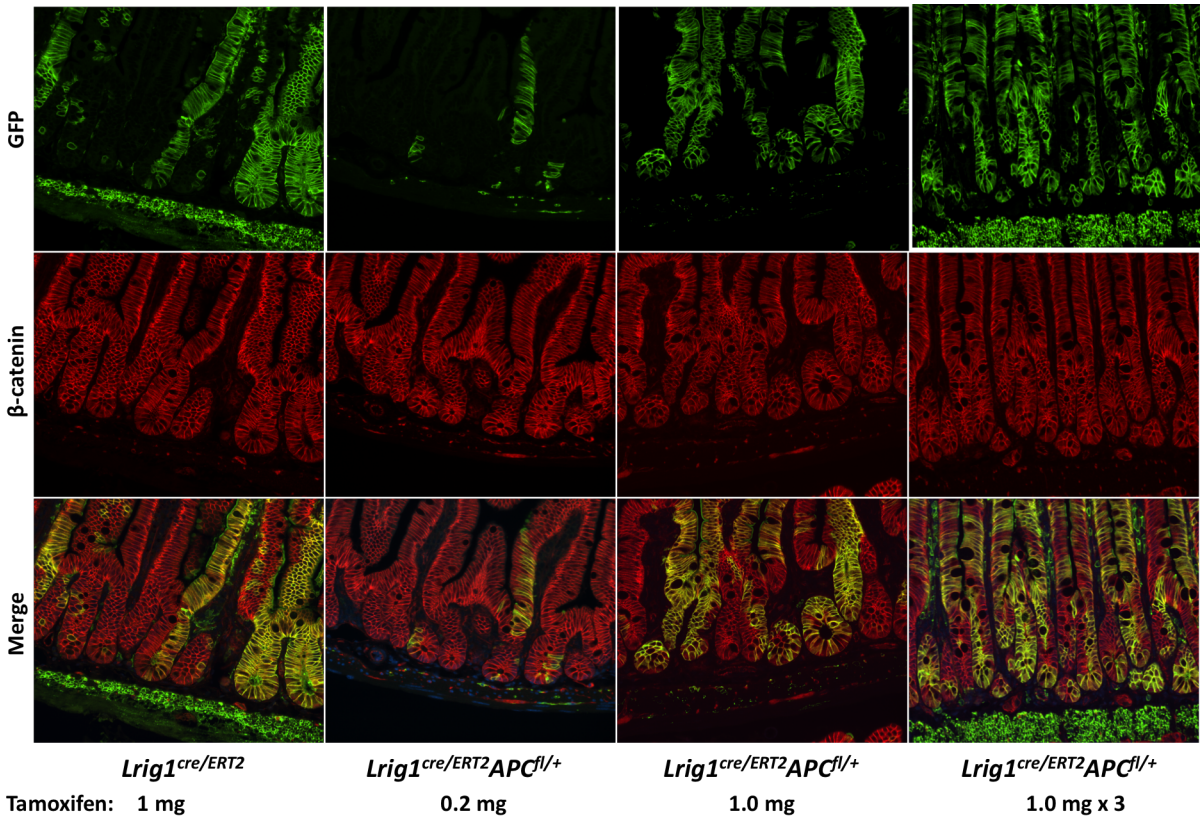

Figure 37. Tamoxifen inducible recombination in *Lrig1-CreER;mTmG reporter mice*. 8-12 week old *mTmG*$^{+/-}$ reporter mice crossed with the *Lrig1-CreER* driver and *Apc*$^{fl/+}$ mice as indicated were treated with varying doses of Tamoxifen. Small intestine tissue was harvested 7 days later and stained for GFP and β-catenin.

To assess the functionality of the *Bves* floxed allele, pure epithelial populations were generated by isolating small intestinal crypts from mice and then treating these enteroids with 4OHT *ex vivo* to induce recombination. As seen in Figure 38, successful recombination of the *mTmG* reporter allele was observed in nearly 100% of enteroids following 4OHT treatment for 96 hours. As the *mTmG* reporter switches from mTomato to GFP, the mTomato signal diminishes while the GFP signal, specifically in the epithelial cells, increases. There is observable background autofluorescence in the GFP channel in the minus 4OHT conditions but this signal is entirely within the dead/apoptotic luminal contents of the enteroids and no "leak" or epithelial GFP expression was observed without 4OHT. While the expression of GFP within the epithelium confirms the activation of cre recombinase and successful cleavage of the *mTmG* reporter, this does not guarantee successful floxing of the *Bves* allele as it is well reported that floxed alleles can have different sensitivities/efficiencies[314]. To determine the degree of recombination occurring within the floxed *Bves* exon, RNA and DNA was isolated from the enteroids depicted in Figure 38 as well as from colonoids treated in an identical fashion. A schematic of the conditional BVES knockout mouse is depicted in Figure 39A. The first loxP site is located within the intronic region between Exon 3 and Exon 4 of *Bves*. A PGK-neomycin selection cassette remains within the intronic region between Exon 4 and Exon 5 of *Bves,* upstream of the second loxP site. The loxP sites are oriented in the same direction meaning that upon cre-mediated recombination, the entire ~4,261 bp fragment which includes all of Exon 4 will be excised. To determine recombination frequency after 4OHT treatment, three pairs of PCR primers were generated. A common forward primer and three different reverse primers. With the addition of 4OHT, the reverse priming site for primers R1 and R2 should be excised which would prevent PCR amplification in these conditions (assuming 100% recombination efficiency). However, as can be seen in Figure 39B, following 4OHT treatment, the reverse priming sites downstream of the loxP site remain intact and PCR

bands of the expected size are generated (see F:R1 and F:R2 bands). There does appear to be a slight reduction in the intensity of the band following 4OHT treatment (and equivalent amounts of genomic DNA were utilized for each PCR reaction) but this is semi-quantitative at best and suggests very low recombination efficiency. The third set of PCR primers spans the entire floxed region and should generate a large, ~4,200 bp product, in the absence of 4OHT but following recombination, the interspersed region is removed which would leave only about a 488 bp product. As can be seen in the bottom two panels of Figure 39B, there is a detectable level of genomic recombination (as demonstrated by the ~500 bp PCR product following 4OHT treatment. While the signal from this band is quite robust, it cannot be compared directly to the 4,200 bp product in the -4OHT condition as the efficiency of a reaction with a PCR product of this size is likely much lower. Overall, these data provide evidence of successful genomic recombination in the *Bves*$^{fl/fl}$ mice but with very low efficiency. Deletion of the neomycin cassette using the FLP-FRT recombination system may dramatically improve efficiency as it will reduce the size of the floxed DNA fragment by >50%.

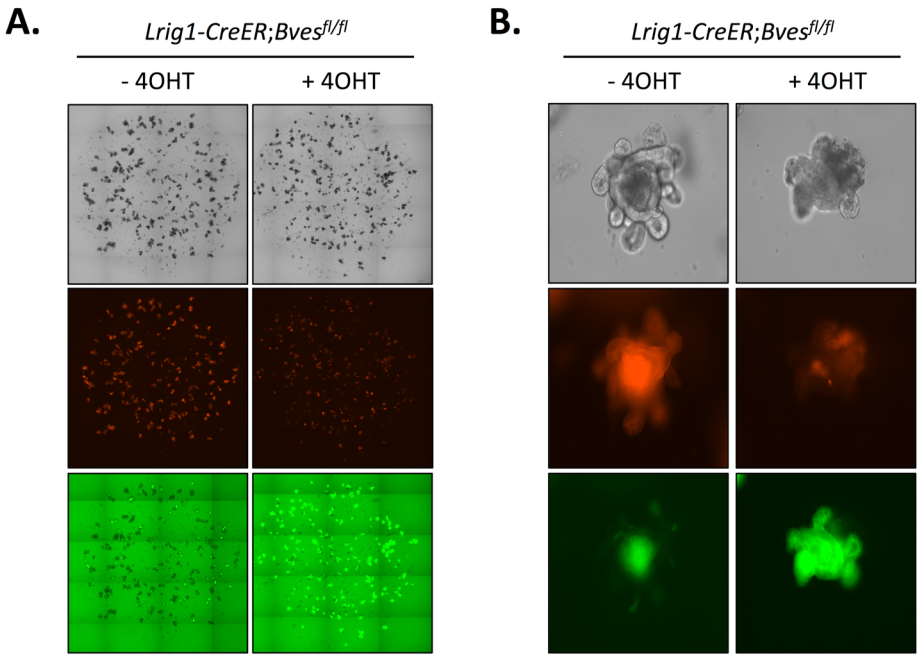

Figure 38. 4-Hydroxytamoxifen treatment of *Lrig1-CreER;Bves$^{fl/fl}$;mTmG* enteroids. (A) Small intestinal crypts from one 10-week old *Lrig1-CreER;Bves$^{fl/fl}$;mTmG$^{+/-}$* mouse were harvested and embedded in Matrigel. 24 hours after isolation, enteroids were treated with 500 μM 4-Hydroxytamoxifen (4OHT) for 96 hours. At the end of treatment, representative Matrigel plugs were imaged and 4x images were tiled together to generate an image of the entire matrigel plug. (B) 20x images of individual enteroids from (A).

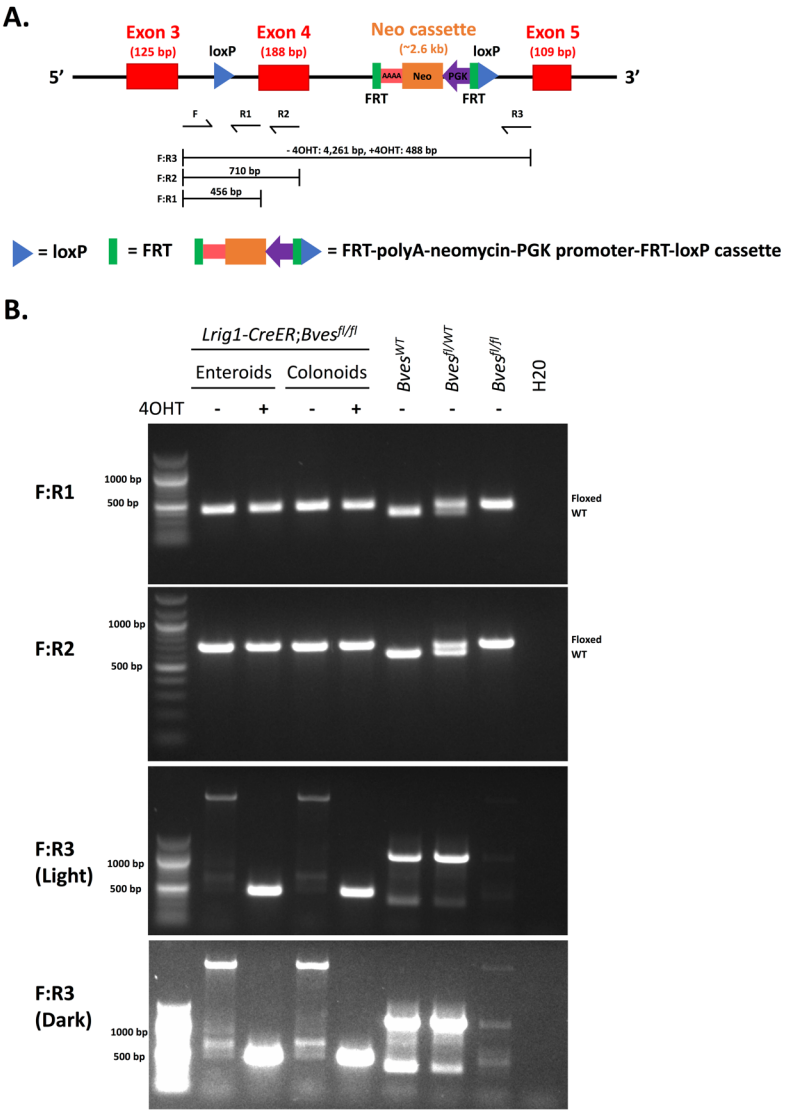

Figure 39. Analysis of recombination in BVES conditional knockout enteroids. (A) Schematic of the *Bves*$^{fl/fl}$ loxP sites. Exon 4 of BVES is floxed. The Neomycin cassette utilized in generating the conditional knockout mice, flanked by FRT sites, is located in the intronic region between Exon 4 and Exon 5. The location of PCR primers utilized to amplify genomic DNA and assess the degree of recombination are depicted, along with expected PCR product sizes generated by amplification using each set of primers. (B) *Lrig1-CreER;Bves*$^{fl/fl}$*;mTmG*$^{+/-}$ enteroids and colonoids were treated with 500 µM 4-Hydroxytamoxifen (4OHT) for 96 hours before harvesting genomic DNA. Control DNA samples from mouse ear punches corresponding to the indicated genotypes are also included in each PCR reaction.

While troubleshooting and characterizing gene deletion in the *Bves*$^{fl/fl}$ mice, a careful assessment of *Bves* transcript levels in multiple mouse tissues was ultimately performed. This analysis evolved because we initially sought to confirm *Bves* deletion at the transcriptional level by assessing *Bves* mRNA levels utilizing a panel of qRT-PCR primers that primed within the floxed *Bves* Exon 4. A summary of this analysis is depicted in Table 7. Initially, qRT-PCR analysis was performed on *Lrig1-CreER;Bves*^{WT}*;mTmG*$^{+/-}$, *Lrig1-CreER;Bves*$^{fl/+}$*;mTmG*$^{+/-}$, and *Lrig1-CreER;Bves*$^{fl/fl}$*;mTmG*$^{+/-}$ duodenal crypts and enteroids (-/+ 4OHT). Utilizing a *Bves* Taqman probe which spans Exons 5 and 6, amplification was detected but there was no change in BVES transcript following 4OHT treatment in the *Bves*$^{fl/fl}$ enteroids. Successful floxing of *Bves* Exon 4 could generate an altered mRNA transcript which undergoes nonsense mediated decay but this is not always the case, which is why some mouse models demonstrate maintained mRNA transcript levels without translation of functional protein. To further assess this, additional Taqman probes that prime within the floxed Exon 4 were utilized on the same cDNA samples but these probes failed to amplify BVES. As the GAPDH CT values were relatively low, additional reactions utilizing more input cDNA were performed but these also failed (despite a 2 CT increase in GAPDH abundance). To test whether the Exon 3-4 and Exon 4-5 Taqman probes were functional, additional analysis was performed on a panel of mouse tissue and mouse cell lines. Overall, all 3 BVES Taqman probes work to varying degrees as does the SYBR Green Exon 4 primer pair but in tissues where *Bves* transcript levels are relatively low (whole intestinal tissue, small intestine and colon crypts, enteroids, and YAMC cells), amplification appear to be less efficient. These data are useful in that they confirm robust *Bves* mRNA expression in heart and muscle tissue and demonstrate relatively low, but generally detectable, levels of *Bves* expression in intestinal tissues of interest.

	Tamoxifen/4OHT	mBVES 00517902 Exon 5-6	mBVES 01192020 Exon 3-4	mBVES 01192021 Exon 4-5	SYBR Green Exon 3/4	SYBR Green Exon4
Lrig1 mTmG SI Crypts	-	35.9/23.3	2 uL: –/23.0 9 uL: –/20.9	–/22.9	Some amp. but melt curves have high baseline and multiple Tm peaks	–/20.6
Lrig BVES fl/+ mTmG Duo Crypts	-	36.0/22.6	–/24.2			31.7/20.0
Lrig BVESfl/fl mTmG Duo Crypts	-	35.7/22.8	–/22.8	–/22.4		31.4/20.0
Lrig Enteroids	-		–/22.0			(–,34.0,38.6)/19.3
Lrig Enteroids	+		–/22.5			–/19.7
LrigBVESfl/+ Enteroids	-		–/22.3			–/19.7
LrigBVESfl/+ Enteroids	+		–/23.2			–/19.7
LrigBVESfl/fl Enteroids	-	36.0/21.6	2 uL: –/21.4 9 uL: –/19.2	–/21.2		–/19.1
LrigBVESfl/fl Enteroids	+	35.9/21.8 *No change in transcript levels*	2 uL: –/21.6 9 uL: –/19.4	–/21.3		(32.6,36.9,37.2)/19.2
MC38 SQ Xenografts LacZ 2		35.2/20.9	35.1/20.9	35.7/20.9		
Mouse Colon Crypts		36.9/22.8	–/22.8	–/22.8		
WT Heart		26.1/17.9	22.1/17.9	22.8/17.9		
WT Muscle		25.7/16.7	21.7/16.7	22.5/16.7		
WT Liver		34.7/20.6	31.8/20.6	31.9/20.6		
WT Brain		31.0/18.8	26.9/18.8	27.6/18.8		
WT Distal Colon		29.2/19.1	25.3/19.1	25.9/19.1		
WT Proximal Duo		31.2/19.3	27.4/19.3	28.0/19.3		
BVES WT MEF - Wnt		32.0/18.3	28.5/18.3	29.3/18.3		
BVES KO MEF - Wnt		36.4/18.4	37.0/18.4	36.6/18.4		
YAMC		30.2/19.9	26.4/19.9	26.8/19.9		
WT Enteroid		36.1/18.7		37.8/18.7		
WT MEF - Wnt					Some amp. but multiple Tm peaks	29.1/17.5
KO MEF - Wnt						35.4/17.6
WT MEF + Wnt						28.8/17.8
KO MEF + Wnt						34.9/17.9
Lrig BVES fl/fl mTmG Heart		23.98/21.1	23.5/21.1	23.5/21.3		23.6/19.8
Lrig BVES fl/fl mTmG Muscle		24.22/20.1	23.6/20.1	23.5/20.2		23.65/18.8
Lrig BVES fl/fl mTmG Proximal Duo		28.8/21.3	28.4/21.3	28.4/21.5		28.2/19.9
Lrig BVES fl/fl mTmG Distal Colon		27.7/22.6	27.1/22.6	27.2/22.7		27/21
Lrig BVES fl/fl mTmG Duo Crypts		35.7/22.8	–/22.8	–/22.3		39.5/20.9
Lrig BVES fl/fl mTmG Colon Crypts		35.0/22.2	–/22.2	37.2/22.2		35.1/20.7
Lrig BVES fl/fl mTmG Duo Enteroids	-	36.3/20.3	–/20.3	38.2/20.4		32.0/18.9
Lrig BVES fl/fl mTmG Duo Enteroids	+	34.9/20.7	–/20.7	37.6/20.8		36.2/19.4
Lrig BVES fl/fl mTmG Colonoids	-	34.9/19.1	–/19.1	38.0/19.3		35.9/17.8
Lrig BVES fl/fl mTmG Colonoids	+	35.2/19.8	–/19.8	37.1/19.9		35.8/18.6
WT MEF + Wnt (Re-ran as + Control)		28.4/19.2	27.6/19.2	27.5/19.2		28.0/17.6

Table 7. Survey of *Bves* transcript levels in mouse tissue. CT values from qRT-PCR experiments performed on indicated tissue shown as BVES CT/GAPDH CT. Average value from three technical replicates are displayed. mBVES 00517902, mBVES 01192020, and mBVES 01192021 are Taqman probes spanning the indicated exons while the SYBR Green Exon3/4 primer set spans Exons 3 and 4 and SYBR Green Exon 4 is internal to Exon 4. Three values are shown in brackets for some BVES CT values to demonstrate the significant variability among technical replicates in some situations. -- = no amplification. Values are color coded as reliable, indeterminate, and unsuccessful based on an analysis of the BVES amplification plots, variability within technical replicates, and melt curves (SYBR Green only). In all samples, GAPDH amplification was reliable.

REFERENCES

1. van der Flier, L.G.; Clevers, H. Stem cells, self-renewal, and differentiation in the intestinal epithelium. *Annu Rev Physiol* **2009**, *71*, 241-260.
2. Mooseker, M.S. Organization, chemistry, and assembly of the cytoskeletal apparatus of the intestinal brush border. *Annu Rev Cell Biol* **1985**, *1*, 209-241.
3. Barker, N.; van Es, J.H.; Kuipers, J.; Kujala, P.; van den Born, M.; Cozijnsen, M.; Haegebarth, A.; Korving, J.; Begthel, H.; Peters, P.J.*, et al.* Identification of stem cells in small intestine and colon by marker gene lgr5. *Nature* **2007**, *449*, 1003-1007.
4. Cheng, H.; Leblond, C.P. Origin, differentiation and renewal of the four main epithelial cell types in the mouse small intestine. V. Unitarian theory of the origin of the four epithelial cell types. *Am J Anat* **1974**, *141*, 537-561.
5. Barker, N.; van de Wetering, M.; Clevers, H. The intestinal stem cell. *Genes Dev* **2008**, *22*, 1856-1864.
6. Umar, S. Intestinal stem cells. *Curr Gastroenterol Rep* **2010**, *12*, 340-348.
7. Crosnier, C.; Stamataki, D.; Lewis, J. Organizing cell renewal in the intestine: Stem cells, signals and combinatorial control. *Nat Rev Genet* **2006**, *7*, 349-359.
8. Tian, H.; Biehs, B.; Chiu, C.; Siebel, C.W.; Wu, Y.; Costa, M.; de Sauvage, F.J.; Klein, O.D. Opposing activities of notch and wnt signaling regulate intestinal stem cells and gut homeostasis. *Cell Rep* **2015**, *11*, 33-42.
9. de Lau, W.; Barker, N.; Low, T.Y.; Koo, B.K.; Li, V.S.; Teunissen, H.; Kujala, P.; Haegebarth, A.; Peters, P.J.; van de Wetering, M.*, et al.* Lgr5 homologues associate with wnt receptors and mediate r-spondin signalling. *Nature* **2011**, *476*, 293-297.
10. Sato, T.; Vries, R.G.; Snippert, H.J.; van de Wetering, M.; Barker, N.; Stange, D.E.; van Es, J.H.; Abo, A.; Kujala, P.; Peters, P.J.*, et al.* Single lgr5 stem cells build crypt-villus structures in vitro without a mesenchymal niche. *Nature* **2009**, *459*, 262-265.
11. Sato, T.; van Es, J.H.; Snippert, H.J.; Stange, D.E.; Vries, R.G.; van den Born, M.; Barker, N.; Shroyer, N.F.; van de Wetering, M.; Clevers, H. Paneth cells constitute the niche for lgr5 stem cells in intestinal crypts. *Nature* **2011**, *469*, 415-418.
12. Durand, A.; Donahue, B.; Peignon, G.; Letourneur, F.; Cagnard, N.; Slomianny, C.; Perret, C.; Shroyer, N.F.; Romagnolo, B. Functional intestinal stem cells after paneth cell ablation induced by the loss of transcription factor math1 (atoh1). *Proc Natl Acad Sci U S A* **2012**, *109*, 8965-8970.
13. Kim, T.H.; Escudero, S.; Shivdasani, R.A. Intact function of lgr5 receptor-expressing intestinal stem cells in the absence of paneth cells. *Proc Natl Acad Sci U S A* **2012**, *109*, 3932-3937.
14. Aoki, R.; Shoshkes-Carmel, M.; Gao, N.; Shin, S.; May, C.L.; Golson, M.L.; Zahm, A.M.; Ray, M.; Wiser, C.L.; Wright, C.V.*, et al.* Foxl1-expressing mesenchymal cells constitute the intestinal stem cell niche. *Cell Mol Gastroenterol Hepatol* **2016**, *2*, 175-188.
15. Potten, C.S. Extreme sensitivity of some intestinal crypt cells to x and gamma irradiation. *Nature* **1977**, *269*, 518-521.
16. Sangiorgi, E.; Capecchi, M.R. Bmi1 is expressed in vivo in intestinal stem cells. *Nat Genet* **2008**, *40*, 915-920.
17. Takeda, N.; Jain, R.; LeBoeuf, M.R.; Wang, Q.; Lu, M.M.; Epstein, J.A. Interconversion between intestinal stem cell populations in distinct niches. *Science* **2011**, *334*, 1420-1424.

18. Montgomery, R.K.; Carlone, D.L.; Richmond, C.A.; Farilla, L.; Kranendonk, M.E.; Henderson, D.E.; Baffour-Awuah, N.Y.; Ambruzs, D.M.; Fogli, L.K.; Algra, S.*, et al.* Mouse telomerase reverse transcriptase (mtert) expression marks slowly cycling intestinal stem cells. *Proc Natl Acad Sci U S A* **2011**, *108*, 179-184.
19. Powell, A.E.; Wang, Y.; Li, Y.; Poulin, E.J.; Means, A.L.; Washington, M.K.; Higginbotham, J.N.; Juchheim, A.; Prasad, N.; Levy, S.E.*, et al.* The pan-erbb negative regulator lrig1 is an intestinal stem cell marker that functions as a tumor suppressor. *Cell* **2012**, *149*, 146-158.
20. Wong, V.W.; Stange, D.E.; Page, M.E.; Buczacki, S.; Wabik, A.; Itami, S.; van de Wetering, M.; Poulsom, R.; Wright, N.A.; Trotter, M.W.*, et al.* Lrig1 controls intestinal stem-cell homeostasis by negative regulation of erbb signalling. *Nat Cell Biol* **2012**, *14*, 401-408.
21. Barker, N.; van Oudenaarden, A.; Clevers, H. Identifying the stem cell of the intestinal crypt: Strategies and pitfalls. *Cell Stem Cell* **2012**, *11*, 452-460.
22. Walko, G.; Castanon, M.J.; Wiche, G. Molecular architecture and function of the hemidesmosome. *Cell Tissue Res* **2015**, *360*, 363-378.
23. Evans, W.H.; Martin, P.E. Gap junctions: Structure and function (review). *Mol Membr Biol* **2002**, *19*, 121-136.
24. Balda, M.S.; Matter, K. Tight junctions and the regulation of gene expression. *Biochimica et biophysica acta* **2009**, *1788*, 761-767.
25. Hermiston, M.L.; Gordon, J.I. Inflammatory bowel disease and adenomas in mice expressing a dominant negative n-cadherin. *Science* **1995**, *270*, 1203-1207.
26. Dorudi, S.; Sheffield, J.P.; Poulsom, R.; Northover, J.M.; Hart, I.R. E-cadherin expression in colorectal cancer. An immunocytochemical and in situ hybridization study. *Am J Pathol* **1993**, *142*, 981-986.
27. Tunggal, J.A.; Helfrich, I.; Schmitz, A.; Schwarz, H.; Gunzel, D.; Fromm, M.; Kemler, R.; Krieg, T.; Niessen, C.M. E-cadherin is essential for in vivo epidermal barrier function by regulating tight junctions. *EMBO J* **2005**, *24*, 1146-1156.
28. Shin, K.; Fogg, V.C.; Margolis, B. Tight junctions and cell polarity. *Annu Rev Cell Dev Biol* **2006**, *22*, 207-235.
29. Zihni, C.; Mills, C.; Matter, K.; Balda, M.S. Tight junctions: From simple barriers to multifunctional molecular gates. *Nat Rev Mol Cell Biol* **2016**, *17*, 564-580.
30. Osler, M.E.; Chang, M.S.; Bader, D.M. Bves modulates epithelial integrity through an interaction at the tight junction. *Journal of cell science* **2005**, *118*, 4667-4678.
31. Brand, T. The popeye domain-containing gene family. *Cell Biochem Biophys* **2005**, *43*, 95-103.
32. Knight, R.F.; Bader, D.M.; Backstrom, J.R. Membrane topology of bves/pop1a, a cell adhesion molecule that displays dynamic changes in cellular distribution during development. *The Journal of biological chemistry* **2003**, *278*, 32872-32879.
33. Hager, H.A.; Bader, D.M. Bves: Ten years after. *Histol Histopathol* **2009**, *24*, 777-787.
34. Kukuruzinska, M.A.; Lennon, K. Protein n-glycosylation: Molecular genetics and functional significance. *Crit Rev Oral Biol Med* **1998**, *9*, 415-448.
35. Osler, M.E.; Smith, T.K.; Bader, D.M. Bves, a member of the popeye domain-containing gene family. *Dev Dyn* **2006**, *235*, 586-593.
36. Kawaguchi, M.; Hager, H.A.; Wada, A.; Koyama, T.; Chang, M.S.; Bader, D.M. Identification of a novel intracellular interaction domain essential for bves function. *PLoS One* **2008**, *3*, e2261.

37. Reese, D.E.; Zavaljevski, M.; Streiff, N.L.; Bader, D. Bves: A novel gene expressed during coronary blood vessel development. *Dev Biol* **1999**, *209*, 159-171.
38. Andree, B.; Hillemann, T.; Kessler-Icekson, G.; Schmitt-John, T.; Jockusch, H.; Arnold, H.H.; Brand, T. Isolation and characterization of the novel popeye gene family expressed in skeletal muscle and heart. *Dev Biol* **2000**, *223*, 371-382.
39. Andree, B.; Fleige, A.; Arnold, H.H.; Brand, T. Mouse pop1 is required for muscle regeneration in adult skeletal muscle. *Molecular and cellular biology* **2002**, *22*, 1504-1512.
40. Wu, Y.C.; Liu, C.Y.; Chen, Y.H.; Chen, R.F.; Huang, C.J.; Wang, I.J. Blood vessel epicardial substance (bves) regulates epidermal tight junction integrity through atypical protein kinase c. *The Journal of biological chemistry* **2012**, *287*, 39887-39897.
41. Williams, C.S.; Zhang, B.; Smith, J.J.; Jayagopal, A.; Barrett, C.W.; Pino, C.; Russ, P.; Presley, S.H.; Peng, D.; Rosenblatt, D.O.*, et al.* Bves regulates emt in human corneal and colon cancer cells and is silenced via promoter methylation in human colorectal carcinoma. *J Clin Invest* **2011**, *121*, 4056-4069.
42. Kim, M.; Jang, H.R.; Haam, K.; Kang, T.W.; Kim, J.H.; Kim, S.Y.; Noh, S.M.; Song, K.S.; Cho, J.S.; Jeong, H.Y.*, et al.* Frequent silencing of popeye domain-containing genes, bves and popdc3, is associated with promoter hypermethylation in gastric cancer. *Carcinogenesis* **2010**, *31*, 1685-1693.
43. Feng, Q.; Hawes, S.E.; Stern, J.E.; Wiens, L.; Lu, H.; Dong, Z.M.; Jordan, C.D.; Kiviat, N.B.; Vesselle, H. DNA methylation in tumor and matched normal tissues from non-small cell lung cancer patients. *Cancer Epidemiol Biomarkers Prev* **2008**, *17*, 645-654.
44. Smith, T.K.; Bader, D.M. Characterization of bves expression during mouse development using newly generated immunoreagents. *Dev Dyn* **2006**, *235*, 1701-1708.
45. Guillot, C.; Lecuit, T. Mechanics of epithelial tissue homeostasis and morphogenesis. *Science* **2013**, *340*, 1185-1189.
46. Ragkousi, K.; Gibson, M.C. Cell division and the maintenance of epithelial order. *The Journal of cell biology* **2014**, *207*, 181-188.
47. Orsulic, S.; Huber, O.; Aberle, H.; Arnold, S.; Kemler, R. E-cadherin binding prevents beta-catenin nuclear localization and beta-catenin/lef-1-mediated transactivation. *Journal of cell science* **1999**, *112*, 1237-1245.
48. Sanchez-Tillo, E.; de Barrios, O.; Siles, L.; Cuatrecasas, M.; Castells, A.; Postigo, A. Beta-catenin/tcf4 complex induces the epithelial-to-mesenchymal transition (emt)-activator zeb1 to regulate tumor invasiveness. *Proc Natl Acad Sci U S A* **2011**, *108*, 19204-19209.
49. Severson, E.A.; Parkos, C.A. Mechanisms of outside-in signaling at the tight junction by junctional adhesion molecule a. *Ann N Y Acad Sci* **2009**, *1165*, 10-18.
50. Jayagopal, A.; Yang, J.L.; Haselton, F.R.; Chang, M.S. Tight junction-associated signaling pathways modulate cell proliferation in uveal melanoma. *Invest Ophthalmol Vis Sci* **2011**, *52*, 588-593.
51. Kavanagh, E.; Buchert, M.; Tsapara, A.; Choquet, A.; Balda, M.S.; Hollande, F.; Matter, K. Functional interaction between the zo-1-interacting transcription factor zonab/dbpa and the rna processing factor symplekin. *Journal of cell science* **2006**, *119*, 5098-5105.
52. Smith, T.K.; Hager, H.A.; Francis, R.; Kilkenny, D.M.; Lo, C.W.; Bader, D.M. Bves directly interacts with geft, and controls cell shape and movement through regulation of rac1/cdc42 activity. *Proc Natl Acad Sci U S A* **2008**, *105*, 8298-8303.
53. Jou, T.S.; Schneeberger, E.E.; Nelson, W.J. Structural and functional regulation of tight junctions by rhoa and rac1 small gtpases. *The Journal of cell biology* **1998**, *142*, 101-115.

54. Russ, P.K.; Pino, C.J.; Williams, C.S.; Bader, D.M.; Haselton, F.R.; Chang, M.S. Bves modulates tight junction associated signaling. *PLoS One* **2011**, *6*, e14563.
55. Hager, H.A.; Roberts, R.J.; Cross, E.E.; Proux-Gillardeaux, V.; Bader, D.M. Identification of a novel bves function: Regulation of vesicular transport. *EMBO J* **2010**, *29*, 532-545.
56. Tayeb, M.A.; Skalski, M.; Cha, M.C.; Kean, M.J.; Scaife, M.; Coppolino, M.G. Inhibition of snare-mediated membrane traffic impairs cell migration. *Exp Cell Res* **2005**, *305*, 63-73.
57. Luftman, K.; Hasan, N.; Day, P.; Hardee, D.; Hu, C. Silencing of vamp3 inhibits cell migration and integrin-mediated adhesion. *Biochemical and biophysical research communications* **2009**, *380*, 65-70.
58. Froese, A.; Breher, S.S.; Waldeyer, C.; Schindler, R.F.; Nikolaev, V.O.; Rinne, S.; Wischmeyer, E.; Schlueter, J.; Becher, J.; Simrick, S.*, et al.* Popeye domain containing proteins are essential for stress-mediated modulation of cardiac pacemaking in mice. *J Clin Invest* **2012**, *122*, 1119-1130.
59. Schindler, R.F.; Scotton, C.; Zhang, J.; Passarelli, C.; Ortiz-Bonnin, B.; Simrick, S.; Schwerte, T.; Poon, K.L.; Fang, M.; Rinne, S.*, et al.* Popdc1(s201f) causes muscular dystrophy and arrhythmia by affecting protein trafficking. *J Clin Invest* **2016**, *126*, 239-253.
60. Amunjela, J.N.; Tucker, S.J. Dysregulation of popdc1 promotes breast cancer cell migration and proliferation. *Biosci Rep* **2017**, *37*.
61. Beese, M.; Wyss, K.; Haubitz, M.; Kirsch, T. Effect of camp derivates on assembly and maintenance of tight junctions in human umbilical vein endothelial cells. *BMC Cell Biol* **2010**, *11*, 68.
62. D'Souza, T.; Agarwal, R.; Morin, P.J. Phosphorylation of claudin-3 at threonine 192 by camp-dependent protein kinase regulates tight junction barrier function in ovarian cancer cells. *The Journal of biological chemistry* **2005**, *280*, 26233-26240.
63. Brabletz, T.; Jung, A.; Spaderna, S.; Hlubek, F.; Kirchner, T. Opinion: Migrating cancer stem cells - an integrated concept of malignant tumour progression. *Nat Rev Cancer* **2005**, *5*, 744-749.
64. Thoreson, M.A.; Reynolds, A.B. Altered expression of the catenin p120 in human cancer: Implications for tumor progression. *Differentiation* **2002**, *70*, 583-589.
65. Knights, A.J.; Funnell, A.P.; Crossley, M.; Pearson, R.C. Holding tight: Cell junctions and cancer spread. *Trends Cancer Res* **2012**, *8*, 61-69.
66. Van Aken, J.; Cuvelier, C.A.; De Wever, N.; Roels, J.; Gao, Y.; Mareel, M.M. Immunohistochemical analysis of e-cadherin expression in human colorectal tumours. *Pathol Res Pract* **1993**, *189*, 975-978.
67. Dhawan, P.; Singh, A.B.; Deane, N.G.; No, Y.; Shiou, S.R.; Schmidt, C.; Neff, J.; Washington, M.K.; Beauchamp, R.D. Claudin-1 regulates cellular transformation and metastatic behavior in colon cancer. *J Clin Invest* **2005**, *115*, 1765-1776.
68. Hewitt, K.J.; Agarwal, R.; Morin, P.J. The claudin gene family: Expression in normal and neoplastic tissues. *BMC Cancer* **2006**, *6*, 186.
69. Chang, T.L.; Ito, K.; Ko, T.K.; Liu, Q.; Salto-Tellez, M.; Yeoh, K.G.; Fukamachi, H.; Ito, Y. Claudin-1 has tumor suppressive activity and is a direct target of runx3 in gastric epithelial cells. *Gastroenterology* **2010**, *138*, 255-265 e251-253.
70. Ni, S.; Xu, L.; Huang, J.; Feng, J.; Zhu, H.; Wang, G.; Wang, X. Increased zo-1 expression predicts valuable prognosis in non-small cell lung cancer. *Int J Clin Exp Pathol* **2013**, *6*, 2887-2895.

71. Martin, T.A.; Watkins, G.; Mansel, R.E.; Jiang, W.G. Loss of tight junction plaque molecules in breast cancer tissues is associated with a poor prognosis in patients with breast cancer. *Eur J Cancer* **2004**, *40*, 2717-2725.
72. Kaihara, T.; Kusaka, T.; Nishi, M.; Kawamata, H.; Imura, J.; Kitajima, K.; Itoh-Minami, R.; Aoyama, N.; Kasuga, M.; Oda, Y.*, et al.* Dedifferentiation and decreased expression of adhesion molecules, e-cadherin and zo-1, in colorectal cancer are closely related to liver metastasis. *J Exp Clin Cancer Res* **2003**, *22*, 117-123.
73. Parang, B.; Kaz, A.M.; Barrett, C.W.; Short, S.P.; Ning, W.; Keating, C.E.; Mittal, M.K.; Naik, R.D.; Washington, M.K.; Revetta, F.L.*, et al.* Bves regulates c-myc stability via pp2a and suppresses colitis-induced tumourigenesis. *Gut* **2017**, *66*, 852-862.
74. Snider, A.J.; Bialkowska, A.B.; Ghaleb, A.M.; Yang, V.W.; Obeid, L.M.; Hannun, Y.A. Murine model for colitis-associated cancer of the colon. *Methods Mol Biol* **2016**, *1438*, 245-254.
75. Waldner, M.J.; Neurath, M.F. Mechanisms of immune signaling in colitis-associated cancer. *Cell Mol Gastroenterol Hepatol* **2015**, *1*, 6-16.
76. De Robertis, M.; Massi, E.; Poeta, M.L.; Carotti, S.; Morini, S.; Cecchetelli, L.; Signori, E.; Fazio, V.M. The aom/dss murine model for the study of colon carcinogenesis: From pathways to diagnosis and therapy studies. *J Carcinog* **2011**, *10*, 9.
77. Ciclitira, P.J.; Macartney, J.C.; Evan, G. Expression of c-myc in non-malignant and pre-malignant gastrointestinal disorders. *J Pathol* **1987**, *151*, 293-296.
78. Brentnall, T.A.; Pan, S.; Bronner, M.P.; Crispin, D.A.; Mirzaei, H.; Cooke, K.; Tamura, Y.; Nikolskaya, T.; Jebailey, L.; Goodlett, D.R.*, et al.* Proteins that underlie neoplastic progression of ulcerative colitis. *Proteomics Clin Appl* **2009**, *3*, 1326.
79. Suzuki, R.; Miyamoto, S.; Yasui, Y.; Sugie, S.; Tanaka, T. Global gene expression analysis of the mouse colonic mucosa treated with azoxymethane and dextran sodium sulfate. *BMC Cancer* **2007**, *7*, 84.
80. Arnold, H.K.; Sears, R.C. A tumor suppressor role for pp2a-b56alpha through negative regulation of c-myc and other key oncoproteins. *Cancer Metastasis Rev* **2008**, *27*, 147-158.
81. Thompson, J.J.; Williams, C.S. Protein phosphatase 2a in the regulation of wnt signaling, stem cells, and cancer. *Genes (Basel)* **2018**, *9*.
82. Nunbhakdi-Craig, V.; Machleidt, T.; Ogris, E.; Bellotto, D.; White, C.L., 3rd; Sontag, E. Protein phosphatase 2a associates with and regulates atypical pkc and the epithelial tight junction complex. *The Journal of cell biology* **2002**, *158*, 967-978.
83. Han, P.; Fu, Y.; Liu, J.; Wang, Y.; He, J.; Gong, J.; Li, M.; Tan, Q.; Li, D.; Luo, Y.*, et al.* Netrin-1 promotes cell migration and invasion by down-regulation of bves expression in human hepatocellular carcinoma. *Am J Cancer Res* **2015**, *5*, 1396-1409.
84. Han, P.; Fu, Y.; Luo, M.; He, J.; Liu, J.; Liao, J.; Tian, D.; Yan, W. Bves inhibition triggers epithelial-mesenchymal transition in human hepatocellular carcinoma. *Dig Dis Sci* **2014**, *59*, 992-1000.
85. Amunjela, J.N.; Tucker, S.J. Popdc1 is suppressed in human breast cancer tissues and is negatively regulated by egfr in breast cancer cell lines. *Cancer Lett* **2017**, *406*, 81-92.
86. Mah, A.T.; Yan, K.S.; Kuo, C.J. Wnt pathway regulation of intestinal stem cells. *J Physiol* **2016**, *594*, 4837-4847.
87. Gregorieff, A.; Clevers, H. Wnt signaling in the intestinal epithelium: From endoderm to cancer. *Genes Dev* **2005**, *19*, 877-890.

88. Reddy, V.K.; Short, S.P.; Barrett, C.W.; Mittal, M.K.; Keating, C.E.; Thompson, J.J.; Harris, E.I.; Revetta, F.; Bader, D.M.; Brand, T.*, et al.* Bves regulates intestinal stem cell programs and intestinal crypt viability after radiation. *Stem Cells* **2016**, *34*, 1626-1636.
89. Choksi, Y.A.; Reddy, V.K.; Singh, K.; Barrett, C.W.; Short, S.P.; Parang, B.; Keating, C.E.; Thompson, J.J.; Verriere, T.G.; Brown, R.E.*, et al.* Bves is required for maintenance of colonic epithelial integrity in experimental colitis by modifying intestinal permeability. *Mucosal Immunol* **2018**.
90. Manning, G.; Whyte, D.B.; Martinez, R.; Hunter, T.; Sudarsanam, S. The protein kinase complement of the human genome. *Science* **2002**, *298*, 1912-1934.
91. Eichhorn, P.J.; Creyghton, M.P.; Bernards, R. Protein phosphatase 2a regulatory subunits and cancer. *Biochimica et biophysica acta* **2009**, *1795*, 1-15.
92. Virshup, D.M.; Shenolikar, S. From promiscuity to precision: Protein phosphatases get a makeover. *Molecular Cell 33*, 537-545.
93. Janssens, V.; Longin, S.; Goris, J. Pp2a holoenzyme assembly: In cauda venenum (the sting is in the tail). *Trends in biochemical sciences* **2008**, *33*, 113-121.
94. Cegielska, A.; Shaffer, S.; Derua, R.; Goris, J.; Virshup, D.M. Different oligomeric forms of protein phosphatase 2a activate and inhibit simian virus 40 DNA replication. *Molecular and cellular biology* **1994**, *14*, 4616-4623.
95. Polakis, P. Wnt signaling in cancer. *Cold Spring Harbor Perspectives in Biology* **2012**, *4*, a008052.
96. The Cancer Genome Atlas, N. Comprehensive molecular characterization of human colon and rectal cancer. *Nature* **2012**, *487*, 330-337.
97. Hartsock, A.; Nelson, W.J. Adherens and tight junctions: Structure, function and connections to the actin cytoskeleton. *Biochimica et Biophysica Acta (BBA) - Biomembranes* **2008**, *1778*, 660-669.
98. Chen, W.C.; Obrink, B. Cell-cell contacts mediated by e-cadherin (uvomorulin) restrict invasive behavior of l-cells. *The Journal of cell biology* **1991**, *114*, 319-327.
99. Liu, C.; Li, Y.; Semenov, M.; Han, C.; Baeg, G.H.; Tan, Y.; Zhang, Z.; Lin, X.; He, X. Control of β-catenin phosphorylation/degradation by a dual-kinase mechanism. *Cell* **2002**, *108*.
100. Clevers, H.; Nusse, R. Wnt/β-catenin signaling and disease. *Cell* **2012**, *149*.
101. Schneikert, J.; Behrens, J. The canonical wnt signalling pathway and its apc partner in colon cancer development. *Gut* **2007**, *56*, 417-425.
102. Yanfeng, W.A.; Tan, C.; Fagan, R.J.; Klein, P.S. Phosphorylation of frizzled-3. *The Journal of biological chemistry* **2006**, *281*, 11603-11609.
103. Klimowski, L.K.; Garcia, B.A.; Shabanowitz, J.; Hunt, D.F.; Virshup, D.M. Site-specific casein kinase 1ε-dependent phosphorylation of dishevelled modulates β-catenin signaling. *FEBS Journal* **2006**, *273*, 4594-4602.
104. Ikeda, S.; Kishida, M.; Matsuura, Y.; Usui, H.; Kikuchi, A. Gsk-3beta-dependent phosphorylation of adenomatous polyposis coli gene product can be modulated by beta-catenin and protein phosphatase 2a complexed with axin. *Oncogene* **2000**, *19*, 537-545.
105. Rubinfeld, B.; Albert, I.; Porfiri, E.; Fiol, C.; Munemitsu, S.; Polakis, P. Binding of gsk3beta to the apc-beta-catenin complex and regulation of complex assembly. *Science* **1996**, *272*, 1023-1026.
106. Yamamoto, H.; Kishida, S.; Kishida, M.; Ikeda, S.; Takada, S.; Kikuchi, A. Phosphorylation of axin, a wnt signal negative regulator, by glycogen synthase kinase-3β regulates its stability. *Journal of Biological Chemistry* **1999**, *274*, 10681-10684.

107. Jho, E.; Lomvardas, S.; Costantini, F. A gsk3beta phosphorylation site in axin modulates interaction with beta-catenin and tcf-mediated gene expression. *Biochemical and biophysical research communications* **1999**, *266*, 28-35.
108. Rivers, A.; Gietzen, K.F.; Vielhaber, E.; Virshup, D.M. Regulation of casein kinase i epsilon and casein kinase i delta by an in vivo futile phosphorylation cycle. *The Journal of biological chemistry* **1998**, *273*, 15980-15984.
109. Budini, M.; Jacob, G.; Jedlicki, A.; Perez, C.; Allende, C.C.; Allende, J.E. Autophosphorylation of carboxy-terminal residues inhibits the activity of protein kinase ck1alpha. *J Cell Biochem* **2009**, *106*, 399-408.
110. Cross, D.A.; Alessi, D.R.; Cohen, P.; Andjelkovich, M.; Hemmings, B.A. Inhibition of glycogen synthase kinase-3 by insulin mediated by protein kinase b. *Nature* **1995**, *378*, 785-789.
111. Frame, S.; Cohen, P.; Biondi, R.M. A common phosphate binding site explains the unique substrate specificity of gsk3 and its inactivation by phosphorylation. *Mol Cell* **2001**, *7*, 1321-1327.
112. Fujiki, H.; Suganuma, M.; Yoshizawa, S.; Nishiwaki, S.; Winyar, B.; Sugimura, T. Mechanisms of action of okadaic acid class tumor promoters on mouse skin. *Environmental Health Perspectives* **1991**, *93*, 211-214.
113. Suganuma, M.; Fujiki, H.; Suguri, H.; Yoshizawa, S.; Hirota, M.; Nakayasu, M.; Ojika, M.; Wakamatsu, K.; Yamada, K.; Sugimura, T. Okadaic acid: An additional non-phorbol-12-tetradecanoate-13-acetate-type tumor promoter. *Proceedings of the National Academy of Sciences of the United States of America* **1988**, *85*, 1768-1771.
114. Maynes, J.T.; Bateman, K.S.; Cherney, M.M.; Das, A.K.; Luu, H.A.; Holmes, C.F.; James, M.N. Crystal structure of the tumor-promoter okadaic acid bound to protein phosphatase-1. *The Journal of biological chemistry* **2001**, *276*, 44078-44082.
115. Bialojan, C.; Takai, A. Inhibitory effect of a marine-sponge toxin, okadaic acid, on protein phosphatases. Specificity and kinetics. *Biochem J* **1988**, *256*, 283-290.
116. Swingle, M.; Ni L Fau - Honkanen, R.E.; Honkanen, R.E. Small-molecule inhibitors of ser/thr protein phosphatases: Specificity, use and common forms of abuse. *Methods Mol Biol* **2007**, 365:323-328.
117. Pallas, D.C.; Shahrik, L.K.; Martin, B.L.; Jaspers, S.; Miller, T.B.; Brautigan, D.L.; Roberts, T.M. Polyoma small and middle t antigens and sv40 small t antigen form stable complexes with protein phosphatase 2a. *Cell* **1990**, *60*, 167-176.
118. Sontag, E.; Fedorov, S.; Kamibayashi, C.; Robbins, D.; Cobb, M.; Mumby, M. The interaction of sv40 small tumor antigen with protein phosphatase 2a stimulates the map kinase pathway and induces cell proliferation. *Cell* **1993**, *75*, 887-897.
119. Ali, S.H.; DeCaprio, J.A. Cellular transformation by sv40 large t antigen: Interaction with host proteins. *Seminars in cancer biology* **2001**, *11*, 15-23.
120. Yu, J.; Boyapati, A.; Rundell, K. Critical role for sv40 small-t antigen in human cell transformation. *Virology* **2001**, *290*, 192-198.
121. Hahn, W.C.; Dessain, S.K.; Brooks, M.W.; King, J.E.; Elenbaas, B.; Sabatini, D.M.; DeCaprio, J.A.; Weinberg, R.A. Enumeration of the simian virus 40 early region elements necessary for human cell transformation. *Molecular and cellular biology* **2002**, *22*, 2111-2123.
122. Chen, W.; Possemato, R.; Campbell, K.T.; Plattner, C.A.; Pallas, D.C.; Hahn, W.C. Identification of specific pp2a complexes involved in human cell transformation. *Cancer Cell* **2004**, *5*, 127-136.

123. Chen, W.; Arroyo, J.D.; Timmons, J.C.; Possemato, R.; Hahn, W.C. Cancer-associated pp2a aα subunits induce functional haploinsufficiency and tumorigenicity. *Cancer Research* **2005**, *65*, 8183-8192.
124. Ruediger, R.; Pham, H.T.; Walter, G. Disruption of protein phosphatase 2a subunit interaction in human cancers with mutations in the a alpha subunit gene. *Oncogene* **2001**, *20*, 10-15.
125. Liu, H.; Gu, Y.; Wang, H.; Yin, J.; Zheng, G.; Zhang, Z.; Lu, M.; Wang, C.; He, Z. Overexpression of pp2a inhibitor set oncoprotein is associated with tumor progression and poor prognosis in human non-small cell lung cancer. *Oncotarget* **2015**, *6*, 14913-14925.
126. Li, M.; Makkinje, A.; Damuni, Z. Molecular identification of i1pp2a, a novel potent heat-stable inhibitor protein of protein phosphatase 2a. *Biochemistry* **1996**, *35*, 6998-7002.
127. Tsujio, I.; Zaidi, T.; Xu, J.; Kotula, L.; Grundke-Iqbal, I.; Iqbal, K. Inhibitors of protein phosphatase-2a from human brain structures, immunocytological localization and activities towards dephosphorylation of the alzheimer type hyperphosphorylated tau. *FEBS Lett* **2005**, *579*, 363-372.
128. Sangodkar, J.; Perl, A.; Tohme, R.; Kiselar, J.; Kastrinsky, D.B.; Zaware, N.; Izadmehr, S.; Mazhar, S.; Wiredja, D.D.; O'Connor, C.M.*, et al.* Activation of tumor suppressor protein pp2a inhibits kras-driven tumor growth. *J Clin Invest* **2017**, *127*, 2081-2090.
129. Oaks, J.J.; Santhanam, R.; Walker, C.J.; Roof, S.; Harb, J.G.; Ferenchak, G.; Eisfeld, A.K.; Van Brocklyn, J.R.; Briesewitz, R.; Saddoughi, S.A.*, et al.* Antagonistic activities of the immunomodulator and pp2a-activating drug fty720 (fingolimod, gilenya) in jak2-driven hematologic malignancies. *Blood* **2013**, *122*, 1923-1934.
130. Yang, Y.; Huang, Q.; Lu, Y.; Li, X.; Huang, S. Reactivating pp2a by fty720 as a novel therapy for aml with c-kit tyrosine kinase domain mutation. *J Cell Biochem* **2012**, *113*, 1314-1322.
131. Perrotti, D.; Neviani, P. Protein phosphatase 2a (pp2a), a drugable tumor suppressor in ph1(+) leukemias. *Cancer Metastasis Rev* **2008**, *27*, 159-168.
132. Arino, J.; Woon, C.W.; Brautigan, D.L.; Miller, T.B., Jr.; Johnson, G.L. Human liver phosphatase 2a: Cdna and amino acid sequence of two catalytic subunit isotypes. *Proc Natl Acad Sci U S A* **1988**, *85*, 4252-4256.
133. Götz, J.; Probst, A.; Ehler, E.; Hemmings, B.; Kues, W. Delayed embryonic lethality in mice lacking protein phosphatase 2a catalytic subunit cα. *Proceedings of the National Academy of Sciences of the United States of America* **1998**, *95*, 12370-12375.
134. McCright, B.; Rivers, A.M.; Audlin, S.; Virshup, D.M. The b56 family of protein phosphatase 2a (pp2a) regulatory subunits encodes differentiation-induced phosphoproteins that target pp2a to both nucleus and cytoplasm. *The Journal of biological chemistry* **1996**, *271*, 22081-22089.
135. Götz, J.; Probst, A.; Mistl, C.; Nitsch, R.M.; Ehler, E. Distinct role of protein phosphatase 2a subunit cα in the regulation of e-cadherin and β-catenin during development. *Mechanisms of Development* **2000**, *93*, 83-93.
136. Buck, E.; Eyzaguirre, A.; Barr, S.; Thompson, S.; Sennello, R.; Young, D.; Iwata, K.K.; Gibson, N.W.; Cagnoni, P.; Haley, J.D. Loss of homotypic cell adhesion by epithelial-mesenchymal transition or mutation limits sensitivity to epidermal growth factor receptor inhibition. *Molecular Cancer Therapeutics* **2007**, *6*, 532-541.
137. Su, Y.; Fu, C.; Ishikawa, S.; Stella, A.; Kojima, M.; Shitoh, K.; Schreiber, E.M.; Day, B.W.; Liu, B. Apc is essential for targeting phosphorylated β-catenin to the scfβ-trcp ubiquitin ligase. *Molecular Cell* **2008**, *32*, 652-661.

138. Stappert, J.; Kemler, R. A short core region of e-cadherin is essential for catenin binding and is highly phosphorylated. *Cell adhesion and communication* **1994**, *2*, 319-327.
139. Choi, H.-J.; Huber, A.H.; Weis, W.I. Thermodynamics of β-catenin-ligand interactions: The roles of the n- and c-terminal tails in modulating binding affinity. *Journal of Biological Chemistry* **2006**, *281*, 1027-1038.
140. Huber, A.H.; Weis, W.I. The structure of the beta-catenin/e-cadherin complex and the molecular basis of diverse ligand recognition by beta-catenin. *Cell* **2001**, *105*, 391-402.
141. Dupre-Crochet, S.; Figueroa, A.; Hogan, C.; Ferber, E.C.; Bialucha, C.U.; Adams, J.; Richardson, E.C.N.; Fujita, Y. Casein kinase 1 is a novel negative regulator of e-cadherin-based cell-cell contacts. *Molecular and cellular biology* **2007**, *27*, 3804-3816.
142. Yokoyama, N.; Malbon, C.C. Phosphoprotein phosphatase-2a docks to dishevelled and counterregulates wnt3a/β-catenin signaling. *Journal of Molecular Signaling* **2007**, *2*, 1-18.
143. Welsh, G.I.; Proud, C.G. Glycogen synthase kinase-3 is rapidly inactivated in response to insulin and phosphorylates eukaryotic initiation factor eif-2b. *Biochemical Journal* **1993**, *294*, 625-629.
144. Mitra, A.; Menezes, M.E.; Pannell, L.K.; Mulekar, M.S.; Honkanen, R.E.; Shevde, L.A.; Samant, R.S. Dnajb6 chaperones pp2a mediated dephosphorylation of gsk3beta to downregulate beta-catenin transcription target, osteopontin. *Oncogene* **2012**, *31*, 4472-4483.
145. Li, L.; Fang, C.; Xu, D.; Xu, Y.; Fu, H.; Li, J. Cardiomyocyte specific deletion of pp2a causes cardiac hypertrophy. *Am J Transl Res* **2016**, *8*, 1769-1779.
146. Seeling, J.M.; Miller, J.R.; Gil, R.; Moon, R.T.; White, R.; Virshup, D.M. Regulation of beta-catenin signaling by the b56 subunit of protein phosphatase 2a. *Science* **1999**, *283*, 2089-2091.
147. Fagotto, F.; Guger, K.; Gumbiner, B.M. Induction of the primary dorsalizing center in xenopus by the wnt/gsk/beta-catenin signaling pathway, but not by vg1, activin or noggin. *Development (Cambridge, England)* **1997**, *124*, 453-460.
148. Li, X.; Yost, H.J.; Virshup, D.M.; Seeling, J.M. Protein phosphatase 2a and its b56 regulatory subunit inhibit wnt signaling in xenopus. *EMBO J* **2001**, *20*, 4122-4131.
149. Yamamoto, H.; Hinoi, T.; Michiue, T.; Fukui, A.; Usui, H.; Janssens, V.; Van Hoof, C.; Goris, J.; Asashima, M.; Kikuchi, A. Inhibition of the wnt signaling pathway by the pr61 subunit of protein phosphatase 2a. *Journal of Biological Chemistry* **2001**, *276*, 26875-26882.
150. Zhang, W.; Yang, J.; Liu, Y.; Chen, X.; Yu, T.; Jia, J.; Liu, C. Pr55 alpha, a regulatory subunit of pp2a, specifically regulates pp2a-mediated beta-catenin dephosphorylation. *The Journal of biological chemistry* **2009**, *284*, 22649-22656.
151. Hino, S.; Tanji, C.; Nakayama, K.I.; Kikuchi, A. Phosphorylation of beta-catenin by cyclic amp-dependent protein kinase stabilizes beta-catenin through inhibition of its ubiquitination. *Molecular and cellular biology* **2005**, *25*, 9063-9072.
152. Fang, D.; Hawke, D.; Zheng, Y.; Xia, Y.; Meisenhelder, J.; Nika, H.; Mills, G.B.; Kobayashi, R.; Hunter, T.; Lu, Z. Phosphorylation of beta-catenin by akt promotes beta-catenin transcriptional activity. *The Journal of biological chemistry* **2007**, *282*, 11221-11229.
153. Hein, A.L.; Seshacharyulu, P.; Rachagani, S.; Sheinin, Y.M.; Ouellette, M.M.; Ponnusamy, M.P.; Mumby, M.C.; Batra, S.K.; Yan, Y. Pr55alpha subunit of protein phosphatase 2a supports the tumorigenic and metastatic potential of pancreatic cancer cells by sustaining hyperactive oncogenic signaling. *Cancer Res* **2016**, *76*, 2243-2253.

154. Henderson, B.R. Nuclear-cytoplasmic shuttling of apc regulates beta-catenin subcellular localization and turnover. *Nat Cell Biol* **2000**, *2*, 653-660.
155. Neufeld, K.L.; Zhang, F.; Cullen, B.R.; White, R.L. Apc-mediated downregulation of β-catenin activity involves nuclear sequestration and nuclear export. *EMBO Reports* **2000**, *1*, 519-523.
156. Ha, N.C.; Tonozuka, T.; Stamos, J.L.; Choi, H.J.; Weis, W.I. Mechanism of phosphorylation-dependent binding of apc to beta-catenin and its role in beta-catenin degradation. *Mol Cell* **2004**, *15*, 511-521.
157. Hsu, W.; Zeng, L.; Costantini, F. Identification of a domain of axin that binds to the serine/threonine protein phosphatase 2a and a self-binding domain. *Journal of Biological Chemistry* **1999**, *274*, 3439-3445.
158. Strovel, E.T.; Wu, D.; Sussman, D.J. Protein phosphatase 2cα dephosphorylates axin and activates lef-1-dependent transcription. *Journal of Biological Chemistry* **2000**, *275*, 2399-2403.
159. Clevers, H.; Loh, K.M.; Nusse, R. Stem cell signaling. An integral program for tissue renewal and regeneration: Wnt signaling and stem cell control. *Science* **2014**, *346*, 1248012.
160. Nusse, R. Wnt signaling and stem cell control. *Cell Res* **2008**, *18*, 523-527.
161. Holland, J.D.; Klaus, A.; Garratt, A.N.; Birchmeier, W. Wnt signaling in stem and cancer stem cells. *Curr Opin Cell Biol* **2013**, *25*, 254-264.
162. de Sousa, E.M.F.; Vermeulen, L. Wnt signaling in cancer stem cell biology. *Cancers (Basel)* **2016**, *8*.
163. Wang, C.; Chang, K.C.; Somers, G.; Virshup, D.; Ang, B.T.; Tang, C.; Yu, F.; Wang, H. Protein phosphatase 2a regulates self-renewal of drosophila neural stem cells. *Development (Cambridge, England)* **2009**, *136*, 2287-2296.
164. Yoon, B.S.; Jun, E.K.; Park, G.; Jun Yoo, S.; Moon, J.H.; Soon Baik, C.; Kim, A.; Kim, H.; Kim, J.H.; Koh, G.Y.*, et al.* Optimal suppression of protein phosphatase 2a activity is critical for maintenance of human embryonic stem cell self-renewal. *Stem Cells* **2010**, *28*, 874-884.
165. Amit, M.; Carpenter, M.K.; Inokuma, M.S.; Chiu, C.P.; Harris, C.P.; Waknitz, M.A.; Itskovitz-Eldor, J.; Thomson, J.A. Clonally derived human embryonic stem cell lines maintain pluripotency and proliferative potential for prolonged periods of culture. *Dev Biol* **2000**, *227*, 271-278.
166. Arnold, H.K.; Sears, R.C. Protein phosphatase 2a regulatory subunit b56alpha associates with c-myc and negatively regulates c-myc accumulation. *Molecular and cellular biology* **2006**, *26*, 2832-2844.
167. Janghorban, M.; Langer, E.M.; Wang, X.; Zachman, D.; Daniel, C.J.; Hooper, J.; Fleming, W.H.; Agarwal, A.; Sears, R.C. The tumor suppressor phosphatase pp2a-b56alpha regulates stemness and promotes the initiation of malignancies in a novel murine model. *PLoS One* **2017**, *12*, e0188910.
168. He, T.C.; Sparks, A.B.; Rago, C.; Hermeking, H.; Zawel, L.; da Costa, L.T.; Morin, P.J.; Vogelstein, B.; Kinzler, K.W. Identification of c-myc as a target of the apc pathway. *Science* **1998**, *281*, 1509-1512.
169. Wilson, A.; Murphy, M.J.; Oskarsson, T.; Kaloulis, K.; Bettess, M.D.; Oser, G.M.; Pasche, A.C.; Knabenhans, C.; Macdonald, H.R.; Trumpp, A. C-myc controls the balance between hematopoietic stem cell self-renewal and differentiation. *Genes Dev* **2004**, *18*, 2747-2763.

170. Waikel, R.L.; Kawachi, Y.; Waikel, P.A.; Wang, X.J.; Roop, D.R. Deregulated expression of c-myc depletes epidermal stem cells. *Nat Genet* **2001**, *28*, 165-168.
171. Siegel, R.L.; Miller, K.D.; Fedewa, S.A.; Ahnen, D.J.; Meester, R.G.S.; Barzi, A.; Jemal, A. Colorectal cancer statistics, 2017. *CA Cancer J Clin* **2017**, *67*, 177-193.
172. Siegel, R.L.; Miller, K.D.; Jemal, A. Cancer statistics, 2018. *CA Cancer J Clin* **2018**, *68*, 7-30.
173. Marikawa, Y.; Elinson, R.P. Beta-trcp is a negative regulator of wnt/beta-catenin signaling pathway and dorsal axis formation in xenopus embryos. *Mech Dev* **1998**, *77*, 75-80.
174. Wehrli, M.; Dougan, S.T.; Caldwell, K.; O'Keefe, L.; Schwartz, S.; Vaizel-Ohayon, D.; Schejter, E.; Tomlinson, A.; DiNardo, S. Arrow encodes an ldl-receptor-related protein essential for wingless signalling. *Nature* **2000**, *407*, 527-530.
175. Pinson, K.I.; Brennan, J.; Monkley, S.; Avery, B.J.; Skarnes, W.C. An ldl-receptor-related protein mediates wnt signalling in mice. *Nature* **2000**, *407*, 535-538.
176. Niehrs, C.; Shen, J. Regulation of lrp6 phosphorylation. *Cell Mol Life Sci* **2010**, *67*, 2551-2562.
177. Jho, E.H.; Zhang, T.; Domon, C.; Joo, C.K.; Freund, J.N.; Costantini, F. Wnt/beta-catenin/tcf signaling induces the transcription of axin2, a negative regulator of the signaling pathway. *Molecular and cellular biology* **2002**, *22*, 1172-1183.
178. Thorne, C.A.; Hanson, A.J.; Schneider, J.; Tahinci, E.; Orton, D.; Cselenyi, C.S.; Jernigan, K.K.; Meyers, K.C.; Hang, B.I.; Waterson, A.G.*, et al.* Small-molecule inhibition of wnt signaling through activation of casein kinase 1alpha. *Nat Chem Biol* **2010**, *6*, 829-836.
179. Bandapalli, O.R.; Dihlmann, S.; Helwa, R.; Macher-Goeppinger, S.; Weitz, J.; Schirmacher, P.; Brand, K. Transcriptional activation of the beta-catenin gene at the invasion front of colorectal liver metastases. *J Pathol* **2009**, *218*, 370-379.
180. Freeman, T.J.; Smith, J.J.; Chen, X.; Washington, M.K.; Roland, J.T.; Means, A.L.; Eschrich, S.A.; Yeatman, T.J.; Deane, N.G.; Beauchamp, R.D. Smad4-mediated signaling inhibits intestinal neoplasia by inhibiting expression of beta-catenin. *Gastroenterology* **2012**, *142*, 562-571 e562.
181. Su, Y.; Ishikawa, S.; Kojima, M.; Liu, B. Eradication of pathogenic beta-catenin by skp1/cullin/f box ubiquitination machinery. *Proc Natl Acad Sci U S A* **2003**, *100*, 12729-12734.
182. Zhan, T.; Rindtorff, N.; Boutros, M. Wnt signaling in cancer. *Oncogene* **2017**, *36*, 1461-1473.
183. Wada, A.M.; Reese, D.E.; Bader, D.M. Bves: Prototype of a new class of cell adhesion molecules expressed during coronary artery development. *Development (Cambridge, England)* **2001**, *128*, 2085-2093.
184. Saito-Diaz, K.; Chen, T.W.; Wang, X.; Thorne, C.A.; Wallace, H.A.; Page-McCaw, A.; Lee, E. The way wnt works: Components and mechanism. *Growth Factors* **2013**, *31*, 1-31.
185. Gao, C.; Chen, Y.G. Dishevelled: The hub of wnt signaling. *Cell Signal* **2010**, *22*, 717-727.
186. Gonzalez-Sancho, J.M.; Greer, Y.E.; Abrahams, C.L.; Takigawa, Y.; Baljinnyam, B.; Lee, K.H.; Lee, K.S.; Rubin, J.S.; Brown, A.M. Functional consequences of wnt-induced dishevelled 2 phosphorylation in canonical and noncanonical wnt signaling. *The Journal of biological chemistry* **2013**, *288*, 9428-9437.
187. Gammons, M.V.; Rutherford, T.J.; Steinhart, Z.; Angers, S.; Bienz, M. Essential role of the dishevelled dep domain in a wnt-dependent human-cell-based complementation assay. *Journal of cell science* **2016**, *129*, 3892-3902.

188. Zeng, X.; Huang, H.; Tamai, K.; Zhang, X.; Harada, Y.; Yokota, C.; Almeida, K.; Wang, J.; Doble, B.; Woodgett, J.*, et al.* Initiation of wnt signaling: Control of wnt coreceptor lrp6 phosphorylation/activation via frizzled, dishevelled and axin functions. *Development (Cambridge, England)* **2008**, *135*, 367-375.
189. Hernandez, F.; Langa, E.; Cuadros, R.; Avila, J.; Villanueva, N. Regulation of gsk3 isoforms by phosphatases pp1 and pp2a. *Mol Cell Biochem* **2010**, *344*, 211-215.
190. Wadzinski, B.E.; Wheat, W.H.; Jaspers, S.; Peruski, L.F., Jr.; Lickteig, R.L.; Johnson, G.L.; Klemm, D.J. Nuclear protein phosphatase 2a dephosphorylates protein kinase a-phosphorylated creb and regulates creb transcriptional stimulation. *Molecular and cellular biology* **1993**, *13*, 2822-2834.
191. Zachos, N.C.; Kovbasnjuk, O.; Foulke-Abel, J.; In, J.; Blutt, S.E.; de Jonge, H.R.; Estes, M.K.; Donowitz, M. Human enteroids/colonoids and intestinal organoids functionally recapitulate normal intestinal physiology and pathophysiology. *The Journal of biological chemistry* **2016**, *291*, 3759-3766.
192. Saito-Diaz, K.; Benchabane, H.; Tiwari, A.; Tian, A.; Li, B.; Thompson, J.J.; Hyde, A.S.; Sawyer, L.M.; Jodoin, J.N.; Santos, E.*, et al.* Apc inhibits ligand-independent wnt signaling by the clathrin endocytic pathway. *Dev Cell* **2018**, *44*, 566-581 e568.
193. Takahashi, M.; Nakatsugi, S.; Sugimura, T.; Wakabayashi, K. Frequent mutations of the beta-catenin gene in mouse colon tumors induced by azoxymethane. *Carcinogenesis* **2000**, *21*, 1117-1120.
194. Maltzman, T.; Whittington, J.; Driggers, L.; Stephens, J.; Ahnen, D. Aom-induced mouse colon tumors do not express full-length apc protein. *Carcinogenesis* **1997**, *18*, 2435-2439.
195. Fajardo, A.M.; Piazza, G.A.; Tinsley, H.N. The role of cyclic nucleotide signaling pathways in cancer: Targets for prevention and treatment. *Cancers (Basel)* **2014**, *6*, 436-458.
196. Bilic, J.; Huang, Y.L.; Davidson, G.; Zimmermann, T.; Cruciat, C.M.; Bienz, M.; Niehrs, C. Wnt induces lrp6 signalosomes and promotes dishevelled-dependent lrp6 phosphorylation. *Science* **2007**, *316*, 1619-1622.
197. Lee, H.J.; Zheng, J.J. Pdz domains and their binding partners: Structure, specificity, and modification. *Cell Commun Signal* **2010**, *8*, 8.
198. Joiner, D.M.; Ke, J.; Zhong, Z.; Xu, H.E.; Williams, B.O. Lrp5 and lrp6 in development and disease. *Trends Endocrinol Metab* **2013**, *24*, 31-39.
199. Goentoro, L.; Kirschner, M.W. Evidence that fold-change, and not absolute level, of beta-catenin dictates wnt signaling. *Mol Cell* **2009**, *36*, 872-884.
200. Ilyas, M.; Tomlinson, I.P.; Rowan, A.; Pignatelli, M.; Bodmer, W.F. Beta-catenin mutations in cell lines established from human colorectal cancers. *Proc Natl Acad Sci U S A* **1997**, *94*, 10330-10334.
201. Giles, R.H.; van Es, J.H.; Clevers, H. Caught up in a wnt storm: Wnt signaling in cancer. *Biochimica et biophysica acta* **2003**, *1653*, 1-24.
202. Fearon, E.R.; Vogelstein, B. A genetic model for colorectal tumorigenesis. *Cell* **1990**, *61*, 759-767.
203. Vervoort, V.S.; Roselli, S.; Oshima, R.G.; Pasquale, E.B. Splice variants and expression patterns of shep1, bcar3 and nsp1, a gene family involved in integrin and receptor tyrosine kinase signaling. *Gene* **2007**, *391*, 161-170.
204. Garron, M.L.; Arsenieva, D.; Zhong, J.; Bloom, A.B.; Lerner, A.; O'Neill, G.M.; Arold, S.T. Structural insights into the association between bcar3 and cas family members, an atypical complex implicated in anti-oestrogen resistance. *J Mol Biol* **2009**, *386*, 190-203.

205. Cai, D.; Felekkis, K.N.; Near, R.I.; O'Neill, G.M.; van Seventer, J.M.; Golemis, E.A.; Lerner, A. The gdp exchange factor and-34 is expressed in b cells, associates with hef1, and activates cdc42. *J Immunol* **2003**, *170*, 969-978.
206. Dodelet, V.C.; Pazzagli, C.; Zisch, A.H.; Hauser, C.A.; Pasquale, E.B. A novel signaling intermediate, shep1, directly couples eph receptors to r-ras and rap1a. *The Journal of biological chemistry* **1999**, *274*, 31941-31946.
207. Gotoh, T.; Cai, D.; Tian, X.; Feig, L.A.; Lerner, A. P130cas regulates the activity of and-34, a novel ral, rap1, and r-ras guanine nucleotide exchange factor. *The Journal of biological chemistry* **2000**, *275*, 30118-30123.
208. Sakakibara, A.; Ohba, Y.; Kurokawa, K.; Matsuda, M.; Hattori, S. Novel function of chat in controlling cell adhesion via cas-crk-c3g-pathway-mediated rap1 activation. *Journal of cell science* **2002**, *115*, 4915-4924.
209. van Agthoven, T.; van Agthoven, T.L.; Dekker, A.; van der Spek, P.J.; Vreede, L.; Dorssers, L.C. Identification of bcar3 by a random search for genes involved in antiestrogen resistance of human breast cancer cells. *EMBO J* **1998**, *17*, 2799-2808.
210. Dorssers, L.C.; van Agthoven, T.; Dekker, A.; van Agthoven, T.L.; Kok, E.M. Induction of antiestrogen resistance in human breast cancer cells by random insertional mutagenesis using defective retroviruses: Identification of bcar-1, a common integration site. *Mol Endocrinol* **1993**, *7*, 870-878.
211. Matsuda, M.; Mayer, B.J.; Fukui, Y.; Hanafusa, H. Binding of transforming protein, p47gag-crk, to a broad range of phosphotyrosine-containing proteins. *Science* **1990**, *248*, 1537-1539.
212. Reynolds, A.B.; Kanner, S.B.; Wang, H.C.; Parsons, J.T. Stable association of activated pp60src with two tyrosine-phosphorylated cellular proteins. *Molecular and cellular biology* **1989**, *9*, 3951-3958.
213. Brinkman, A.; van der Flier, S.; Kok, E.M.; Dorssers, L.C. Bcar1, a human homologue of the adapter protein p130cas, and antiestrogen resistance in breast cancer cells. *J Natl Cancer Inst* **2000**, *92*, 112-120.
214. Defilippi, P.; Di Stefano, P.; Cabodi, S. P130cas: A versatile scaffold in signaling networks. *Trends Cell Biol* **2006**, *16*, 257-263.
215. Cai, D.; Clayton, L.K.; Smolyar, A.; Lerner, A. And-34, a novel p130cas-binding thymic stromal cell protein regulated by adhesion and inflammatory cytokines. *J Immunol* **1999**, *163*, 2104-2112.
216. Mahankali, M.; Peng, H.J.; Cox, D.; Gomez-Cambronero, J. The mechanism of cell membrane ruffling relies on a phospholipase d2 (pld2), grb2 and rac2 association. *Cell Signal* **2011**, *23*, 1291-1298.
217. Cai, D.; Iyer, A.; Felekkis, K.N.; Near, R.I.; Luo, Z.; Chernoff, J.; Albanese, C.; Pestell, R.G.; Lerner, A. And-34/bcar3, a gdp exchange factor whose overexpression confers antiestrogen resistance, activates rac, pak1, and the cyclin d1 promoter. *Cancer Res* **2003**, *63*, 6802-6808.
218. Cross, A.M.; Wilson, A.L.; Guerrero, M.S.; Thomas, K.S.; Bachir, A.I.; Kubow, K.E.; Horwitz, A.R.; Bouton, A.H. Breast cancer antiestrogen resistance 3-p130(cas) interactions promote adhesion disassembly and invasion in breast cancer cells. *Oncogene* **2016**, *35*, 5850-5859.
219. Wallez, Y.; Riedl, S.J.; Pasquale, E.B. Association of the breast cancer antiestrogen resistance protein 1 (bcar1) and bcar3 scaffolding proteins in cell signaling and antiestrogen resistance. *The Journal of biological chemistry* **2014**, *289*, 10431-10444.

220. Painter, M.W.; Davis, S.; Hardy, R.R.; Mathis, D.; Benoist, C.; Immunological Genome Project, C. Transcriptomes of the b and t lineages compared by multiplatform microarray profiling. *J Immunol* **2011**, *186*, 3047-3057.
221. Lyons, Y.A.; Wu, S.Y.; Overwijk, W.W.; Baggerly, K.A.; Sood, A.K. Immune cell profiling in cancer: Molecular approaches to cell-specific identification. *NPJ Precis Oncol* **2017**, *1*, 26.
222. Jablonski, K.A.; Amici, S.A.; Webb, L.M.; Ruiz-Rosado Jde, D.; Popovich, P.G.; Partida-Sanchez, S.; Guerau-de-Arellano, M. Novel markers to delineate murine m1 and m2 macrophages. *PLoS One* **2015**, *10*, e0145342.
223. Maeda, M.; Nishimura, Y.; Hayashi, H.; Kumagai, N.; Chen, Y.; Murakami, S.; Miura, Y.; Hiratsuka, J.; Kishimoto, T.; Otsuki, T. Reduction of cxc chemokine receptor 3 in an in vitro model of continuous exposure to asbestos in a human t-cell line, mt-2. *Am J Respir Cell Mol Biol* **2011**, *45*, 470-479.
224. Kanduri, K.; Tripathi, S.; Larjo, A.; Mannerstrom, H.; Ullah, U.; Lund, R.; Hawkins, R.D.; Ren, B.; Lahdesmaki, H.; Lahesmaa, R. Identification of global regulators of t-helper cell lineage specification. *Genome Med* **2015**, *7*, 122.
225. Smith, J.J.; Deane, N.G.; Wu, F.; Merchant, N.B.; Zhang, B.; Jiang, A.; Lu, P.; Johnson, J.C.; Schmidt, C.; Bailey, C.E.*, et al.* Experimentally derived metastasis gene expression profile predicts recurrence and death in patients with colon cancer. *Gastroenterology* **2010**, *138*, 958-968.
226. Riggins, R.B.; Quilliam, L.A.; Bouton, A.H. Synergistic promotion of c-src activation and cell migration by cas and and-34/bcar3. *The Journal of biological chemistry* **2003**, *278*, 28264-28273.
227. Near, R.I.; Zhang, Y.; Makkinje, A.; Vanden Borre, P.; Lerner, A. And-34/bcar3 differs from other nsp homologs in induction of anti-estrogen resistance, cyclin d1 promoter activation and altered breast cancer cell morphology. *J Cell Physiol* **2007**, *212*, 655-665.
228. Makkinje, A.; Near, R.I.; Infusini, G.; Vanden Borre, P.; Bloom, A.; Cai, D.; Costello, C.E.; Lerner, A. And-34/bcar3 regulates adhesion-dependent p130cas serine phosphorylation and breast cancer cell growth pattern. *Cell Signal* **2009**, *21*, 1423-1435.
229. Vanden Borre, P.; Near, R.I.; Makkinje, A.; Mostoslavsky, G.; Lerner, A. Bcar3/and-34 can signal independent of complex formation with cas family members or the presence of p130cas. *Cell Signal* **2011**, *23*, 1030-1040.
230. Wilson, A.L.; Schrecengost, R.S.; Guerrero, M.S.; Thomas, K.S.; Bouton, A.H. Breast cancer antiestrogen resistance 3 (bcar3) promotes cell motility by regulating actin cytoskeletal and adhesion remodeling in invasive breast cancer cells. *PLoS One* **2013**, *8*, e65678.
231. Ibrahim, R.; Lemoine, A.; Bertoglio, J.; Raingeaud, J. Human enhancer of filamentation 1-induced colorectal cancer cell migration: Role of serine phosphorylation and interaction with the breast cancer anti-estrogen resistance 3 protein. *Int J Biochem Cell Biol* **2015**, *64*, 45-57.
232. Cunningham-Edmondson, A.C.; Hanks, S.K. P130cas substrate domain signaling promotes migration, invasion, and survival of estrogen receptor-negative breast cancer cells. *Breast Cancer (Dove Med Press)* **2009**, *1*, 39-52.
233. Patwardhan, P.; Shen, Y.; Goldberg, G.S.; Miller, W.T. Individual cas phosphorylation sites are dispensable for processive phosphorylation by src and anchorage-independent cell growth. *The Journal of biological chemistry* **2006**, *281*, 20689-20697.

234. Sakai, R.; Iwamatsu, A.; Hirano, N.; Ogawa, S.; Tanaka, T.; Mano, H.; Yazaki, Y.; Hirai, H. A novel signaling molecule, p130, forms stable complexes in vivo with v-crk and v-src in a tyrosine phosphorylation-dependent manner. *EMBO J* **1994**, *13*, 3748-3756.
235. Mace, P.D.; Wallez, Y.; Dobaczewska, M.K.; Lee, J.J.; Robinson, H.; Pasquale, E.B.; Riedl, S.J. Nsp-cas protein structures reveal a promiscuous interaction module in cell signaling. *Nat Struct Mol Biol* **2011**, *18*, 1381-1387.
236. Sun, G.; Cheng, S.Y.; Chen, M.; Lim, C.J.; Pallen, C.J. Protein tyrosine phosphatase alpha phosphotyrosyl-789 binds bcar3 to position cas for activation at integrin-mediated focal adhesions. *Molecular and cellular biology* **2012**, *32*, 3776-3789.
237. Oh, M.J.; van Agthoven, T.; Choi, J.E.; Jeong, Y.J.; Chung, Y.H.; Kim, C.M.; Jhun, B.H. Bcar3 regulates egf-induced DNA synthesis in normal human breast mcf-12a cells. *Biochemical and biophysical research communications* **2008**, *375*, 430-434.
238. Boyer, A.P.; Collier, T.S.; Vidavsky, I.; Bose, R. Quantitative proteomics with sirna screening identifies novel mechanisms of trastuzumab resistance in her2 amplified breast cancers. *Mol Cell Proteomics* **2013**, *12*, 180-193.
239. Batt, D.B.; Roberts, T.M. Cell density modulates protein-tyrosine phosphorylation. *The Journal of biological chemistry* **1998**, *273*, 3408-3414.
240. Roskoski, R., Jr. Src protein-tyrosine kinase structure and regulation. *Biochemical and biophysical research communications* **2004**, *324*, 1155-1164.
241. Hunter, T. A tail of two src's: Mutatis mutandis. *Cell* **1987**, *49*, 1-4.
242. Reddy, R.J.; Gajadhar, A.S.; Swenson, E.J.; Rothenberg, D.A.; Curran, T.G.; White, F.M. Early signaling dynamics of the epidermal growth factor receptor. *Proc Natl Acad Sci U S A* **2016**, *113*, 3114-3119.
243. Sigismund, S.; Algisi, V.; Nappo, G.; Conte, A.; Pascolutti, R.; Cuomo, A.; Bonaldi, T.; Argenzio, E.; Verhoef, L.G.; Maspero, E.*, et al.* Threshold-controlled ubiquitination of the egfr directs receptor fate. *EMBO J* **2013**, *32*, 2140-2157.
244. Capuani, F.; Conte, A.; Argenzio, E.; Marchetti, L.; Priami, C.; Polo, S.; Di Fiore, P.P.; Sigismund, S.; Ciliberto, A. Quantitative analysis reveals how egfr activation and downregulation are coupled in normal but not in cancer cells. *Nat Commun* **2015**, *6*, 7999.
245. Euhus, D.M.; Hudd, C.; LaRegina, M.C.; Johnson, F.E. Tumor measurement in the nude mouse. *J Surg Oncol* **1986**, *31*, 229-234.
246. Thompson, J.J.; Short, S.P.; Parang, B.; Brown, R.E.; Li, C.; Ng, V.H.; Saito-Diaz, K.; Choksi, Y.A.; Washington, M.K.; Smith, J.J.*, et al.* Blood vessel epicardial substance (bves) reduces lrp6 receptor and cytoplasmic -catenin levels to modulate wnt signaling and intestinal homeostasis. *Carcinogenesis* **2019**.
247. Near, R.I.; Smith, R.S.; Toselli, P.A.; Freddo, T.F.; Bloom, A.B.; Vanden Borre, P.; Seldin, D.C.; Lerner, A. Loss of and-34/bcar3 expression in mice results in rupture of the adult lens. *Mol Vis* **2009**, *15*, 685-699.
248. Basu, S.; Haase, G.; Ben-Ze'ev, A. Wnt signaling in cancer stem cells and colon cancer metastasis. *F1000Res* **2016**, *5*.
249. Yan, K.S.; Janda, C.Y.; Chang, J.; Zheng, G.X.Y.; Larkin, K.A.; Luca, V.C.; Chia, L.A.; Mah, A.T.; Han, A.; Terry, J.M.*, et al.* Non-equivalence of wnt and r-spondin ligands during lgr5(+) intestinal stem-cell self-renewal. *Nature* **2017**, *545*, 238-242.
250. Bellam, N.; Pasche, B. Tgf-beta signaling alterations and colon cancer. *Cancer Treat Res* **2010**, *155*, 85-103.
251. Xu, Y.; Pasche, B. Tgf-beta signaling alterations and susceptibility to colorectal cancer. *Hum Mol Genet* **2007**, *16 Spec No 1*, R14-20.

252. Guo, J.; Canaff, L.; Rajadurai, C.V.; Fils-Aime, N.; Tian, J.; Dai, M.; Korah, J.; Villatoro, M.; Park, M.; Ali, S.*, et al.* Breast cancer anti-estrogen resistance 3 inhibits transforming growth factor beta/smad signaling and associates with favorable breast cancer disease outcomes. *Breast Cancer Res* **2014**, *16*, 476.
253. van Agthoven, T.; Sieuwerts, A.M.; Meijer-van Gelder, M.E.; Look, M.P.; Smid, M.; Veldscholte, J.; Sleijfer, S.; Foekens, J.A.; Dorssers, L.C. Relevance of breast cancer antiestrogen resistance genes in human breast cancer progression and tamoxifen resistance. *J Clin Oncol* **2009**, *27*, 542-549.
254. Shiou, S.R.; Singh, A.B.; Moorthy, K.; Datta, P.K.; Washington, M.K.; Beauchamp, R.D.; Dhawan, P. Smad4 regulates claudin-1 expression in a transforming growth factor-beta-independent manner in colon cancer cells. *Cancer Res* **2007**, *67*, 1571-1579.
255. Pino, M.S.; Kikuchi, H.; Zeng, M.; Herraiz, M.T.; Sperduti, I.; Berger, D.; Park, D.Y.; Iafrate, A.J.; Zukerberg, L.R.; Chung, D.C. Epithelial to mesenchymal transition is impaired in colon cancer cells with microsatellite instability. *Gastroenterology* **2010**, *138*, 1406-1417.
256. Wang, J.P.; Hielscher, A. Fibronectin: How its aberrant expression in tumors may improve therapeutic targeting. *J Cancer* **2017**, *8*, 674-682.
257. Guinney, J.; Dienstmann, R.; Wang, X.; de Reynies, A.; Schlicker, A.; Soneson, C.; Marisa, L.; Roepman, P.; Nyamundanda, G.; Angelino, P.*, et al.* The consensus molecular subtypes of colorectal cancer. *Nat Med* **2015**, *21*, 1350-1356.
258. Siena, S.; Sartore-Bianchi, A.; Marsoni, S.; Hurwitz, H.I.; McCall, S.J.; Penault-Llorca, F.; Srock, S.; Bardelli, A.; Trusolino, L. Targeting the human epidermal growth factor receptor 2 (her2) oncogene in colorectal cancer. *Ann Oncol* **2018**, *29*, 1108-1119.
259. Short, S.P.; Thompson, J.J.; Bilotta, A.J.; Chen, X.; Revetta, F.L.; Washington, M.K.; Williams, C.S. Serine threonine kinase 17a maintains the epithelial state in colorectal cancer cells. *Mol Cancer Res* **2019**.
260. Xu, Q.; Wang, Y.; Dabdoub, A.; Smallwood, P.M.; Williams, J.; Woods, C.; Kelley, M.W.; Jiang, L.; Tasman, W.; Zhang, K.*, et al.* Vascular development in the retina and inner ear: Control by norrin and frizzled-4, a high-affinity ligand-receptor pair. *Cell* **2004**, *116*, 883-895.
261. Kategaya, L.S.; Changkakoty, B.; Biechele, T.; Conrad, W.H.; Kaykas, A.; Dasgupta, R.; Moon, R.T. Bili inhibits wnt/beta-catenin signaling by regulating the recruitment of axin to lrp6. *PLoS One* **2009**, *4*, e6129.
262. Sanjana, N.E.; Shalem, O.; Zhang, F. Improved vectors and genome-wide libraries for crispr screening. *Nat Methods* **2014**, *11*, 783-784.
263. Sato, T.; Stange, D.E.; Ferrante, M.; Vries, R.G.; Van Es, J.H.; Van den Brink, S.; Van Houdt, W.J.; Pronk, A.; Van Gorp, J.; Siersema, P.D.*, et al.* Long-term expansion of epithelial organoids from human colon, adenoma, adenocarcinoma, and barrett's epithelium. *Gastroenterology* **2011**, *141*, 1762-1772.
264. Heijmans, J.; van Lidth de Jeude, J.F.; Koo, B.K.; Rosekrans, S.L.; Wielenga, M.C.; van de Wetering, M.; Ferrante, M.; Lee, A.S.; Onderwater, J.J.; Paton, J.C.*, et al.* Er stress causes rapid loss of intestinal epithelial stemness through activation of the unfolded protein response. *Cell Rep* **2013**, *3*, 1128-1139.
265. Chavez, A.; Scheiman, J.; Vora, S.; Pruitt, B.W.; Tuttle, M.; E, P.R.I.; Lin, S.; Kiani, S.; Guzman, C.D.; Wiegand, D.J.*, et al.* Highly efficient cas9-mediated transcriptional programming. *Nat Methods* **2015**, *12*, 326-328.

266. Manchado, E.; Eguren, M.; Malumbres, M. The anaphase-promoting complex/cyclosome (apc/c): Cell-cycle-dependent and -independent functions. *Biochemical Society transactions* **2010**, *38*, 65-71.
267. Higashi, T.; Arnold, T.R.; Stephenson, R.E.; Dinshaw, K.M.; Miller, A.L. Maintenance of the epithelial barrier and remodeling of cell-cell junctions during cytokinesis. *Curr Biol* **2016**, *26*, 1829-1842.
268. Greussing, R.; Unterluggauer, H.; Koziel, R.; Maier, A.B.; Jansen-Durr, P. Monitoring of ubiquitin-proteasome activity in living cells using a degron (dgn)-destabilized green fluorescent protein (gfp)-based reporter protein. *J Vis Exp* **2012**.
269. Li, W.; Ye, Y. Polyubiquitin chains: Functions, structures, and mechanisms. *Cell Mol Life Sci* **2008**, *65*, 2397-2406.
270. Jones, C.M.; Chen, J.S.; Johnson, A.E.; Elmore, Z.C.; Cullati, S.N.; Beckley, J.R.; Gould, K.L. Relief of the dma1-mediated checkpoint requires dma1 autoubiquitination and dynamic localization. *Mol Biol Cell* **2018**, *29*, 2176-2189.
271. Jorgensen, J.P.; Lauridsen, A.M.; Kristensen, P.; Dissing, K.; Johnsen, A.H.; Hendil, K.B.; Hartmann-Petersen, R. Adrm1, a putative cell adhesion regulating protein, is a novel proteasome-associated factor. *J Mol Biol* **2006**, *360*, 1043-1052.
272. Jang, S.H.; Park, J.W.; Kim, H.R.; Seong, J.K.; Kim, H.K. Adrm1 gene amplification is a candidate driver for metastatic gastric cancers. *Clin Exp Metastasis* **2014**, *31*, 727-733.
273. Jiang, R.T.; Yemelyanova, A.; Xing, D.; Anchoori, R.K.; Hamazaki, J.; Murata, S.; Seidman, J.D.; Wang, T.L.; Roden, R.B.S. Early and consistent overexpression of adrm1 in ovarian high-grade serous carcinoma. *J Ovarian Res* **2017**, *10*, 53.
274. Logue, J.S.; Whiting, J.L.; Tunquist, B.; Sacks, D.B.; Langeberg, L.K.; Wordeman, L.; Scott, J.D. Akap220 protein organizes signaling elements that impact cell migration. *The Journal of biological chemistry* **2011**, *286*, 39269-39281.
275. Bauman, A.L.; Scott, J.D. Kinase- and phosphatase-anchoring proteins: Harnessing the dynamic duo. *Nat Cell Biol* **2002**, *4*, E203-206.
276. Palorini, R.; Votta, G.; Pirola, Y.; De Vitto, H.; De Palma, S.; Airoldi, C.; Vasso, M.; Ricciardiello, F.; Lombardi, P.P.; Cirulli, C.*, et al.* Protein kinase a activation promotes cancer cell resistance to glucose starvation and anoikis. *PLoS Genet* **2016**, *12*, e1005931.
277. Taylor, S.S.; Yang, J.; Wu, J.; Haste, N.M.; Radzio-Andzelm, E.; Anand, G. Pka: A portrait of protein kinase dynamics. *Biochimica et biophysica acta* **2004**, *1697*, 259-269.
278. Fernandez-Marcos, P.J.; Auwerx, J. Regulation of pgc-1alpha, a nodal regulator of mitochondrial biogenesis. *Am J Clin Nutr* **2011**, *93*, 884S-890.
279. Dang, C.V. Myc, metabolism, cell growth, and tumorigenesis. *Cold Spring Harb Perspect Med* **2013**, *3*.
280. Everett, L.J.; Le Lay, J.; Lukovac, S.; Bernstein, D.; Steger, D.J.; Lazar, M.A.; Kaestner, K.H. Integrative genomic analysis of creb defines a critical role for transcription factor networks in mediating the fed/fasted switch in liver. *BMC Genomics* **2013**, *14*, 337.
281. Sakurai, H. Targeting of tak1 in inflammatory disorders and cancer. *Trends Pharmacol Sci* **2012**, *33*, 522-530.
282. Sakurai, H.; Nishi, A.; Sato, N.; Mizukami, J.; Miyoshi, H.; Sugita, T. Tak1-tab1 fusion protein: A novel constitutively active mitogen-activated protein kinase kinase kinase that stimulates ap-1 and nf-kappab signaling pathways. *Biochemical and biophysical research communications* **2002**, *297*, 1277-1281.

283. Choo, M.K.; Sakurai, H.; Koizumi, K.; Saiki, I. Tak1-mediated stress signaling pathways are essential for tnf-alpha-promoted pulmonary metastasis of murine colon cancer cells. *Int J Cancer* **2006**, *118*, 2758-2764.
284. Neil, J.R.; Schiemann, W.P. Altered tab1:I kappab kinase interaction promotes transforming growth factor beta-mediated nuclear factor-kappab activation during breast cancer progression. *Cancer Res* **2008**, *68*, 1462-1470.
285. Strippoli, R.; Benedicto, I.; Foronda, M.; Perez-Lozano, M.L.; Sanchez-Perales, S.; Lopez-Cabrera, M.; Del Pozo, M.A. P38 maintains e-cadherin expression by modulating tak1-nf-kappa b during epithelial-to-mesenchymal transition. *Journal of cell science* **2010**, *123*, 4321-4331.
286. Liu, T.; Zhang, L.; Joo, D.; Sun, S.C. Nf-kappab signaling in inflammation. *Signal Transduct Target Ther* **2017**, *2*.
287. Foletta, V.C.; Segal, D.H.; Cohen, D.R. Transcriptional regulation in the immune system: All roads lead to ap-1. *J Leukoc Biol* **1998**, *63*, 139-152.
288. Wagner, E.F.; Eferl, R. Fos/ap-1 proteins in bone and the immune system. *Immunol Rev* **2005**, *208*, 126-140.
289. el Marjou, F.; Janssen, K.P.; Chang, B.H.; Li, M.; Hindie, V.; Chan, L.; Louvard, D.; Chambon, P.; Metzger, D.; Robine, S. Tissue-specific and inducible cre-mediated recombination in the gut epithelium. *Genesis* **2004**, *39*, 186-193.
290. Provenzano, P.P.; Inman, D.R.; Eliceiri, K.W.; Beggs, H.E.; Keely, P.J. Mammary epithelial-specific disruption of focal adhesion kinase retards tumor formation and metastasis in a transgenic mouse model of human breast cancer. *Am J Pathol* **2008**, *173*, 1551-1565.
291. Moossavi, S.; Bishehsari, F. Inflammation in sporadic colorectal cancer. *Arch Iran Med* **2012**, *15*, 166-170.
292. Muller, M.F.; Ibrahim, A.E.; Arends, M.J. Molecular pathological classification of colorectal cancer. *Virchows Arch* **2016**, *469*, 125-134.
293. Lu, Y.; Brush, J.; Stewart, T.A. Nsp1 defines a novel family of adaptor proteins linking integrin and tyrosine kinase receptors to the c-jun n-terminal kinase/stress-activated protein kinase signaling pathway. *The Journal of biological chemistry* **1999**, *274*, 10047-10052.
294. Dorssers, L.C.; van Agthoven, T.; Brinkman, A.; Veldscholte, J.; Smid, M.; Dechering, K.J. Breast cancer oestrogen independence mediated by bcar1 or bcar3 genes is transmitted through mechanisms distinct from the oestrogen receptor signalling pathway or the epidermal growth factor receptor signalling pathway. *Breast Cancer Res* **2005**, *7*, R82-92.
295. Kim, D.I.; Jensen, S.C.; Noble, K.A.; Kc, B.; Roux, K.H.; Motamedchaboki, K.; Roux, K.J. An improved smaller biotin ligase for bioid proximity labeling. *Mol Biol Cell* **2016**, *27*, 1188-1196.
296. Gumbiner, B.M.; Kim, N.G. The hippo-yap signaling pathway and contact inhibition of growth. *Journal of cell science* **2014**, *127*, 709-717.
297. Sudol, M. Yap1 oncogene and its eight isoforms. *Oncogene* **2013**, *32*, 3922.
298. Yuan, M.; Tomlinson, V.; Lara, R.; Holliday, D.; Chelala, C.; Harada, T.; Gangeswaran, R.; Manson-Bishop, C.; Smith, P.; Danovi, S.A*., et al.* Yes-associated protein (yap) functions as a tumor suppressor in breast. *Cell Death Differ* **2008**, *15*, 1752-1759.
299. Hansen, C.G.; Moroishi, T.; Guan, K.L. Yap and taz: A nexus for hippo signaling and beyond. *Trends Cell Biol* **2015**, *25*, 499-513.
300. Imajo, M.; Ebisuya, M.; Nishida, E. Dual role of yap and taz in renewal of the intestinal epithelium. *Nat Cell Biol* **2015**, *17*, 7-19.

301. Li, C.; Wang, S.; Xing, Z.; Lin, A.; Liang, K.; Song, J.; Hu, Q.; Yao, J.; Chen, Z.; Park, P.K.*, et al.* A ror1-her3-lncrna signalling axis modulates the hippo-yap pathway to regulate bone metastasis. *Nat Cell Biol* **2017**, *19*, 106-119.
302. Dinkel, H.; Van Roey, K.; Michael, S.; Kumar, M.; Uyar, B.; Altenberg, B.; Milchevskaya, V.; Schneider, M.; Kuhn, H.; Behrendt, A.*, et al.* Elm 2016--data update and new functionality of the eukaryotic linear motif resource. *Nucleic Acids Res* **2016**, *44*, D294-300.
303. Glotzer, M.; Murray, A.W.; Kirschner, M.W. Cyclin is degraded by the ubiquitin pathway. *Nature* **1991**, *349*, 132-138.
304. Welcker, M.; Clurman, B.E. Fbw7 ubiquitin ligase: A tumour suppressor at the crossroads of cell division, growth and differentiation. *Nat Rev Cancer* **2008**, *8*, 83-93.
305. Welcker, M.; Orian, A.; Jin, J.; Grim, J.E.; Harper, J.W.; Eisenman, R.N.; Clurman, B.E. The fbw7 tumor suppressor regulates glycogen synthase kinase 3 phosphorylation-dependent c-myc protein degradation. *Proc Natl Acad Sci U S A* **2004**, *101*, 9085-9090.
306. Tong, J.; Tan, S.; Zou, F.; Yu, J.; Zhang, L. Fbw7 mutations mediate resistance of colorectal cancer to targeted therapies by blocking mcl-1 degradation. *Oncogene* **2017**, *36*, 787-796.
307. Wagner, S.A.; Beli, P.; Weinert, B.T.; Scholz, C.; Kelstrup, C.D.; Young, C.; Nielsen, M.L.; Olsen, J.V.; Brakebusch, C.; Choudhary, C. Proteomic analyses reveal divergent ubiquitylation site patterns in murine tissues. *Mol Cell Proteomics* **2012**, *11*, 1578-1585.
308. Udeshi, N.D.; Mertins, P.; Svinkina, T.; Carr, S.A. Large-scale identification of ubiquitination sites by mass spectrometry. *Nat Protoc* **2013**, *8*, 1950-1960.
309. Doyle, A.; McGarry, M.P.; Lee, N.A.; Lee, J.J. The construction of transgenic and gene knockout/knockin mouse models of human disease. *Transgenic Res* **2012**, *21*, 327-349.
310. Li, E.; Bestor, T.H.; Jaenisch, R. Targeted mutation of the DNA methyltransferase gene results in embryonic lethality. *Cell* **1992**, *69*, 915-926.
311. Bouabe, H.; Okkenhaug, K. Gene targeting in mice: A review. *Methods Mol Biol* **2013**, *1064*, 315-336.
312. Means, A.L.; Freeman, T.J.; Zhu, J.; Woodbury, L.G.; Marincola-Smith, P.; Wu, C.; Meyer, A.R.; Weaver, C.J.; Padmanabhan, C.; An, H.*, et al.* Epithelial smad4 deletion up-regulates inflammation and promotes inflammation-associated cancer. *Cell Mol Gastroenterol Hepatol* **2018**, *6*, 257-276.
313. Kondo, J.; Powell, A.E.; Wang, Y.; Musser, M.A.; Southard-Smith, E.M.; Franklin, J.L.; Coffey, R.J. Lrig1 regulates ontogeny of smooth muscle-derived subsets of interstitial cells of cajal in mice. *Gastroenterology* **2015**, *149*, 407-419 e408.
314. Liu, J.; Willet, S.G.; Bankaitis, E.D.; Xu, Y.; Wright, C.V.; Gu, G. Non-parallel recombination limits cre-loxp-based reporters as precise indicators of conditional genetic manipulation. *Genesis* **2013**, *51*, 436-442.